DEVELOPMENT OF INNOVATIVE POLYMERIC MEMBRANES USING GREEN APPROACHES FOR WATER AND ENERGY SUSTAINABILITY

A Thesis Submitted to
the Graduate School of Engineering and Sciences of
İzmir Institute of Technology
in Partial Fulfillment of the Requirements for the Degree of

DOCTOR OF PHILOSOPHY

in Chemical Engineering

by
Elif GÜNGÖRMÜŞ DELİİSMAİL

December 2022
İZMİR

ACKNOWLEGMENT

I would like to express my deep and sincere gratitude to my supervisor Prof. Dr. Sacide ALSOY ALTINKAYA for her supervision, encouragements, and guide throughout the thesis. Besides, I would like to thank my sincere gratitude to my PhD Thesis Committee and Jury Members, Prof. Dr. Mustafa Muammer DEMİR, Assoc. Prof. Dr. Özgenç EBİL, Prof. Dr. Nalan KABAY, Assoc. Prof. Dr. Yılmaz YÜREKLİ for their constructive criticism to improve the overall quality of my thesis.

I warmly express my special thanks to my lab mates and my close friends for their help and support. I would like to thank the Biotechnology and Bioengineering Application and Research Center, Center for Materials Research, and Environmental Development Application and Research Center at İzmir Institute of Technology for providing technical support.

Finally, I would like to thank my dear husband Özgün DELIISMAIL and my family for their never-ending love, support, and encouragement. Special thanks go to my dear son, Ayaz DELİİSMAİL for making me stronger and better than I could have ever imagined.

ABSTRACT

DEVELOPMENT OF INNOVATIVE POLYMERIC MEMBRANES USING GREEN APPROACHES FOR WATER AND ENERGY SUSTAINABILITY

In this thesis, innovative polymeric membranes with fast, simple, and easily scalable manufacturing procedures were developed to demonstrate the potential of membrane technology in making chemical processes more sustainable. In this scope, firstly, it was focused on minimizing the adverse chemical, environmental, and economic effects of conventional drying processes by integrating membrane technology into the production of nano/microparticles. Acid-resistant polyaniline based ultrafiltration (UF) membrane and solvent-resistant poly (ether imide sulfone) based UF membrane were developed to produce aluminum sulfate powder and silica powder, respectively. The developed high-performance and antifouling membranes made the production of powders more sustainable and environmentally friendly by enabling the recovery of the acid/solvent used in the synthesis and the reduction of energy consumption for drying. The third part of the thesis focused on biodiesel production with a high-performance, antifouling, alumina-calcium oxide catalyst-modified polyethersulfone UF membrane. Combining membrane technology with reaction engineering allowed for the elimination of the catalyst recovery step, shortened the reaction time to reach a desirable yield, and reduced energy consumption, resulting in more sustainable biodiesel production than existing production techniques. In the last part of the thesis, a high-performance, antibiofouling/antibacterial citric acid doped polyaniline based UF membrane was developed. Ensuring sustainability improvement in membrane production in all applications was the main objective of this thesis. By reducing the number of steps in membrane production, the amount of wastewater generated, and toxic waste released during membrane production was minimized, and energy consumption was significantly reduced.

ÖZET

SU VE ENERJİ SÜRDÜRÜLEBİLİRLİĞİ İÇİN YEŞİL YAKLAŞIMLAR KULLANILARAK YENİLİKÇİ POLİMERİK MEMBRANLARIN GELİŞTİRİLMESİ

Bu tezde, membran teknolojisinin kimyasal süreçleri daha sürdürülebilir hale getirme potansiyelini göstermek için hızlı, basit ve kolayca ölçeklenebilir üretim prosedürlerine sahip yenilikçi polimerik membranlar geliştirildi. Bu kapsamda öncelikle, nano/mikropartikül üretimine membran teknolojisi entegre edilerek, geleneksel kurutma proseslerinin olumsuz kimyasal, çevresel ve ekonomik etkilerinin en aza indirilmesine odaklanılmıştır. Aside dayanıklı polianilin bazlı ultrafiltrasyon (UF) membranı ve çözücülere dayanıklı poli (eter imid sülfon) bazlı UF membranı, sırasıyla, alüminyum sülfat tozu ve silika tozu üretimleri için geliştirilmiştir. Geliştirilen yüksek performanslı ve kirlenmeye dirençli membranlar, sentez aşamasında kullanılan asidin/çözücünün geri kazanımını ve kurutma aşamasındaki enerji tüketiminin azaltılmasını sağlayarak, tozların üretimini daha sürdürülebilir ve çevre dostu hale getirmiştir. Tezin üçüncü bölümünde, biyodizel üretiminde kullanılmak üzere yüksek performansa sahip, kirlenmeye dirençli, alümina-kalsiyum oksit katalizörü ile modifiye edilmiş polietersülfon UF membranı geliştirilmiştir. Membran teknolojisinin reaksiyon mühendisliği ile birleştirilmesi, katalizör geri kazanım adımının ortadan kaldırılmasını, istenilen verime ulaşmak için gerekli reaksiyon süresinin kısalmasını ve enerji tüketiminin azalmasını sağlayarak, mevcut üretim yöntemlerine göre daha sürdürülebilir biyodizel üretimi gerçekleştirilmiştir. Tezin son bölümünde ise yüksek performanslı, biyolojik kirlilik önleyici/antibakteriyel sitrik asit katkılı polianilin bazlı UF membranı geliştirilmiştir. Tüm bu uygulamalarda membran üretiminde sürdürülebilir iyileştirmenin sağlanması bu tezin temel amacı olmuştur. Membran üretimindeki adım sayısı azaltılarak, membran üretimi sırasında oluşan atık su miktarı ve açığa çıkan zehirli atık miktarı en aza indirilmiş ve enerji tüketimi önemli ölçüde azaltılmıştır.

TABLE OF CONTENTS

LIST OF FIGURES.....x

LIST OF TABLES.....xv

CHAPTER 1. INTRODUCTION.....1

1.1. Overview of Membrane Separation Processes and Fabrications.....2

1.2. Membrane Based Processes for Sustainable Production 3

1.3. Sustainability Assessment of Membrane Fabrications.....4

1.4. Motivations.....6

1.5. Thesis Overview.....6

1.6. Contributions to the Literature.....7

CHAPTER 2. A HIGH-PERFORMANCE ACID-RESISTANT POLYANILINE BASED ULTRAFILTRATION MEMBRANE: APPLICATION IN THE PRODUCTION OF ALUMINIUM SULFATE POWDER FROM ALUMINA SOL.....9

2.1. Introduction.....9

2.2. Materials and Methods.....11

2.2.1. Materials.....11

2.2.2. Synthesis of the Emeraldine Base (EB) Form of PANI.....12

2.2.3. Preparation of the EB and H_2SO_4 Doped Emeraldine Salt (ES) Membranes.....12

2.2.4. Performance Tests of the EB and H_2SO_4 Doped ES Membranes.....13

2.2.5. Characterization of the EB and H_2SO_4 doped ES Membranes.....14

2.2.6. Acid Resistance of the H_2SO_4 Doped ES Membrane.....15

2.2.7. Preparation of Alumina Sol and Determination of its Particle Size Distribution.....15

2.2.8. Alumina Sol Filtration Performance of the H_2SO_4 Doped ES Membranes.....15

2.2.9. Preparation and Characterization of Powder Obtained with and without Filtration of Alumina Sol.....16

2.3. Results and Discussion 17

2.3.1. Characterization of the EB and H_2SO_4 Doped ES Membranes.....17

2.3.2. Stability of the H_2SO_4 Doped ES Membranes.....22

2.3.3. Alumina Sol Filtration Performance of the H_2SO_4 Doped ES Membranes.....28

2.3.4. The Effect of Membrane Filtration on the Chemical and Physical Properties of the Aluminium Sulfate Powder.....30

2.4. Conclusion.....35

CHAPTER 3. A NEW-GENERATION POLY (ETHER IMIDE SULFONE) BASED SOLVENT RESISTANT ULTRAFILTRATION MEMBRANE FOR A SUSTAINABLE PRODUCTION OF SILICA NANOPOWDER.....36

3.1. Introduction.....36

3.2. Materials and Methods.....39

3.2.1. Materials.....39

3.2.2. Amine Functionalization of TiO_2 Nanoparticles.....40

3.2.3. Preparation of Pristine and Amine-functionalized TiO_2 Coated Poly (ether imide sulfone) Membranes.....40

3.2.4. Performance Tests of Pristine and Amine-functionalized TiO_2 Coated Poly (ether imide sulfone) Membranes.....41

3.2.5. Characterization of Pristine and Amine-functionalized TiO_2 Coated Poly (ether imide sulfone) Membranes.....42

3.2.6. Synthesis and Characterization of Colloidal Silica Suspension.....43

3.2.7. Filtration of Colloidal Silica Suspension through the Amine-functionalized TiO_2 Coated Poly (ether imide sulfone)

Membranes.....43

3.2.8. Stability of Amine-functionalized TiO_2 Coated Poly (ether imide sulfone) Membrane.....44

3.2.9. Preparation and Characterization of Powder Obtained with and without Filtration of Colloidal Silica Suspension.....45

3.3. Results and Discussion 45

3.3.1. Preparation of Amine-functionalized TiO_2 Coated Poly (ether imide sulfone) Membranes.....45

3.3.2. Characterization of Pristine and Amine-functionalized TiO_2 Coated Poly (ether imide sulfone) Membranes.....48

3.3.3. Colloidal Silica Suspension Filtration Performance and Stability of the Amine-functionalized TiO_2 Coated Poly (ether imide sulfone) Membrane.....51

3.3.4. The Chemical and Physical Properties of the Silica Nanopowder Produced by Membrane Filtration and Drying-Based Methods and Economics of Each Method.....55

3.4. Conclusion 58

CHAPTER 4. A HIGHLY ACTIVE ALUMINA-CALCIUM OXIDE CATALYST IMMOBILIZED POLY (ETHER SULFONE) MEMBRANE FOR SUSTAINABLE BIODIESEL PRODUCTION.....59

4.1. Introduction.....59

4.2. Materials and Methods.....62

4.2.1. Materials.....62

4.2.2. Catalyst Preparation.....62

4.2.3. Membrane Preparation.....63

4.2.4. Characterization and Performance Tests of the Membranes.....63

4.2.5. Optimization of Transesterification Reaction Parameters to Produce Biodiesel on the Cat/PDA/PES Membrane Surface.....64

4.2.6. Long-term Catalytic Activity and Fouling of the Cat/PDA/PES

Membrane.....66
4.2.7. Stability of the Cat/PDA/PES Membrane 67
4.3. Results and Discussion 67
4.3.1. Characterization of Alumina-calcium Oxide Catalyst Immobilized Polydopamine Modified Poly (Ether Sulfone) Membrane.....67
4.3.2. Optimization of Reaction Parameters of Transesterification of Canola Oil to Produce Biodiesel on the Cat/PDA/PES) Membrane Surface.....71
4.3.3. Catalytic Activity and Performance Changes of the Cat/PDA/PES Membrane in Long-term reaction period.....76
4.3.4. Stability of the Cat/PDA/PES Membrane 82
4.4. Conclusion 83

CHAPTER 5. FACILE FABRICATION OF ANTI-BIOFOULING POLYANILINE ULTRAFILTRATION MEMBRANE BY GREEN CITRIC ACID DOPING PROCESS.....85

5.1. Introduction.....85
5.2. Materials and Methods.....89
5.2.1. Materials.....89
5.2.2. Polymer Synthesis..... 89
5.2.3. Membrane Fabrication and Modification.....90
5.2.4. Membrane Performance Tests and Characterization.....90
5.2.5. Antibacterial Activity Tests.....92
5.2.6. Antibiofouling Performance Tests.....92
5.2.7. Stability Test for the Citric Acid Doped ES Membrane.....93
5.3. Results and Discussion 94
5.3.1. Effect of Citric Acid Doping on the Structure, Chemical Composition and Surface Properties of the EB Membrane

Activity of the Membranes.....94
5.3.2. Antibacterial Activities of the Membranes.....100
5.3.3. Antibiofouling Performance of the Membranes.....104
5.3.4. Antibacterial Stability of Citric Acid Doped ES Membrane.....107
5.4. Conclusion.....110
CHAPTER 6. CONCLUSION.....111
REFERENCES.....114
APPENDICES.....146
APPENDIX A. PERMISSIONS FOR REPRODUCING PUBLISHED ARTICLES.....146
APPENDIX B. SUPPLEMENTARY INFORMATION FOR CHAPTER 3.....148

LIST OF FIGURES

Figure **Page**

Figure 2.1. ATR-FTIR spectra of a) synthesized and b) commercial EB in the form of polymer, c) EB membrane, d) H_2SO_4 doped ES membrane and e) H_2SO_4 doped ES membrane after 30 days of H_2SO_4 exposure under static exposure under static conditions.....18

Figure 2.2. SEM-EDX elemental analysis and mapping of a) EB membrane, b) H_2SO_4 doped ES membrane, and c) H_2SO_4 doped ES membrane after 30 days of H_2SO_4 exposure under static conditions.....19

Figure 2.3. Cross-section SEM images of a-b) EB membrane, c-d) H_2SO_4 doped ES membrane and e-f) H_2SO_4 doped ES membrane after 30 days of H_2SO_4 exposure under static conditions.....20

Figure 2.4. AFM images of a-b) EB membrane and c-d) H_2SO_4 doped ES membrane.....20

Figure 2.5. Zeta potential of EB and H_2SO_4 doped ES membranes as a function of pH.....21

Figure 2.6. Performance of H_2SO_4 doped ES membrane during 5-cycle alumina sol filtration.....28

Figure 2.7. Flux recovery, irreversible and reversible fouling ratios, and alumina sol recoveries for each cycle during filtration of alumina sol.....29

Figure 2.8. Particle size distributions of a) the prepared alumina sol and powder dried b) at 25°C after filtering 80 % of sol, c) at 25°C without filtration, d) at 100°C in an oven without filtration, e) in a freeze dryer without filtration.....32

Figure **Page**

Figure 2.9. SEM images of the powders dried a-b) at 25°C after filtering 80 % of sol, c-d) at 25°C without filtration, e-f) at 100°C in an oven without filtration, g-h) in a freeze dryer without filtration.....33

Figure 2.10. XRD patterns of the aluminium sulfate powders prepared with membrane filtration and traditional drying methods.....34

Figure 3.1. a) Chemical structure of poly (ether imide sulfone), b) amine functionalization of TiO_2 nanoparticles, and c) schematic illustration of the membrane modification by amine-functionalized TiO_2 nanoparticles.....39

Figure 3.2. a) PEG rejections and b) the pore size distribution of pristine and amine-functionalized TiO_2 coated poly (ether imide sulfone) membranes.....47

Figure 3.3. ATR-FTIR spectra of the pristine and amine-functionalized TiO_2 coated polyetherimide sulfone membranes.....49

Figure 3.4. Surface SEM images, cross-sectional SEM images and SEM-EDX elemental analysis and mapping of the pristine (a, c, e) and the amine-functionalized TiO_2 coated poly (ether imide sulfone) membranes (b,d,f).....49

Figure 3.5. AFM images of a) pristine and b) amine-functionalized TiO_2 coated poly (ether imide sulfone) membranes.....50

Figure 3.6. Zeta potential of the pristine and amine-functionalized TiO_2 coated poly (ether imide sulfone) membranes as a function of pH.....50

Figure 3.7. TGA and dTG (derivative thermogravimetry) curves of the polyethylene terephthalate nonwoven fabric, pristine and amine-functionalized TiO_2 coated poly (ether imide sulfone) membranes, and amine-functionalized TiO_2 nanoparticles 51

Figure **Page**

Figure 3.8. a) The changes in flux of amine-functionalized TiO_2 coated poly (ether imide sulfone) membrane and the recovery of nanoparticles, b) The change in the flux recovery ratio, irreversible and reversible fouling resistances during filtration of colloidal silica suspension.....52

Figure 3.9. Antifouling mechanism of amine-functionalized TiO_2 coated poly (ether imide sulfone) membranes and recovery of silica nanoparticles from the suspension by using the membrane.....53

Figure 3.10. Stability of the amine-functionalized TiO_2 coated poly (ether imide sulfone) membrane: a) % release of amine-functionalized TiO_2 nanoparticles from the membrane surface as a function of time and b) The change in the PWP and PEG 10 kDa rejection of the membrane after storing in water up to 30 days.....54

Figure 3.11. The change in the PWP and PEG rejections of the membranes after storing in a-b) the 40% ethanol aqueous solution and c-d) silica nanoparticle synthesis solution consisting of ammonia: ethanol: water.....54

Figure 3.12. a) Total energy consumption (kWh), b) batch operation times, c) utility costs ($), and d) equipment costs for producing 1 kg nanopowder by membrane filtration and classical drying methods.....57

Figure 3.13. Comparison of silica nanopowder production by membrane filtration and drying-based methods.....57

Figure 4.1. The proposed binding mechanism between PDA/PES membrane and alumina-calcium oxide catalyst.....68

Figure 4.2. ATR-FTIR spectra of the PES, PDA/PES, and Cat/PDA/PES membranes.....68

Figure **Page**

Figure 4.3. SEM surface image and EDX elemental mapping of the a) PES, b) PDA/PES, and c) Cat/PDA/PES membranes.....70

Figure 4.4. The effect of ball milling time on the particle size distribution of alumina-calcium oxide catalyst.....70

Figure 4.5. AFM images of the a) PES, b) PDA/PES, and c) Cat/PDA/PES membranes 71

Figure 4.6. The effect of stirring speed on the biodiesel yield.....72

Figure 4.7. Combined effects of:a) butanol:oil molar ratio and temperature, b) pressure and temperature and c)pressure and butanol:oil molar ratio on the biodiesel yield.....75

Figure 4.8. GC/MS chromatograms of a) biodiesel standard diluted 10-fold and b) biodiesel sample produced under optimum reaction conditions.....76

Figure 4.9. The change of catalytic activity of the Cat/PDA/PES membrane under a) dynamic filtration and b) static conditions.....78

Figure 4.10. Normalized flux of the Cat/PDA/PES membrane as a function of time during 24 h reaction mixture filtration.....78

Figure 4.11. Schematic illustration of batch and flow-through mode of operations.....78

Figure 4.12. Flux recovery, irreversible and reversible fouling ratios of the Cat/PDA/PES membrane. a) flow-through mode of operation b) batch operation.....79

Figure 4.13 Stability of the Cat/PDA/PES membrane: a) The change in the % of alumina-calcium oxide catalyst remained on the membrane surface as a function of time and b) The change in the butanol permeability and % biodiesel yields of the membrane after storing in reactant mixture.....83

Figure **Page**

Figure 4.14. TGA spectra of the PES, PDA/PES, and Cat/PDA/PES membranes and alumina-calcium oxide catalyst.....83

Figure 5.1. ATR-FTIR spectra of EB membrane and citric acid doped ES membrane.....94

Figure 5.2. SEM cross-sectional images, surface images, and EDX elemental analysis of the EB membrane and the citric acid doped ES membranes.....96

Figure 5.3 AFM images of the a) EB membrane and b) citric acid doped ES membrane.....97

Figure 5.4. Zeta potential as a function of pH for the EB membrane and citric acid doped ES membrane.....97

Figure 5.5. TGA and dTG analysis of citric acid, EB membrane and citric acid doped ES membrane.....98

Figure 5.6. The MWCO of the a) EB membrane and b) citric acid dopec ES membrane.....99

Figure 5.7. Bactericidal rates within 24 hr and 1 hr incubation times for the EB and citric acid doped ES membrane.....101

Figure 5.8. Normalized flux of the EB membrane and citric acid doped ES membranes as a function of volume filtered per unit area during a) *E.coli* and b) *S.aureus* filtrations.....105

Figure 5.9. Flux recovery ratio and biofouling resistances of the membranes during a) *E.coli* and b) *S.aureus* filtrations.....106

Figure 5.10. Surface SEM images of the membranes at the end of 1st cycle (a,b) *E.coli* and (c,d) *S.aureus* filtrations.....106

Figure 5.11. Stability test results of citric acid doped ES membrane.....109

Figure 5.12. Bactericidal rates within 24 hr incubation time for the citric acid doped ES membranes after 1-month storage in 1 M NaCl solution.....109

LIST OF TABLES

Table **Page**

Table 2.1. H_2SO_4 stability of different polymeric membranes 25

Table 2.2. Comparison of energy cost of powder production with membrane filtration and solely drying-based techniques.....34

Table 4.1 Box–Behnken experimental design for biodiesel production.....65

Table 4.2 Normalized peak area ratios different peaks determined from ATR-FTIR spectra of the PES, PDA/PES, and Cat/PDA/PES membranes.....69

Table 4.3. The Box-Behnken design matrix.....73

Table 4.4. Analysis of variance (ANOVA) for quadratic model and regression statistics.....73

Table 4.5. The catalytic activity of the membranes in the literature used for continuous-flow biodiesel production.....80

Table 5.1 Properties of the prepared membranes.....96

Table 5.2. The PWP of commercial membranes with comparable MWCO manufactured by different companies.....99

Table 5.3 Static antibacterial activity of the UF membranes in the literature.....102

CHAPTER 1

INTRODUCTION

In the middle of the 20th century, it has begun to be understood/recognized that with increasing global warming, climate change and greenhouse gas emissions, if human beings do not take appropriate measures, they will cause irreversible damage to the planet (Paramonova, 2016). Then, the concept of sustainability started to draw attention with the report called Our Common Future prepared by the United Nations World Commission on Environment and Development in 1987. In the report, sustainable development is defined as the development that meets the needs of the present without compromising the ability of future generations (Brundtland, 1987). Sustainability employs three interrelated pillars: economic, social, and environmental development (Purvis et al., 2019).

Over the past few decades, membrane-based technologies have led to significant innovation in processes and products to advance sustainable industrial growth. Compared to conventional technologies, membrane operations do not require high temperatures, chemical additives, or phase change; they are modular and easy to scale up. Their energy consumption and waste production are low; thus, they have a remarkable potential for more sustainable usage, production of raw materials, and recovery and reuse of products. The membrane technology can break the water-energy nexus to provide water and energy more sustainably. In addition to well-established membrane-based desalination processes for water recovery, new membrane operations can produce green energy by using sustainable resources. However, the main limitation in all applications is membrane fouling, which increases both chemical and energy consumption during operation. Sustainable production of energy, water, and raw materials with membranes cannot be the complete solution if the membrane production harms the environment.

This thesis aims to demonstrate the role of membrane technology in sustainable micro/nanoparticle production and sustainable biodiesel production. While developing the membranes, the main focus was to adjust the membrane properties required for the target application. Additionally, simplifying the protocols, thus reducing the number of steps, energy, and water consumption required for membrane production and enhancing the fluxes and antifouling/antibiofouling properties of the surfaces were other concerns.

This chapter will discuss the potential of membrane technology in achieving sustainable production and the factors influencing green membrane production. The motivation and specific contributions of the thesis to the literature will also be mentioned.

1.1. Overview of Membrane Separation Processes and Fabrications

Pressure-driven membrane processes are divided into four categories as microfiltration (MF), ultrafiltration (UF), nanofiltration (NF), and reverse osmosis (RO). MF membranes can separate particles, viruses, and bacteria. They have the largest pores within a range of 0.1-10 μm and require the lowest pressure (< 2 bar) compared with other filtration processes. MF's dominant sieving transport mechanism leads to separate particles according to their dimensions, although some charge or adsorptive separation is possible. UF membranes have smaller pores (1-100 nm) and are operated at relatively high pressure (< 10 bar). A typical UF membrane application removes macromolecules, colloids, and solutes with MW > 10,000 from low molecular weight species, based on the components' size difference and surface charge. NF membrane has a pore size of around 1 nm; operated at high pressure (< 40 bar). The selectivity of NF membranes is based on the sieving effect and Donnan exclusion (charge effect). Donnan exclusion allows the removal of ions with a size below the pore size of the membrane. RO membranes have the smallest pores (< 2 nm) and operate at very high pressure (60-70 bar). Selectivity is a result of the solution-diffusion mechanism. RO membranes are used in desalination to separate monovalent salts (Baker, 2012).

While the membrane market continues to grow, especially in water treatment, gas separation, healthcare, bioprocess, and solvent separation applications, about 50% of this market includes UF and MF membranes produced by the phase inversion method (Kim, 2020). The phase inversion method was first reported in 1960 by Loeb and Sourirajan (1960). Nonsolvent-induced phase separation (NIPS), thermally induced phase separation (TIPS), vapor-induced phase separation (VIPS), and evaporation-induced phase separation (EIPS) are different types of phase inversion methods. NIPS is the most commonly used method due to its versatility and possibility of preparing many membranes (Mulder, 1996). A stable homogeneous solution, prepared by dissolving a polymer in an organic solvent, is cast onto a glass plate or a nonwoven support material using a casting knife with the desired thickness. Next, the solution-casted support is

immersed into a coagulation bath (including non-solvent), where the exchange of solvent and non-solvent takes place. As the solvent moves from the polymer solution to the coagulation bath, the non-solvent does the opposite, forming the membrane. Thermodynamics defines interactions among polymer, solvent, and non-solvent in a coagulation bath. The exchange rate of solvent and non-solvent and the speed of the phase separation depend on the kinetics (Tasselli, 2016). Both the thermodynamics and kinetics of the phase inversion process strongly influence the morphology and performance of the membranes. In NF and RO processes, thin-film composite (TFC) membranes are most commonly used due to their very thin, highly selective layer on a porous UF support. The selective layer is commonly prepared through interfacial polymerization (Asadi Tashvigh et al., 2021).

1.2. Membrane Based Processes for Sustainable Production

Increasing demand for water, energy, raw materials, and products requires new solutions to support sustainable industrial growth. Global needs for water and energy are critical challenges in the 21st century. Energy is needed for water treatment and purification, while water is needed for energy production. The membrane technology has great potential to break the water-energy nexus. Desalination is a standard technology to produce fresh water. Compared to distillation techniques adopted for desalination, such as multi-stage flash, multi-effect distillation, vacuum vapor compression, etc., reverse osmosis technology consumes ten folds less energy (Ali et al., 2017). New RO membranes are still being investigated to improve the energy efficiency of the process. Desalination of seawater to produce drinking water (Lee et al., 2011; Matsuura, 2001); desalination of produced water in oil and gas industries (Çakmakce et al., 2008; Zaidi et al., 1992; Lee and Frankiewicz, 2005); production of partially desalinated water for agriculture use (Beltrán and Koo-Oshima, 2006; Burn et al., 2015); are some of the applications for the sustainable water production with membranes. The membrane technology used in the treatment of spent mining water (Juby, 1992; Harries, 1985); and industrial and municipal wastewater containing toxic chemicals such as heavy metals and trace organic contaminants (Barakat, 2011; Jeppesen et al., 2009; Cicek et al., 1998; Minami, 1994; Zaloum et al., 1994) can contribute to environmental and economic sustainability. Chemical processes utilize a substantial amount of solvent to perform

reactions and achieve separation. Conventional energy-intensive distillation processes can generate high-purity solvents. The organic solvent nanofiltration (OSN) can become an alternative to distillation. Rundquist et al. (2012) demonstrated that OSN could recover organic solvent with a suitable purity for re-use as an active pharmaceutical ingredient (API) and uses 25 times less energy per L of the recovered solvent when compared to distillation.

Membrane technology also plays a significant role in energy sustainability. New processes such as pressure-retarded osmosis and reverse electrodialysis are currently being utilized to convert seawater or wastewater into electricity (Skilhagen et al., 2008; Gerstandt et al., 2008). Additionally, membranes are used in energy storage for renewable energy sources (fuel cells and batteries) (Lee et al., 2014; Huang, 2011) or become part of the production in separating biofuels, bioethanol, and biogas from the reaction environment. Catalytic membrane reactors can provide remarkable advantages in sustainable energy production by eliminating the need for catalyst recovery and selective removal of products from the reaction mixture to prevent consecutive reactions or to break the equilibrium limitation (Shuit et al., 2012). Micro or nanopowder production is currently done with energy-intensive drying processes. The process increases greenhouse gas emissions and harms the environment due to the loss of solvents to the atmosphere if not recovered. Distillation is mainly used to recover the solvents requiring significant energy input. The membrane technology offers significant advantages in sustainable nano/micro particle production; however, this area has yet to be exploited. The main challenge in all applications is fouling, which causes increased energy and chemical consumption to recover the initial performance. Thus, there is a need to develop membranes with enhanced separation and antifouling properties to comply with the principles of the sustainability concept.

1.3. Sustainability Assessment of Membrane Fabrication

While discussing the potential of membrane technology for sustainable production, different strategies to make membrane production greener should also be considered without compromising its performance. The principles of manufacturing greener membranes can be ranked under four categories: 1) Replacing conventional solvents used in membrane manufacture with greener solvents and using low-toxicity

chemicals that reduces their environmental impact and making the process safer. 2) Reducing the number of steps during production could minimize energy consumption and toxic waste. 3) Using renewable raw materials, making membrane production more sustainable. 4) Dissolving polymers and crosslinking at room temperature results in lower energy consumption (Szekely et al., 2014). Mass intensity (amount of spent reagent per product mass) should also be considered, and this value should be kept to a minimum as much as possible.

The polymers commonly used in membrane production, such as polyvinylidene fluoride (PVDF), polyethersulfone (PES), and polysulfone (PSU), are dissolved in hard polar aprotic solvents (e.g., N-methyl pyrrolidone (NMP), dimethylacetamide (DMAc) and dimethylformamide (DMF)) to prepare casting solutions. These types of solvents are toxic and are on the watch list of the European Chemicals Agency and will soon be banned in large-scale production (Kim et al., 2016). Therefore, some of the current membrane studies focus on green solvents that can replace these toxic solvents (Sherwood et al., 2014; Kim, 2016; Marino et al., 2019; Rasool and Vankelecom, 2019). Most of the waste generated in membrane production (> 95% by weight) is solvent-contaminated wastewater in a coagulation bath (Kim et al., 2018). The proposed potential solutions applied for the sustainable treatment of this wastewater are organophilic pervaporation to selectively permeate the solvent (Lipnizki et al., 1999; Liu et al., 2011) and adsorption technologies utilizing molecularly imprinted polymers to capture solvent molecules within wastewater selectively (Razali et al., 2015). The other option to produce greener membranes is to reduce extra steps in membrane fabrication, thus eliminating the need for extra solvent and energy consumption. The membranes are generally crosslinked with post-treatment to enhance their stability and rejection characteristics. Soroko et al., 2011; Vanherck et al., 2013 and Cihanoğlu and Alsoy Altınkaya, 2018 made the membrane fabrication process greener by crosslinking the membrane during the phase inversion process by adding the crosslinker into the coagulation bath or replacing the crosslinking medium containing alcohol with water to eliminate alcohol washing steps before and after membrane crosslinking. Replacing fossil-based polymers with potential green polymers, such as bio-based polymers, can make membrane production greener. Compared to petro-derived conventional polymers, bio-based polymers are less toxic, environmentally friendly, and produced from renewable sources such as sugar, corn, starch, microorganisms, plants, and animals. Among many bio-based materials, cellulose, which can be abundantly found in nature, was mainly investigated in previous studies (Zhang et

al., 2001; Li et al., 2006; Mao et al., 2010; Li et al., 2011), but its dissolution using a green solvent is still a problem. Besides cellulose, chitosan, alginate, and polylactic acid are other biomaterials used in the production and modification of membranes (Lackner, 2015; Aburabie et al., 2017; Le Phuong et al., 2019; Aburabie et al., 2020).

1.4. Motivations

Sustainable development goals impose demands on new, innovative, green solutions for separation technologies and manufacturing methods. Nanotechnology has a significant role in supporting the United Nations' Sustainable Development Goals (SDGs). Green production of nanotechnology products is as essential as the role of nanotechnology in sustainable development. One of the motivations for this thesis study was to contribute to developing membranes and applying membrane technology for the green and more sustainable production of micro and nanoparticles. The sixth sustainable development goal of the United Nations is to ensure access to water and sanitation for all. It is estimated that the current rates of progress should be increased fourfold to reach universal access to drinking water, sanitation, and hygiene by 2030. Goal 7 ensures access to affordable, reliable, sustainable, and modern energy. Biofuels mainly contribute to SDG 7 and SDG 13 (climate action). Although biofuel usage positively impacts clean energy, green biofuel production should also be seriously considered. The role of membrane technology in producing clean water has been proven. The second motivation in the thesis was to develop green protocols for producing novel membranes with improved long-term stability and permeability. The last motivation was to contribute to sustainable biodiesel production by developing a novel catalytic membrane.

1.5. Thesis Overview

The details of each chapter of this PhD thesis were described below:

a. Chapter 2: A new class of acid-resistant UF membrane fabricated from polyaniline (PANI) was reported based on its self-acid doping ability through H_2SO_4. The prepared membrane recovered aluminum sulfate particles from a highly acidic synthesis

environment and green production of aluminum sulfate powder through membrane filtration without a dryer.

b. Chapter 3: A new-generation poly (ether imide sulfone) based solvent-resistant UF membrane for sustainable production of silica nanopowder was reported. Integrating membrane technology into nanoparticle production minimizes the adverse effects caused by conventional drying processes. It makes production more sustainable and environmentally friendly through solvent recovery and reduced energy consumption.
c. Chapter 4: A novel catalytically active polydopamine-modified poly (ether sulfone) membrane immobilized with alumina-calcium oxide catalyst was reported for use in sustainable biodiesel production. The integration of membrane technology using the flow-through operation system made biodiesel production more cost-effective and environmentally friendly.
d. Chapter 5: A green antibacterial agent doped PANI-based membrane was developed to obtain a high-performance anti-biofouling UF membrane by using a fast, simple, facile, and easily scalable protocol that can be adapted for large-scale production. Biofouling was simulated by long-term filtering Gram-negative and Gram-positive model bacteria suspensions through the membranes.

1.6. Contributions to the Literature

The contributions of this PhD thesis to the literature are listed below:

a. Chapter 2: Research efforts on developing acid-resistant membranes were primarily focused on the NF category. However, NF membranes are not the best choice for recovering nano/microparticles due to their low permeabilities. UF membranes are more economical alternatives than NF membranes since they can be operated at lower pressures. In addition to the energy cost, the overall cost of recovering particles with membranes is also determined by the cost of the membrane polymer. Acid-resistant semicrystalline polymers are limited to small-scale membrane production due to high raw material costs. Also, their extreme hydrophobicities result in low-flux membranes with a high fouling tendency. The review of current studies then clearly indicated that efficient and cost-effective acid-resistant UF membranes are needed. In light of the literature, the novelty of this study lies in three points. First, it proposes a new acid-resistant PANI-based UF membrane that can easily be obtained through a simple acid

doping process. Second, it is shown for the first time that acid doped PANI membrane can recover aluminum sulfate particles from a highly acidic synthesis environment without the permanent attachment of particles on the surface. Third, this study is the first which demonstrates the production of aluminum sulfate powder from the sol through membrane filtration without using a dryer.

b. Chapter 3: The existing drying-based processes used for nanopowder production are highly energy-intensive. Increasing demand for reducing greenhouse gases emission and more sustainable production requires novel approaches within nanotechnology. It was shown that integrating membrane technology into nanoparticle production can minimize the adverse effects caused by conventional drying processes and make production more sustainable and environmentally friendly through solvent recovery and reduced energy consumption. Another contribution of the study reported in Chapter 3 is the new type of solvent-resistant UF membrane. Despite many publications on OSN membranes, studies investigating solvent-resistant UF membranes are limited. Poly (ether imide sulfone) based solvent-resistant membrane was developed for the first time for sustainable silica nanopowder production.

c. Chapter 4: A novel catalytically active polydopamine-modified poly (ether sulfone) membrane immobilized with alumina-calcium oxide catalyst was reported for use in sustainable biodiesel production. Integrating membrane technology by using the flow-through mode of the operation system made biodiesel production more cost-effective and environmentally friendly.

d. Chapter 5: There is still a need for alternative methods/materials which are scalable and cost-effective for large-scale industrial production of UF membranes possessing both anti-adhesion and antibacterial properties. Also, sustainable development goals impose demands on new, innovative, and green solutions for membrane production. The protocol proposed in our study is fast, simple, facile, and easily scalable for large-scale production. Using a green antibacterial agent and its loading with a one-step process without consuming chemicals or functionalizing the support makes the proposed method environmentally friendly.

CHAPTER 2

A HIGH-PERFORMANCE ACID-RESISTANT POLYANILINE BASED ULTRAFILTRATION MEMBRANE: APPLICATION IN THE PRODUCTION OF ALUMINIUM SULFATE POWDER FROM ALUMINA SOL

2.1. Introduction

Most of the polymeric membranes are adversely affected by extremely acidic (pH≤2) conditions. Acid-resistant membranes are needed for the recovery of nano/microparticles and various applications in metal (Qin et al., 2005; Gonzalez-Munoz et al., 2006), mining (Hayryne et al., 2009; Ricci et al., 2015), electroplating (Boricha and Murthy, 2009), paper (Manttari and Nystrom, 2004; Manttari et al., 2006) industries and bio-refineries (Koschuh et al., 2005; Weinwurm et al., 2015). Among these applications, nano/microparticle recovery is attractive but highly challenging due to difficulty in preventing the permanent attachment of the particles on the membrane surface. The production of nano/microparticles in powder form is often required to lower the cost for storage and transport and for improving the stability of the particles. Previously, membranes were used for the short-term filtration of metallic nanoparticles, but the filtration medium was water, and the main objective was improving the efficiency of the recovery process for small scale separations (Gaborski et al., 2010; Mudalige et al., 2015; Meisterjahn et al., 2016; Alele et al., 2016; Van Goethem et al., 2018). So far, the application of membranes for separation of particles from extremely acidic synthesis environment has not been reported. This is due to the lack of membranes with sufficient performance. Research efforts on developing acid-resistant membranes were mostly focused on the NF category (Liu et al., 2012; Zeng et al., 2018; He et al., 2019; Hoseinpour et al., 2016). Unfortunately, NF membranes are not the best choice for

---

This chapter has been published as:
Gungormus, E., Alsoy Altınkaya S., 2020. A high-performance acid-resistant polyaniline based ultrafiltration membrane: Application in the production of aluminium sulfate powder from alumina sol. Chemical Engineering Journal, 389, 124393.

the recovery of nano/microparticles due to their low permeabilities. UF membranes are more economical alternatives than NF membranes since they can be operated at lower pressures. In addition to the energy cost, the overall cost of recovering particles with membranes is also determined by the cost of the membrane polymer. Semicrystalline polymers such as polytetrafluoroethylene (PTFE), polyethylene (PE), polyvinylidene fluoride (PVDF), poly (ether ether ketone) (PEEK), ethylene chlorotrifluoroethylene (ECTFE), chlorinated polyvinyl chloride (CPVC), and perfluoroalkoxy alkane (PFA) are known to be acid-resistant (Yeerken et al., 2019; Zhang et al., 2013; Peng et al., 2012; Park et al., 2018; da Silva Burgal et al., 2015; McKeen, 2016; Ebnesajjad, 2003). However, the usage of these polymers is limited to small scale membrane production due to high raw material costs. Also, their extreme hydrophobicities result in low-flux membranes with a high fouling tendency. The review of current studies then clearly indicated that efficient and cost-effective acid-resistant UF membranes are needed.

This study aims to fill the gap in the literature regarding the development of acid-resistant UF membranes. PANI was chosen as a membrane polymer since it can be synthesized using low-cost monomers and easily doped by protonic acids (Shen et al., 2018) to impart acid resistance. Besides, it has high thermal and chemical stability and a hydrophilic structure (Boeva et al., 2014). The performance of this membrane was tested through filtration of aluminium sulfate particles (alumina sol) synthesized in an extremely acidic H_2SO_4 solution. The separation of particles from the acid solution is required for both controlling the size, size distribution of the particles and for obtaining powder. Traditionally, aluminium sulfate powder is produced by freeze-drying, spray-drying, and conventional drying of alumina sol in an oven at different temperatures and pressures (Ponthieu et al., 1997; Varma et al., 1994). However, the production method solely utilizing drying has serious disadvantages. First, drying times are typically long due to low solid content in the sol. This causes both very high energy usage and a reduction in the service life of the dryers due to corrosion. Second, Van der Waals forces and Brownian motion can cause agglomeration in a conventional drying process (Kwon and Messing et al., 1997; Rahman et al., 2008; Frey and Halloran, 1984). This is certainly undesirable since the powder with a narrow size distribution is required for applications. Third, a significant amount of acid loss occurs during drying which is not only an economic loss but has also a negative impact on the environment. Membrane filtration prior to drying can help to minimize these disadvantages. However, to scale up the use of membranes for concentrating the sol from the acid solution, they should have long-term

acid resistance and antifouling properties. This study focused on both of these challenges. In this context, the acid resistance of the developed membrane was evaluated by determining the change in chemical structure, surface morphology, elemental compositions, and pore size of the membrane upon long-term exposure to H_2SO_4 acid solution. The fouling tendency of the membrane was evaluated through following flux change during alumina sol filtration and comparing the pure water fluxes of the clean and backwashed membranes after sol filtration. In addition, the impact of membrane filtration on the chemical and physical properties of the aluminium sulfate powder was investigated. In light of the literature, the novelty of this study lies in three points. First, it proposes a new acid-resistant PANI based UF membrane which can easily be obtained through a simple acid doping process. Second, it is shown for the first time that acid-doped PANI membrane can be used for the recovery of aluminium sulfate particles from extremely acidic synthesis environment without the permanent attachment of particles on the surface. Third, this study is the first which demonstrates the production of aluminium sulfate powder from the sol through membrane filtration without using a dryer.

2.2. Materials and Methods

2.2.1. Materials

Aniline (Sigma-Aldrich, ACS reagent, ≥99.50% purity), ammonium persulfate ($(NH_4)_2S_2O_8$, Sigma-Aldrich, ACS reagent, ≥98% purity), HCl fuming 37% (Merck), 25% ammonia solution (NH_4OH, Merck), and methanol (Sigma-Aldrich, ACS reagent, ≥99.80% purity) were utilized to synthesize PANI. Commercial EB (average Mw~ 100,000) was supplied from Sigma Aldrich. Triethylamine (Riedel-de Haën) and N-methyl-2-pyrrolidone (NMP, Merck, anhydrous, greater than 99.5%) were used to prepare casting solution. PEG 1000, 4000, 6000, 10000, and 20000 Da provided by Sigma Aldrich were used to determine *MWCO*. H_2SO_4 (≥98% purity) used in membrane doping process and alumina sol synthesis and aluminum isopropoxide (≥98% purity) used in the preparation of alumina sol were all purchased from Sigma-Aldrich.

2.2.2. Synthesis of the Emeraldine Base (EB) Form of PANI

EB is the most extensively studied form of PANI due to having higher environmental stability compared to other forms. PANI was synthesized through chemical oxidative polymerization of aniline in a medium of HCl aqueous solution by using $(NH_4)_2S_2O_8$ as an oxidizing agent. Aniline and $(NH_4)_2S_2O_8$ were separately dissolved in 1 M HCl solution and their concentrations were adjusted to 10% (v/v) and 5% (w/v), respectively. The prepared solutions were cooled to 0°C, then the oxidant solution was added dropwise to aniline solution under constant stirring. The polymerization reaction was carried out first at 0°C for 4 h to limit secondary reactions and then at 25°C for 20 hr. At the end of the reaction, the color of the mixture turned from transparent to dark green, and a solid deposit was formed. The deposit was filtered and rinsed first with 1 M HCl solution and next with deionized water (DI). The washing process was continued until the pH of the washing solution became 7. The filtered emeraldine hydrochloride precipitate was treated with 1 M NH_4OH solution for 3 h to obtain EB, rinsed with DI water until the pH of DI water was reached and finally washed with water: methanol mixture and then filtered. The dark blue EB powder was dried for 48 h under vacuum. The general procedure for EB synthesis was adapted from the studies conducted by Gomes and Oliveira, 2012 and Ibrahim, 2017.

2.2.3. Preparation of the EB and H_2SO_4 Doped Emeraldine Salt (ES) Membranes

The synthesized EB was dried at 70°C for 4 h to remove moisture. NMP was mixed with gel inhibitor trimethylamine, next EB was gradually added, and the mixture was stirred continuously for 1 h at 300 rpm (T=25°C). The concentrations of EB, trimethylamine, and NMP in the solution were adjusted to 15 wt.%, 1.50 wt.%, and 83.50 wt.%, respectively. In order to eliminate air bubbles, the solution was held without stirring for 1 h, and then cast on a polyester nonwoven fabric (Type TH, Hirose Paper Mfg. Co. Ltd.) with the help of an automated film applicator (Sheen Instrument Ltd., model number: 1133N) and finally immediately immersed into water bath at 20°C. The initial thickness of the cast membrane was adjusted as 200 µm. This membrane was first compacted at 2 bar until reaching steady-state condition, then, doped by filtering 0.27 M

H_2SO_4 aqueous solution (pH=0.55) at 2 bar for 3 h. These prepared un-doped and acid doped membranes will be referred to as the EB and H_2SO_4 doped ES membranes, respectively. The doping time of 3 h was enough to achieve a constant flux.

2.2.4. Performance Tests of the EB and H_2SO_4 Doped ES Membranes

A dead-end cell filtration system with a cell volume of 10 mL and an effective surface area (A) of 4.10 cm^2 (Millipore, Amicon Stirred Cell 8010) was used in performance tests of the membranes. The prepared membranes were compacted until reaching steady state conditions, then the volume of permeated water (ΔV) was recorded for every one minute (Δt) at a constant transmembrane pressure difference (ΔP) of 1 bar. Pure water permeability (PWP, $Lm^{-2}hr^{-1}bar^{-1}$) of the membranes was calculated by using Eq.2.1.

$$PWP = \frac{\Delta V}{A \times \Delta t \times \Delta P} \tag{2.1}$$

The rejection properties of the membranes were tested with aqueous solutions of PEG (1 g/L) with a molecular weight of 1000, 4000, 6000, 10000, and 20000 Da, separately. The PEG solutions were filtered at 1 bar under a constant stirring rate of 200 rpm, and the concentrations of feed (C_F), retentate (C_R), and permeate (C_P) solutions were detected by using Rudolph-J357 Automatic Refractometer. The rejection levels (R, %) were calculated from

$$R(\%) = \left(1 - \frac{C_P}{0.5 \times (C_F + C_R)}\right) \times 100 \tag{2.2}$$

The feed concentration in the module (C_f) changes with time due to the decrease in volume and increase in amount rejected by the membrane. In order to take the change in concentration on the feed side into account, an arithmetic average of the concentrations measured at the beginning (C_f) and at the end of the rejection experiment (C_r) were used (Luo et al., 2010).

2.2.5. Characterization of the EB and H_2SO_4 Doped ES Membranes

Pore size of the membrane was predicted from the rejection data collected using PEG solutions. For uncharged solutes, at high pore Peclet number, the rejection of a solute is given by the following equations by assuming that pores in the membrane are cylindrical (Combe et al., 1999; Bowen and Doneva, 2000):

$$R_{\lim} = 1 - \Phi K_{i,c} \tag{2.3}$$

$$\Phi = (1-\lambda)^2 \tag{2.4}$$

$$K_{i,c} = (2-\Phi)(1 + 0.054\lambda - 0.988\lambda^2 + 0.441\lambda^3) \tag{2.5}$$

$$\lambda = \frac{r_s}{r_p} \tag{2.6}$$

where ϕ, $K_{i,c}$, r_s, and r_p are the steric partition coefficient, the hindrance factor for convection, the solute and pore radii (in nm), respectively. The radius of PEG was predicted from Eq. 2.7 which was derived from Stokes-Einstein law by assuming PEG as a spherical particle.

$$r_s = 0.045 \times MW^{0.44} \tag{2.7}$$

where the unit of molecular weight (*MW*) is Da.

The chemical structure of the dried membranes was determined with Attenuated Total Reflectance Fourier Transformed Infrared Spectrometer (ATR-FTIR, Perkin Elmer) at ambient temperature over a scanning range of 650–4000 cm^{-1} with a resolution of 4.00 cm^{-1}. The surface and bulk morphology of the membranes was observed with the scanning electron microscope (SEM) (FEI Quanta 250 FEG) and elemental compositions on the surface were determined with energy dispersive X-ray analysis (EDX). The membranes were fractured in liquid nitrogen and sputter-coated with gold to obtain a clear cross-section. The surface roughness of the membranes was determined with atomic force microscopy (AFM, MMSPM Nanoscope 8 Bruker) by taking topographic images of 2 μm×2 μm sized dried membrane surfaces at a rate of 1 Hz. Zeta potential values of the membranes in 10 mM NaCl solution were measured by NanoPlus Micromeritics Instrument. NaCl solution was adjusted to five different pH level in the range of 3-11, by using HCl and NaOH for acidic and basic pH, respectively. Membrane hydrophilicity was characterized by measuring dynamic contact angles of the dried membrane (Attension Optical tensiometer) with 5 μl of the deionized water droplet.

2.2.6. Acid Resistance of the H_2SO_4 Doped ES Membrane

The dense surface of the H_2SO_4 doped ES membrane was exposed to a 0.27 M H_2SO_4 solution for one month at room temperature. The *PWP* and PEG 6000 rejection of the membrane were measured before and after acid exposure (exposure to acid solution). In addition, the chemical structure, surface morphology, and elemental compositions of the fresh and acid-exposed membranes were investigated by using ATR-FTIR, SEM, and EDX analyses.

2.2.7. Preparation of Alumina Sol and Determination of its Particle Size Distribution

Alumina sol was synthesized using the procedure given in the study of Yoldas, 1975. Deionized water at 85°C and aluminum isopropoxide was mixed and stirred for 1 h at 85°C. H_2SO_4 was added to the mixture (aluminum isopropoxide: H_2SO_4: water 1g: 0.65ml: 10.25ml), stirred again for 1 h at the same temperature and finally, a clear sol was formed. The prepared alumina sol was kept at room temperature for 1 day before further use. The particle size distribution of the sol was determined using DI water as a solvent (NanoPlus Micromeritics).

2.2.8. Alumina Sol Filtration Performance of the H_2SO_4 Doped ES Membrane

The alumina sol was filtered through H_2SO_4 doped ES membrane at 1 bar under a constant stirring rate of 200 rpm until the volume of the sol was reduced to 20% of the feed solution. Experiments started with the measurement of *PWP* of the membrane. After filtering 40 ml of the sol, the membrane (A = 4.10 cm^2) was backwashed with water for 30 minutes and the *PWP* was re-measured to evaluate the extent of flux recovery. This cycle was repeated for 4 times and 80% volume reduction of the sol was achieved in 5 cycles. The recovery of the alumina sol (*Rec.*) was calculated from Eq.2.8 by measuring the mass of dried feed (W_F), retentate (W_R), permeate (W_P) and backwashing (W_B) solutions.

$$\mathrm{Re}c(\%) = \left(\frac{W_R + W_B}{W_F} \right) \times 100 \tag{2.8}$$

Flux recovery ratios (*FRR*), reversible fouling (R_r) and irreversible fouling (R_{ir}) resistances were calculated by using the following equations.

$$FRR(\%) = \frac{J_R}{J_W} \times 100 \tag{2.9}$$

$$R_r(\%) = \frac{J_R - J_P}{J_W} \times 100 \tag{2.10}$$

$$R_{ir}(\%) = \frac{J_W - J_R}{J_W} \times 100 \tag{2.11}$$

where J_W and J_R are the pure water fluxes of the clean and backwashed membranes after sol filtration, respectively, while J_P is the flux of alumina sol.

2.2.9. Preparation and Characterization of Powder Obtained with and without Filtration of Alumina Sol

After filtering 80 % of alumina sol, concentrated particles were converted into powder form simply by drying at room temperature without using a dryer. For a comparison, alumina sol was also dried in a freeze dryer and in an oven at 100°C without applying filtration. Drying continued until reaching a constant weight of powder. The shapes of powders were observed by SEM (FEI Quanta 250 FEG), while the particle size distribution was determined with NanoPlus Micromeritics Instrument by dispersing the powder in deionized water. Each measurement was made in triplicate to ensure repeatability. The crystal structure of the powders was characterized by X-ray diffractometer (XRD, Philips X'pert Pro Diffractometer – operated at 40 kV, 45 mA) with Ni-filtered CuKα radiation ($\lambda = 0.15406$ nm) in the range of 5–80° 2θ angle. The crystalline phases in powders were identified using Powder Diffraction File of International Centre for Diffraction Data, 2000.

2.3. Results and Discussion

2.3.1. Characterization of the EB and H_2SO_4 Doped ES Membranes

Figure 2.1 shows that the IR spectra of the synthesized and commercial EB polymers are equivalent which proved the success of polymer synthesis. For EB in the form of polymer and membrane, the typical peaks located at 1600 and 1500 cm^{-1} are respectively assigned to the stretching vibration of nitrogen quinoid and benzenoid (Dognani et al., 2019), as shown in Figure 2.1.a-c. The band at 1300 cm^{-1} also originated from the C-N stretch of a secondary amine group. The aromatic C–H in-plane bending modes were observed in the region of 1010-1170 cm^{-1} (Wang et al., 2019c; Trchová et al., 2004; Huang et al., 2015). H_2SO_4 doping caused shifting in the peaks of the quinoid, benzenoid, and the secondary amine to 1563, 1480, and 1291 cm^{-1}, respectively (Figure 2.1.d). This indicates the quinone and benzene ring-stretching deformations, due to the protonation of the nitrogen of amine and imine groups in the EB chain (Trchová et al., 2004; Blinova et al., 2007). The peaks at 1200, 1147, and 1054 cm^{-1} are assigned to C–N^+ stretching vibration, –NH^+= stretching vibration, and S=O bonds which are formed during protonation of EB with H_2SO_4. The aromatic C–H in-plane vibration and out-of-plane vibration are also observed in the range of 1010-1170 cm^{-1} and 807-881 cm^{-1}, respectively. These peaks overlap a broad absorption extending from 850 to 1200 cm^{-1}. The appearance of the specific peaks exhibiting chemical bonds of EB and H_2SO_4 doped ES membranes approves the successful EB membrane synthesis and effective acid doping process to the EB membrane.

The elemental composition of the membrane surfaces obtained from EDX analysis is shown in Figure 2.2. Compared to the pristine EB membrane, the presence of sulfur and oxygen in the modified membrane also proved successful H_2SO_4 doping. SEM-EDX mapping images demonstrated a homogeneous distribution of sulfur and oxygen on the surface. Cross-section SEM images shown in Figure 2.3 illustrate that both doped and un-doped membranes have typical finger-like pores in the sublayer along with a thin dense active layer on top of the porous support layer. Acid doping did not significantly change the bulk morphology of the membrane, on the other hand, the surface morphologies were affected by doping. The AFM images in Figure 2.4 show that the H_2SO_4 doped ES membrane has a relatively rough surface with a plating structure while

the pristine EB membrane demonstrates a comparatively uniform ridge-and-valley morphology. The roughness parameters (R_a and R_q) after the H_2SO_4 doping process increased from 2.67 nm and 3.36 nm to 5.35 nm and 6.61 nm, respectively.

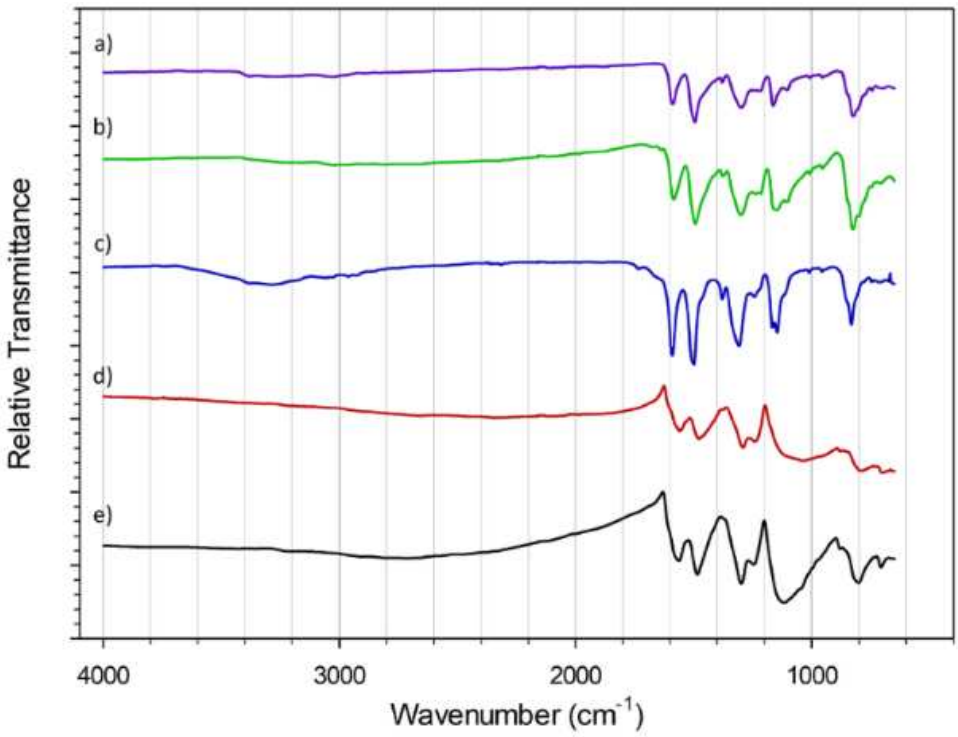

Figure 2.1. ATR-FTIR spectra of a) synthesized and b) commercial EB in the form of polymer, c) EB membrane, d) H_2SO_4 doped ES membrane and e) H_2SO_4 doped ES membrane after 30 days of H_2SO_4 exposure under static conditions.

EB and H_2SO_4 doped ES membranes display an opposite trend in their charge densities as a function of pH (Figure 2.5). This can be explained by the self-doping/dedoping mechanism of the PANI as shown in Scheme 2.1. At low pH values, the EB membrane has a relatively larger amount of amino and imino-functional groups, hence higher charge density. H_2SO_4 doping protonates the amine and imine groups, resulting in positively charged nitrogen (Kang and Neoh, 1998). On the other hand, negatively charged counter-ion, HSO_4^-, bind ionically to the positively charged nitrogen (Kang et al., 1990) resulting in electroneutrality of the polymer backbone. At basic pH values, ES membrane deprotonates due to the removal of H_2SO_4 from the polymer backbone by OH groups. This resulted in an increase in the positive charge density. EB form of PANI is blue in color while protonation of EB form results in the green ES form (Ogoshi et al., 2011). As shown in Figure 2.5, the color of the H_2SO_4 doped ES membrane changed from green at pH 3 to blue at pH 11 which simply confirmed the dedoping of ES

membrane at basic pH. The results in Figure 2.5 suggest that the H_2SO_4 doped ES membrane is not suitable for treatments in basic environments.

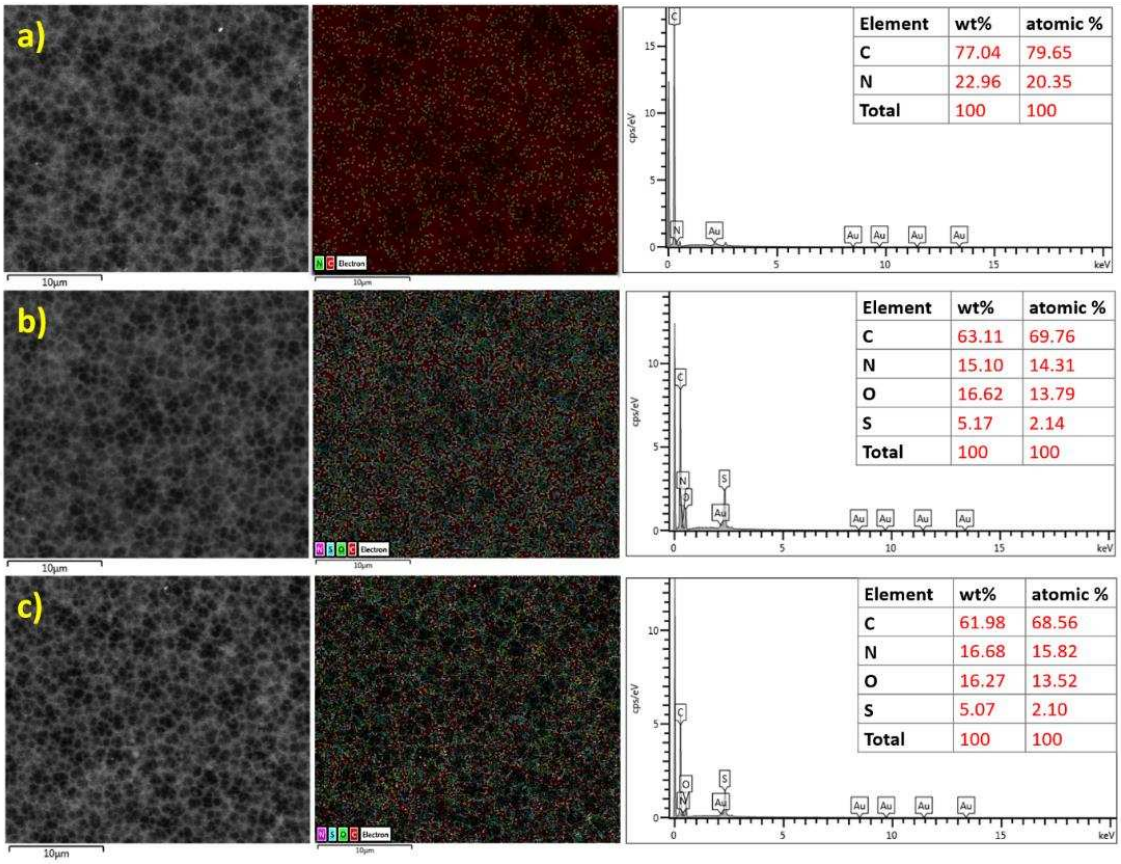

Figure 2.2. SEM-EDX elemental analysis and mapping of a) EB membrane, b) H_2SO_4 doped ES membrane, and c) H_2SO_4 doped ES membrane after 30 days of H_2SO_4 exposure under static conditions.

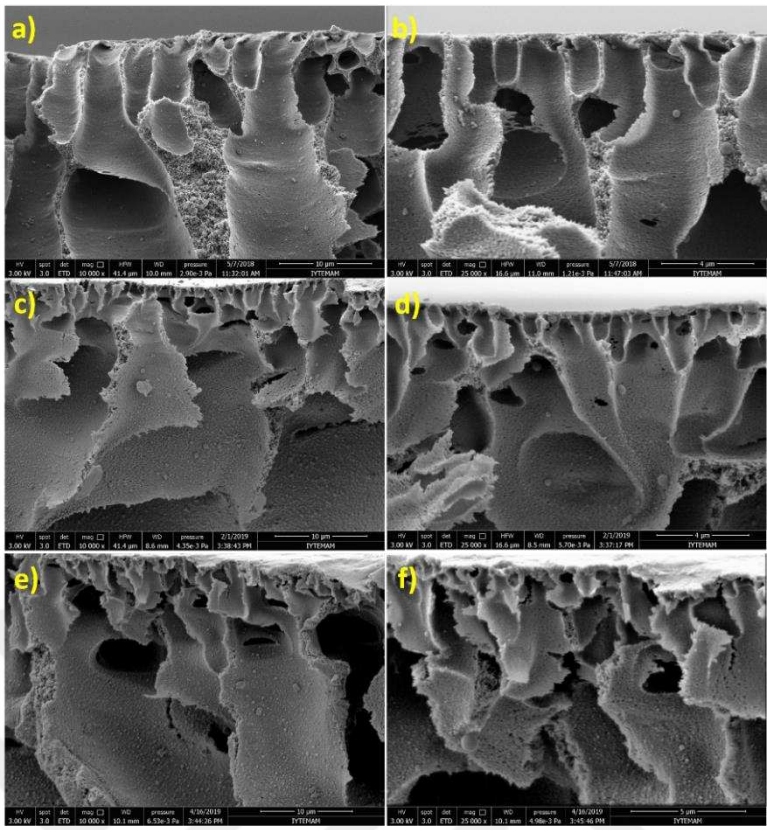

Figure 2.3. Cross-section SEM images of a-b) EB membrane, c-d) H_2SO_4 doped ES membrane and e-f) H_2SO_4 doped ES membrane after 30 days of H_2SO_4 exposure under static conditions with a magnification of ×10000 and ×25000, respectively.

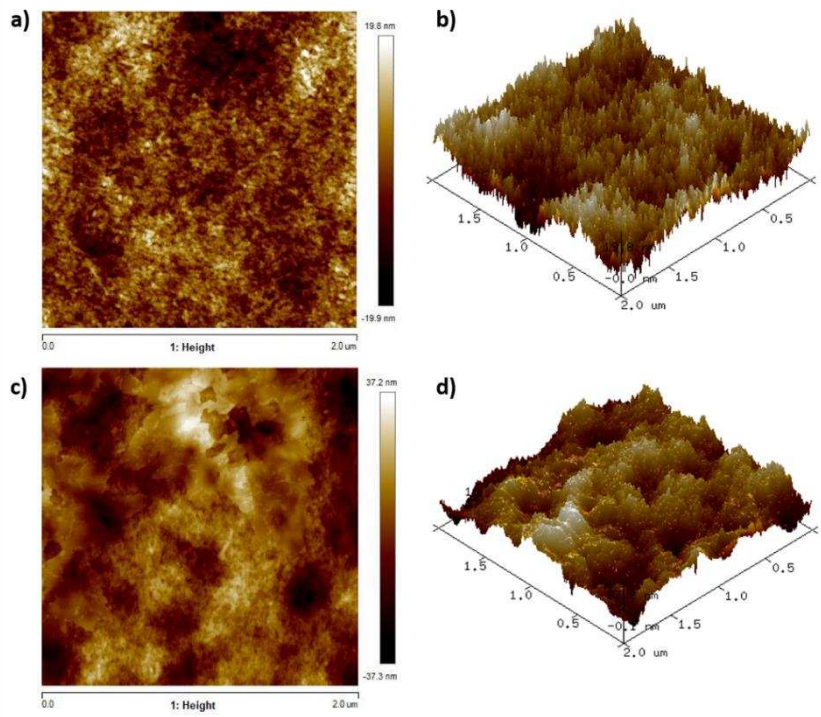

Figure 2.4. AFM images of a-b) EB membrane and c-d) H_2SO_4 doped ES membrane.

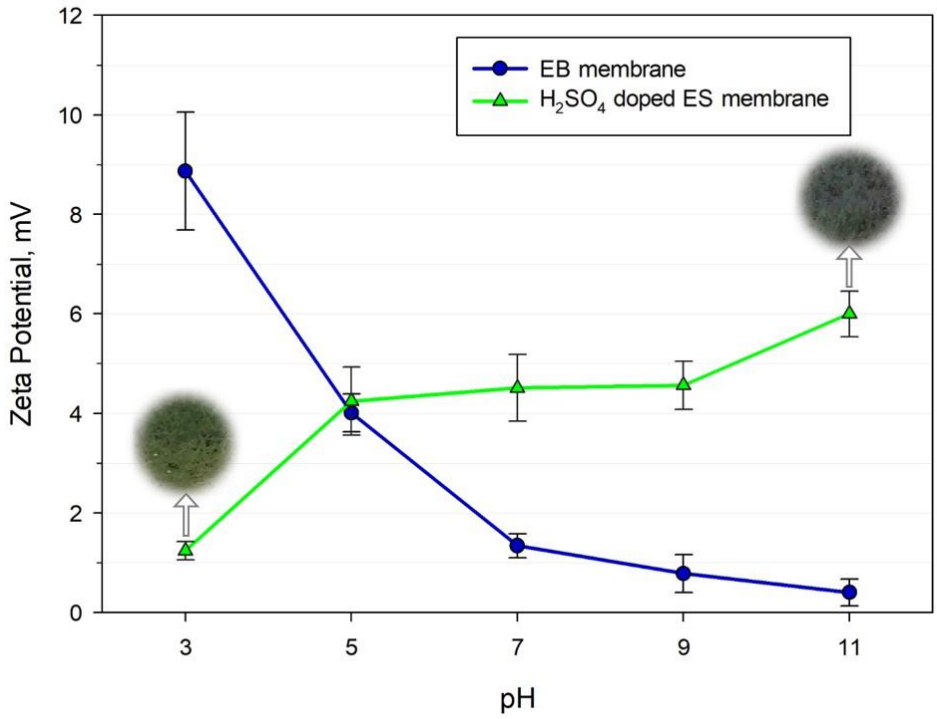

Figure 2.5. Zeta potential of EB and H_2SO_4 doped ES membranes as a function of pH.

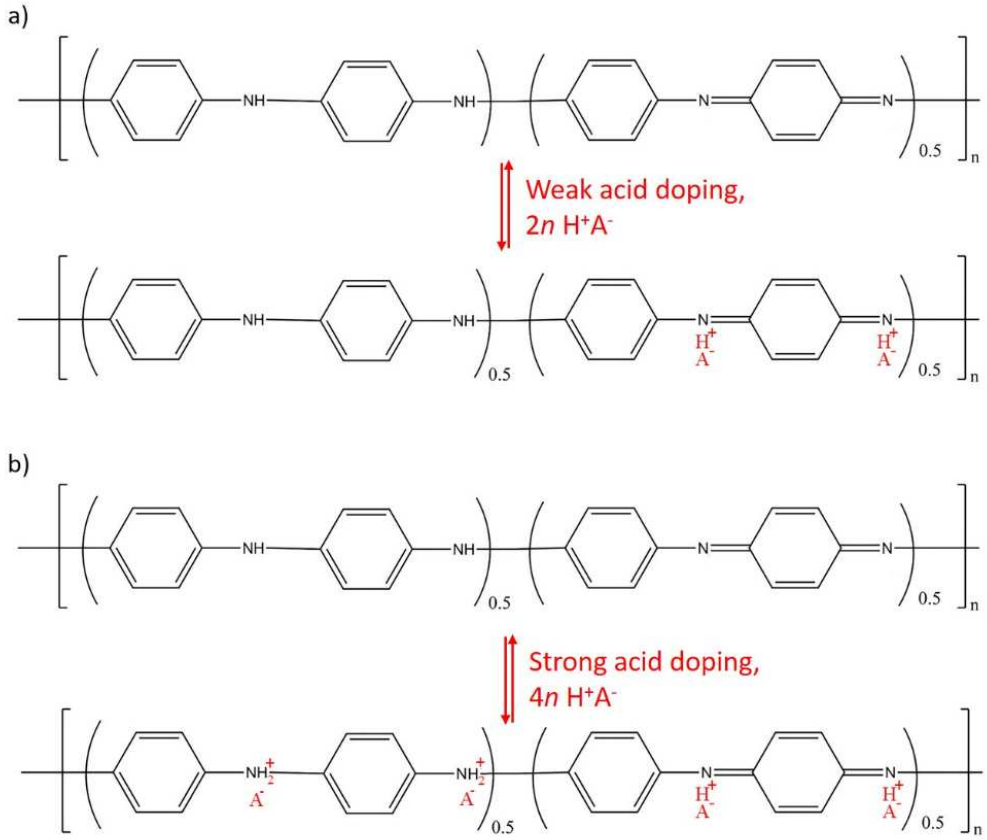

Scheme 2.1. Rearrangement reaction mechanism between the EB and ES polymers through a) weak protonic acid b) strong protonic acid doping and dedoping in alkaline medium. A^- is an anion of the protonic acid.

The contact angle value of the EB membrane decreased from 76.22°±0.85° to 64.75°±2.40° upon H_2SO_4 doping. The increment of hydrophilicity was due to the hydrophilic sulfonic functional groups of the dopant. Similarly, Liu et al., 1994 and Blinova et al., 2008 reported an improvement in the hydrophilicity of EB polymer in the presence of doped ions.

Acid doping reduced the *PWP*, *MWCO*, and pore radius of the EB membrane from 97.57±1.53 $Lm^{-2}hr^{-1}bar^{-1}$, 7500 Da, and 3.13 nm to 25.47±0.06 $Lm^{-2}hr^{-1}bar^{-1}$, 6750 Da, and 2.75 nm, respectively. Slight decreases in the *MWCO* and pore size of the membrane were other evidence of successful acid doping. The acid doping occurred not only on the membrane surface but also in the bulk of the membrane since H_2SO_4 can easily penetrate the pores. The decrease in the *PWP* after acid doping can be attributed to pore narrowing within a region near the surface. The proposed mechanism for pore size reduction due to H_2SO_4 doping is shown in Scheme 2.2.

2.3.2. Stability of the H_2SO_4 Doped ES Membrane

The stability of the H_2SO_4 doped ES membrane was evaluated by comparing the permeability, rejection, surface, bulk morphology, and the chemical structure of the membrane before and after 30 days of H_2SO_4 exposure under static conditions. The chemical structures of the fresh and acid–exposed ES membrane were found the same as shown in the ATR-FTIR spectra in Figure 2.1.d and 2.1.e. Quantitative analysis of SEM-EDX mapping images showed that mass and atomic fractions of O and S elements and their uniform distribution on the surface almost unchanged after acid exposure (Figure 2.2.b and 2.2.c). In addition, the bulk morphologies of the acid-exposed ES membrane and its fresh counter-part were observed to be similar (Figure 2.3.c-2.3.f). Furthermore, no changes were measured in the *PWP* and PEG 6000 rejection of the doped membrane after long-term acid exposure.

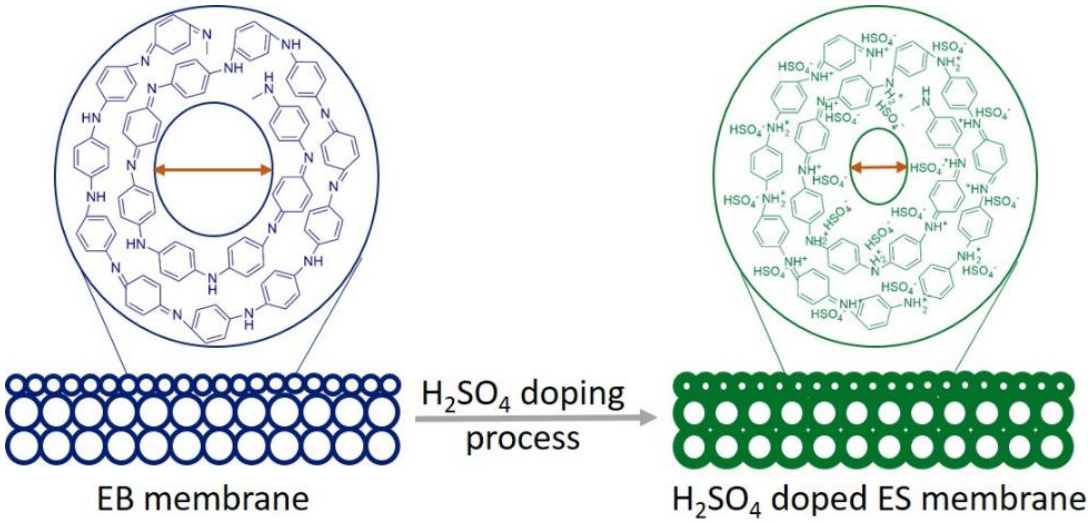

Scheme 2.2. Proposed mechanism for pore size reduction in the bulk of the membrane due to H_2SO_4 doping.

Table 2.1 compares the long-term H_2SO_4 stability of membranes prepared from different polymers (Liu et al., 2012; Zeng et al., 2018; He et al., 2019; Hoseinpour et al., 2016; Ricci et al., 2017; Platt et al., 2004; Wang et al., 2019a; Zhu et al., 2020). Except the poly(2,5-benzimidazole) based membrane (*MWCO*: 6 kDa) which is in the UF category (Lohokare et al., 2018), all other membranes tested are in NF range. In the tests, storage time in acid solution ranged from 24 h up to 4 months while the acid concentration was between 0.1 M and 2 M. Exposure to the H_2SO_4 concentration higher than 1 M resulted in a significant change in the permeability and rejection properties of the membranes. When the H_2SO_4 concentration was less than 1 M, the doped PANI membrane prepared in our study demonstrated the best performance. Although the commercial NF membrane, MPF-34, was exposed to a significantly lower H_2SO_4 concentration than that used in our study, its magnesium and nickel rejections decreased by 27 % while *PWP* increased by a factor of 3 (Ricci et al., 2017). Degradation of the MPF-34 was also shown with SEM and AFM analysis and contact angle measurement.

EB could be easily doped by various organic and inorganic acids. The localized sigma bond in amine groups ($-NH_2^+-$) along the EB backbone forms a strong chemical bond, while the less strongly localized pi bond in imine groups ($-NH^+=$) provides a weaker chemical bond (Rimbu et al., 2006). The strengths of the acid and the amine and imine groups in the EB chain determine the ability of the interaction between EB and proton of acid (Hatchett et al., 1999). The acid dissociation constants (pKa) for the amine and imine groups in the EB chain were reported as 2.50 and 5.50, respectively (Menardo

et al., 1988). As shown in Scheme 2.3, H_2SO_4 protonates both amine and imine groups in the EB chain since it is a strong acid (pKa=1.92). Protonation equilibria in the H_2SO_4 doped ES membrane are influenced by the presence of counterions and change in the pH of the feed solution. When pH becomes higher than the pKa of amine and imine groups, the deprotonation of these groups occur and ES membrane returns to EB form. This is a major limitation and restricts the use of H_2SO_4 doped ES membrane in a basic pH environment. If the membrane is exposed to a different type of acid solution, the displacement of the anion, HSO_4^-, in the polymer backbone ($R\text{-}HSO_4^-$) with counter anion in solution (X^-) is expected to take place through following ion exchange reaction (Endo et al., 2001).

$$R - HSO_4^- + X^- \leftrightarrow R - X^- + HSO_4^-$$

The EB membrane was doped with the same acid and at the same pH used in the synthesis of alumina sol. Therefore, the performance of the resulting H_2SO_4 doped ES membrane did not change during acidic alumina sol filtration or after 1-month storage in the H_2SO_4 solution (Scheme 2.3).

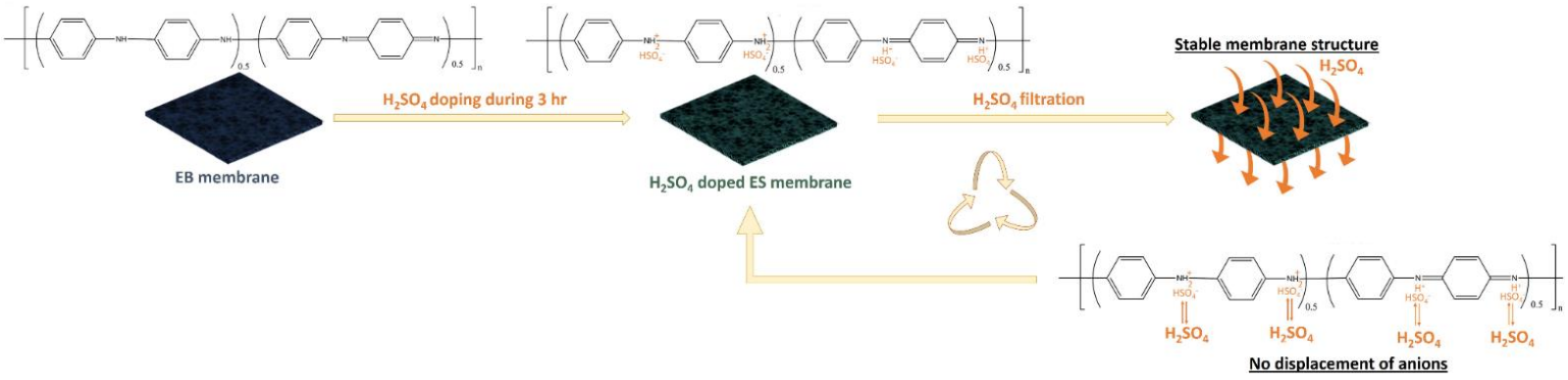

Scheme 2.3. Acid resistance mechanism of the H_2SO_4 doped ES membrane

Table 2.1. H_2SO_4 stability of different polymeric membranes

Membrane	Membrane Chemistry	Storage time and temperature	Molarity of H_2SO_4 solution	Permeability increment ($Lm^{-2}hr^{-1}bar^{-1}$)	Rejection decline	Ref.
BPT-NF-1-006	Melamine polyamine with polyether sulphone support membrane	30 days, 80°C	2.04	1.7-3.9 to 23.2-27.3	83-91.5% to 28.5-30.4% for sucrose in water 75-88% to 14.9-19.8% for glucose in water	Platt et al. (2004)
		2 months, 80°C		1.7-3.9 to 60.8-65	83-91.5% to 8.6-12.9% for sucrose in water 75-88% to 8-8.9% for glucose in water	
		30 days, 20°C		1.7-3.9 to 3-3.2	83-91.5% to 81.5-82% for sucrose in water 75-88% to 77.7-82% for glucose in water	
		4 months, 20°C		1.7-3.9 to 3-3.1	83-91.5% to 85.2-86 for sucrose in water 75-88% to 82-82.8% for glucose in water	
		30 days, 20°C	1.22	2.22 to 2.3	96% to 95% for sucrose in water 92% to 90% for glucose in water	
		3 months, 20°C		2.22 to 4.3	96% to 90% for sucrose in water 92% to 82% for glucose in water	

(Cont. on next page)

Table 2.1. (Cont.)

Membrane	Membrane Chemistry	Storage time and temperature	Molarity of H_2SO_4 solution	Permeability increment ($Lm^{-2}hr^{-1}bar^{-1}$)	Rejection decline	Ref.
BPT-NF-2-015	Melamine polyamine with polyether sulphone support membrane	30 days, 80°C	2.04	1.8-4.9 to 41.3-54.6	88-97% to 8.1-16.2% for sucrose in water 78-93% to 6.2-9.8% for glucose in water	Platt et al. (2004)
		2 months, 80°C		1.8-4.9 to 85.8-129	88-97% to 6.1-9.9% for sucrose in water 78-93% to 1.6-5.9% for glucose in water	
		30 days, 20°C		1.8-4.9 to 4.7-4.8	88-97% to 90.8-92.9% for sucrose in water 78-93% to 82.7-87.5% for glucose in water	
		4 months, 20°C		1.8-4.9 to 5.3-5.4	88-97% to 82.2-83% for sucrose in water 78-93% to 70.2% for glucose in water	
PIP-NTSC	Piperazine-naphthalene-1,3,6-trisulfonylchloride composite	2 months, 25°C	2.04	5.72 to 6.5	~90% to 86% for Na_2SO_4 in water	Liu et al. (2012)
PIP-PA	Piperazine-polyamide	24 hr, 55°C	1.02	~1.44 to –[a,b]	~72% to –[b] for $MgSO_4$ in water	Hoseinpour et al. (2016)
MPD-PA	M-phenylenediamine-polyamide			~1.18 to –[a,b]	~96% to –[b] for $MgSO_4$in water	
PIP-PASA	Piperazine-poly(amide-sulfonamide)			~2.24 to 6.6[a]	~68% to 32 for $MgSO_4$ in water	
MPD-PASA	M-phenylenediamine-poly(amide-Sulfonamide)			~1.82 to 9.4[a]	~70% to 20 for $MgSO_4$ in water	
PIP-PSA	Piperazine-Polysulfonamide			~2.6 to 2.8[a]	~46% to 44 for $MgSO_4$ in water	
MPD-PSA	M-phenylenediamine-Polysulfonamide			~1.56 to 1.8[a]	~32% to 25 for $MgSO_4$ in water	
MPF-34	Proprietary composite	4 weeks, 20°C	0.15	3.1 to 13.3	97% to 70% for $MgSO_4$ in water 97% to 84% for $CoSO_4$ in water 98% to 71% for $NiSO_4$ in water	Ricci et al. (2017)
MPF-34	Proprietary composite	8 weeks, 20°C			97% to 19% for $MgSO_4$ in water 97% to 19% for $CoSO_4$ in water 98% to 33% for $NiSO_4$ in water	

(Cont. on next page)

Table 2.1. (Cont.)

Membrane	Membrane Chemistry	Storage time and temperature	Molarity of H_2SO_4 solution	Permeability increment ($Lm^{-2}hr^{-1}bar^{-1}$)	Rejection decline	Reference
TPT-TMC/PSf	1,3,5-(tris-piperazine)-triazine- trimesoyl Chloride/Polysulfone	30 days, 25±1°C	0.05	~8 to 12	97% to ~92% for $MgSO_4$ in water	Zeng et al. (2018)
PIP-TMC/PSf	Piperazine- trimesoyl Chloride/Polysulfone			7.11 to 15.16	95% to 62% for $MgSO_4$ in water	
PES-PSA5	Polyethersulphone-polysulfonamide	24 hr, 90°C	2.04	3.03 to 5.49	99.81% to 95.92% for Na_2SO_4 in water	He et al. (2019)
Control IP	2,4,6-tris(chlorosulfonyl)phenol- piperazine			1.49 to 3.21	98.31% to 95.97% for Na_2SO_4 in water	
TMC-PIP	Trimesoyl Chloride- piperazine			9.23 to 23.55	99.16% to 28.49% for Na_2SO_4 in water	
NF270	Polyamide			11.64 to 50.04	99.42% to 4.36% for Na_2SO_4 in water	
M1	Poly(2,5-benzimidazole)-polypropylene	24 hr, 20°C	12.5	8.2 ± 1.2 to 10.14	-	Lohokare et al. (2018)
M6				15.1± 1.5 to 20.55		
NF6	Polysulfonamide	30 days, 21°C	2.04	6.8 to 7.6	92% to 88% for $MgCl_2$ in water	Wang et al. (2019a)
PSA-PSF	Polysulfonamide-polysulfone	24 hr, 25±5°C	0.82	~0.5 to 0.48	~86% to 87 for Na_2SO_4 in water	Zhu et al. (2020)
PSA/SPEEK-PSF	Polysulfonamide/sulfonated poly(ether ether ketone)-polysulfone			~2.5 to 4.2	~89% to 88 for Na_2SO_4 in water	
SPEEK-PSF	sulfonated poly(ether ether ketone)-polysulfone			~3.2 to 7	~88% to 75 for Na_2SO_4 in water	
H_2SO_4 doped ES membrane	ES	30 days, 20±1°C	0.27	25.47±0.06 to 25.59±0.07	87.78±0.38% to 87.92±0.29% for PEG 6000 in water	This study

2.3.3. Alumina Sol Filtration Performance of the H_2SO_4 Doped ES Membrane

The H_2SO_4 doped ES membrane was used to concentrate alumina sol by filtering the H_2SO_4 aqueous solution in sol. Figure 2.6 shows the change in flux during 5-cycle sol filtration. The pure water and alumina sol fluxes measured as 25.47±0.06 L/m^{2}h and 15.75 L/m^{2}h at the end of the first cycle decreased to 22.22±0.03 L/m^{2}h and 14.87 L/m^{2}h when 5-cycle filtration was completed. In each cycle, the alumina sol flux decreased rapidly in a short period due to the accumulation of particles on the membrane surface. However, most of the flux was recovered after backwashing the membrane with water for 30 minutes. Backwashing after 5 h filtration (first cycle) resulted in a 96% flux recovery. The recovery decreased to 87% at the end of the fifth cycle as a result of a gradual increase in irreversible fouling from 4.0% up to 12.70% (Figure 2.7). High flux recoveries were observed since the fouling due to accumulation of particles on the surface was mostly reversible.

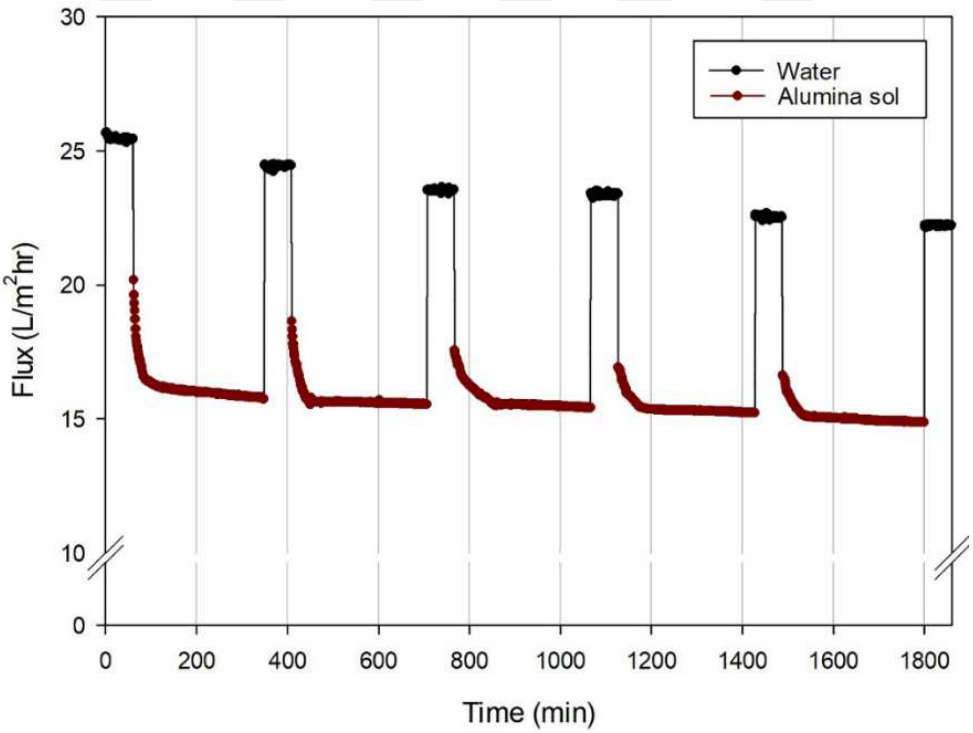

Figure 2.6. Performance of H_2SO_4 doped ES membrane during 5-cycle alumina sol filtration.

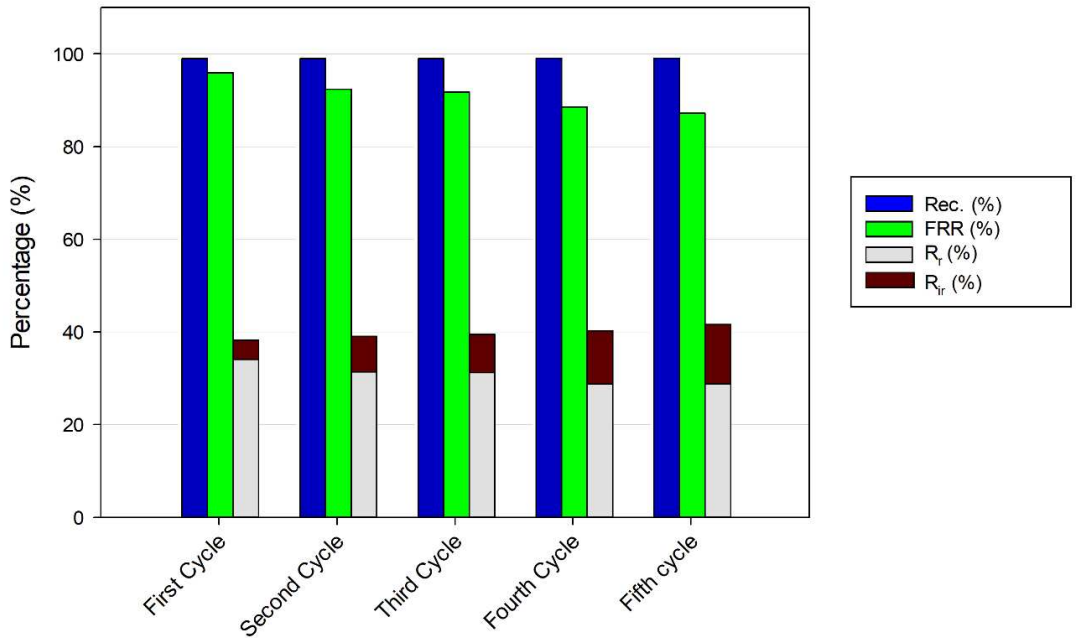

Figure 2.7. Flux recovery, irreversible and reversible fouling ratios, and alumina sol recoveries for each cycle during filtration of alumina sol.

Figure 2.7 demonstrates that 99% of the aluminium sulfate particles were recovered in the retentate stream. The pores on the surface were not clogged by aluminium sulfate particles. This was confirmed by measuring the PEG 6000 rejection at the beginning (87.78±0.38%) and at the end of 5th filtration cycle (89.41±0.15%). The results suggest that the H_2SO_4 doped ES membrane is a suitable acid-resistant membrane to concentrate alumina sol due to full recovery of particles, high flux restoration achieved after short-time backwashing with DI water and stable rejection performance at the end of 25 h filtration of extremely acidic alumina sol solution (pH=0.55).

The antifouling property of the H_2SO_4 doped ES membrane can be attributed to the hydrophilicity, surface roughness and net-zero charge of the surface at the filtration pH. The effects of roughness on membrane fouling can vary depending on the interplay between the size of foulant particulates and roughness of the surface (Bai et al., 2020). As shown in AFM images (Figure 2.4), the ES membrane does not contain large valleys on its surface. The roughness of the membrane is very low compared to the size of the particles and the surface does not have a morphology that can entrap the particles. The hydrophilic charged groups on the polymer backbone create a hydration layer on the surface (Liu et al., 2019a; Zhu et al., 2017), which acts as a physical and energy barrier and prevents the accumulation of the particles. From a thermodynamic point of view, a large amount of energy is needed to break this hydration layer (He et al., 2016). The

H_2SO_4 doped ES membrane contains both positively and negatively charged groups (Scheme 2.4) and has a neutral charge at the filtration pH (Figure 2.5). The negatively charged HSO_4^- and the positively charged nitrogen are closely connected through an ionic bond. This bonding simply avoids interaction of the charged particles with the membrane surface, as shown in Scheme 2.4. In summary, the antifouling mechanism of the H_2SO_4 doped ES membrane can be explained by the formation of a hydration layer on the surface and steric hindrance effect of the charged groups, as well as a relatively smooth surface morphology.

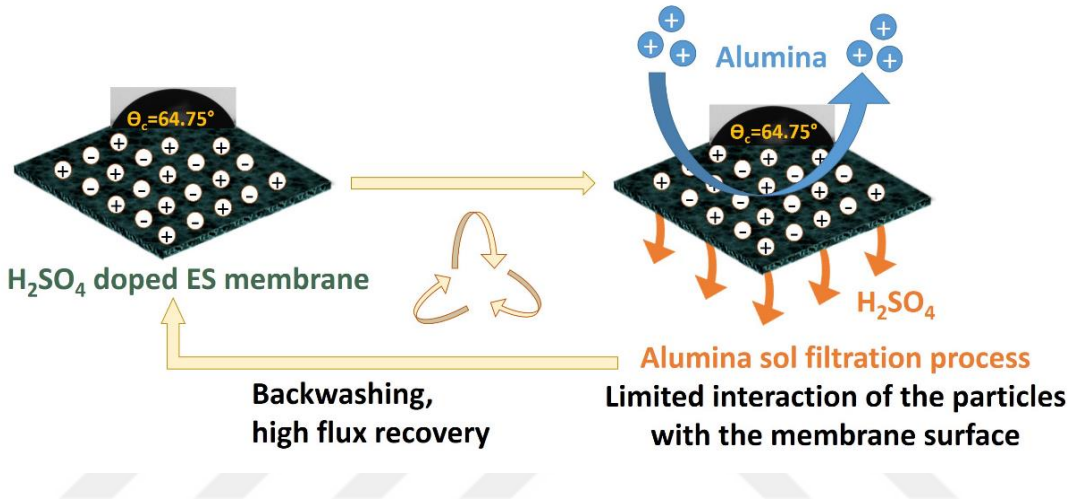

Scheme 2.4. Antifouling mechanism of the H_2SO_4 doped ES membrane

2.3.4. The Effect of Membrane Filtration on the Chemical and Physical Properties of the Aluminium Sulfate Powder

To evaluate the influence of membrane filtration on the chemical and physical properties of aluminium sulfate powder, the particle size distribution, morphology, and crystalline structures of the powder were determined. After filtering 80 % of the H_2SO_4 solution, the concentrated particles were dried at room temperature without using a dryer.

The mean particle diameter of virgin alumina sol was measured as 1494±201 nm while its polydispersity index (PDI) was 0.495 (Figure 2.8). The membrane filtration did not change the size and size distribution of the particles (1211±62 nm, PDI: 0.386). If no filtration was applied, the drying time of the sol at room temperature extended from 24 h to 72 h. Also, larger-sized particles (2102±181 nm with a PDI value of 0.386) were obtained due to their continuous growth during drying of a large volume. For comparison

purposes, the powder was also obtained with two additional classical drying techniques without applying filtration, namely, freeze-drying and oven drying at 100°C. Compared to the membrane filtration usage, the powder produced with freeze-drying had similar size distribution (1760±79 nm, PDI: 0.476) but drying was completed in a longer time (48 h). At 100 °C, the sol was dried in 24 h, however, resulting powder had a larger size and broad size distribution (22040±2785 nm and PDI: 22.42). Agglomeration of the particles is enhanced at high temperatures due to the combined effects of Van der Waals forces and Brownian motion (Kwon and Messing et al., 1997; Rahman et al., 2008; Frey and Halloran, 1984).

SEM images of the powder produced by membrane filtration and traditional drying techniques are shown in Figure 2.9. The powder obtained with membrane filtration did not include any aggregates and had a fairly smooth appearance (Figure 2.9.a and 2.9.b). A similar morphology was also observed for the powder dried at room temperature without applying any filtration (Figure 2.9.c and 2.9.d). Freeze-drying of the sol resulted in a rough structure of fiber layers (Figure 2.9.g and 2.9.h) while drying in an oven at 100°C caused interwoven short and stacked fine, needle-like aggregate formation (Figure 2.9.e and 2.9.f).

XRD patterns shown in Figure 2.10 demonstrate that the crystalline structure of the powder dried at room temperature was not deteriorated due to filtration. Except for the powder dried at 100°C, all the samples contained alunogen ($Al_2(SO_4)_3.17H_2O$) which is simple aluminium sulfate, including very high-water content. Two intense XRD peaks were observed at 2θ values of ~6.60° and 19.90°, followed by ~26.60° and 29.60°. Freeze-drying reduced the crystallinity of the powder as confirmed by the decrease in the intensity of XRD peaks while oven drying at 100°C caused even disappearance of the specific XRD peaks at 2θ values of ~26.60° and 29.60°.

Table 2.2 demonstrates that membrane filtration can significantly reduce the energy cost of powder production (0.095 $/gram) compared to the cost of traditional drying-based techniques. When operating the filtration unit, energy is needed only in pressurizing the feed using nitrogen. Membrane filtration allows recovering most of the acid and this has also a positive impact both on the cost of production and the environment. The characterization results demonstrated that membrane filtration usage allowed producing aluminium sulfate powder with the most desirable structural features at the lowest energy cost. Filtration of the sol not only reduces drying time but also

prevents agglomeration of particles and maintains crystalline structure. These structural properties, in turn, are required for many applications such as the production of high-quality ceramics to obtain uniform particle packing and fully dense materials.

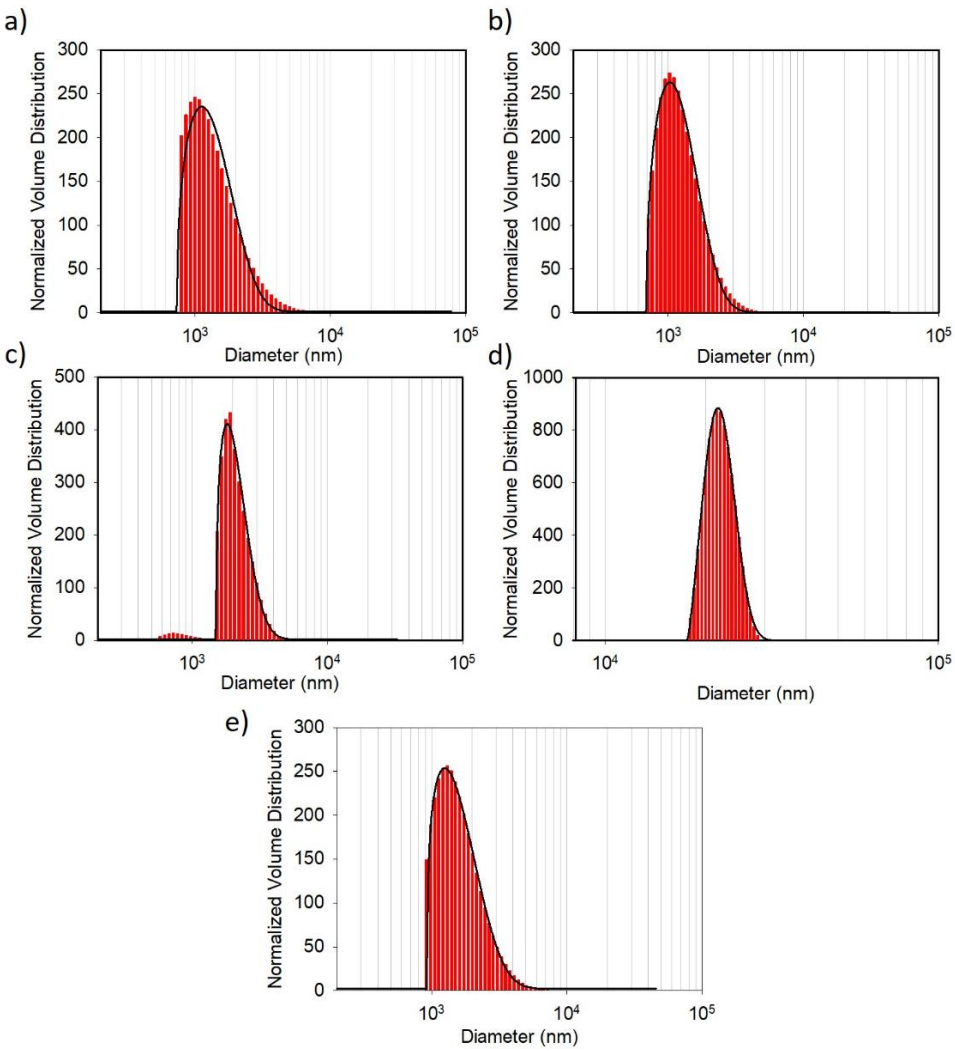

Figure 2.8. Particle size distributions of a) the prepared alumina sol and powder dried b) at 25°C after filtering 80 % of sol, c) at 25°C without filtration, d) at 100°C in an oven without filtration, e) in a freeze dryer without filtration.

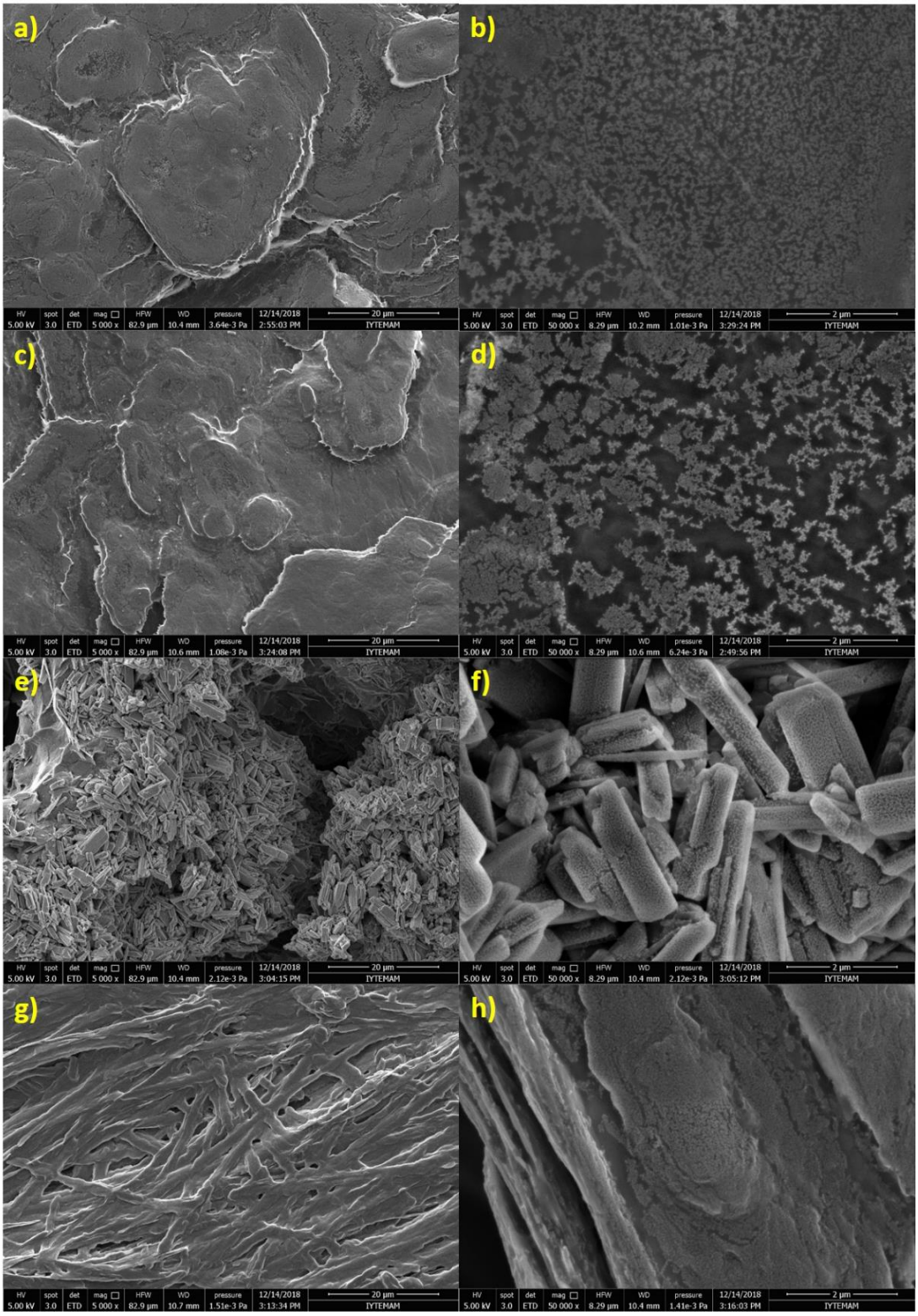

Figure 2.9. SEM images of the powders dried a-b) at 25°C after filtering 80 % of sol, c-d) at 25°C without filtration, e-f) at 100°C in an oven without filtration, g-h) in a freeze dryer without filtration. Magnifications are ×5000 and ×50000, respectively.

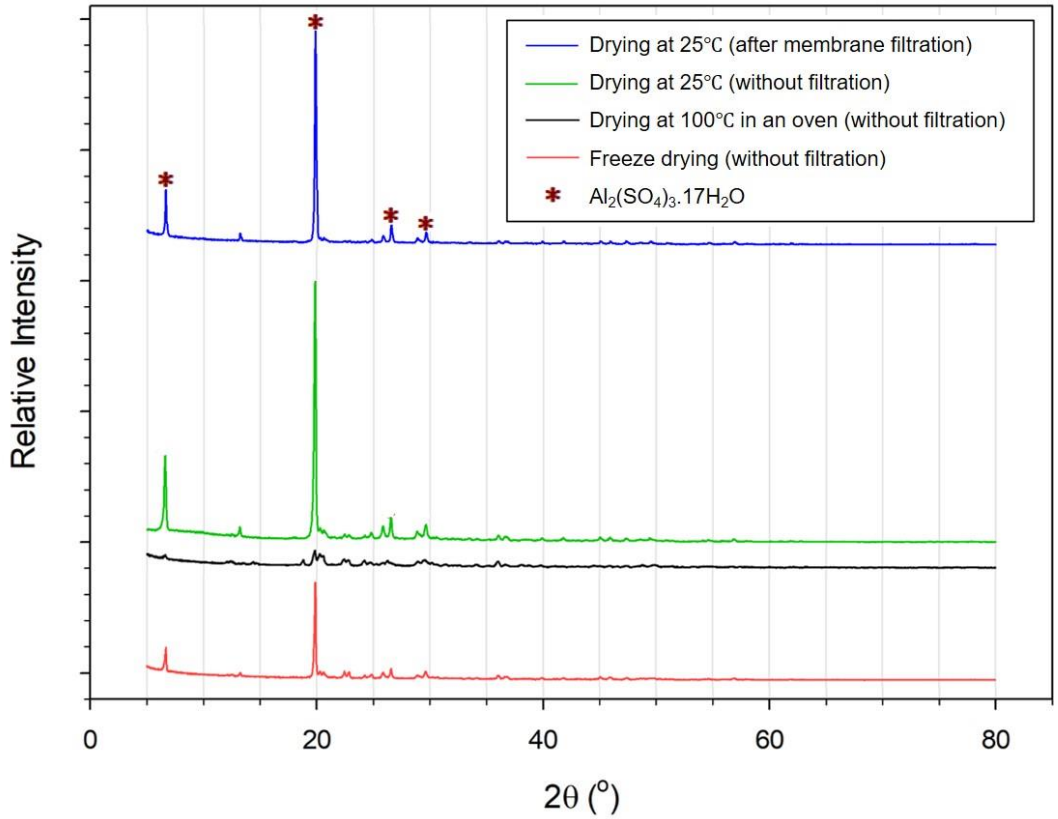

Figure 2.10. XRD patterns of the aluminium sulfate powders prepared with membrane filtration and traditional drying methods

Table 2.2. Comparison of energy cost of powder production with membrane filtration and solely drying-based techniques

Drying Method	**Drying Period**	**Energy Cost ($/g)**
Drying at 25°C (after filtering 80 % of sol in 25 h)	24 h	0.095
Drying at 25°C (without filtration)	72 h	-
Freeze-drying (without filtration)	48 h	0.958
Drying at 100°C in an oven (without filtration)	24 h	0.477

2.4. Conclusion

The self-acid doping ability of PANI is a facile approach to prepare acid-resistant membranes from this polymer. The acid doping procedure proposed in this study is a simple method and can be easily adapted in commercial membrane fabrication processes. The H_2SO_4 doped PANI membrane preserved its chemical structure and separation performance after 30 days of exposure to the H_2SO_4 solution under static conditions. In order to obtain long-term acid resistance, the membrane should be doped with the acid in the feed solution and the pH of the dopant should be the same as the pH of feed solution. The H_2SO_4 doped membrane was successfully used in concentrating the alumina sol synthesized in the H_2SO_4 solution. Almost 100% of the particles were recovered in the retentate stream and flux loss during filtration was mostly recovered through simple backwashing with water. Concentrating the sol through filtration minimized the risk of uncontrolled particle growth. The concentrated particles were converted into powder form in 24 h simply by drying at room temperature without using a dryer. The features such as long-term acid stability, high particle recovery, low fouling tendency, and low materials and processing costs make acid doped PANI membrane a potential candidate in the production of aluminium sulfate powder from alumina sol. On the other hand, the membrane can also be used in numerous other applications for the treatment of acid-containing feeds.

CHAPTER 3

A NEW-GENERATION POLY (ETHER IMIDE SULFONE) BASED SOLVENT RESISTANT ULTRAFILTRATION MEMBRANE FOR A SUSTAINABLE PRODUCTION OF SILICA NANOPOWDER

3.1. Introduction

Nanoparticles provide unprecedented opportunities to address global challenges in water purification, clean energy technologies, greenhouse gas management, materials supply/ utilization, green manufacturing, and chemistry (Diallo et al., 2013). The sol-gel process allows highly porous nanomaterials synthesis using low temperature and relatively mild conditions (Meng, 2012). In this process, a colloidal solution and a solid gel state are formed in an organic solvent via a sol-gel transformation. The main challenge is the removal of large solvent volumes to produce powder-form nanoparticles, which many applications require. Supercritical drying, freeze-drying, and conventional oven-drying are standard techniques used to obtain nanopowder. Supercritical drying involves hazardous high pressures, while freeze drying encounters technical difficulties due to the low freezing temperature of alcohols, and conventional oven drying carries a risk of particle aggregation. The common disadvantages inherent in these drying-based methods are their greenhouse gas emission due to electricity and fossil fuel usage. Additionally, solvent, catalyst emissions, and water loss negatively impact the environment. Organic solvents lost during drying are usually recycled and reused using the distillation process. However, distillation is thermally driven and requires high energy input. Consequently, there is a demand for an energy-efficient nanopowder manufacturing process with a low-carbon footprint and environmental impact.

This chapter has been published as:
Gungormus, E., Alsoy Altınkaya S., 2023. A new-generation poly (ether imide sulfone) based solvent resistant ultrafiltration membrane for a sustainable production of silica nanopowder. Separation and Purification Technology, 304, 122351.

The integration of membrane technology into conventional nanopowder production can bring important advantages. First, the energy consumption required for drying is significantly decreased by reducing the suspension volume through continuous filtration. Second, the solvent, catalyst, and water are recovered without requiring phase change; thus, production with a lower greenhouse gas emission, raw material cost, and environmental impact is possible. Third, the agglomeration potential of the nanoparticles is minimized by reducing particle-particle interaction through volume reduction of solvent (Rahman et al., 2008). The nanoparticles can be recovered using pressure-driven (UF) and centrifugal force-driven (centrifugal filtration) membrane technologies, depending on the driving force. Centrifugal filtration systems have a quick filtration function compared to pressure-driven membrane separation processes (Hangzhou Cobetter Filtration Equipment Co Ltd, 2022); however, their technical design still needs to be improved (Hangzhou Cobetter Filtration Equipment Co Ltd, 2022; Bonhomme et al., 2013). Additionally, the price of these units is high, and the need to replace the centrifugal filter unit before each operation (Miilipore Corporation, 2022) increases the cost and negatively affects the environment and sustainability of the production due to the frequent disposal of used units. The pressure-driven dead-end cell filtration systems have a relatively simple design and can be easily operated and scaled up; furthermore, the membrane in the unit can be used for a long time. The heart of membrane-assisted nanopowder production technology is the membrane itself. The essential properties expected from an ideal membrane are high solvent resistance and low fouling tendency to maintain the membrane's separation ability for the long term and prevent/minimize the attachment of the particles on the membrane surface. Both properties extend the lifetime of the membrane. Another bottleneck for membrane-assisted nanopowder production is water used for washing the membrane to remove the particles and wastewater generated at the end of the washing process. Also, the discontinuity of the production to collect particles from the membrane surface can be recognized as an additional limitation of the membrane technology.

This work demonstrates the feasibility of using a membrane for sustainable nano-silica powder production. Currently, nano-silica powder has many applications in adhesives, food additives, sealants, paints, cosmetics, inks, fiber optic strands, polymers, coatings, and cement-based building materials (Hessien et al., 2009) due to its high pore volume, large specific surface area, high porosity, low refractive index and ultralow dielectric constant (Soleimani Dorcheh and Abbasi, 2008). The global nano-silica market

is expected to grow at a CAGR of 7.6% from 2016-2025 (GRV, 2017). Nano-sized silica can be recovered from the suspension using the membranes in the nanofiltration and ultrafiltration categories. Although both membranes satisfy pore size requirements, ultrafiltration processes require lower energy consumption. A large number of publications exist on OSN membranes (Hendrix et al., 2013; da Silva Burgal et al., 2015; Valtcheva et al., 2015; Falca et al., 2019; Feng et al., 2019; Karimi et al., 2020; Liang et al., 2020; Shinde et al., 2020; Zhang et al., 2019c; Fu et al., 2021) however, studies investigating solvent-resistant UF membranes (Kang et al., 2008; de Souza Araki et al., 2010; Jeon et al., 2012; Penha et al., 2015; Saxena et al., 2015; Lee et al., 2016; Ursino et al., 2016; Yang et al., 2019; Zhang et al., 2019a) are very limited. The selection of polymer plays a critical role in manufacturing solvent-resistant membranes. Hydrophilic polymers are prone to swelling during solvent exposure; thus, cross-linkers and high-temperature annealing are needed to overcome swelling and compaction effects (Asabi Tashvigha et al., 2018). Hydrophobic polymers, polytetrafluoroethylene, and polyethylene have high solvent resistance, but they cannot be processed with phase inversion techniques due to their insolubility in common solvents.

In this study, we have chosen poly (ether imide sulfone), commercially named EXTEM, as a membrane polymer because it can be dissolved in different solvents (Mazinani et al., 2017), and the (ether (-O-), isopropylidene ($-C(CH_3)_2-$), and sulfone (S=O) groups in the structure (Figure 3.1.a) provide superior resistance to chemicals, high thermal-oxidative stability, and good processability. In addition, EXTEM is a semicrystalline polymer, and crystalline domains in its structure (Kim and Nunes, 2017) prevent the chains' free rotation and the membrane's compression (Mallevialle et al., 1996). To date, EXTEM membranes have been tested for gas separation (Xia et al., 2010; Peng et al., 2010) and ultrafiltration applications (Jalal et al., 2014; Kim and Nunes, 2017; Mazinani et al., 2017), but their solvent resistance has not yet been demonstrated. We prepared the EXTEM membrane with the classical nonsolvent induced phase inversion method and modified it with TiO_2 nanoparticle adsorption to make surface antifouling and reduce pore size. We extensively compared membrane-assisted silica nanopowder production with freeze-drying and oven-drying methods in terms of particle size distribution and economic factors such as capital investment, operating costs, batch production times, and total energy consumption. The proof of concept demonstrated in the current study can also be applied to other nanopowder productions as long as a suitable membrane is available. To the best of our knowledge, this is the first study that developed

a solvent-resistant, antifouling, TiO_2 coated poly (ether imide sulfone) membrane and illustrated the benefits of integrating a membrane for a more sustainable silica nanopowder production.

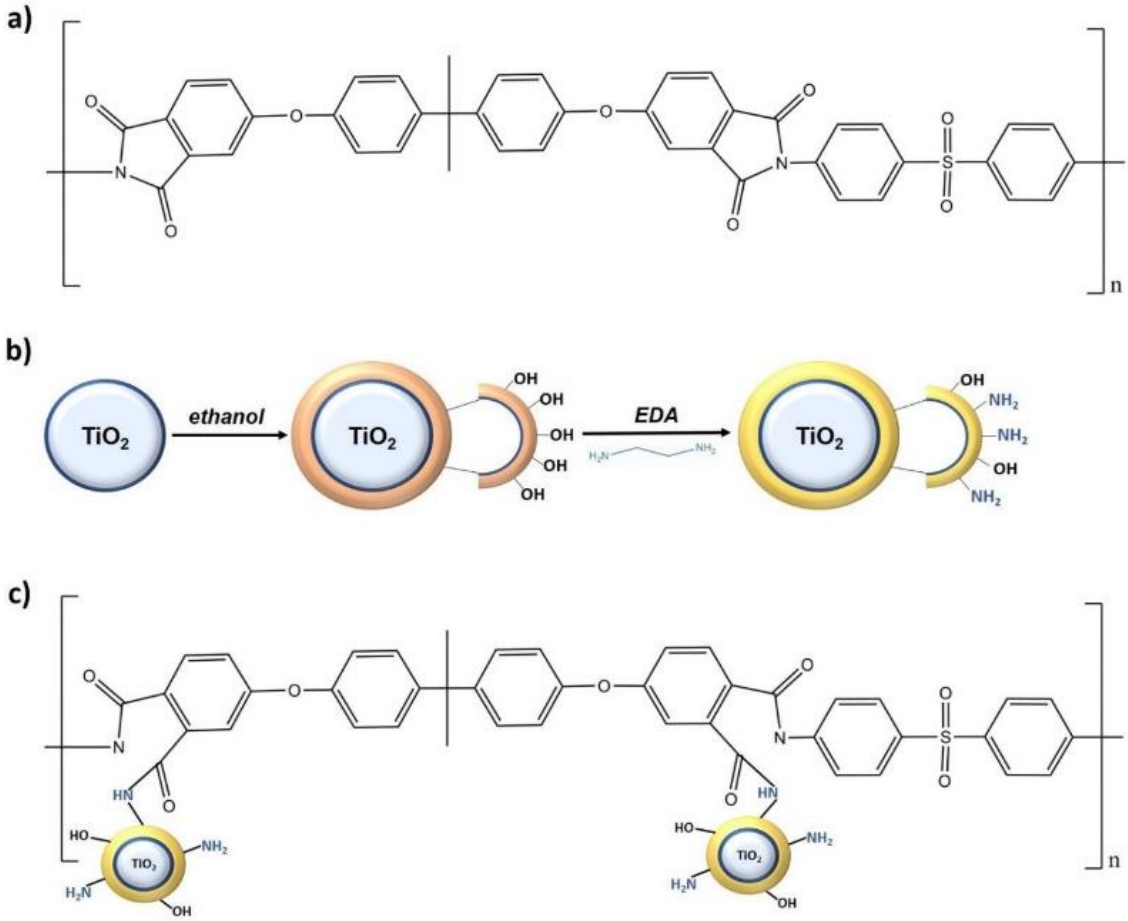

Figure 3.1. a) Chemical structure of poly (ether imide sulfone), b) amine functionalization of TiO_2 nanoparticles, and c) schematic illustration of the membrane modification by amine-functionalized TiO_2 nanoparticles

3.2. Materials and Methods

3.2.1. Materials

The chemicals used in the amine functionalization of TiO_2 nanoparticles were TiO_2 (Riedel, Reagent Grade, ≥99%), ethylenediamine (EDA, Alfa Aeser, 99% purity), and ethanol (EtOH, Merck, ≥99.9% purity). Poly (ether imide sulfone), Extem® XH1005, (Figure 3.1.a) was kindly supplied by SABIC. N, N-Dimethylformamide (DMF, Sigma-Aldrich, anhydrous, greater than 99.8%) was used to prepare casting solutions. PEG

10000, 20000, 35000, and 100000 Da provided by Sigma Aldrich were used for molecular weight cutoff (MWCO) measurements. Silica nanoparticles were synthesized by using TEOS (Fluka, 98% purity), ethanol (Merck, ≥99.9% purity), deionized water, and ammonia solution (NH_4OH, Merck).

3.2.2. Amine Functionalization of TiO_2 Nanoparticles

The TiO_2 nanoparticles were amine-functionalized to increase their stability on the membrane surface using the procedure adapted from Dehghani Kiadehi et al. (2014) (Figure 3.1.b). Briefly, 1 gr of TiO_2 particles was dispersed in 50 ml ethanol by sonication. EDA was added dropwise to the TiO_2 solution, and its concentration was adjusted to 0.3, 0.6, 0.9, and 1.5 M. The reaction was carried out at 65°C for 3 hours under constant stirring. The volatile part of the mixture was refluxed with a condenser, and the powder was washed with ethanol twice to remove any residual chemicals. The modified particles were dried for 24 h under vacuum. The prepared powders were denoted as 0.3 M EDA-TiO_2, 0.6 M EDA-TiO_2, 0.9 M EDA-TiO_2, and 1.5 M EDA-TiO_2. The chemical structure of the bare and amine-functionalized TiO_2 nanoparticles was determined with Attenuated Total Reflectance Fourier Transform Infrared Spectrometer (ATR-FTIR, Perkin Elmer) at ambient temperature over a scanning range of 425-4000 cm^{-1} with a resolution of 4.00 cm^{-1}. Optimum EDA concentration was selected based on the nanoparticles' zeta potentials and particle size distributions (NanoPlus Micromeritics Instrument).

3.2.3. Preparation of Pristine and Amine-functionalized TiO_2 Coated Poly (ether imide sulfone) Membranes

Membranes were prepared by nonsolvent induced phase inversion technique. The poly (ether imide sulfone) was first dried at 175°C for 3 h to remove moisture and then dissolved (17 wt%) in DMF. The mixture was stirred continuously for 24 h at 25°C and waited for another 24 h without stirring to eliminate air bubbles. The solution was spread on a polyethylene terephthalate nonwoven fabric (Type 2413 Novatexx, Freudenberg Filtration Technologies India Pvt. Ltd.) with the help of an automated film applicator (Sheen Instrument Ltd., model number: 1133N), followed by immediate immersion into

a water bath at 25°C. The initial wet thickness of the cast membrane was adjusted to 250 μm. The membrane was compacted at 2 bar until reaching steady-state condition before coating with amine-functionalized TiO_2 nanoparticles. The active membrane surface was contacted with the fresh nanoparticle solution at different temperatures (25°C, 50°C, 70°C, and 90°C), and the contact times (30, 60, and 90 min). The concentration of the nanoparticles was adjusted to 0.3, 0.5, and 0.8 wt% in water. Schematic illustration of the membrane modification by amine-functionalized TiO_2 nanoparticles is shown in Figure 3.1.c.

3.2.4. Performance Tests of Pristine and Amine-functionalized TiO_2 Coated Poly (ether imide sulfone) Membranes

The membranes' pure water permeability (PWP) was measured using a dead-end filtration (Sterlitech HP4750) stirred cell. The active membrane area was 14.6 cm^2, and the pressure was adjusted to 1 bar. The prepared membranes were first compacted until reaching steady-state conditions, then the PWP ($Lm^{-2}h^{-1}bar^{-1}$) was calculated from Eq. 3.1.

$$PWP = \frac{\Delta V}{A \times \Delta t \times \Delta P} \tag{3.1}$$

where ΔV (L) is the volume of permeated water, A (m^2) is the active membrane area, Δt (h) is permeation time, and ΔP (bar) is the transmembrane pressure difference.

MWCO values of the pristine and amine-functionalized TiO_2 coated membranes were determined by measuring the rejection of different PEGs (10000-100000 Da). PEG aqueous solutions (1 g/L) were filtered at 1 bar under a constant stirring rate of 300 rpm. The PEG concentrations in the feed and permeate were detected by using the Rudolph-J357 Automatic Refractometer, and rejection (R) was calculated by the following equation:

$$R(\%) = \left(1 - \frac{C_P}{0.5 \times (C_F + C_R)}\right) \times 100 \tag{3.2}$$

where C_F, C_R, and C_P are the concentrations of feed, retentate, and permeate solutions, respectively. All membrane performance tests were made at least in triplicate to ensure repeatability.

The pore size distribution of the membranes was estimated by using the most common form of the two-parameter log-normal distribution function with the assumptions of no interaction (steric and hydrodynamic) between the neutral PEG molecules and pores of the membranes (Atchariyawut et al., 2006; Liu et al., 2015; Cihanoğlu and Alsoy Altınkaya, 2020):

$$\frac{dR(r_p)}{dr_p} = \frac{1}{r_p \ln(\sigma_p)\sqrt{2\pi}} \exp\left[-\frac{1}{2}\left(\frac{\ln(r_p/\mu_p)}{\ln(\sigma_p)}\right)^2\right] \tag{3.3}$$

where the geometrical mean radius of the solute (μ_p) was obtained at R=50%, and the geometrical standard deviation of the solute (σ_p) was defined as the ratio of r_p of R=84.13% to that of R=50%. The radii of PEG and PEO were predicted from Eq. 3.4 and 3.5, respectively, which were derived from Stokes-Einstein law by assuming a spherical particle (Sing et al., 1998).

$$r_p = 16.73 \times 10^{-12} \times MW^{0.557} \tag{3.4}$$

$$r_p = 10.44 \times 10^{-12} \times MW^{0.587} \tag{3.5}$$

where the unit of molecular weight (MW) is Da.

3.2.5. Characterization of Pristine and Amine-functionalized TiO_2 Coated Poly (ether imide sulfone) Membranes

The chemical structure of the dried pristine and coated poly (ether imide sulfone) membranes was determined with ATR-FTIR (Perkin Elmer) at ambient temperature over the scanning range of 425-4000 cm^{-1} with a resolution of 4.00 cm^{-1}. Scanning electron microscope (SEM) (FEI Quanta 250 FEG) was used to observe the surface and bulk morphology of the membranes. Before taking images, the membranes were fractured in liquid nitrogen and sputter-coated with gold. The elemental composition changes on the membrane due to TiO_2 coating were determined with energy dispersive X-ray analysis (EDX). Atomic force microscopy (AFM, MMSPM Nanoscope 8 Bruker) was utilized to measure the surface roughness of the membranes. Topographic images were taken for 2 μm×2 μm sized dried membrane surfaces at a rate of 1 Hz. The zeta potential of the membrane surface was characterized by NanoPlus Micromeritics Instrument using NaCl

(10 mM) as the electrolyte. The pH of the solution was adjusted in the range of 3-9 with HCl and NaOH. The hydrophilicity of the membranes was evaluated by a water contact angle device (Attension Optical tensiometer) with 5 µl of the deionized water droplet. Thermogravimetric analysis (TGA) was carried out using a Setaram, Labsys, TG-DTA/DSC to determine the amount of TiO_2 coated to the membrane. The heating rate was adjusted to 10°C/min from 25°C to 800°C under the nitrogen atmosphere. Each measurement was repeated 3 times.

3.2.6. Synthesis and Characterization of Colloidal Silica Suspension

Silica nanoparticles were synthesized by the sol-gel process through the hydrolysis and condensation of TEOS in ethanol: water mixture using ammonia as a base catalyst (Rahman et al., 2007). Deionized water and ethanol were mixed to adjust ethanol concentration at 13, 38, and 50%, and the mixtures were sonified for 10 min at 50°C. Next, 1 mol/L of TEOS was added to the mixtures and sonified for 2 h at the same temperature. Finally, ammonia (2 mol/L) was added dropwise at a 0.03 mL/min flow rate and sonified again for 5 h at 50°C; then, colloidal silica suspension was obtained. NanoPlus Micromeritics Instrument determined the suspension's zeta potential and particle size distribution. Results were given in Supporting Information (Figure B.1 and B.2).

3.2.7. Filtration of Colloidal Silica Suspension through the Amine-functionalized TiO_2 Coated Poly (ether imide sulfone) Membrane

The 250 ml colloidal silica suspension was filtered at 1 bar under a constant stirring rate of 300 rpm via a dead-end filtration cell (Sterlitech HP4750, active membrane area: 14.6 cm^2) until the initial volume was reduced to 10%. Following filtration, the membrane was backwashed with water for 30 min, then PWP was re-measured, and this cycle was repeated 5 times. The silica nanoparticles in backwash solution were recovered through gravity-settling without energy. The masses of nanoparticles in feed (250 ml colloidal silica suspension) (W_F), in retentate (W_R), and settled from backwash solution (W_B) were determined by drying the solutions at room temperature. The antifouling

property of the membrane was evaluated by determining flux recovery ratio (FRR), reversible fouling (R_r), and irreversible fouling (R_{ir}) resistances, calculated in Eq. 3.6-3.8.

$$FRR(\%) = \frac{J_R}{J_W} \times 100 \tag{3.6}$$

$$R_r(\%) = \frac{J_R - J_P}{J_W} \times 100 \tag{3.7}$$

$$R_{ir}(\%) = \frac{J_W - J_R}{J_W} \times 100 \tag{3.8}$$

where J_W and J_R are the pure water fluxes of the clean and backwashed membranes after colloidal silica suspension filtration, respectively, while J_P is the flux of the suspension.

Recovery of the silica nanoparticles (Rec) was calculated by the following equation:

$$\text{Rec}\,(\%) = \left(\frac{W_R + W_B}{W_F}\right) \times 100 \tag{3.9}$$

where W_F, W_R, and W_B are the mass of silica nanoparticles in feed, retentate and separated from backwash solutions, respectively.

The chemical content of the permeate was determined by ATR-FTIR (Perkin Elmer) analysis at ambient temperature over a scanning range of 425-4000 cm^{-1} with a resolution of 4.00 cm^{-1}.

3.2.8. Stability of Amine-functionalized TiO_2 Coated Poly (ether imide sulfone) Membrane

The stability of the coated poly (ether imide sulfone) membrane was evaluated by measuring the amount of TiO_2 nanoparticles released into the water at the end of 1, 3, 7, 15, and 30 days of storage. The concentration of nanoparticles was determined by inductively coupled plasma optical emission spectrometry (ICP-OES, Agilent 5110). The PWP and PEG (10 kDa) rejection values of the stored membranes were also measured. Additionally, the change in the PWP and PEG rejection of the pristine and TiO_2 coated membranes before and after storing in 40% aqueous ethanol solution and nanoparticle synthesis solution consisting of ammonia: ethanol: water (1: 5.02: 9.36, v/v) was followed

up to 30 days. Furthermore, both storage media was analyzed with ICP to determine the leached nanoparticles at the end of 30 days. The results were reported as the % release calculated by dividing the amount released in the storage media x100 by the initial amount loaded to the membrane**.** The temperature during these experiments was 25°C.

3.2.9. Preparation and Characterization of Powder Obtained with and without Filtration of Colloidal Silica Suspension

After 90% volume reduction through filtration, the colloidal silica suspension was converted into powder form by drying at room temperature (25°C) without using an oven. The suspension was also freeze-dried and oven-dried at 80°C without reducing its volume by filtration. Samples were dried until reaching a constant weight of powder and calcined at 500°C for 2 h to remove impurities. The chemical structure of the nanoparticles was determined with Attenuated Total Reflectance Fourier Transform Infrared Spectrometer (ATR-FTIR, Perkin Elmer) at ambient temperature over a scanning range of 425-4000 cm^{-1} with a resolution of 4.00 cm^{-1}. The particle size distributions of the samples were determined by using NanoPlus Micromeritics Instrument.

3.3. Results and Discussion

3.3.1. Preparation of the Amine-functionalized TiO_2 Coated Poly (ether imide sulfone) Membranes

Membrane-assisted silica nanopowder production requires membrane development with high antifouling properties, solvent resistance, high negative surface charge, and suitable pore size and size distribution. Solvent resistance is needed for the long-term stability of the membrane. At the same time, antifouling property, negative surface charge, and right pore size are required to prevent the attachment of the particles to the surface and maximize the recovery of negatively charged silica nanoparticles from the suspension when filtered through the membrane. The poly (ether imide sulfone) has desirable structural features to make the membrane solvent resistant. The membranes from this polymer were cast on a polyester nonwoven fabric with a 250 µm wet thickness

by varying the polymer concentration from 15 to 17%. Only the membrane prepared at 17% polymer concentration exhibited 90% PEG 100 kDa rejection, but the pure water permeability was very low (19.82±0.63 $Lm^{-2}h^{-1}bar^{-1}$). Below 17%, polymer concentration was not enough to form a thin membrane layer on the nonwoven fabric. The nonwoven fabric type was changed to a more porous PET and casting 17% EXTEM (wet thickness:250 µm) on this fabric improved the PWP significantly (from 19.82±0.63 $Lm^{-2}h^{-1}bar^{-1}$ for polyester nonwoven to 70.23±0.65 $Lm^{-2}h^{-1}bar^{-1}$ for PET nonwoven) without compromising the PEG 100 kDa rejection (84.61%, Figure 3.2.a). The membrane, however, had a large pore size distribution (μ_p: 5.86 nm and σ_p:1.46 nm) ranging from 2.5 to 12.3 nm (Figure 3.2.b) and was not suitable for the full recovery of silica nanoparticles (size range: 8.15-16.70 nm). Increasing polymer concentration from 17% to 20% decreased the PWP to 5.51±0.76 $Lm^{-2}h^{-1}bar^{-1}$ without significantly reducing the surface pore size. Thus, it was decided to apply the surface modification to reduce the pore size, narrow pore size distribution, enhance the flux and make the membrane surface highly negatively charged. TiO_2 nanoparticles were selected for surface modification due to their strong chemical stability and hydrophilic nature (Fischer et al., 2018), and they were amine-functionalized to attach them to the surface covalently. The FTIR spectra of bare and modified samples were taken to prove the success of the functionalization. In addition to the typical peaks around 480 and 1620 cm^{-1} that belong to the Ti-O bending mode and deformative vibration of the Ti-OH stretching mode (Chougala et al., 2017) for TiO_2 nanoparticles (Figure B.3 and Figure B.4), new peaks at around 3200 and 3400 cm^{-1} after EDA modification confirmed -the NH groups' attachment to the TiO_2 nanoparticles. As illustrated in Figure 3.1.b, upon adding EDA, the -OH groups on the nanoparticle surface are replaced with $-NH_2$ groups. The effect of EDA concentration on amine functionalization was evaluated based on the surface charge and size of the modified nanoparticles. It was desired to make the membrane surface highly negatively charged and pore size smaller than the size of the silica nanoparticles upon attaching TiO_2 nanoparticles to the membrane surface. These features are needed to improve the membrane antifouling properties and maximize the recovery of negatively charged silica nanoparticles from the suspension when filtered through the membrane. The highest degree of functionalization was achieved with 0.6 M EDA, as confirmed by the largest peak area ratio for -NH to Ti-OH groups (Table B.1). Additionally, the amine functionalization with 0.6 M EDA resulted in the highest negative surface charge and the smallest increase in the particle size (bare: 50.9±2.90 nm, PDI=0.37; 0.6M-

EDA:60.23±2.80 nm, PDI=0.32) (Table B.2). On the other hand, modification with 1.5 M EDA increased particle size from 50.9±2.90 nm to 206±11 nm (PDI=0.46) and decreased the negative charge on the surface (bare: -34.82±0.95 mV and 1.5 M EDA: -26.64±0.66). Based on the results in Tables B.1 and B.2, 0.6 M EDA was chosen as optimum for the amine functionalization of TiO_2 nanoparticles.

The pristine EXTEM membrane was coated with modified TiO_2 nanoparticles by varying the nanoparticle concentration, coating time, and temperature. The coating time and temperature were changed between 20 and 90°C and 30 and 90 minutes. The PWP of the support increased from 70.23±0.65 $Lm^{-2}h^{-1}bar^{-1}$ to 76.71±1.25, 81.65±1.91, and 82.04±2.01 $Lm^{-2}h^{-1}bar^{-1}$, after coating the surface with 0.3, 0.5, and 0.8 wt% functionalized TiO_2 nanoparticles for 60 min at 70°C, respectively. Based on the maximum enhancement in the membrane's permeability (Table B.3), the coating temperature of 70°C, the coating time of 60 min, and the TiO_2 concentration of 0.5% were found to be optimum coating conditions. In agreement with our study, different groups also conducted the chemical crosslinking between amine groups and one of the carbonyl functions of the imide groups at 70°C (Albrecht et al., 2003; Trimpert et al., 2006; Ba et al., 2009; Sun et al., 2011). Modification of the membrane at the optimum coating conditions did not only increase the PWP but also reduced the MWCO of the membrane from >100 kDa to 22 kDa and made the pore size distribution narrower (μ_p:2.37 nm and σ_p:1.48 nm) (Figure 3.2.b). After coating, the membrane's pore size (ranging from 0.95 to 5.62 nm; 5th to 95th percentile) became suitable for fully recovering silica nanoparticles from the suspension.

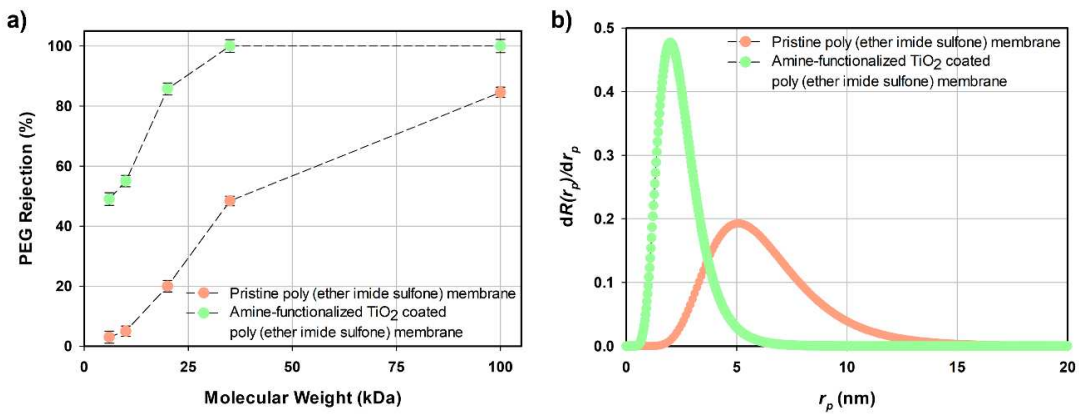

Figure 3.2. a) PEG rejections and b) the pore size distribution of pristine and amine-functionalized TiO_2 coated poly (ether imide sulfone) membranes

3.3.2. Characterization of the Pristine and Amine-functionalized TiO_2 Coated Poly (ether imide sulfone) Membranes

Figure 3.3 shows the FTIR spectra of the pristine and amine-functionalized TiO_2 coated poly (ether imide sulfone) membranes. The bands around 1732 cm^{-1} and 1783 cm^{-1} belong to C=O symmetric and asymmetric stretches of imide groups, respectively. The strong peak at 1366 cm^{-1} was assigned to the C-N stretch of imide groups, which overlapped the asymmetric stretch of $-SO_2-$ peak at 1320 cm^{-1}. However, the symmetric stretch of the $-SO_2-$ absorption band appeared at 1159 cm^{-1}. These peaks are common for both the pristine and coated membranes and agree with the previously reported bands of Xia et al. (2010). The new peaks observed only in the FTIR spectra of the coated membrane at 481 cm^{-1}, 2918 cm^{-1}, and 2850 cm^{-1} that belong to Ti-O and N-H groups confirmed the successful coating of the TiO_2 nanoparticles. When coated on the surface, the N-H peak for the nanoparticle (Figure B.3) slightly shifted to a smaller wavenumber.

The SEM images demonstrated the TiO_2 nanoparticles on the surface (Figure 3.4), and the SEM-EDX analysis quantified the Ti element (Figure 3.4.f). Both pristine and modified membranes showed typical finger-like pores in the sublayer and a thin dense skin layer near the surface (Figures 3.4.c and 3.4.d). AFM topology images (Figure 3.5) demonstrated a slight increase in the membrane's roughness after nanoparticle coating. The negatively charged TiO_2 nanoparticles increased the negative charge density at all pH values and shifted the isoelectric point of the pristine membrane from pH 6.1 to 5.3 (Figure 3.6). In addition, the coating significantly improved the hydrophilicity of the membrane, as confirmed by the decrease in the contact angle value from 76.60°±1.11° to 57.2°±0.53°. The results suggested that improved hydrophilicity and increased surface roughness can explain the enhanced flux of the membrane after coating. Figure 3.7 shows a double-step decomposition of nonwoven fabric and the membranes. For the unmodified membrane, the first degradation step was from 365°C to 490°C, and the second degradation step ended at 650°C, at which point the total mass was zero. On the other hand, 1.4 wt% of the total mass remained in the modified membrane at 650°C. Considering the nondegradability of TiO_2 up to 800°C, the amount of nanoparticles on the membrane was determined to be 1.4 wt% (represented 2217 mg/m^2).

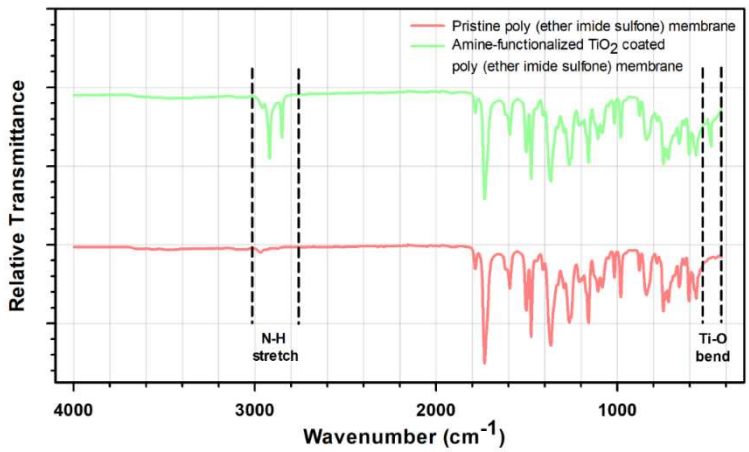

Figure 3.3. ATR-FTIR spectra of the pristine and amine-functionalized TiO_2 coated polyetherimide sulfone membranes

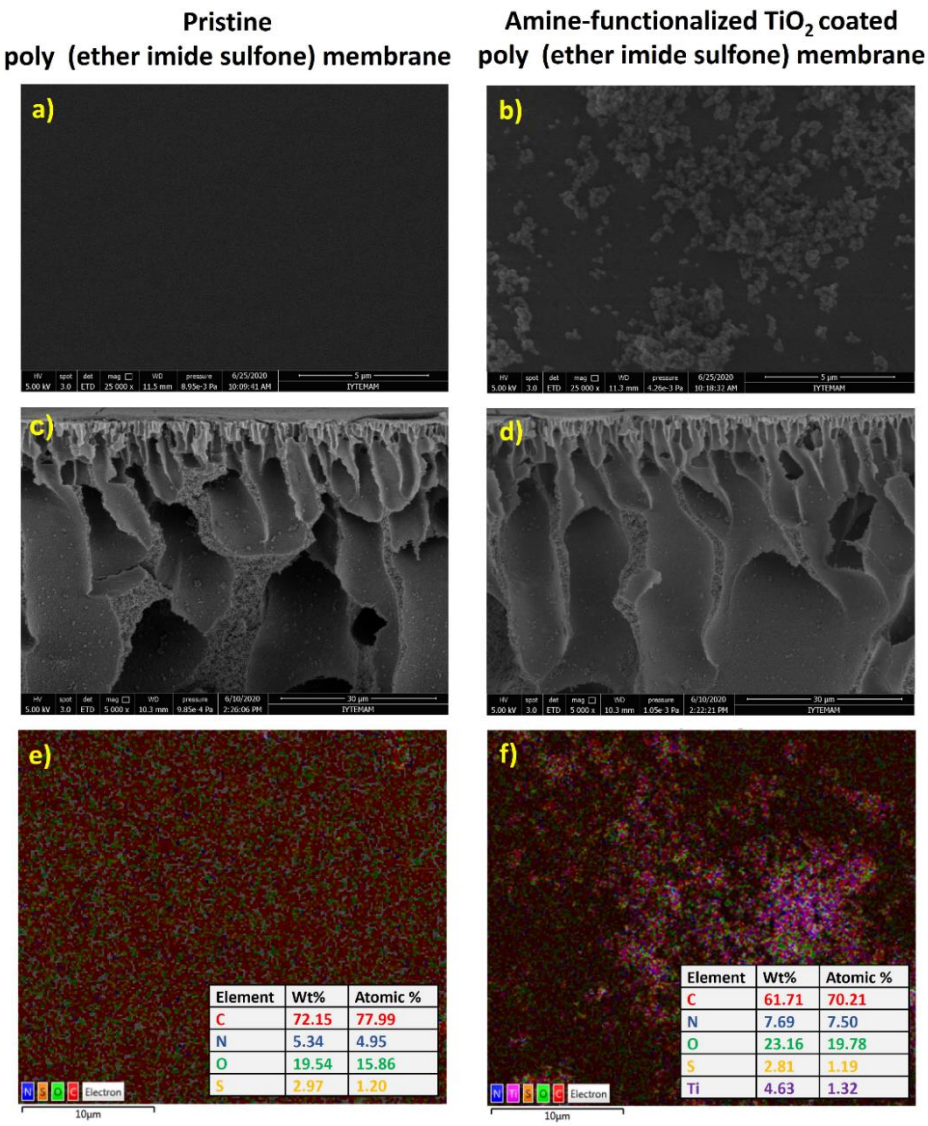

Figure 3.4. Surface SEM images, cross-sectional SEM images and SEM-EDX elemental analysis and mapping of the pristine (a, c, e) and the amine-functionalized TiO_2 coated poly (ether imide sulfone) membranes (b, d, f)

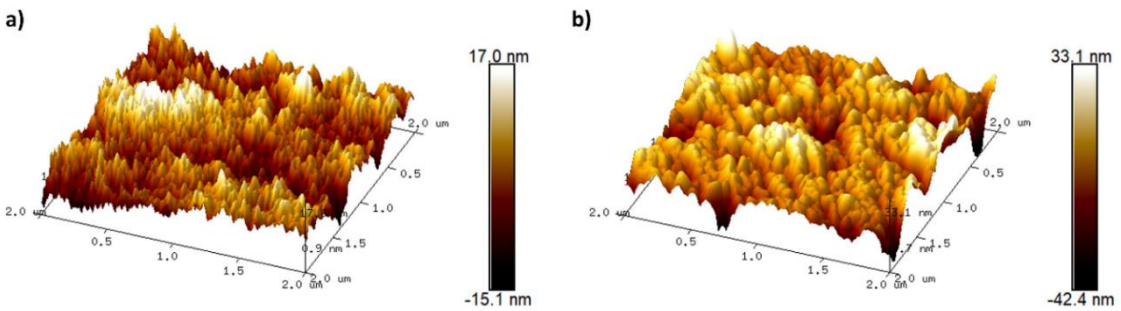

Ra (nm)	Rq (nm)	Rmax (nm)
2.05	2.52	16.9

Ra (nm)	Rq (nm)	Rmax (nm)
5.03	7.18	53

Figure 3.5. AFM images of a) pristine and b) amine-functionalized TiO_2 coated poly (ether imide sulfone) membranes

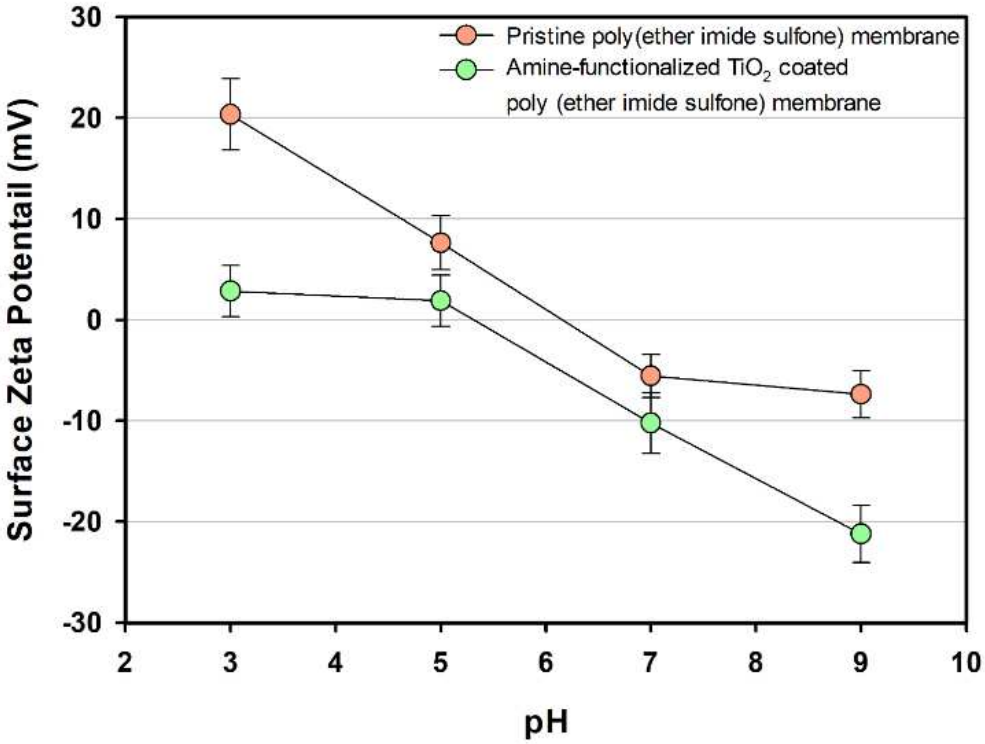

Figure 3.6. Zeta potential of the pristine and amine-functionalized TiO_2 coated poly (ether imide sulfone) membranes as a function of pH

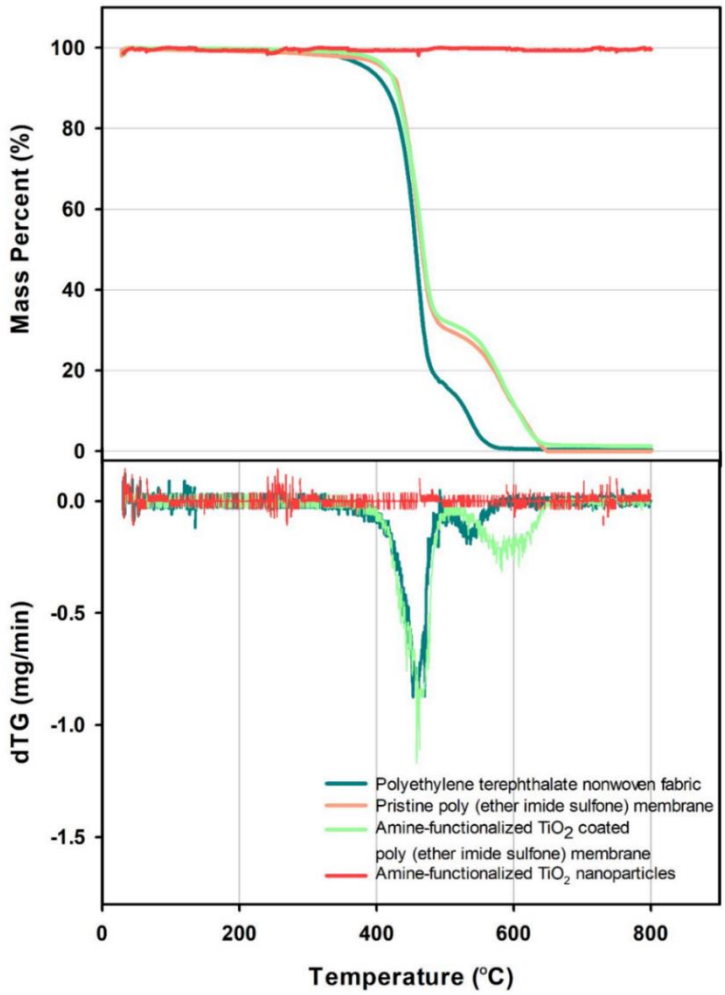

Figure 3.7. TGA and dTG (derivative thermogravimetry) curves of the polyethylene terephthalate nonwoven fabric, pristine and amine-functionalized TiO_2 coated poly (ether imide sulfone) membranes, and amine-functionalized TiO_2 nanoparticles

3.3.3. Colloidal Silica Suspension Filtration Performance and Stability of the Amine-Functionalized TiO_2 Coated Poly (Ether Imide Sulfone) Membrane

Membrane-assisted silica nanopowder production becomes feasible if the membrane exhibits antifouling properties to reduce energy and chemical consumption. The coated membrane was exposed to a 5-cycle filtration test to evaluate the antifouling property. Each cycle consisted of 60 min water flux measurement followed by 250 mL silica suspension filtration and 30 min backwashing of the membrane with water (Figure 3.8.a). At the end of the first cycle, the flux decreased from 80.79±0.44 $Lm^{-2}h^{-1}$ to 60 $Lm^{-2}h^{-1}$; backwashing recovered 96.5% of the flux. Irreversible fouling was

low (3.5%) and backwashing quickly removed the reversible foulant layer (Figure 3.8.b). The FRR slightly decreased to 93.3% at the end of the fifth cycle. A hydrophilic and negatively charged surface imparted antifouling properties to the membrane. The hydration layer provided by the hydrophilic TiO_2 particles on the surface and electrostatic repulsion between negatively charged membrane surface (-21.21±2.83 mV at pH=9) and silica nanoparticles (-24.63±0.69 mV) prevented their attachment to the surface (Figure 3.9). At the end of each cycle, 99.5% recovery of the particles was possible with the suitable pore size distribution of the membrane, smaller than the particle size of the nanoparticles in suspension, along with the antifouling property (Figure 3.8.a). We used dead-end cell filtration due to simple operation, high product recovery, and low solid content in the suspension. Crossflow filtration modules allow continuous operation and cause thinner filter cake formation; however, they require recirculation of the processed samples to achieve higher recovery (Enten et al., 2020), which increases energy consumption. The silica suspension becomes a concentrated mixture due to the permeation/removal of water, solvent, and catalyst. However, during the 5-cycle filtration test (Figure 3.8.a), the flux changed about 1-2% for each cycle, indicating the negligible effect of concentrated feed due to the strong antifouling property of the membrane.

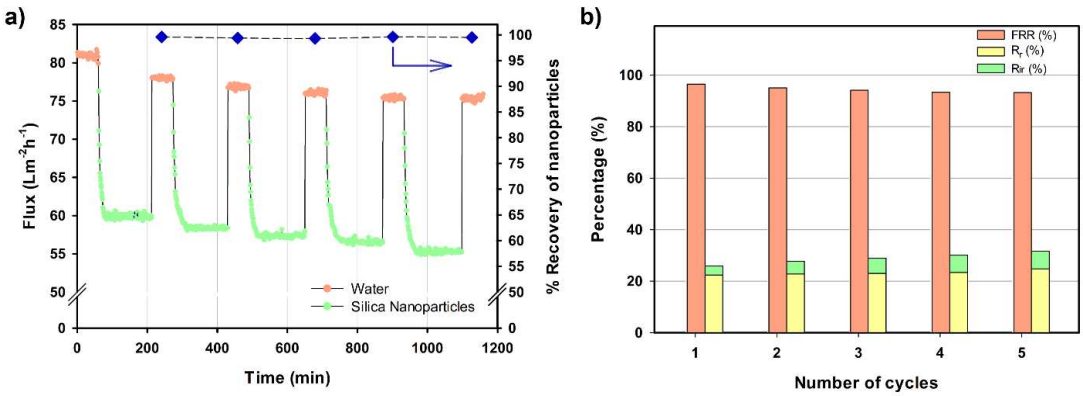

Figure 3.8. a) The changes in flux of amine-functionalized TiO_2 coated poly (ether imide sulfone) membrane and the recovery of nanoparticles, b) The change in the flux recovery ratio, irreversible and reversible fouling resistances during filtration of colloidal silica suspension

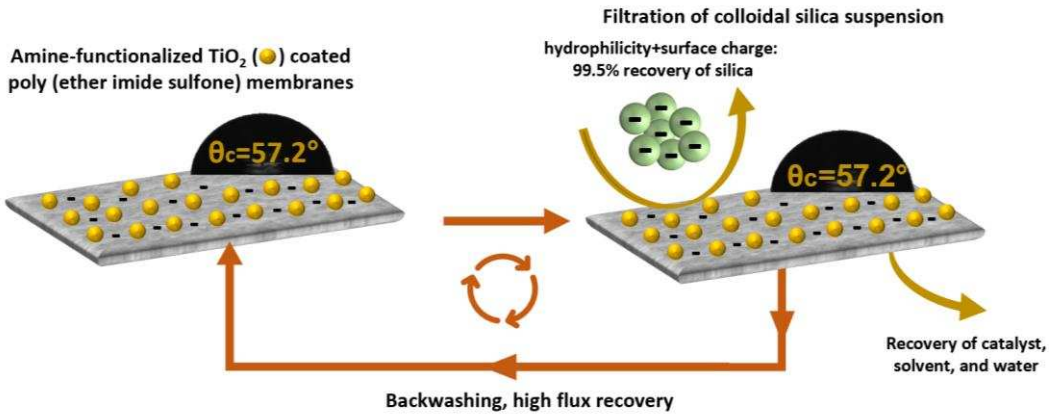

Figure 3.9. Antifouling mechanism of amine-functionalized TiO_2 coated poly (ether imide sulfone) membranes and recovery of silica nanoparticles from the suspension by using the membrane

Figure 3.10.a shows the TiO_2 nanoparticle leaching into the water. The released amount in 1 day was 1.86±0.08% and increased to 2.60±0.11% at the end of 15 days, then almost stabilized (2.79±0.08% at the end of 30 days). The leached amount was found independent of the storage medium, and 97% of the nanoparticles remained in the membrane after 30 days of storage in 40% ethanol and the silica synthesis solution. This result demonstrated that only physically adsorbed TiO_2 nanoparticles were released from the membrane. The PWP and PEG rejection of the coated membrane remained constant during one-month of storage in water (Figure 3.10.b), 40% ethanol (Figure 3.11.b), and silica synthesis solution (Figure 3.11.d). Unchanged permeability and rejection values were other evidence for the coated layer's stability. Additionally, the flux of the coated membrane was also stable during 13.5 h continuous filtration of the silica suspension (Figure 3.8.a). The performance of the pristine membrane also did not change when exposed to 40% ethanol and silica synthesis solutions (Figure 3.11.a and 3.11.c). Good leaching stability of the modified TiO_2 nanoparticles can be explained by the NHC=O bond formed by amine functionalization between nitrogen elements in the TiO_2 nanoparticles and the carbonyl group of the polymer chain, as shown schematically in Figure 3.1.c. The binding energy required to break this bond is very high, about 401.1 eV (Beck et al., 2005) higher than the binding energies for the coordination of plain Ti^{+4} to the oxygen of ether and sulfone groups (for the S=O-Ti^{+4}: 173.5 eV and C-O-Ti^{+4}: 288.6 eV) (Gupta et al., 2005; Ren et al., 2007) or by the H bond between the surface hydroxyl group of TiO_2 and oxygen of the polymer (1.73 eV) (Steiner et al., 2002). Thus, amine functionalization was applied to ensure a strong attachment of the particles to the surface.

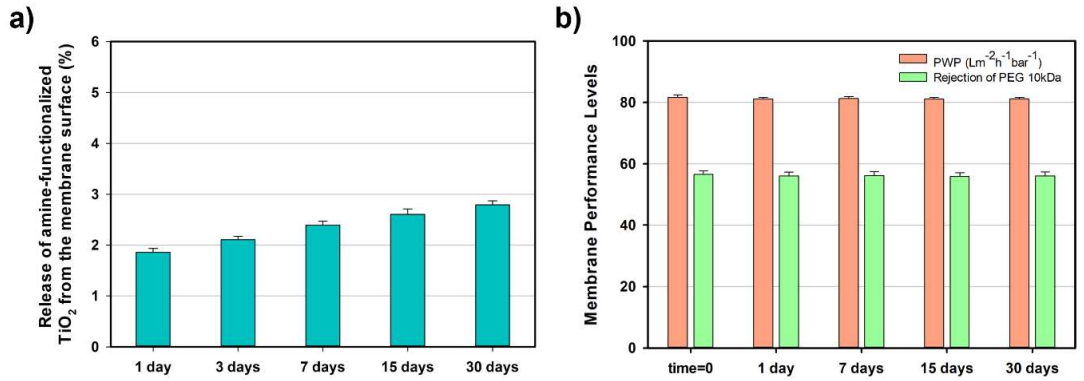

Figure 3.10. Stability of the amine-functionalized TiO_2 coated poly (ether imide sulfone) membrane: a) % release of amine-functionalized TiO_2 nanoparticles from the membrane surface as a function of time and b) The change in the PWP and PEG 10 kDa rejection of the membrane after storing in water up to 30 days

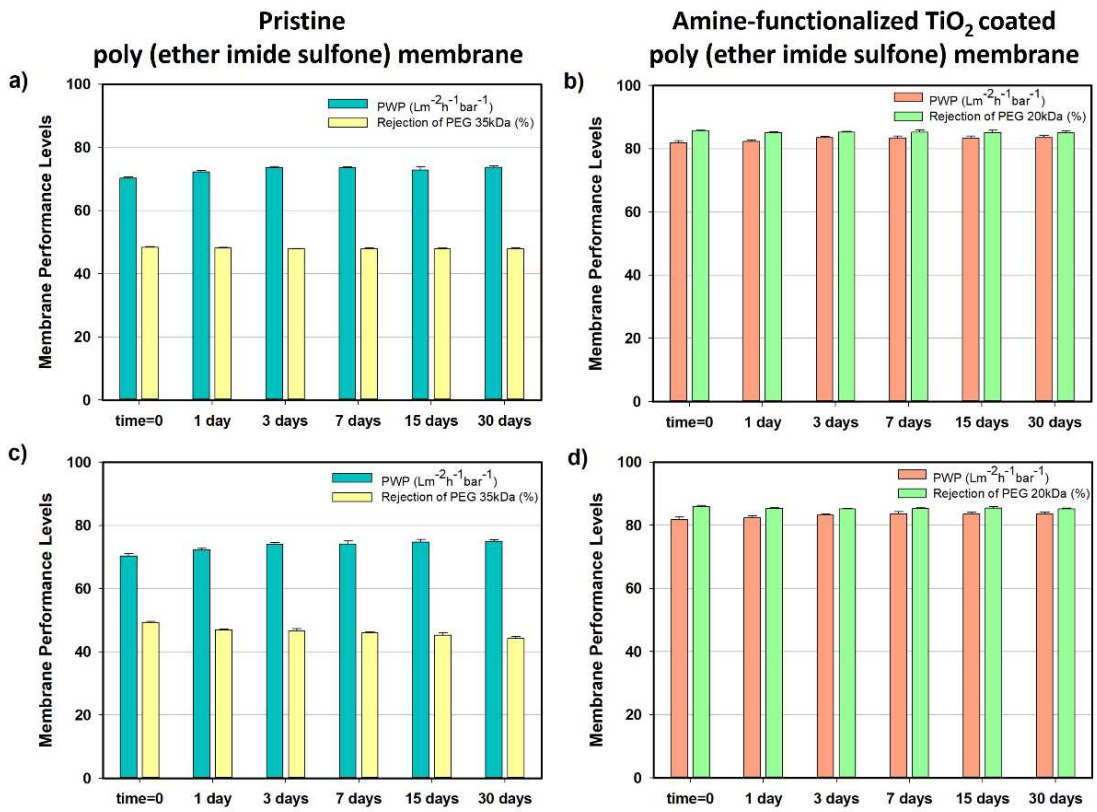

Figure 3.11. The change in the PWP and PEG rejections of the membranes after storing in a-b) the 40% ethanol aqueous solution and c-d) silica nanoparticle synthesis solution consisting of ammonia: ethanol: water

3.3.4. The Chemical and Physical Properties of the Silica Nanopowder Produced by Membrane Filtration and Drying-Based Methods and Economics of Each Method

The bands observed for all samples at about 1050, 800, and 450 cm^{-1}, attributed to the asymmetric Si–O–Si stretching, Si-OH bending, and Si–O bond rocking (Parida et al., 2006), respectively, confirmed the silica nanoparticle production (Figure B.5). The size of the freeze-dried nanoparticles ranged from 10.1 to 16.9 nm (5th to 95th percentile, mean=13.45±2.47 nm, PDI=0.94, Figure B.6). The particles obtained by membrane filtration without a drier were slightly larger with a mean value of 39.8±6.36 nm (PDI=1.13; 5th to 95th percentile range from 32.7 nm to 57.8 nm). Oven drying of the suspension at 80°C without filtration resulted in wide size distribution (PDI:0.47; 5th to 95th percentile: 84.7 nm to 171.8 nm) with an average of 115.5±0.53 nm. Drying at room temperature (25°C) without using an oven and without filtering the suspension narrowed the size distribution (PDI:1.16; 5th to 95th percentile: 53.4 nm to 92.5 nm), but the average size of the nanoparticle (mean=65.9±2.33 nm) was above 50 nm.

The drying of the powder obtained by membrane filtration, freeze-drying, room-temperature (25°C) drying, and oven-drying at 80°C was completed in 8 h, 36 h, 72 h, and 24 h, respectively. We used the ATR-FTIR spectra to determine the permeate content qualitatively (Figure B.7). The broadband at 3000-3500 cm^{-1} and the band at 1635 cm^{-1} indicated O–H stretching in water, ethanol, ammonia solution, and the O–H–O scissors bending in water (Mojet et al., 2010), respectively. The peak at 1644 cm^{-1} belonging to the N-H groups in ammonia solution overlapped with the O–H–O scissors bending; however, the NH_4^+ groups were observed at 1450 cm^{-1} (Max et al., 2013). The bands at 2900-3000 cm^{-1} and 1000-1100 cm^{-1} were due to C-H and C-O groups in ethanol (Mudalip et al., 2013). The specific IR peaks of TEOS at 793 cm^{-1} (Si-O asymmetric stretching), 960 cm^{-1} (CH_3 in TEOS), 1100 cm^{-1} (Si-O-Si symmetric stretching in the linear structure), and 1073 cm^{-1} (Si-O-Si symmetric stretching in the cyclic structure) (Rubio et al., 1998) were not detected. Then, it was concluded that the permeate was a mixture of water, solvent, and catalyst. The permeate composition can be determined using high-performance liquid chromatography or gas chromatography (Meseguer-Lloret et al., 2005; Watherly et al., 2014). By adding a make-up solution consisting of the lost amount of water, ethanol, and ammonia needed for the synthesis, recovered permeate

could be reused to synthesize silica nanoparticles without further treatment. Solvent, water, and catalyst recovery could improve nanopowder production's efficiency and sustainability by reducing water usage, waste generation, the emission of greenhouse gases, and purchase and disposal costs. In the case of drying-based methods, distillation is commonly used to recover water and solvent with high energy input; thus, they contribute to greenhouse gas emissions. Water usage for washing the membrane to remove the foulant layer and wastewater generated at the end of the washing process are the bottlenecks for membrane-assisted nanopowder production. However, the gravitational settling of nanoparticles in backwash solution allows recovering backwash water and attached particles on the membrane surface. Silica nanoparticles (0.2 wt% in water) in the beaker with a height of 15 cm settled down quickly in 15.5±0.5 min with the help of gravity. Under these conditions, an analytical expression developed by Liyanage et al. (2016) predicted a close settling time (12 min) to the experimental value. Using this model, the settling time for 0.2 wt% silica nanoparticles was estimated 40 min when the height of the backwash solution collected in a large tank was 2 m. Then, the cycle, including filtration, backwashing, and settling of backwash solution, is completed in approximately 2.5 h.

An economic analysis was carried out based on equipment and utility costs to demonstrate further the membrane-assisted nanoparticle production's energy and cost efficiency. Freeze-drying and oven-drying at 80°C required 8.1 kWh and 5.3 kWh energy to process 1 kg nanoparticle solution while, for membrane filtration, the power consumption was only 0.1 kWh/kg (Figure 3.12.a). Integrating membrane into production resulted in the shortest batch time (Figure 3.12.b) and reduced the utility cost by 3.2 and 5 times compared to oven and freeze-drying (Figure 3.12.c). The utility cost included the expenses for N_2 gas consumption, water consumption used in backwashing the membrane, and electricity needed to stir the solution in the filtration unit. The N_2 volumetric flowrate required to supply 1 barg was 11.2 L/min. The water consumption was about 370 mL for filtering 1 kg silica nanoparticle solution. Membrane cost was estimated at 57.5\$/m^2 by considering the amounts/prices of polymer, solvent, and nonwoven used in membrane preparation, energy consumption due to stirring of casting solution, and water consumption in the coagulation bath. Assuming one year of lifetime, the annual replacement cost of the membrane would be only 0.084\$. The utility cost for membrane-assisted production will even be lower if the recovered solvent and catalyst are reused in the synthesis. The price of a filtration unit is comparable to a classical oven

and cheaper than a freezer dryer (Figure 3.12.d). The calculations shown in Figure 3.12 suggest that it is possible to reduce the manufacturing cost of nanopowder while improving the sustainability of the production (Figure 3.13).

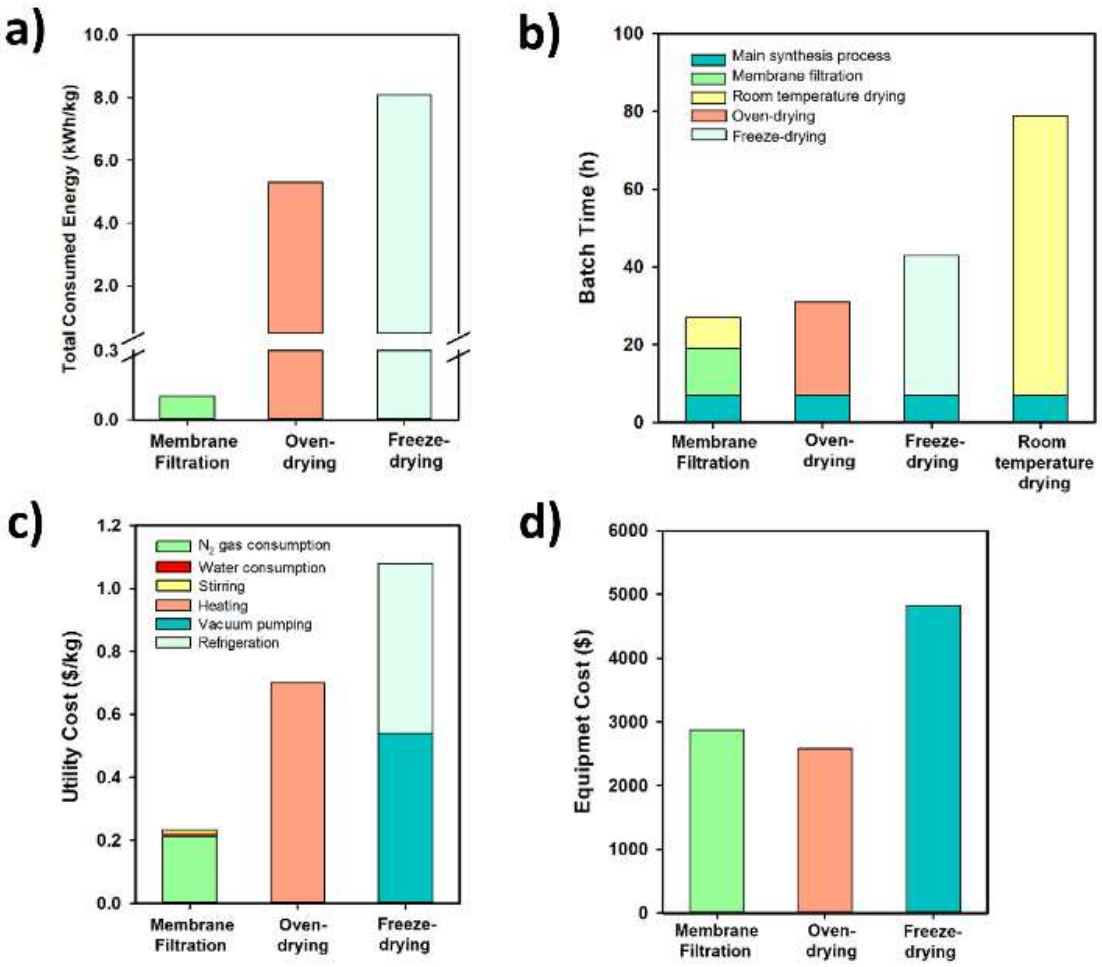

Figure 3.12. a) Total energy consumption (kWh), b) batch operation times, c) utility costs ($), and d) equipment costs for producing 1 kg nanopowder by membrane filtration and classical drying methods

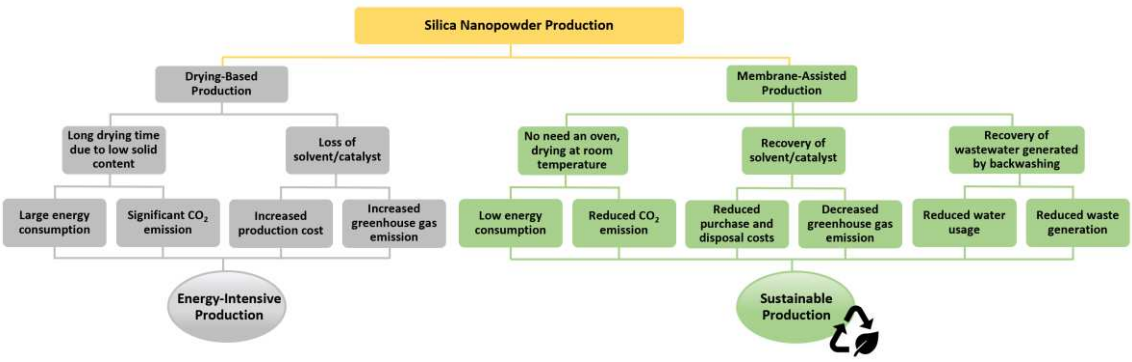

Figure 3.13. Comparison of silica nanopowder production by membrane filtration and drying-based methods

3.4. Conclusion

The work presented here demonstrated the feasibility of using a membrane during silica nanopowder production. A new TiO_2-coated poly (ether imide sulfone) membrane was developed to recover silica nanoparticles from the synthesis solution by reducing the solution's 90 % volume. The membrane durability and antifouling property are the bottlenecks that hinder commercializing membrane-assisted nanoparticle production. We demonstrated that selecting the suitable membrane material and tuning the surface properties could resolve both issues. The membrane maintained its performance in the long term when exposed to 40% ethanol and the synthesis solution consisting of ammonia: ethanol: water. In addition, it exhibited good leaching stability and high antifouling property, allowing the recovery of 99.5% of the particles. Another bottleneck for membrane-assisted nanopowder production is water used for washing the membrane and wastewater generated at the end of the washing process. This problem can be solved by separating silica nanoparticles and water through gravity-settling without energy; thus, recovered water can be reused. Membrane-assisted production can reduce energy consumption, batch production time, and utility cost and allows water, solvent, and catalyst recovery without requiring phase change. Thus, membrane technology can make nanopowder manufacturing more sustainable than conventional drying-based processes. Due to its ethanol resistance, the EXTEM membrane developed in this study can also find other applications in food (e.g., vegetable oil extraction, waste oil purification) and refinery processing fields. It should be pointed out that the literature on the implementation of membranes as part of nanoparticle production is very scarce. These studies did not focus on the economic aspect of the process or powder production. The current work aimed to fill the gap in the literature; however, further scale-up studies are needed for membrane-assisted production to become a mature technology.

CHAPTER 4

A HIGHLY ACTIVE ALUMINA-CALCIUM OXIDE CATALYST IMMOBILIZED POLY (ETHER SULFONE) MEMBRANE FOR SUSTAINABLE BIODIESEL PRODUCTION

4.1. Introduction

The gradual decrease in petrochemical resources and the environmental problems caused by fossil fuel usage have made biodiesel production attractive. Biodiesel can positively impact air pollution, global warming, and climate change by decreasing the growing emission of carbon dioxide, particulate matter, sulfur dioxide, hydrocarbons, and volatile organic compounds (VOCs) from the combustion of fossil fuels (USEPA, 2008). Homogeneous, heterogeneous catalysts, enzymes, and supercritical alcohol can catalyze biodiesel production (Shuit et al., 2012). Homogeneous acid catalysts are corrosive and require high reaction temperatures, a high alcohol-to-oil molar ratio, and a long reaction time (Lotero et al., 2005). On the other hand, homogeneous alkaline catalysts are sensitive to the purity of the reactant; the presence of water and free fatty acids in the feedstock could induce saponification, complicating the subsequent separation process (Vicente et al., 2004). The recovery of homogeneous catalysts results in a massive amount of wastewater which can cause an increase in production costs due to the need for wastewater treatment. The biocatalytic transesterification process is not popular since the reaction times are prolonged, and the enzyme quickly loses its activity (Dizge et al., 2009). Supercritical alcohol transesterification is possible at high temperatures and pressures, thus, needs more resistant and expensive reactors (Yin et al., 2008). Heterogeneous catalysts can resolve many of the problems that result from homogeneous catalysts. Their most important advantages are easy recovery, longer catalyst lifetime, and the possibility of reusing them in the biodiesel production process (Thangaraj et al., 2018). While the methods such as extraction, vacuum distillation, or centrifugation are commonly used for the recovery of heterogeneous catalysts (Miceli et al., 2021), they

increase biodiesel production costs and adversely affect the sustainability of the production due to extra energy and chemical consumption.

Recently, catalytic membranes have been proposed to solve the limitation of heterogeneous catalysts arising from their recoveries. The catalyst neutralization unit required in the conventional production plant can be eliminated since the catalyst is embedded inside the polymer matrix and would not mix with the reactant. The deactivation of heterogeneous catalysts is a serious problem resulting in the loss of catalytic activity with time (Argyle and Bartholomew, 2015). Regeneration processes, including washing, abrasion, and oxidation, followed by reduction (Trimm, 2001), cause negative economic and environmental impacts. The catalytic membrane reduces the need for a frequent catalyst activation process (Vankelecom, 2002), thus making biodiesel production more environmentally friendly. In addition, simple backwashing of the membrane allows for recovering the catalyst activity lost due to deposited reactants/products on the catalyst surface. Another attractive feature of catalytic membranes for biodiesel production is their ability to overcome the limitation imposed by chemical equilibrium. The transesterification reaction is reversible, and according to Le Chatelier's principle, using a catalytic membrane could break the equilibrium limitations by removing the products from the reaction mixture (Shuit et al., 2012). Furthermore, if the membrane has a suitable pore size, combining separation and reaction processes in one stage is possible (Dittmeyer et al., 2004).

In literature, catalytic membranes for biodiesel production were prepared by alkalization of polysulfone (Shi et al., 2016b; Shi et al., 2022) or by blending polymers containing acid groups (Zhu et al., 2010; Shi et al., 2011; Shi et al., 2013; Shi et al., 2015; Corzo-González et al., 2017; Shi et al., 2021), ion exchange resins (Zhang et al., 2012; Casimiro et al., 2014), and acid catalysts (Shi et al., 2010; Hou et al., 2016; Shi et al., 2016a; Aca-Aca et al., 2018; Tian et al., 2020; Zhang et al., 2020a; Zhang et al., 2020b) with good film-forming polymers such as poly(vinyl alcohol) and poly (ether sulfone). Modifying polymers to obtain acid-containing groups produces large amounts of acid waste, causing environmental pollution. Additionally, membranes bearing acid groups are prone to swelling due to absorbing alcohol during the transesterification reaction (Zhang et al., 2020b). Similarly, cation ion-exchange resins, composed of acid groups as the active site, also have high swelling capacity due to retaining the produced water during the esterification, leading to poor reusability (Zhang et al., 2020a). Blending acidic polymers or ion exchange resins with membrane polymer is an easy preparation method.

However, the active groups in the membrane bulk structure may not fully participate in the catalytic reaction. The noticeable drawbacks of the current membranes used in biodiesel production are low conversion (Shi et al., 2016a; Hapońska et al., 2019), reduction in chemical stability (Houng et al., 2016; Zhang et al., 2020a; Shi et al., 2021), and harsh chemical requirements for membrane production (Zhang et al., 2020a; Zhang et al., 2020b). Maintaining the membrane's catalytic activity for the long term is still a challenge. Fouling due to the adsorption of products or by-products on the catalyst's surface is primarily responsible for decreased catalytic activity. Additionally, the adsorption of oil particles to the membrane surface is undesirable due to causing flux reduction and eventually leading to high energy consumption for production. Increased energy consumption, cleaning frequency, and premature membrane replacement due to membrane fouling overshadow the benefits of biodiesel usage. Unfortunately, none of the previous studies focused on fouling for the catalytically active membranes used in biodiesel production. Thus, new catalytic membranes with antifouling properties are needed that significantly advance biodiesel production performance.

In this study, commercial poly (ether sulfone) (PES) UF membrane has been used as a support due to its excellent thermal stability and chemical resistance (Alenazi et al., 2017), which are the required properties not to be affected by the reaction medium. The CaO/Al_2O_3 has been chosen as a solid base catalyst since it has high chemical and thermal stability and superior catalytic activity under mild reaction conditions (Turkkul et al., 2020). The high basicity and mild basic strength of CaO/Al_2O_3 catalysts resulted in higher biodiesel yield than pure CaO or Al_2O_3 (Umdu, 2008). The catalyst was covalently bonded to the support surface through the intermediate polydopamine (PDA) layer, which formed a bridge between the PES membrane and the catalyst. Optimization of transesterification reaction parameters on the membrane surface, long-term catalytic activity, and performance changes of the membrane was investigated by flow-through mode of operation. The advantages of continuous production, such as breaking the equilibrium limitation, achieving higher yield values, and maintaining catalytic activity, were demonstrated by comparing it with a batch operation. To the best of our knowledge, this study is the first that systematically investigated the relationship between fouling tendency and the catalytic activity of the membrane used for biodiesel production.

4.2. Materials and Methods

4.2.1. Materials

The commercial PES ultrafiltration support membrane (NADIR® PM UP150) was supplied by Microdyn Nadir and pretreated with isopropyl alcohol (IPA) (Sigma-Aldrich). Dopamine hydrochloride, tris hydrochloride buffer, and sodium hydroxide, used for forming polydopamine coating, were purchased from Sigma-Aldrich. The alumina-calcium oxide catalyst was synthesized using alumina isopropoxide (AIP, ≥ 98 % purity, Aldrich), nitric acid (68 wt%, VWR Chemicals), and calcium nitrate tetrahydrate (≥ 99 % purity, Fluka Analytical). Commercially available canola oil (Soyyigit Food Industry and Trade Inc.) and 1-butanol (99.9% purity, Aldrich) were purchased for the transesterification reaction. KOH (Merck) was used as a homogeneous catalyst to prepare biodiesel standard. HCl fuming 37% (Merck) was used for the biodiesel washing steps.

4.2.2. Catalyst Preparation

Alumina-calcium oxide catalyst, 60 wt% CaO on Al_2O_3, was synthesized using the procedure reported by Turkkul et al. (2020). Briefly, aluminum isopropoxide was added to deionized water that was already at 85°C. Then, a necessary amount of HNO_3 acid was added to the mixture at the same temperature and stirred until a clear sol was formed. To obtain 60%CaO on Al_2O_3, a required amount of calcium nitrate tetrahydrate was added to the alumina sol and then, the mixture was slowly evaporated until gel was formed. The gel was dried and calcined as reported by Turkkul et al. (2020). The calcined catalyst was further sieved and ground to less than 44 µm of particle size with the procedure developed in this study. The catalyst was first roughly ground and then mixed in butanol using a planetary ball mill (Retsch PM 100) in a high-density polyethylene jar with yttria-stabilized zirconia balls for 9, 18, and 36 h. Particle size reduction was determined by using NanoPlus Micromeritics Instrument.

4.2.3. Membrane Preparation

The PES membrane was first pretreated by immersion into 25% (v/v) IPA solution for one h, followed by overnight storage in deionized water. The pretreated coupon was compacted at 2 bar until reaching steady-state condition. First, PDA was coated onto the PES membrane by using a custom-designed coating device adapted from the study of Dobosz et al. (2019). The device limited the coating to only one side (active side) of the PES membrane (Cihanoğlu et al. 2022). A 50 mL reaction solution, consisting of 2 mg/mL dopamine hydrochloride dissolved in 10 mM trizma hydrochloride buffer solution (pH 8.5), was poured onto the active side of the membrane. The solution was stirred at 100 rpm, and the reaction was stopped at the end of 1 h. N_2 was continuously fed from the porous side (backside) of the membrane at 0.25 bar to prevent monomer penetration into the pores. The modified membrane was washed with DI water to remove uncoated molecules from the surface. Alumina-calcium oxide catalyst was immobilized onto the PDA-modified PES membrane by filtering catalyst: butanol mixture (concentration: 0.16 mg/ml) at 1 bar. The unmodified, PDA-modified, and catalyst-immobilized PDA-modified PES membranes will be referred to as PES, PDA/PES, and Cat/PDA/PES membranes, respectively.

4.2.4. Characterization and Performance Tests of the Membranes

The pure butanol permeability (PBP) was measured using a dead-end filtration stirred cell (Millipore, Amicon Stirred Cell 50 mL). The active membrane area was 13.4 cm^2, and the pressure was adjusted to 1 bar. Before the permeability test, membranes were stored in pure butanol for 24 h for conditioning. The PBP ($Lm^{-2}h^{-1}bar^{-1}$) was calculated from Eq 4.1.

$$PBP = \frac{\Delta V}{A \times \Delta t \times \Delta P} \tag{4.1}$$

where ΔV (L) is the volume of permeated butanol, A (m^2) is the active membrane area, Δt (h) is permeation time, and ΔP (bar) is the transmembrane pressure difference.

The chemical structures of the dried PES, PDA/PES, and Cat/PDA/PES membranes were determined with Attenuated Total Reflectance Fourier Transform Infrared Spectrometer (ATR-FTIR, Perkin Elmer) at ambient temperature over a scanning

range of 650-4000 cm^{-1} with a resolution of 4.00 cm^{-1}. The membranes' surface morphology was characterized using a scanning electron microscope (SEM, FEI Quanta 250 FEG), and the elemental mapping on the surface was determined by energy dispersive X-ray analysis (EDX). All samples were coated with a thin layer of gold before the analysis. The surface roughness of the membranes was evaluated by atomic force microscopy (AFM, AFM/SPM MMSPM Nanoscope 8 Bruker) images taken in tapping mode with a 5 µm × 5 µm scanning area. The contact angles of dried membrane surfaces were measured with five µL of butanol to determine the surface's wettability with alcohol. The amount of catalyst immobilized onto the PDA/PES membrane was quantified with inductively coupled plasma optical emission spectrometry (ICP-OES, Agilent 5110). Before ICP-OES analysis, membrane samples were pretreated by mixing with 10 mL HNO_3 and 1 mL H_2O_2 and then microwave-digested (MARS 6) at 200°C for 30 min. The digested samples were filtered and analyzed for their Ca and Al ion contents.

4.2.5. Optimization of Transesterification Reaction Parameters to Produce Biodiesel on the Cat/PDA/PES Membrane Surface

The reactant mixture (butanol: oil) was continuously filtered through the Cat/PDA/PES membrane using a dead-end filtration module (Millipore, Amicon Stirred Cell 50 mL). The stirring speed was varied between 300 and 900 rpm to investigate the effect of mass transfer limitation under the following reaction conditions: 9:1 of butanol: oil molar ratio; 50°C of the reaction temperature; and 0.5 bar of the applied pressure. Continuous filtration was provided using a reservoir including a reactant mixture at the reaction temperature. After a one-h reaction period, the retentate and permeate were collected and mixed with (1100 rpm) 3 vol% HCl aqueous solution (reaction medium: acid solution volume ratio of 1:1) at 25°C. The mixtures were centrifuged at 6000 rpm and at 25°C for 10 minutes to obtain three phases: butanol and fatty acid butyl esters (FABEs) rich upper phase, oil-rich middle phase, and glycerol containing acid solution rich bottom phase (Akin, 2021). The upper phase was collected and dried in an oven at 100°C to evaporate butanol and determine the FABEs amount. Biodiesel yield was calculated using the following equations:

$$\% \text{ Biodiesel yield} = \frac{\text{Actual yield}}{\text{Theoretical yield}} \times 100\% \tag{4.2}$$

$$\text{Actual yield (wt\%)} = \frac{\text{Amount of FABE (g) in retentate and permeate}}{\text{Amount of oil (g) contacted with membrane}} \times 100\% \quad (4.3)$$

$$\text{Theoretical yield (wt\%)} = \frac{\text{Amount of FABE (g) obtained when all the limiting reagent has reacted}}{\text{Amount of limiting reagent (oil, g) contacted with membrane}} \times 100\% \quad (4.4)$$

Biodiesel yield was also calculated from the stoichiometric ratio by measuring the amount of unreacted oil in the middle phase of the centrifuged mixture. Further validation was done by analyzing the contents of biodiesel with an Agilent 6890N / 5973N gas chromatography-mass spectrometer (GC-MS) and a capillary HP-5MS column. Helium was the carrier gas, and its flow rate and split ratio were set at 1 ml/min and 50, respectively. The initial oven temperature was held at 175 °C for 5 min and raised to 220 °C at 3°C/min, to 250°C at 5°C/min, and finally to 300 °C at 40 °C/min. The total analysis time was 37 min, and the injector and detector temperatures were 280°C. Compounds were identified based on their retention times and quantified using the biodiesel standard prepared using KOH as a homogeneous catalyst. The biodiesel standard was produced in a batch-type reactor at 50 °C with butanol: oil molar ratio of 60:1, catalyst: oil weight ratio of 2×10^{-3}, and the reaction time was four h. The standard deviations of biodiesel yields were calculated based on the directly measured biodiesel amounts.

Experiments were performed using a Box-Behnken design with three factors and three coded levels (Table 4.1). The factors used for the statistical design of the experiments were reaction temperature, the molar ratio of butanol: oil, and transmembrane pressure applied for filtration. Each test was repeated three times. Experimental results were analyzed using ANOVA to evaluate whether the effect and the interaction among the investigated factors are significant concerning the experimental error.

Table 4.1. Box–Behnken experimental design for biodiesel production

Factors	Coded and Real Values		
	-	0	+
A: Reaction temperature (°C)	30	50	70
B: Molar ratio of butanol: oil	9:1	27:1	45:1
C: Pressure (bar)	0.5	2.5	4.5

4.2.6. Long-Term Catalytic Activity and Fouling of the Cat/PDA/PES Membrane

The catalytic activity of the Cat/PDA/PES membrane was followed up to 24 h using batch and flow-through mode operations. The transesterification reactions were carried out at the optimum conditions corresponding to a reaction temperature of 55.3 °C, butanol: oil molar ratio of 36.5:1, and stirring speed of 600 rpm. The transmembrane pressure was 2.5 bar and 0 bar in flow-through and batch modes. The reaction cycles were repeated eight times within 24 h. In each cycle, the samples were collected at 30th min, 1st h, 2nd h, and 3rd h from the retentate and permeate sides during dynamic filtration and the reaction mixture during the static test. The samples were analyzed to determine the biodiesel yield using the same procedures described in Section 4.2.5.

The fouling tendency of the catalytic membrane was evaluated under dynamic and static conditions. For flow-through mode, experiments started with the butanol flux measurement (J_B), followed by filtration of the reaction mixture for three h. Next, the membrane (A = 13.4 cm^2) was backwashed with butanol for 15 min, and the butanol flux was re-measured. Experiments under static conditions were conducted similarly, except that the transmembrane pressure was set to zero. In this case, no permeate was collected since the filtration was driven by pressure. Flux recovery ratio (*FRR*), reversible fouling (R_r), and irreversible fouling (R_{ir}) resistances of the Cat/PDA/PES membrane under dynamic and static conditions were calculated by using Eqs 4.5-4.7.

$$\mathrm{FRR}\,(\%) = \frac{J_R}{J_B} \times 100 \tag{4.5}$$

$$R_r(\%) = \frac{J_R - J_P}{J_B} \times 100 \tag{4.6}$$

$$R_{ir}(\%) = \frac{J_B - J_R}{J_B} \times 100 \tag{4.7}$$

where J_B and J_R are the pure butanol fluxes of the clean and backwashed membranes after each reaction cycle, respectively, while J_P is the flux of the reaction mixture. Reversible fouling of the membrane cannot be defined when the biodiesel is produced under static conditions.

4.2.7. Stability of the Cat/PDA/PES membrane

The stability of the Cat/PDA/PES membrane was evaluated by storing it in the reaction mixture (butanol: oil molar ratio of 36.5:1) for 1, 3, 7, 15, and 30 days. ICP-OES determined the catalyst concentration remained on the surface after the pretreatment of membrane samples with the protocol described in Section 4.2.4. The butanol permeability of the stored membranes and biodiesel yield at the end of the one-h reaction were also measured. The thermal stability of the Cat/PDA/PES membrane was determined by thermogravimetric analysis (TGA) using a Setaram, Labsys, TG-DTA/DSC. The heating rate was adjusted to 10°C/min from 20°C to 800°C under the nitrogen atmosphere.

4.3. Results and Discussion

4.3.1. Characterization of Alumina-Calcium Oxide Catalyst Immobilized Polydopamine Modified Poly (Ether Sulfone) Membrane

The alumina-calcium oxide catalyst directly deposited on the PES support was easily leached from the surface. An intermediate PDA layer was first formed to solve this issue, which acted as a bridge between the PES membrane and catalyst particles. The catechol groups in dopamine molecules are thought to play a central role in adhesion onto substrates (Tsai et al., 2011); however, the exact adhesion mechanism of PDA remains elusive (Liu et al., 2014). Figure 4.1 illustrates the proposed binding mechanism between the PDA and catalyst layer that is based on the catechol dissociation and catalyst-OH dehydration reactions, including bidentate chelating bonding, bridged bidentate bonding, monodentate bonding/mixed monodentate-bidentate bonding or hydrogen bonding (Ye et al., 2011).

The surface chemistry of the membrane was analyzed by ATR-FTIR spectroscopy. A combination of spectra from the PES support, the PDA, and the catalyst layers was observed, as shown in Figure 4.2. For example, three peaks at 1578, 1486, and 1412 cm^{-1} correspond to benzene, the bands around 1324 cm^{-1} and 1300 cm^{-1} belong to the ether functional group, while two stretching peaks at 1151 cm^{-1} and 1106 cm^{-1}

originate from sulfone functional in PES (Qu et al., 2010; Alenazi et al., 2018). A new peak at 1662 cm^{-1} and 3434 cm^{-1} for PES/PDA membrane is attributed to the aromatic rings stretching and N–H bending vibrations and stretching frequencies of O-H and N-H groups (Davari et al., 2021; Xing et al., 2018). The characteristic peaks due to Ca-O and Al-O bonds at 875 cm^{-1} and 558 cm^{-1} (Atrak et al., 2018; Bharathiraja et al., 2018) overlapped with the benzene ring out-of-plane bend (Jung et al., 2018). On the other hand, the peak area ratios of the 875 cm-^{1} (A(Cat/PDA/PES) / A(PDA/PES): 1.31) and 556 cm^{-1} (A(Cat/PDA/PES) / A(PDA/PES): 1.62) peaks for the Cat/PDA/PES to PDA/PES membranes were above one which proved the presence of catalyst on the PDA/PES membrane surface (Table 4.2). The catalyst immobilization caused a decrease in the stretching frequencies of O-H groups due to the interaction between the catechol groups and the alumina-calcium oxide catalyst (A(Cat/PDA/PES) / A(PDA/PES) for the wavenumber of 3434 cm^{-1} = 0.74).

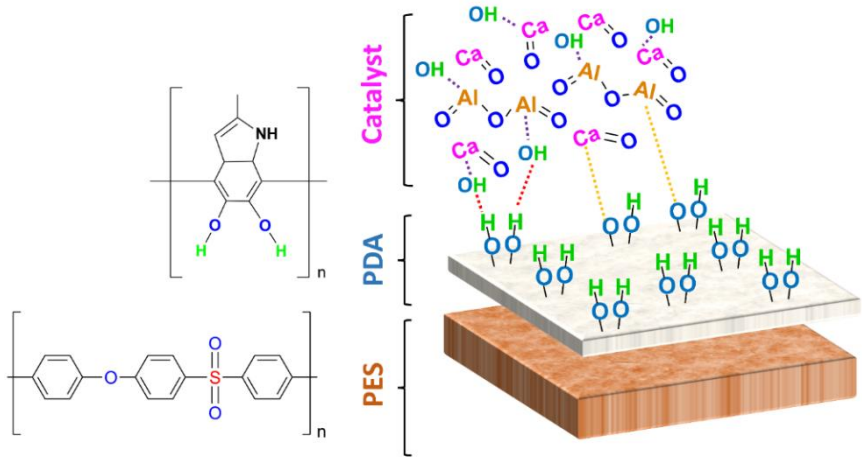

Figure 4.1. The proposed binding mechanism between PDA/PES membrane and alumina-calcium oxide catalyst

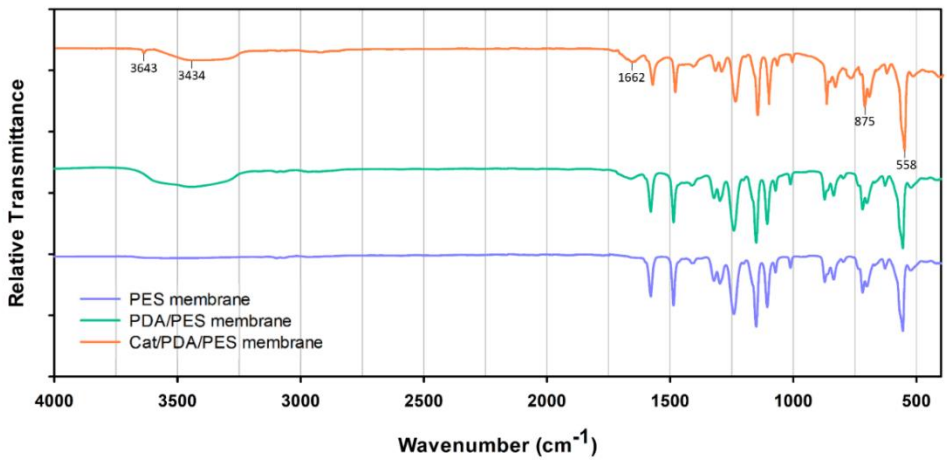

Figure 4.2. ATR-FTIR spectra of the PES, PDA/PES, and Cat/PDA/PES membranes

Table 4.2. Normalized peak area ratios different peaks determined from ATR-FTIR spectra of the PES, PDA/PES, and Cat/PDA/PES membranes

Wave-number (cm^{-1})	**Functional Group Name**	**Peak Area for PES membrane, $A_{(PES)}$**	**Peak Area for PDA/PES membrane, $A_{(PDA/PES)}$**	**Peak Area for Cat/PDA/PES membrane, $A_{(Cat/PDA/PES)}$**	**$A_{(PDA/PES)}$ / $A_{(PES)}$**	**$A_{(Cat/PDA/PES)}$ / $A_{(PDA/PES)}$**
3643	O-H	0	0	0.04	-	-
3434	O-H, N-H	0	1	0.74	-	0.74
1662	N–H	0	0.18	0.19	-	1.06
1578	Benzene ring mode	0.19	0.2	0.21	1.05	1.06
1486	Benzene ring mode	0.2	0.25	0.28	1.25	1.10
1412	Benzene ring mode	0.09	0.11	0.13	1.22	1.16
1324	C-O	0.11	0.12	0.13	1.09	1.06
1300	C-O	0.11	0.11	0.11	1.00	0.96
1151	S=O	0.32	0.33	0.32	1.03	0.96
1106	S=O	0.19	0.21	0.21	1.11	1.01
875	benzene ring, out-of-plane bend, Ca-O	0.12[a]	0.13[a]	0.17[b]	1.08	1.31
558	benzene ring, out-of-plane bend, Al-O	0.4[a]	0.42[a]	0.68[b]	1.05	1.62

[a] including only benzene ring, out-of-plane bend
[b] including benzene ring, out-of-plane bend and Ca-O or Al-O functional group

The PDA layer contains nitrogen, and the catalyst-coated PDA layer additionally includes Ca and Al, while the underlying support layer does not have these elements. This elemental contrast allowed us to perform SEM-EDX measurements, as depicted in Figure 4.3. The smooth surface morphology of the PES membrane remained similar after PDA modification. The PDA layer covered the PES support homogeneously, as evidenced by the nitrogen element's homogeneous distribution shown in Figure 4.3.b. Similarly, the Ca and Al element maps illustrated uniform coating of the catalyst on the PDA/PES membrane (Figure 4.3.c). The catalyst particle size was reduced to nanoscale using a ball mill to increase the coating's homogeneity and effective surface area. The first nine h ball milling process reduced the particle size from 44 μm to 496±36 nm (Figure 4.4). Increasing ball milling time to 18 h and 36 h caused a further reduction in particle sizes to 330±9 nm and 333±17 nm, respectively. The data suggested that 18 hours ball milling period is sufficient to reach minimum particle size.

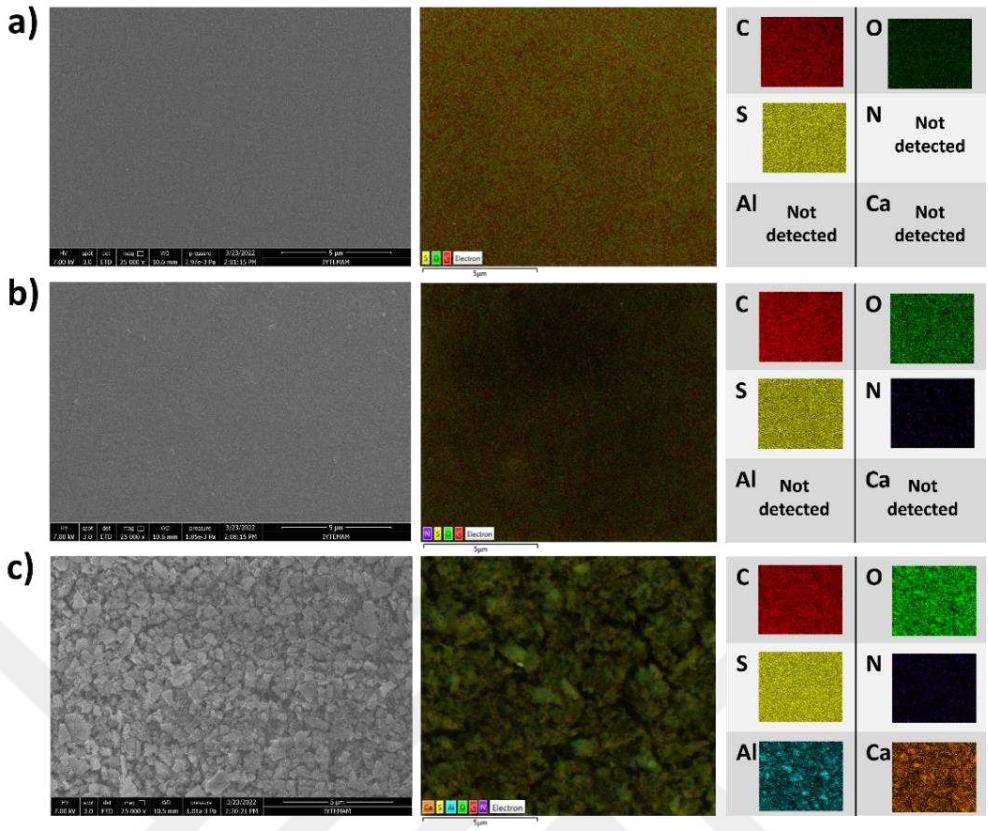

Figure 4.3. SEM surface image and EDX elemental mapping of the a) PES, b) PDA/PES, and c) Cat/PDA/PES membranes

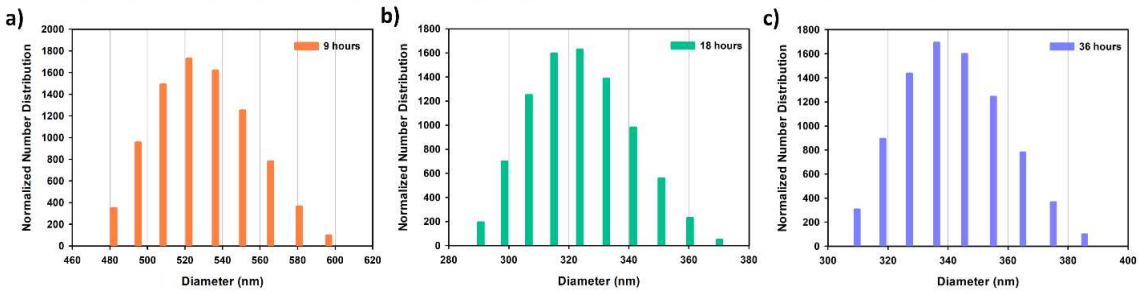

Figure 4.4. The effect of ball milling time on the particle size distribution of alumina-calcium oxide catalyst

AFM images (Figure 4.5) demonstrated that the roughness of the PES support nearly did not change after PDA coating. The roughness values (R_a and R_q) were 2.70 nm and 3.44 nm for the PES membrane; 2.91 nm and 3.65 nm for the PDA/PES membrane. Both PES and PDA/PES membranes had uniform ridge-and-valley morphology. However, after catalyst coating, surface roughness increased approximately 16 folds (R_a: 46.6 nm and R_q: 59.6 nm) due to the three-dimensional bonding structure between the alumina-calcium oxide catalyst and PDA layers. The measured contact angles between pure butanol and the PES, PDA/PES, and Cat/PDA/PES membranes were 22.38±1.19°,

21.12±0.96°, and 16.58±1.27°, respectively. A low contact angle of the Cat/PDA/PES membrane is desirable to enhance the transesterification performance.

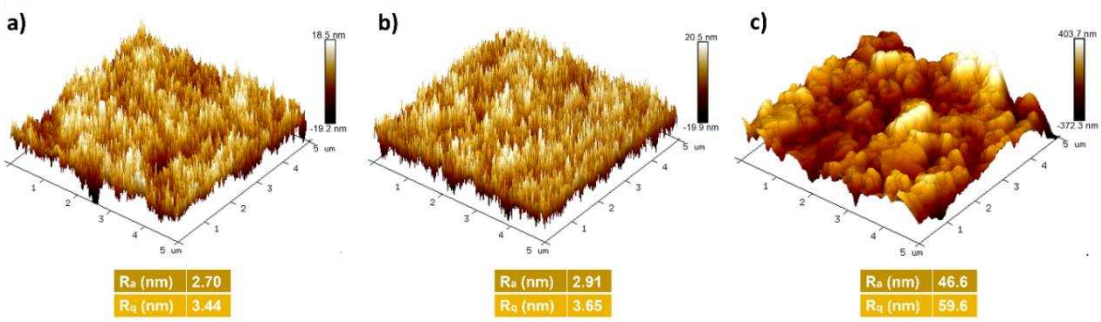

Figure 4.5. AFM images of the a) PES, b) PDA/PES, and c) Cat/PDA/PES membranes

Alumina-calcium oxide catalyst was immobilized onto the PDA/PES membrane by filtering 10 ml catalyst: butanol mixture at 1 bar. Following filtration, the membrane was backwashed with butanol at 1 bar for 15 min to remove the unbounded catalyst, and the butanol flux was remeasured. Filtration and washing cycles were repeated until the flux value no longer changed. The immobilized amount of catalyst was determined to be 952±3.82 mg/m^2 from ICP/OES analysis. The pure butanol permeabilities of the PES, PDA/PES, and Cat/PDA/PES membranes were measured as 82±1.23, 79±1.05, and 90±1.16 Lm^{-2}h^{-1}bar^{-1}, respectively. Catalyst immobilization increased the butanol permeability of the membrane due to enhanced filtration area and wettability of the surface by butanol.

4.3.2. Optimization of Reaction Parameters of Transesterification of Canola Oil to Produce Biodiesel on the Cat/PDA/PES Membrane Surface

The effect of external mass transfer limitation on the transesterification reaction was investigated by measuring biodiesel yields at various stirring speeds (Figure 4.6). The yield increased from 4.97±0.27% to 5.95±0.16% and 7.10±0.20% at stirring speeds of 300 rpm, 450 rpm, and 600 rpm, respectively. The results suggested that 600 rpm is enough to eliminate the mass transfer effect on the reaction since the yield values did not change above this stirring speed.

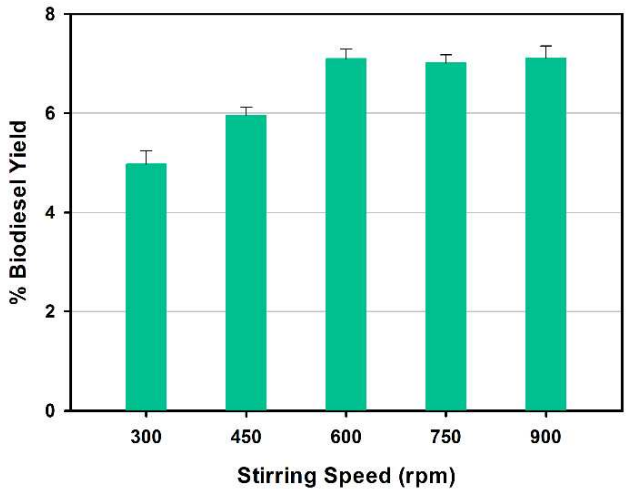

Figure 4.6. The effect of stirring speed on the biodiesel yield

Many parameters affect the transesterification reaction; we tested three important and easily controlled parameters during industrial production: temperature, butanol-to-oil ratio, and transmembrane pressure applied during filtration. The parameters were studied at three levels, and the response was biodiesel yield at the specified reaction time. The transesterification reaction is reversible, and the stoichiometric molar ratio of alcohol to oil is 3:1. We set the minimum and maximum ratios to increase the contact between the alcohol and triglyceride and shift the reaction toward completion (Lee and Saka 2010, Musa 2016) and to minimize the energy and chemical consumptions for separation of butanol from products. Similarly, energy consumption was the primary concern while selecting the upper limits for the temperature and transmembrane pressure. Because the biodiesel formed with butanol exhibits higher combustion energy (Nimcevic, Puntigam et al. 2000) and improved cold-flow properties when mixed with the conventional biodiesel (Pappu, Yanez et al. 2011), we used butanol for transesterification. Table 4.3 shows the Box-Behnken design matrix and biodiesel yield values. The quadratic model given in Eq 4.8 fitted the experimental data.

$$R = -67.453 + 1.696 \times A + 3.014 \times B + 12.479 \times C - 0.004 \times A \times B + 6.42 \times 10^{-18} \times A \times C \\ -0.111 \times B \times C - 0.014 \times A^2 - 0.034 \times B^2 - 1.646 \times C^2 \quad (4.8)$$

where R is % biodiesel yield, A is reaction temperature (°C), B is molar ratio of butanol: oil, C is the transmembrane pressure applied through the membrane (bar). The statistical analysis of variance (ANOVA) performed by the software is shown in Table 4.4. The p-value of the model (p: 0.0148) is less than 0.05, indicating that the model terms are significant and can be used in predicting the biodiesel yield. Additionally, the large

Fischer variance ratio (F = 8.52) demonstrated that the regression equation explained most of the response variation. Lack of fit shows the consistency between model predictions and experimental data, while adequate precision (AP) defines the signal-to-noise ratio. A very small p-value of lack of fit (0.0943) implies that the model fits all the data. The adequate precision of 8.56, greater than four, means an adequate signal, and the model can cover the design space. The coefficient of variance (CV) represents the ratio of the standard error of estimate to the mean value of the observed response. The CV value of 15.2% > 10% indicates good model precision and experimental data reliability.

Table 4.3. The Box-Behnken design matrix

Run	**A: Reaction temperature (°C)**	**B: Molar ratio of butanol: oil**	**C: Pressure (bar)**	**R: % Biodiesel yield obtained**
1	30	9	2.5	15.07
2	70	9	2.5	27.96
3	30	45	2.5	35.12
4	70	45	2.5	42.36
5	30	27	0.5	28.78
6	70	27	0.5	33.63
7	30	27	4.5	35.21
8	70	27	4.5	40.05
9	50	9	0.5	7.10
10	50	45	0.5	46.87
11	50	9	4.5	18.73
12	50	45	4.5	43.41
13	50	27	2.5	45.05
14	50	27	2.5	48.76
15	50	27	2.5	45.92

Table 4.4. Analysis of variance (ANOVA) for quadratic model and regression statistics

Source	**F value**	**p-value**
Model	8.52	0.0148 (significant)
A	4.15	0.0973
B	44.24	0.0012
C	1.84	0.2327
AB	0.3317	0.5896
AC	1.67×10^{-14}	1

(Cont. on next page)

Table 4.4. (Cont.)

Source	F value	p-value
BC	2.36	0.1852
A^2	4.24	0.0945
B^2	16.27	0.0095
C^2	5.90	0.0595
Lack of fit	9.77	0.0943 (not significant)

	SD	Mean	CV%	R^2	Adj R^2	AP
R	5.21	34.27	15.20	0.94	0.8287	8.5624

SD: standard deviation, CV: coefficient of variance,
R^2: coefficient of determination, AP: adequate precision

Figure 4.7 shows the three-dimensional surface plots of the predicted biodiesel yield. The yield initially increased with the increased butanol: oil molar ratio, the reaction temperature, and the transmembrane pressure. However, as the maximum butanol: oil molar ratio was approached, it slightly decreased due to the dilution effect on reagents (Pardal et al., 2010). Enhanced solubility of triglyceride with pressure (Lee and Saka, 2010) resulted in an improvement in yield values. However, at transmembrane pressures higher than ~2.8 bar, a shorter contact time between the reactant and the catalyst led to lower yield values. The biodiesel yield increased from 30 to ~55°C, but after that did not show a significant change. Consistent with our observation, heterogeneous catalysts, especially involving alkaline metal oxides, showed high activity under mild temperatures (Baskar and Aiswarya, 2016). Similarly, the change in yield with the alcohol: oil ratio agrees with the previous studies (Eevera et al., 2009; Lee and Saka, 2010; Wu and Leung, 2011; Musa, 2016). The predicted optimal reaction conditions giving maximum biodiesel yield (50.95±5.21%) are a reaction temperature of 55.3 °C, a butanol: oil molar ratio of 36.5:1, and the applied pressure of 2.5 bar. The experiment repeated three times under the optimum reaction conditions resulted in a 49.44±0.72% yield. An error of 1.51% between the predicted and measured biodiesel yield proved the accuracy of the generated model in predicting the biodiesel yield.

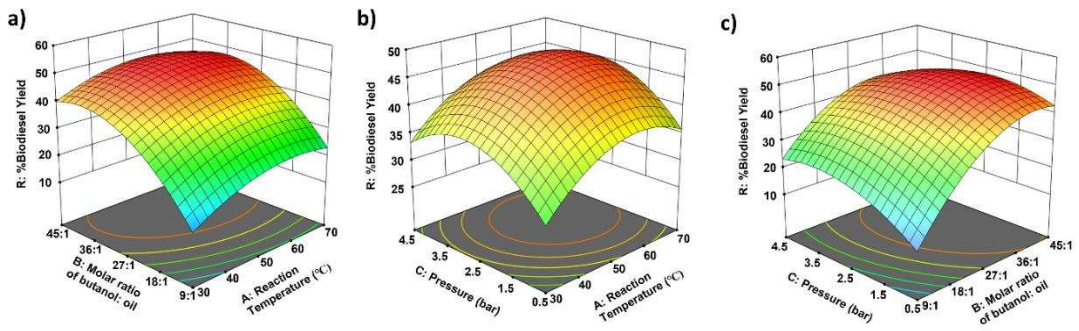

Figure 4.7. Combined effects of a) butanol:oil molar ratio and temperature, b) pressure and temperature and c) pressure and butanol:oil molar ratio on the biodiesel yield

The biodiesel produced at the predicted optimum condition was also analyzed using GC-MS to validate the drying method. Two methods resulted in a maximum of 3% difference in the biodiesel yields calculated from the average of three repeat experiments. The biodiesel standard and the biodiesel samples obtained with the Cat/PDA/PES membrane gave the peaks at nearly the same retention times (Figure 4.8). Using NIST mass spectral database, the compounds in the biodiesel sample were identified as palmitic acid butyl ester (6.12%), linoleic acid butyl ester (17.64%), oleic acid butyl ester (74.68%), and stearic acid butyl ester (1.56%). In literature, the fatty acids in canola oil (and their wt%) were listed as palmitic acid (3.9%), linoleic acid (20.4%), oleic acid (64.4%), stearic acid (1.1%), and linolenic acid (9.6%) (Batista et al., 2015). Except for linolenic acid, not observed in our samples, the weight percent of fatty acids biodiesel standard and samples obtained with the Cat/PDA/PES membrane were similar to the values reported in the literature.

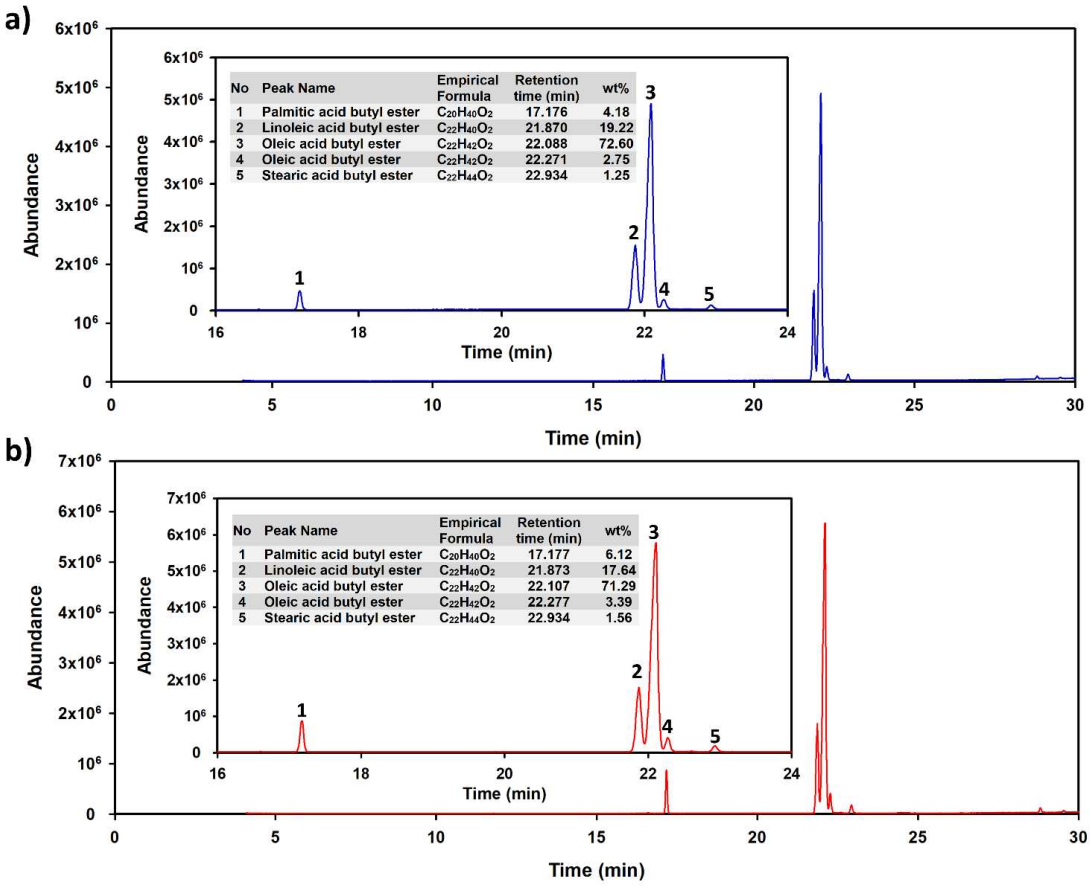

Figure 4.8. GC/MS chromatograms of a) biodiesel standard diluted 10-fold and b) biodiesel sample produced under optimum reaction conditions.

4.3.3. Catalytic Activity and Performance Changes of the Cat/PDA/PES Membrane in Long-Term Reaction Period

We evaluated the catalytic activities of the Cat/PDA/PES membrane under static and dynamic conditions within 24 h (8-cycle). During filtration, the biodiesel yield decreased from 54.54±0.65% to 47.31±0.70% in the first three cycles and stayed constant at 47.00±0.19% (Figure 4.9.a). On the other hand, the yield continuously dropped from 25.42±0.57% to 17.19±0.58% under static conditions (Figure 4.9.b). We hypothesized that the reduction in yield values occurs due to fouling, and to prove our hypothesis, we followed the flux change during the transesterification reaction. As seen in Figure 4.10, the pure butanol and reaction mixture fluxes measured as 230±1.48 and 57.21±1.37 L/m^{2}h at the end of the first cycle decreased to 218±1.34 and 45.85±0.64 L/m^{2}h when completing the 8-cycle filtration. The physical deposition of the reactants/products from the reaction mixture onto the catalyst surface causes flux reduction. Like the change in

yield values, flux decline remained constant after the first three cycles, proving fouling is responsible for the decrease in the yield values. One remarkable observation from the data in Figure 4.9 is the higher yield values achieved under dynamic conditions. Flow through mode of operation allows the removal of products and byproducts from the catalyst surface, resulting in better catalytic activity of the membrane. Thus, this data is additional proof for our hypothesis that the yield value is influenced by the deposition on the catalyst surface (Figure 4.11). Another observation in Figure 4.9 is the decrease in yield values at the beginning of each cycle. One possible explanation for this trend is the dominance of the backward transesterification reaction of triglycerides. The by-product glycerol formed with FABE (Eq 4.9 - 4.11) (Koberg and Gedanken, 2013) involves in glycerolysis reactions (Eq 4.12-4.14) (Zhong el al., 2013) leading to an increase in mono and diglycerides amounts. This increase, in turn, drives the backward transesterification reaction.

$$\text{Triglyceride} + R^1\text{-OH} \leftrightarrow \text{Diglyceride} + RCOOR^1 \quad (4.9)$$

$$\text{Diglyceride} + R^1\text{-OH} \leftrightarrow \text{Monoglyceride} + RCOOR^1 \quad (4.10)$$

$$\text{Monoglyceride} + R^1\text{-OH} \leftrightarrow \text{Glycerol} + RCOOR^1 \quad (4.11$$

$$\text{Triglyceride} + 2\ \text{Glycerol} \leftrightarrow 3\ \text{Monoglyceride} \quad (4.12)$$

$$\text{Triglyceride} + \text{Glycerol} \leftrightarrow \text{Monoglyceride} + \text{Diglyceride} \quad (4.13)$$

$$\text{Diglyceride} + \text{Glycerol} \leftrightarrow 2\ \text{Monoglyceride} \quad (4.14)$$

The initial drop in biodiesel yields varied in the range of 3.19-4.44% for flow-through mode, whereas it was between 13.47 and 18.31% when there was no filtration. The lower drop in yield under flow conditions is because of the continuous filtration of FABE and glycerol, minimizing their accumulation on the catalyst surface. Following the initial drop, between the 1st and 3rd h in each cycle, yield values remained constant for the batch mode of operation, indicating that the equilibrium yield was achieved. In contrast, the increase in yield under dynamic conditions demonstrated the advantages of the flow-through mode of operation in breaking the thermodynamic equilibrium limitation. At the end of each reaction cycle, the butanol fluxes of the membranes were remeasured after backwashing them with butanol for 15 min. The FRRs ranged from 91.33±1.36% to 86.57±1.33% when the membrane was operated continuously, while the values were slightly higher (94.66±0.49% - 87.74±0.42%) for the batch conditions (Figure 4.12). Even though reactants, products, and byproducts accumulated on the membrane surface

when operated batch-wise, batch and dynamic operations resulted in similar irreversible fouling resistances. This observation indicates that most fouling on the surface was reversible and easily removed by backwashing, proving the antifouling property of the membrane.

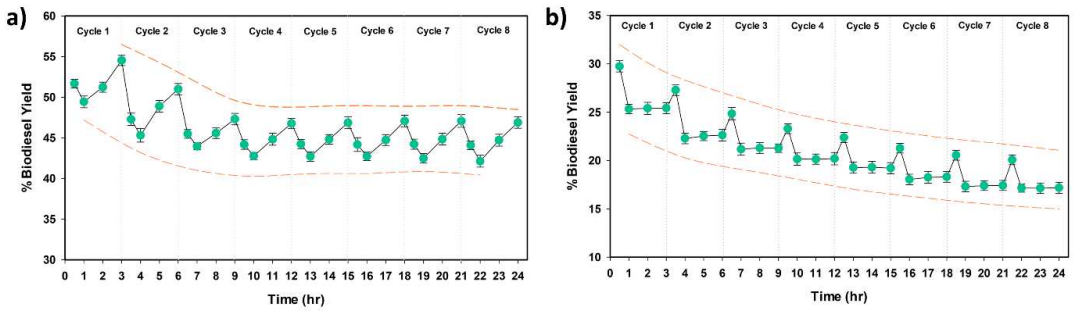

Figure 4.9. The change of catalytic activity of the Cat/PDA/PES membrane under a) dynamic filtration and b) static conditions

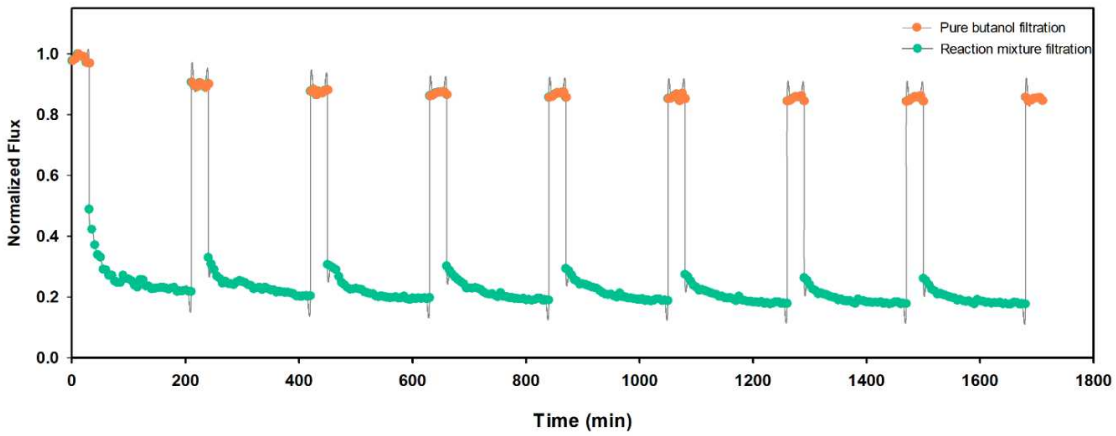

Figure 4.10. Normalized flux of the Cat/PDA/PES membrane as a function of time during 24 h (8-cycles) reaction mixture filtration

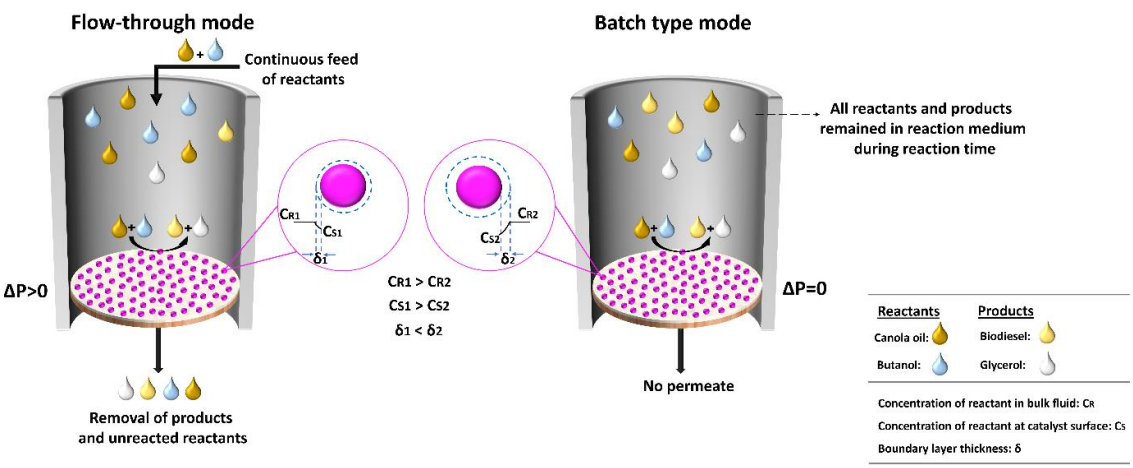

Figure 4.11. Schematic illustration of batch and flow-through mode of operations

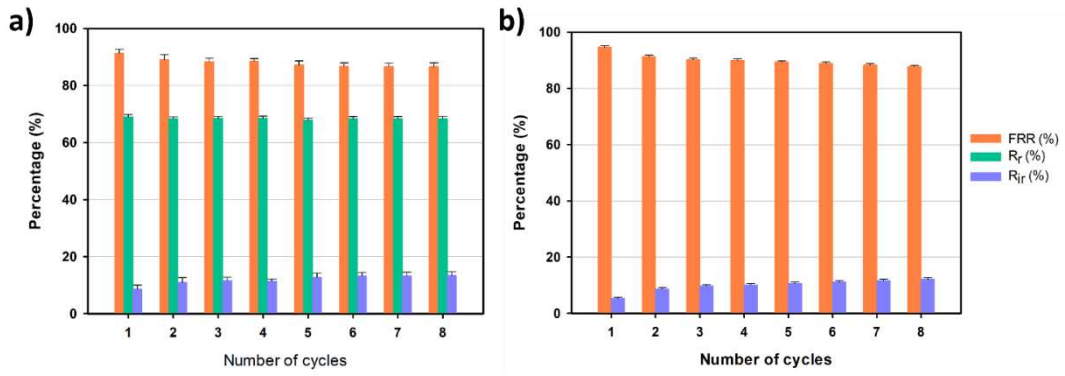

Figure 4.12. Flux recovery, irreversible and reversible fouling ratios of the Cat/PDA/PES membrane a) flow-through mode of operation b) batch operation

Table 4.5 compares the catalytic activities of different membranes used in biodiesel production in continuous-flow systems. Catalytic activities were reported in terms of biodiesel yield or oil conversion. However, a fair comparison is only possible with the yield values since oil conversion considers the formation of desired and undesired products. Shi et al. (2021) reached ~95% biodiesel yield using a 1.73 mm thick polyvinyl guanidine acetic membrane with a 1 ml/min flow rate. Their high yield value can be attributed to the high catalyst loading within a thick membrane and seven times recycling of the permeate stream, increasing the contact time with the catalyst. They tested the reusability of the membrane only under batch conditions, although they proposed flow through mode of operation. Compared to this study, our biodiesel yield is lower; however, our membrane is thinner; thus, catalyst loading is much lower (1.2 wt%), and contact time is lower since we did not recycle the permeate stream. Hou et al. (2016) also recycled the outlet stream to the feed tank in their membrane reactor system and reported a 43% biodiesel yield at the end of 2 h. Although the catalyst loading amount (38%) was very high, their yield value is relatively low compared to ours (51.24±0.62%). Additionally, they used a large methanol-to-oil ratio of about 95:1, which would increase the cost of the overall process; and they did not report the long-term catalytic activity of the membrane. None of the previous studies reported in Table 4.5 focused on the antifouling property of the membrane and its effect on the biodiesel yield. Our study is the first which demonstrated the relation between the fouling tendency and catalytic activity performance of the membrane.

Table 4.5. The catalytic activity of the membranes in the literature used for continuous-flow biodiesel production

Catalytic Membrane Type	Feedstock : Alcohol (Ratio)	Catalyst Loading	Conditions	Yield/ Conversion	Yield/ Conversion Reduction[c]	Ref
Polyvinyl guanidineacetic membrane	Soybean oil: Methanol (Mass ratio = 1:3)	2 wt%	65°C, membrane thickness: 1.73 mm, seven times recyling of permeate	~95%[a] for the feed flowrate of 1 ml/min, ~65%[a] for the feed flowrate of 2 ml/min	2.1% [a] for 5 runs (Each run: 24 h, no flow)	Shi et al. (2021)
Agarose membrane with embedded $H_3PW_{12}O_{40}$	Eruca Sativa Gars oil : Methanol (Molar ratio = 1:95)	38 wt%	65°C, up to 8 h, 33 mL/min flow rate	43% for 2 h[a] 90% for 8 h[a]	-	Hou et al. (2016)
Sulfonated polyethersulfone/ polyethersulfone/ non-woven fabric(SPES/PES/NWF) membrane	Oleic acid: Methanol (Mass ratio = 1:3)	~50 wt% SPES	65°C, membrane thickness of 8.615 mm, 1.2 mL/min flow rate	98%[b]	No reduction[b] up to 500 h	Shi et al. (2013)
Phosphotungstic acid/ polyvinyl alcohol (PWA/PVA) nanofiber composite membranes	Acidified oil: Methanol (Mass ratio = 1:3)	12 wt% PVA 20 wt% PWA	65°C, membrane layers of five, membrane thickness of 1 mm	40.5%[b]	No reduction[b] up to 10 days	Shi et al. (2016)
Amberlyst-15 (A-15)/PVA membrane	Waste cooking oil: Methanol (Mass ratio = 1:2.5)	-	65°C, 25% membrane/oil, 1.2 mL/min flow rate	96.2 [b] % for 10 h	-	Zhang et al. (2020a)
Poly(phenylene sulfide) catalytic membrane through a heterogeneous sulfonation with sulfur trioxide	Oleic acid: Methanol (Mass ratio = 1:3)	8 wt% (IEC = 0.7 mmol/g)	65°C, 35 min, membrane layers of six, membrane thickness of 1.6 mm	98%[b]	<~3% [c] for 50 h	Zhang et al. (2020b)

(Cont. on next page)

Table 4.5. (Cont.)

Catalytic Membrane Type	Feedstock : Alcohol (Ratio)	Catalyst Loading	Conditions	Yield/ Conversion	Yield/ Conversion Reduction[c]	Ref
Phosphotungstic acid (PWA)/PES membrane Alkalized polysulfone membrane (APSF)	Esterification: Oleic acid/soybean oil : Methanol (Molar ratio = 1:6) Transesterification: Oleic acid/soybean oil : Methanol (Molar ratio = 1:12)	60 wt% PWA -	Esterification: 65°C, membrane layers of seven, 30 mL/min flow rate Transesterification: 65°C, co-solvent (n-hexane) of 50 wt%, membrane layers of 9 and 15 mL/min flow rate	Esterification: 98.7%[b] Transesterification: 91.2%[b]	-	Shi et al. (2022)
SrO immobilized polysulfone membrane	Sunflower oil: Methanol (Molar ratio = 1:12)	-	65±3°C, 2 h, 40-48.5 mL/min flow rate	ND	-	Hapońska et al. (2019)
Polypropylene nonwoven fabric membrane modified with Na_2SiO_3 and N-[(2-hydroxy-3-trimethyl ammonium)propyl] chitosan chloride	Soybean oil: Methanol (Molar ratio = 1:9)	81.7 wt%	60°C, 65 min, 1 mL/min flow rate	97%[b]	<~2% [b] for 40 h	Luo et al. (2017)
Cat/PDA/PES membrane	Canola oil: Butanol (Molar ratio = 1:36.5)	1.2 wt%	55.3°C, 2.56 bar, ~1.3 mL/min flow rate	49.44±0.72% for 1 h[a] 51.24±0.62% for 1 h[a] 54.54±0.65% for 3 h[a]	No reduction[a] from 3rd to 8th cycle (Each cycle: 3 h)	This study

[a] Yield = $(2\times ACH_3)/(3\times ACH_2) \times 100\%$ where ACH_3 is integration area of the protons of the methyl esters (the strong singlet peak) and ACH_2 is integration area of the methylene protons.

[b] Conversion = the rate of change of acid value before and after reaction with the initial acid value

4.3.4. Stability of Cat/PDA/PES membrane

The expected properties of an ideal catalytic membrane for biodiesel production are long-term stability in alcohol, high catalytic activity, and high antifouling property. We stored the membrane in a reactant mixture for up to 30 days to test the stability of the catalyst coating. Figure 4.13.a shows the change in catalyst amount that remained on the surface with respect to the initial loading (952±3.82 mg/m^2). The catalyst leached from the surface in the first five days of storage corresponds to the physically adsorbed amount. In the following period, 95% of the initial catalyst loading remained constant in the membrane. Similarly, the biodiesel yield and butanol permeability of the membrane was stable between the 5th and 30th days of storage (Figure 4.13.b). The high stability of the immobilized catalyst layer was due to its strong binding to the PDA/PES membrane through catechol dissociation followed by catalyst-OH dehydration reactions, as described in Figure 4.1. The binding energies required to break the bonds between catechol and CaO (for Ca-O-C and Ca-$(OH)_2$ bonds: 531.4 eV (Qin et al., 2021)) and between catechol and Al_2O_3 (for Al-O-C bond: 284 eV (Liu et al., 2019b) and Al-OH bond: 532.2 eV (Yang et al., 2000)) are very high which explain the high stability of the catalyst layer on the membrane surface.

Thermal stabilities of the PES, PDA/PES, and Cat/PDA/PES membranes were analyzed by TGA. A sharp weight was lost from 380°C to 560°C for the PES membrane, as shown in Figure 4.14. The PDA/PES membrane started to decompose at 100°C due to the loss of water molecules bonded to catechol groups of PDA, followed by a second decomposition step between 200°C and 360°C with 5% weight loss corresponding to PDA layer degradation and a third decomposition step between 380°C to 560°C due to presence of PES membrane (Cheng et al., 2012). The TGA spectrum of the Cat/PDA/PES membrane was similar to that of the PDA/PES membrane. The extra 1.2 wt of the remained mass in Cat/PDA/PES membrane compared to PDA/PES membrane proved the presence of nanoparticles on the membrane surface, which are nondegradable up to 800°C. The continuous weight loss in all membranes when the temperature exceeded 560°C indicated that membranes would have no thermal stability at high temperatures. However, all the membranes are thermally stable at this study's applied reaction temperature range from 30°C to 70°C.

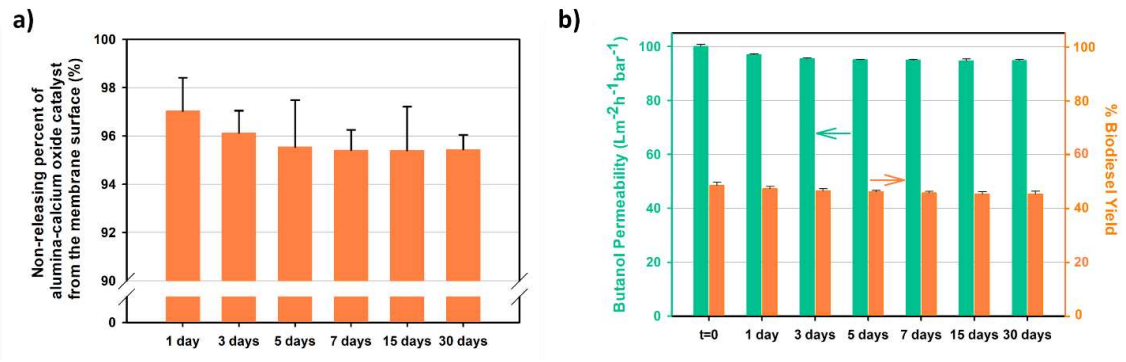

Figure 4.13. Stability of the Cat/PDA/PES membrane: a) The change in the % of alumina-calcium oxide catalyst remained on the membrane surface as a function of time and b) The change in the butanol permeability and % biodiesel yields of the membrane after storing in reactant mixture

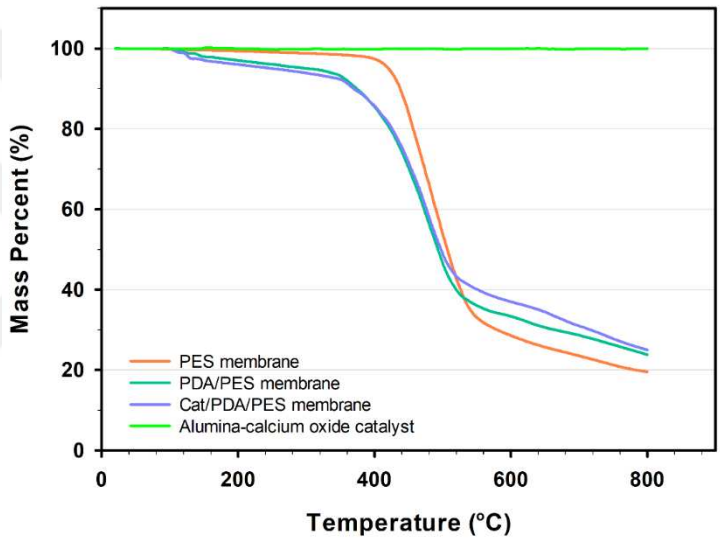

Figure 4.14. TGA spectra of the PES, PDA/PES, and Cat/PDA/PES membranes and alumina-calcium oxide catalyst

4.4. Conclusion

We prepared a novel catalytic membrane using a PES UF support and immobilizing alumina-calcium oxide catalyst through an intermediate layer produced from dopamine polymerization. The presence of catalyst on the surface was shown with FTIR spectroscopy, SEM-EDX, and the ICP/OES measurements. Thanks to the presence of catechol groups in polydopamine, the catalyst was strongly attached to the surface through catechol dissociation and catalyst-OH dehydration reactions. The ICP/OES analysis showed that 95% of the initially loaded particles were still on the surface after

storing the membrane in a reactant mixture for up to 1 month. Unchanged biodiesel yields and butanol fluxes of the membrane during one month of storage were other evidence for the catalyst stability. We demonstrated the advantages of the flow-through mode of operation by measuring the biodiesel yields under batch and continuous conditions. Under dynamic conditions, biodiesel yield was higher, the equilibrium limitation was not observed, and the yield values remained constant after the first three cycles. For batch operation, the yield values decreased continuously within eight cycles (24 h) and were limited by thermodynamic equilibrium. The similarity between flux and yield declines during dynamic filtration proved our hypothesis that catalyst fouling is responsible for the drop in yield values. Most fouling on the membrane surface was reversible and easily removed by butanol backwashing.

Biodiesel production with catalytic membranes is more environmentally friendly and cheaper due to reduced energy/water consumption required for separating the catalyst from the reaction medium. However, the importance of the antifouling property of the membrane on sustainable biodiesel production was underestimated by others. Frequent membrane cleaning with alcohol or other chemicals to recover catalytic activity and flux causes high maintenance costs and a short membrane lifetime and reduces biodiesel production's sustainability. Therefore, future biodiesel production studies with catalytic membranes should focus on the membrane's catalytic activity and antifouling properties.

CHAPTER 5

FACILE FABRICATION OF ANTI-BIOFOULING POLYANILINE ULTRAFILTRATION MEMBRANE BY GREEN CITRIC ACID DOPING PROCESS

5.1. Introduction

Biofouling is a commonly encountered problem in the environmental applications of membrane technology. Biological fouling, which accounts for more than 45% of all membrane fouling (Komlenic, 2010), results from bacterial colonization on the membrane surface (Zhang et al., 2017; Zhang et al., 2016). Severe adverse effects such as reduction in fluxes, increase in energy consumption, decrease in permeate water quality, and eventually, premature replacement of membranes are some of the consequences of biofouling. Currently, pretreatment of feed or aggressive cleaning procedures to reduce and remove biofouling are not preferred solutions due to the self-replicating nature of biofouling organisms and damage to the membrane. Unlike these options, new membrane development or modification of existing membranes is accepted as the primary strategy towards reducing biofouling.

Membrane modification is carried out to achieve anti-biofouling activity through enhancing anti-adhesion and antibacterial properties. Electrostatic repulsion between the membrane surface and foulant both carrying the same charge prevents the adhesion of the foulant on the membrane surface. However, not all foulants in water are completely negatively or positively charged (Wang et al., 2021; Louie et al., 2006; Al-Juboori et al., 2012). A negatively charged membrane surface becomes unsuitable for treating water containing positively charged foulants or vice versa. To achieve high anti-adhesion properties surfaces are highly preferred (Kumar and Ismail, 2015). Additionally, hydrophilic, and against both positively and negatively charged foulant molecules,

---

This chapter has been published as:
Gungormus, E., Alsoy Altınkaya S., 2021. Facile fabrication of anti-biofouling polyaniline ultrafiltration membrane by green citric acid doping process. Separation and Purification Technology, 279, 119756.

neutrally charged smooth surfaces have less fouling tendency. Zwitterionic polymers combine charge neutrality and high hydrophilicity to obtain an anti-adhesive membrane surface. Researchers have made efforts to use different zwitterionic polymers to improve the anti-biofouling properties of membranes (Wang et al., 2015; Yang et al., 2010; Razi et al., 2012a; Saeki et al., 2014; Liu et al., 2017; Chiang et al., 2012; Karkhanechi et al.,2014; Zhang et al., 2013; Bernstein et al., 2011; Meng et al., 2014; Chiang et al., 2009; Zhang et al., 2006). To date, zwitterionic polymer-based membranes have been prepared by using redox-initiated graft polymerization (Wang et al., 2015), UV graft polymerization (Yang et al., 2010), photografting (Razi et al., 2012a), and surface initiated atomic transfer radical polymerization (Saeki et al., 2014; Zhang et al., 2006). These methods require high energy; besides, zwitterionic monomers are expensive, resulting in a significant increase in membrane fabrication cost. Furthermore, achieving uniform polymerization on a large surface area is highly challenging. The anti-adhesive membranes can only control the bacteria attachment and the rate of early biofilm formation. Mitigating bacteria growth and proliferation for a while is only possible with antibacterial membranes since these membranes can attack, disperse, or suppress the activity of attached organisms. Antibacterial functionalization of the membranes was commonly carried out with nanoparticles (e.g., silver, copper, TiO_2, ZnO, MgO). The modified membranes showed their antibacterial action through the continuous release of the nanoparticles (Ben-Sasson et al., 2014; Zodrow et al., 2009; Koseoglu-Imer et al., 2013; Li et al., 2013; Sawada et al., 2012). This release-killing mechanism causes a shorter lasting period for antibacterial action and raises concern about environmental health. Recently metal-organic frameworks and carbon-based nanomaterials (carbon nanotubes, graphene oxide (GO), and carbon dots) have been used to impart antibacterial activity to the membranes (Seyedpour et al., 2019; Prince et al., 2014; Zeng et al., 2016; Anand et al., 2019; Liu and Xu, 2016; Das et al., 2014; Zhao and Chung, 2018; Hegab and Zou, 2015). Among these materials, GO has especially received significant attention due to its physicochemical properties, including sheet morphology, size/size distribution, oxygen-containing group density, electronic mobility, and carbon radicals which can substantially impact its antimicrobial activity. Nevertheless, despite its favorable antibacterial property with contact-killing properties, for the moment, procedures for graphene synthesis are time-consuming. They cannot readily produce defect-free samples in large quantities with high yields (Zhang et al., 2018a). In many studies, functionalization of membrane surfaces with positively charged quaternary ammonium

compounds (QACs) has been shown to produce stable and long-lasting antibacterial activities (Zhang et al., 2017; Zhang et al., 2016a; Zhang et al., 2016b; Wen et al, 2019a; Ping et al., 2019; Razi et al., 2012b; Wang et al., 2018; Wu et al., 2018; Zhang et al., 2018b). Different QACs have been introduced into membranes through blending during fabrication (Zhang et al., 2017; Zhang et al., 2016a; Zhang et al., 2016b; Wen et al, 2019a; Kakihana et al., 2017), graft polymerization (Zeng et al., 2016; Ping et al., 2019; Razi et al., 2012b; Wang et al., 2018; Wu et al., 2018; Zhang et al., 2018b) and coating on the membrane surface (Xu et al., 2015). Grafting and coating methods require abundant chemical usage, extensive procedures (Zeng et al., 2016; Ping et al., 2019; Razi et al., 2012b; Wang et al., 2018; Wu et al., 2018; Zhang et al., 2018b; Xu et al., 2015) and may cause a change in the bulk and surface properties (Zeng et al., 2016; Wu et al., 2018). In a recent study, we proposed a facile approach for preparing antibacterial polysulfone-sulfonated polyethersulfone (SPES) based UF membrane (Cihanoğlu and Alsoy Altınkaya, 2020). QAC, added in the coagulation bath, made strong electrostatic interaction with the negatively charged functional groups of the SPES at the membrane surface, hence, provided high antibacterial activity. The only drawback of the QACs is their hydrophobic nature. Although progress has been made, there is still a need for alternative methods/materials which are scalable and cost-effective for large-scale industrial production of UF membranes possessing both anti-adhesion and antibacterial properties. Also, sustainable development goals impose demands on new, innovative, and green solutions for membrane production.

In this study, a new type of anti-biofouling PANI UF membrane was developed via a facile, simple, and fast route with citric acid doping under dynamic conditions. The most attractive feature of PANI comes from its self-doping ability by protonic acids (Shen et al., 2018). Among various acids, citric acid was chosen due to its well-known antibacterial activity (Smith and Wayman, 1986; Georgopoulou, 1994; Su et al., 2014). It was doped to the membrane through a simple filtration step at low pressure. Citric acid doping protonates the imine groups of PANI and produces positively charged nitrogen (Kang et al., 1998). The protonated groups are ionically bound to the negatively charged counter-ion, $C_6H_7O_7^-$, (Kang et al., 1990); thus, the polymer backbone becomes electroneutral (Scheme 5.1). Also, the integration of carboxyl and hydroxyl functional groups to the structure through acid doping increases the hydrophilicity of the resulting membrane. Thus, the PANI membrane modified with citric acid acts like a zwitterion displaying anti-adhesive and antibacterial properties. To date, only a few studies reported

the usage of PANI in the development of antibacterial water treatment membranes. In these studies, PANI was used either as a filler in the membrane casting solution (Zhao et al., 2017) or a grafting layer on the commercial RO membrane (Khajouei et al., 2018). The antibacterial property was imparted through in situ silver reduction after dopamine coating (Zhao et al., 2017) or copper nanoparticle coating (Khajouei et al., 2018). Both studies utilized many steps and long procedures to prepare the membranes which limit the application of protocols in large scale. The scalability of a membrane production protocol depends on factors such as availability of all materials in large quantities, energy consumption, number of steps, necessity for post treatment or pretreatment, need for harsh chemicals/conditions etc. These factors are closely related with economic considerations where the main motivation is to minimize unit production cost. Herein, we used the PANI as the main membrane polymer that can be synthesized using low-cost monomers and has high thermal, chemical stability, and a hydrophilic structure (Boeva and Sergeyev, 2014). We enhanced its anti-biofouling property through citric acid doping. The proposed doping method is a green solution since the citric acid is a naturally derived, water-soluble antibacterial agent and it also has a low cost. Additionally, there is no need either for the post-treatment of the pristine membrane or crosslinking agent for acid doping. Membrane modification by filtration of citric acid can be implemented in large-scale using commercially available dead end or cross flow filtration units (manufactured by Pall Corporation, Fluence Corporation, Salher etc). Overall, the proposed membrane fabrication technique is fast, simple, facile, and can easily be scaled up for large-scale production.

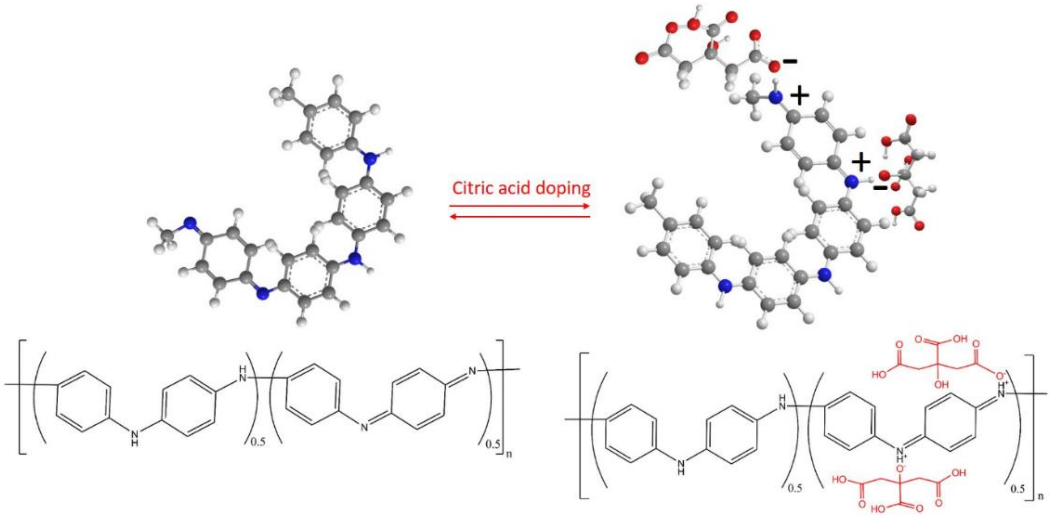

Scheme 5.1. Rearrangement reaction mechanism between the EB and ES polymers through citric acid doping and dedoping in alkaline medium

5.2. Materials and Methods

5.2.1. Materials

The most commonly used form of PANI, the EB form, was synthesized using aniline (Sigma-Aldrich, ACS reagent, ≥99.5% purity), ammonium persulfate ($(NH_4)_2S_2O_8$, Sigma-Aldrich, ACS reagent, ≥98% purity), HCl fuming 37% (Merck), 25% ammonia solution (NH_4OH, Merck), and methanol (Sigma-Aldrich, ACS reagent, ≥99.8% purity). Triethylamine (Riedel-de Haën) and N-methyl-2-pyrrolidone (NMP, Merck, anhydrous, greater than 99.5%) used as gel inhibitor and solvent were utilized in the preparation of membrane casting solution. Molecular weight cut-off (*MWCO*) of the membranes were determined by using polyethylene glycol (PEG) 1000, 4000, 6000, 10000, and 20000 Da (Sigma Aldrich). The citric acid (ACS reagent, ≥99.5% purity) was purchased from Sigma-Aldrich for the membrane doping process. Gram-negative (*Escherichia coli*, ATCC 25922) and Gram-positive (*Staphylococcus aureus*, RSKK 1009) bacteria were used for antibacterial and anti-biofouling tests. NaCl for stability test and phosphate-buffered saline for the antibacterial and anti-biofouling test were purchased from Sigma-Aldrich.

5.2.2. Polymer Synthesis

The EB form of PANI was prepared by chemical oxidative polymerization of aniline. The procedure was adapted from the studies conducted by Ibrahim, 2017 and Gomes and Oliveira, 2012. The oxidizing agent and monomer were separately dissolved in a 1 M HCl aqueous solution, and the resulting solutions were mixed at 0°C. The mixture was first stirred at 0°C for 4 hr and then at 25°C for 20 hr. After 24 hr of reaction, the emeraldine hydrochloride precipitate was collected, washed, and filtered to remove unreacted chemicals. The filtered precipitate was treated with 1 M NH_4OH solution to form EB, washed with DI water, and then DI water: methanol mixture and refiltered. Finally, the EB powder was collected and vacuum dried. The detailed procedure was described in our previous study (Gungormus and Altinkaya, 2020).

5.2.3. Membrane Fabrication and Modification

The membrane casting solution was prepared by dissolving 15 wt. % EB in a mixture of 1.5 wt. % trimethylamine and 83.5 wt. % NMP. The mixture was homogenized by stirring for one hr at 300 rpm (T = 25 °C), degassed, then cast on a polyester nonwoven fabric (Type TH, Hirose Paper Mfg. Co. Ltd.) with the help of an automated film applicator (Sheen Instrument Ltd., model number: 1133N). The casted solution was immersed in a coagulation bath (DI water, 20°C) to induce phase inversion and kept in DI water for 24 hr to complete phase separation. The prepared EB membranes were first compacted at 2 bar and then doped with citric acid by filtering aqueous acid solution (pH=3) at 1 bar for 4.5 hr until reaching a constant flux. The doped membrane will be referred to as citric acid doped ES membrane.

5.2.4. Membrane Performance Tests and Characterization

The chemical structures of the dried pristine and citric acid doped ES membranes were determined with Attenuated Total Reflectance Fourier Transform Infrared Spectrometer (ATR-FTIR, Perkin Elmer) at ambient temperature over a scanning range of 650–4000 cm^{-1} with a resolution of 4.00 cm^{-1}. A scanning electron microscope (FEI Quanta 250 FEG) and energy dispersive X-ray analysis (EDX) were used for characterizing the surface and bulk morphology of the membranes and for determining the elemental compositions on the membrane surface. The samples were fractured in liquid nitrogen and coated with a thin layer of gold before the analysis. Atomic force microscopy (AFM) images with a 2 µm×2 µm scanning area were taken in tapping mode to evaluate the surface roughness of the membranes (AFM/SPM MMSPM Nanoscope 8 Bruker). Membrane hydrophilicity was characterized by measuring dynamic contact angles of dried membrane surfaces with a 5 µl of a deionized water droplet (Attension Optical tensiometer). The zeta potentials of the pristine and acid doped membranes were measured in 10 mM NaCl solutions at the pH ranges from 3 to 9 at 25°C (NanoPlus Micromeritics). Thermogravimetric analysis (TGA) was carried out by using a Setaram, Labsys, TG-DTA/DSC to determine the amount of citric acid doped to the membrane. The heating rate was adjusted to 10°C/min from 25°C to 900 °C under the nitrogen atmosphere.

Performances of the membranes were evaluated by measuring pure water permeability (*PWP*) and rejection of different-sized PEGs (1000, 4000, 6000, 10000, and 20000 Da). Filtration experiments were carried out by using a dead-end cell filtration system with an effective surface area (*A*) of 13.4 cm^2 (Millipore, Amicon Stirred Cell 50 mL). The membranes were first compacted until reaching steady-state condition. Following compaction, the permeate volume (ΔV) was measured over a specific time period (Δt) at the transmembrane pressure (ΔP) of 1 bar. The *PWP* and water flux (J_W) were then calculated by using Eq. 5.1.

$$PWP = \frac{\Delta V}{A \times \Delta t \times \Delta P} = \frac{J_W}{\Delta P} \tag{5.1}$$

The PEG rejection (*R*, %) was calculated from Eq. 5.2 using the PEG concentrations of the feed (C_F:1 g/L), permeate (C_P) and retentate (C_R) streams measured with Rudolph-J357 Automatic Refractometer.

$$R(\%) = \left(1 - \frac{C_P}{0.5 \times (C_F + C_R)}\right) \times 100 \tag{5.2}$$

The pore size distribution of the membranes was estimated from Eq. 5.3 using the two-parameter log-normal distribution function (Wang et al., 2018; Atchariyawut et al., 2006; Liu et al., 2015; Lin et al., 2016) with the assumptions of no interaction (steric and hydrodynamic) between the neutral PEG molecules and pores of the membranes (Wang et al., 2018; Lin et al., 2016):

$$\frac{dR(r_p)}{dr_p} = \frac{1}{r_p \ln(\sigma_p)\sqrt{2\pi}} \exp\left[-\frac{1}{2}\left(\frac{\ln(r_p/\mu_p)}{\ln(\sigma_p)}\right)^2\right] \tag{5.3}$$

where the geometrical mean radius of the solute (μ_p) was obtained at *R*=50% and the geometrical standard deviation of the solute (σ_p) was defined as the ratio of r_p of *R*=84.13% to that of *R*=50%. The radii of PEG were predicted from Eq. 5.4, which was derived from Stokes-Einstein law by assuming a spherical particle (Singh et al., 1998).

$$r_p = 16.73 \times 10^{-12} \times MW^{0.557} \tag{5.4}$$

where the unit of molecular weight (*MW*) is Da.

5.2.5. Antibacterial Activity Tests

The antibacterial activities of the membranes were determined according to ASTM E2180 standard protocol. *E.coli* and *S.aureus* cells, used as model Gram-negative and Gram-positive bacteria, were incubated in nutrient agar and soy agar, respectively, for 24 hr at 37 °C up to reaching exponential growth phase of bacteria. Bacterial suspensions were prepared in 0.1% (w) peptone water with a concentration of 0.5 McFarland, then diluted with nutrient and soy broth to obtain final concentrations of 3.5×10^6 and 4.2×10^6 CFU/mL for *E.coli* and *S.aureus*, respectively. The membrane coupons (active surface area: 3 cm x 3 cm) were sterilized with UV for 30 min and then placed into Erlenmeyer flasks. Each membrane coupon was incubated in the bacterial solution (300 µL) for either 1 hr or 24 hr at 37 °C. Following incubation, 50 mL phosphate-buffered saline solution (PBS, pH = 7.4) was added to the Erlenmeyer flask, which was subjected to 10 min bath sonication to remove bacteria attached to the membrane coupon. The obtained *E.coli* and *S.aureus* suspensions were spread on plates including nutrient agar and soy agar, respectively, incubated for 24 hr at 37 °C, and finally, the colonies on the plates were counted. All samples were analyzed in quintuplicate.

The reduction rate of the bacteria was calculated from the following equation by counting the number of colonies on the agar plate after contacting with the pristine (N_{EB}) and citric acid doped (N_{ES}) membranes.

$$\text{Reduction Rate}\,(\%) = \frac{N_{EB} - N_{ES}}{N_{EB}} \times 100 \tag{5.5}$$

5.2.6. Antibiofouling Performance Tests

Antibiofouling performance tests were carried out using a dead-end filtration cell (effective membrane area 13.4 cm^2). The concentrations of *E.coli* and *S.aureus* suspensions in PBS (pH = 7.4) were adjusted to $1.75\text{x}10^8$ and $2.1\text{x}10^8$ CFU/mL, respectively. Membranes were sterilized with UV light for 20 min. Following compaction at 2 bar, the initial pure water fluxes of both membranes (J_W) were adjusted to similar values (about 50 L/m^2hr). Next, 250 ml of *E.coli* and *S.aureus* solutions were filtered through pristine and acid-doped membranes. The treated membranes were rinsed with

PBS for 10 min, and pure water fluxes were remeasured (J_R). This cycle was repeated for 5 times. The flux recovery ratio (*FRR*) was then calculated from

$$FRR(\%) = \frac{J_R}{J_W} \times 100 \tag{5.6}$$

The antifouling property of the membrane was further evaluated by determining reversible fouling (R_r), and irreversible fouling (R_{ir}) resistances, calculated in Eq. 5.7 and Eq. 5.8.

$$R_r(\%) = \frac{J_R - J_P}{J_W} \times 100 \tag{5.7}$$

$$R_{ir}(\%) = \frac{J_W - J_R}{J_W} \times 100 \tag{5.8}$$

where J_P is the flux of bacteria suspension passing through the membrane.

The surface images of unmodified and citric acid doped membranes after 1st cycle bacteria filtrations were taken by using SEM (FEI Quanta 250 FEG).

5.2.7. Stability Test for the Citric Acid Doped ES Membrane

The stability of the citric acid doped ES membrane was tested by storing in 1 M NaCl solution (25°C) for up to 5 months. To this end, the concentration of citric acid in the solution was measured with Total Organic Carbon (TOC) analyzer (Shimadzu TOC-Vcph (TNM-1/SSM-5000A). The results were reported as % of citric acid released into storage medium with respect to its initial amount loaded to the membrane. Additionally, the *PWP* and rejection of the membrane (with PEG 6000 Da) were determined. Furthermore, the antibacterial activity of the citric acid doped ES membrane at the end of 1-month storage in 1 M NaCl solution (25°C) was also determined according to ASTM E2180 standard protocol with the same antibacterial activity test conditions mentioned in Section 5.2.5.

5.3. Results and Discussion

5.3.1. Effect of Citric Acid Doping on the Structure, Chemical Composition, and Surface Properties of the EB Membrane

The FTIR spectra of EB membrane and citric acid doped ES membrane are shown in Figure 5.1. The typical peaks for nitrogen quinoid and benzenoid were found at 1600 and 1500 cm^{-1}, respectively (Dognani et al., 2019). The C–N stretch of a secondary amine group was observed at 1300 cm^{-1}, and the aromatic C–H in-plane bending modes were originated in the region of 1010–1170 cm^{-1} (Wang et al., 2019c; Trchová et al. 2004; Huang et al., 2015). A new peak appeared at the band of 1729 cm^{-1} due to the C=O stretching (Junior et al., 2019; Thuy and Minh et al., 2012) and increased band width at 3400 cm^{-1} due to the stretching frequencies of OH and NH groups (Rajasekharan et al., 2013) proved citric acid doping to the membrane.

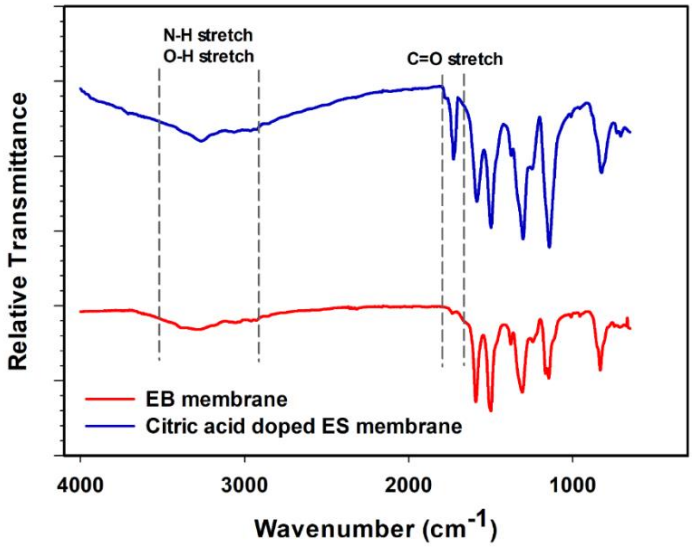

Figure 5.1. ATR-FTIR spectra of EB membrane* and citric acid doped ES membrane

*Reprinted from Chemical Engineering Journal, Vol. 389, E. Gungormus, S.A. Altinkaya, "A high-performance acid-resistant polyaniline based ultrafiltration membrane: Application in the production of aluminium sulfate powder from alumina sol". Page 124393, Copyright (2020), with permission from Elsevier

Figure 5.2 shows the cross-section and surface images of the membranes, including EDX-SEM mapping for carbon, nitrogen, and oxygen. Both pristine and citric acid doped membranes showed a typical asymmetric membrane structure consisting of a

thin, dense skin top layer and a porous sublayer with finger-like macrovoid morphology, as shown in Figures 5.2.a and 5.2.b. The acid doping in the porous sublayer did not change the bulk structure due to the small size of the citric acid. Also, surface structures of the pristine and doped membranes were found similar (Figure 5.2.c and 5.2.d). The EDX analysis confirmed the successful citric acid doping by detecting oxygen only in the ES membrane (Figure 5.2.f). In addition, the C:N ratio (atomic-based) increased from 3.91 to 5.10 upon doping (Figure 5.2.e and Figure 5.2.f).

The EB membrane exhibited a comparatively uniform ridge-and-valley morphology (Figure 5.3.a), while the ES membrane demonstrated a plating structure with a relatively rough surface (Figure 5.3.b). The roughness parameters (R_a and R_q) were determined as 2.67 nm and 3.36 nm for the EB membrane (Gungormus and Altinkaya, 2020); 4.59 nm and 5.74 nm for the citric acid doped ES membrane (Table 5.1). Citric acid doping enhanced the hydrophilicity of the EB membrane as confirmed by the decrease of the contact angle from 76.22±0.85° (Gungormus and Altinkaya, 2020) to 59.41±0.85°. The enhanced hydrophilicity is due to the hydrophilic carboxyl and hydroxyl functional groups of citric acid attached to the polymer backbone.

The pristine EB membrane is positively charged at pH 3 and 5 and becomes neutral at pH 7 and 9 (Gungormus and Altinkaya, 2020). The doped membrane is almost neutral in all pH values, as shown in Figure 5.4. The electroneutrality results from the attachment of the negatively charged counter-ion $C_6H_7O_7^-$ to the protonated imino functional groups of PANI (Scheme 5.1). The deprotonation of the ES membrane at high pH causes the removal of citric acid from the polymer backbone by the OH group, resulting in returning the membrane to the EB form with a higher positive charge density (Gungormus and Altinkaya, 2020).

Figure 5.5 shows the TGA curves of both membranes. The EB membrane degraded between 400°C and 585°C; finally, the degraded products became carbonized after 585°C. On the other hand, a new degradation step was detected for the modified membrane from 148°C to 260°C. By comparing with the TGA curve of pure citric acid, the weight loss between 148°C and 260°C was attributed to the loss of citric acid and was used to calculate citric acid loading in the membrane (16% where 1 m^2 of the 200 µm thick membrane contains 16.53 gram of citric acid). The molecular size of citric acid (192 Da) is much smaller than the pore size of the membrane (*MWCO* of the unmodified membrane:7500 Da, see Table 5.1). As a result, the carboxyl and hydroxyl functional

groups of citric acid are attached at the surface and the interior pore walls of the membrane.

Table 5.1. Properties of the prepared membranes

	EB membrane	**Citric acid doped ES membrane**
R_a (nm)	2.67	4.59
R_q (nm)	3.36	5.74
Contact Angle (°)	76.22 ± 0.85	59.41±0.85
PWP ($Lm^{-2}hr^{-1}bar^{-1}$)	97.57±1.53	52.62±0.74
MWCO (Da)	7500	6600
Pore radius (95th percentile, nm)	2.89	2.52

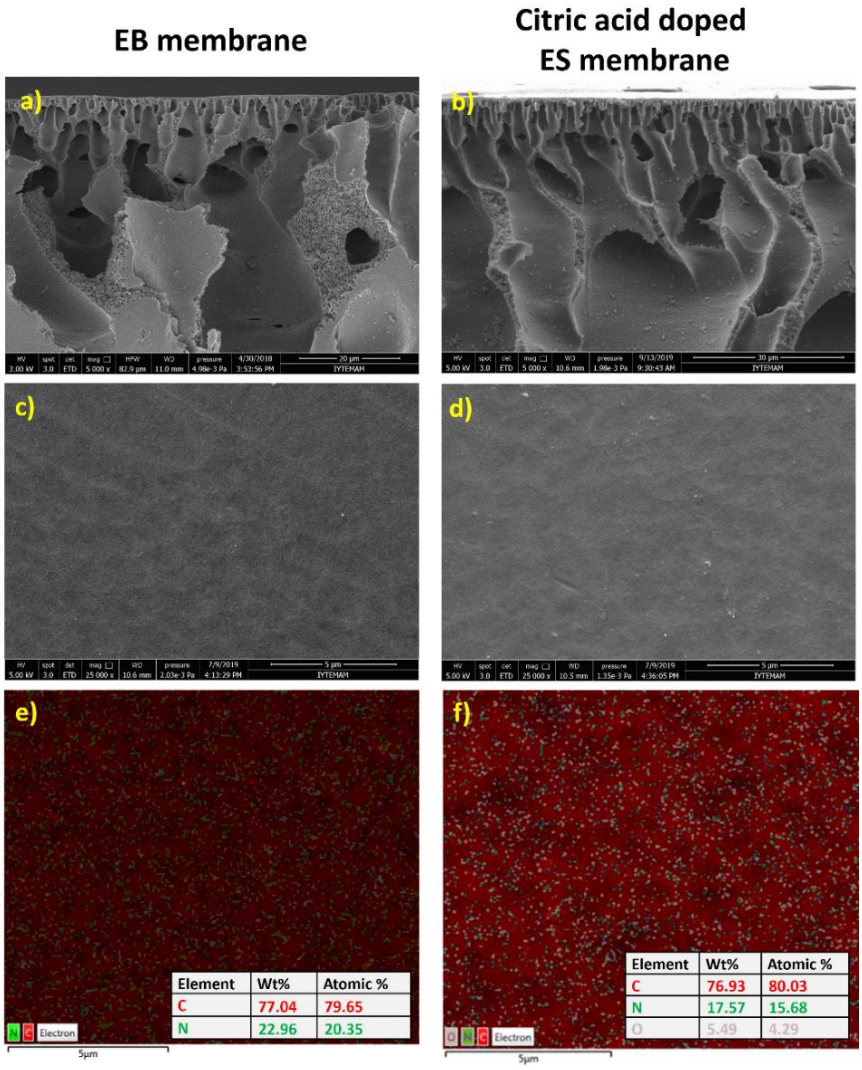

Figure 5.2. SEM cross-sectional images, surface images, and EDX elemental analysis of the EB membrane and the citric acid doped ES membranes

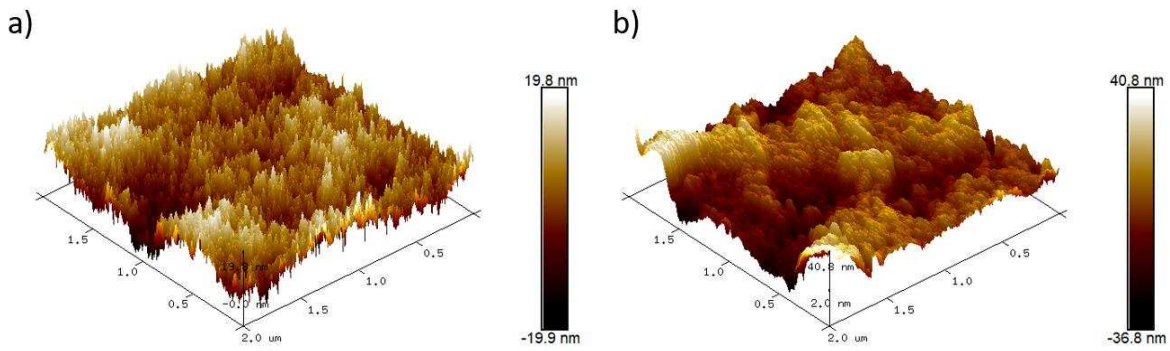

Figure 5.3. AFM images of the a) EB membrane* and b) citric acid doped ES membrane.

*Reprinted from Chemical Engineering Journal, Vol. 389, E. Gungormus, S.A. Altinkaya, "A high-performance acid-resistant polyaniline based ultrafiltration membrane: Application in the production of aluminium sulfate powder from alumina sol". Page 124393, Copyright (2020), with permission from Elsevier.

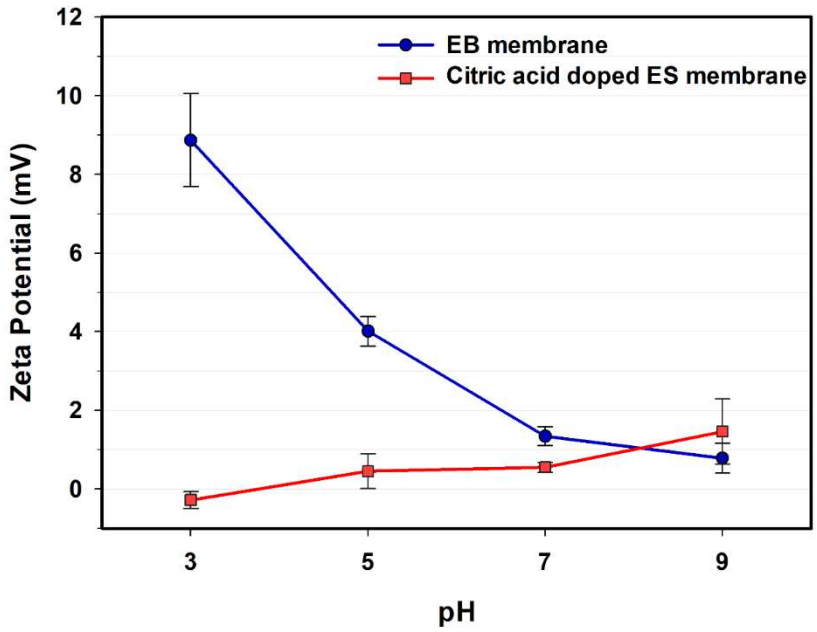

Figure 5.4. Zeta potential as a function of pH for the EB membrane and citric acid doped ES membrane

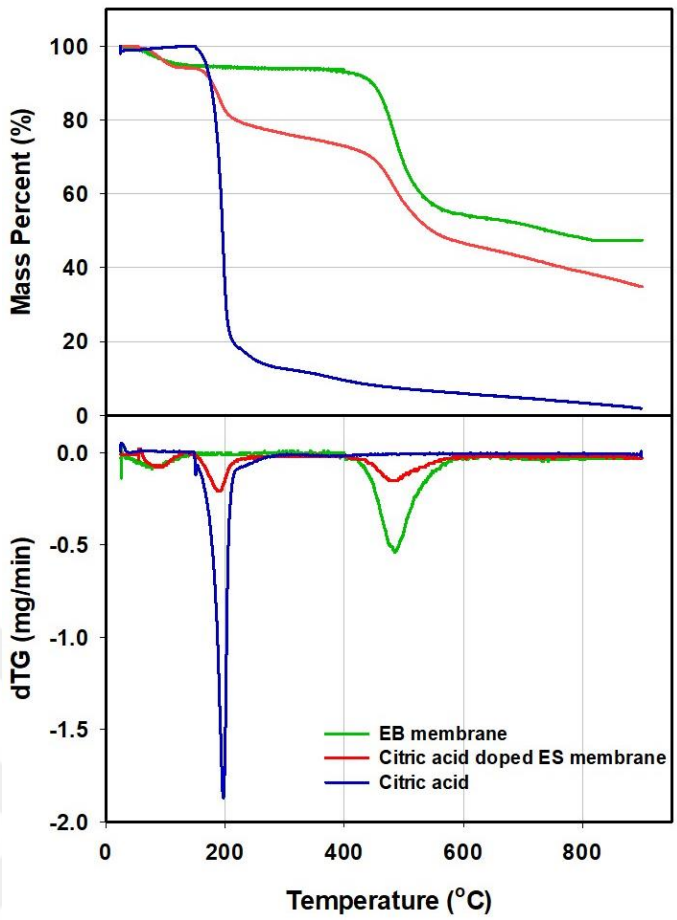

Figure 5.5. TGA and dTG (derivative thermogravimetry) analysis of citric acid, EB membrane, and citric acid doped ES membrane

The *PWP* and *MWCO* values of the unmodified EB membrane decreased from 97.57±1.53 $Lm^{-2}hr^{-1}bar^{-1}$ and 7500 Da (Gungormus and Altinkaya, 2020) to 52.62±0.74 $Lm^{-2}hr^{-1}bar^{-1}$ and 6600 Da upon citric acid doping (Table 5.1). Pore size of the membranes can be accurately estimated by choosing the correct model to evaluate the solute rejection data. If the model solutes used in rejection experiments and membrane surface are charged, then, charge-charge interaction should be considered (Causserand et al., 2004). On the other hand, Causserand et al., 2004 reported that when neutral solutes are used and membrane charge density is low, then, the energy of interaction between the solutes and the membrane can be assumed negligible. We used neutral PEGs as model solutes and at the filtration pH, the membranes are almost neutral (zeta potential value at pH=7: 1.34±0.55 mV for EB membrane and 0.24±0.13 mV for citric acid doped membrane). Therefore, the effect of membrane charge on the pore size calculation was considered negligible. Both the pristine and doped membranes have exhibited higher permeabilities than the commercial membranes with comparable *MWCO* manufactured from different

polymers (Table 5.2). Although citric acid doping enhanced surface hydrophilicity and roughness, the *PWP* decreased after modification. Hydrophilicity increases membrane's water uptake and wettability through enhanced interaction between water molecules and pore wall. On the other hand, since the pore size is on the sub nanometer scale (Table 5.1), water molecules interact stronger with pore walls resulting in increased friction and reduced flow velocity (Xu et al., 2018). Increased surface roughness positively affects the *PWP* by increasing the effective surface area available for permeation of water molecules (Liu and Chen, 2013), however, the results showed that the roughness did not have a dominant effect on the permeability. The decrease in the *PWP* was due to a reduced pore radius from 2.89 nm to 2.52 nm (95th percentile), as shown in Figure 5.6.

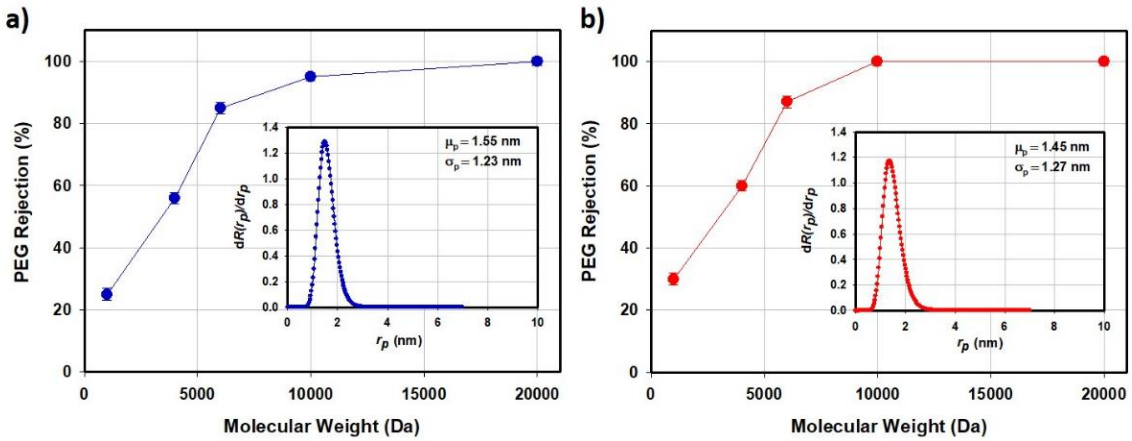

Figure 5.6. The *MWCO* of the a) EB membrane and b) citric acid doped ES membrane

Table 5.2. The *PWP* of commercial membranes with comparable *MWCO* manufactured by different companies

Supplier	**Code**	***MWCO***	**Polymer Type**	**Permeability ($Lm^{-2}hr^{-1}bar^{-1}$)**
Millipore Ultracel	PLC5	5000 Da	Regenerated Cellulose	14.5
	PLCC	5000 Da	Regenerated Cellulose	21.8
Sartorius	RC	5000 Da	Regenerated Cellulose	20
	PES	5000 Da	Regenerated Cellulose	20
TriSep™	UF5	5000 Da	Polyethersulfone	12
	UF10	10000 Da	Polyethersulfone	74
Microdyn™	UP005	5000 Da	Polyethersulfone	10
	UP010	10000 Da	Polyethersulfone	50
Synder™	ST	10000 Da	Polyethersulfone	65-83

5.3.2. Antibacterial Activity of the Membranes

Figure 5.7 shows the antibacterial activities of the pristine and acid-doped membranes against *E.coli* and *S.aureus*. After 24 hr incubation, the EB membrane did not demonstrate inactivation on both bacteria (Figures 5.7.a and 5.7.c). On the other hand, the citric acid doped membrane exhibited excellent antibacterial activity and achieved 100% bacterial inactivation rates (Figures 5.7.b and 5.7.d). The doped membrane was effective even at a short contact time, killed 99% *E.coli* and 70% *S.aureus* in 1 hr (Figure 5.7.f and 5.7.h). *S.aureus* has a thicker peptidoglycan layer (≈30 nm) consisting of a network of crosslinking carbohydrates and peptides (Delcour et al., 1999). This layer acts as a barrier to external stresses; thus, 1 hr contact time was not enough for its disruption. Unlike *S.aureus,* the peptidoglycan layer in *E.coli* is thinner (≈ 10 nm) (Beveridge, 1999), easily disrupted by the ES membrane even in 1 hr contact. The number of bacteria on the EB membrane increased with time (Figures 5.7.a, 5.7.c, 5.7.e, and 5.7.g). Table 5.3 compares the antibacterial activities of different UF membranes against *E.coli* and *S.aureus*. As seen in the table, the initial number of bacteria, incubation time, and membrane area used in these studies vary significantly. A fair comparison of the antibacterial activities is only possible based on the number of bacteria exposed to a 1 cm^2 membrane area. Wang et al., 2014 and Wang et al., 2019b reported 100% and 99.93% *E.coli* inactivation rates at the end of 24 hr incubation. However, the initial number of bacteria used in their study was 10 times lower (1.5×10^4 CFU/cm^2 (Wang et al., 2014) and 2.4×10^3 CFU/cm^2 (Wang et al., 2019b)) than the amount used in our study (11.7×10^4 CFU/cm^2). The inactivation rate of *S.aureus* by different membranes within 24 hr contact varied between 92.6% to 100% (Cihanoğlu and Alsoy Altınkaya, 2020; Kang et al., 2016; Chen et al., 2013; Yu et al., 2020). However, the absence of some critical data such as membrane area or initial bacteria concentration did not allow the comparison of these membrane's performances. We recently developed a polysulfone-sulfonated polyethersulfone UF membrane containing cetyltrimethylammonium bromide (CTAB) as an antibacterial agent (Cihanoğlu and Alsoy Altınkaya, 2020). This membrane was tested under the same conditions as the current study and exhibited 100% and 99.9% inactivation of *E.coli and S.aureus*. Zeng et al., 2016 observed a higher inactivation rate for *S.aureus* (77.9%) within 1 hr incubation than ours (70%). However, their membrane

preparation protocol requires many steps and a large amount of chemical consumption; thus, it cannot be easily scaled up.

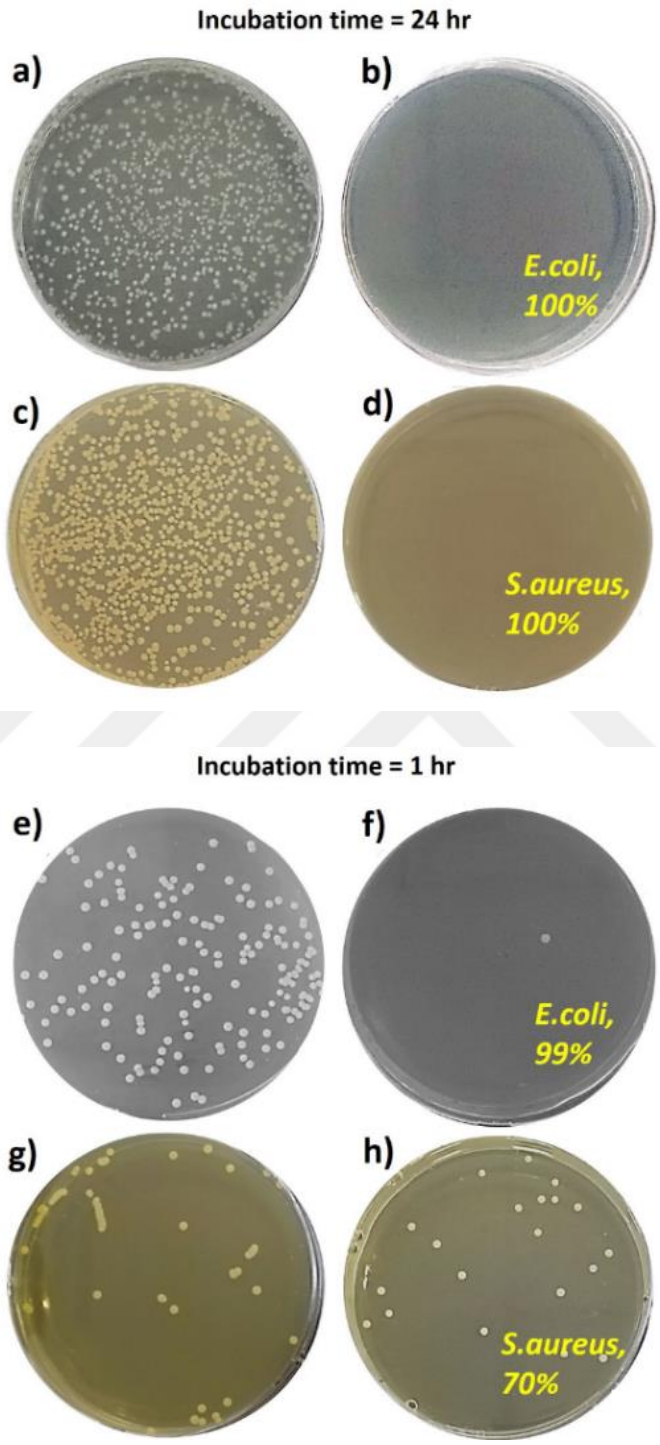

Figure 5.7. Bactericidal rates within (a,b,c,d) 24 hr and (e,f,g,h) 1 hr incubation times for the EB and citric acid doped ES membranes (Bacteria suspensions were diluted 100-fold, before spreading on these plates)

Table 5.3. Static antibacterial activity of the UF membranes in the literature

Membranes	Contact time	Contact area (cm^2)	Volume of bacteria		Bacteria concentration (CFU/mL)		Antibacterial rate (%)		Ref.
			E.coli	*S.aureus*	*E.coli*	*S.aureus*	*E.coli*	*S.aureus*	
PEK-N-Cl	30 min /1 hr	4	20 µL	-	10^6	-	94.6/100	-	Hou et al. (2017)
GOQDs-PVDF	1 hr	2	1 mL	1 mL	10^7	10^7	88.9	77.9	Zeng et al. (2016)
MBHBA/AA-PSF	24 hr	4	100 µL	-	6×10^5	-	100	-	Wang et al. (2014)
PVDF/MWNTs-g-CDDAC	24 hr	-	50 µL	-	10^6	10^6	92.7	95.2	Kang et al. (2016)
(PA-$CuCl_2$)/PSf	4 hr	4	10 ml	-	10^7	-	99	-	Rodríguez et al. (2018)
PS-P4VP-Z	4 hr	-	-	-	10^6	-	73.81	-	Tripathi et al. (2013)
GO-AgNPs	2 hr/4 hr	-	-	-	10^5	-	86/100	-	Sun et al. (2015)
N-PPS, N-T-PPS	18 hr	-	3 ml	-	10^5	-	99	-	Wang et al. (2018)
PDA-b-PBA	48 hr	-	120 ml	120 ml	10^6	10^6	92.70	81.3	Wang et al. (2017)
HPEI-GO/PES	24 hr	-	5 ml	-	10^6	-	74.88	-	Yu et al. (2013)
GO-p-PES	3 hr	1.54	100 µL	-	10^5	-	80	-	Zhang et al. (2018a)
Chitosan/BPPO	12 hr	9	10 ml	-	-	-	70	-	Feng et al. (2014)
HNTs-CS@Ag/PES	24 hr	-	5 ml	5 ml	10^6	10^6	94	92.6	Chen et al. (2013)
MOF-199@PVDF	2 hr	6	100 µL	100 µL	10^6-10^7	10^6-10^7	100	100	Wang et al. (2020)
PSf/PES-AM-VT 1.0	24 hr	3	-	-	-	-	92.3	-	Zhang et al. (2020c)

(Cont. on next page)

Table 5.3. (Cont.)

Membranes	Contact time	Contact area (cm^2)	Volume of bacteria		Bacteria concentration (CFU/mL)		Antibacterial rate (%)		Ref.
			E.coli	*S.aureus*	*E.coli*	*S.aureus*	*E.coli*	*S.aureus*	
PES/SPSf/GO	18 hr	-	45 ml	-	-	-	90	-	Hu et al. (2019)
PSF/GO-Ag	6 hr	6	-	-	10^7	10^7	70.7	61.8	Ali et al. (2019)
rGO-ZnO/PES	3 hr	1.13	100 µL	100 µL	10^6	10^6	95	<10	Zhang et al. (2019b)
PVDF–TiO_2/oxine	3 hr	1.77	-	-	10^8	-	>60	-	Manoharan et al. (2020)
PLA/TiO_2 nfs-15%	24 hr	0.3[a]	2 ml	2 ml	-	-	95	99.9	Yu et al. (2020)
Fe-Al-Mn@chitosan-CA	12 hr	7.5	1 ml	1 ml	10^5	10^5	-[b]	-[b]	Chaudhary and Maiti (2020)
Z-PAEO	8 hr	3.14	20 ml	-	10^6	-	<98	-	Guoet al. (2020)
PI-Ag/CM	24 hr				10^5		99	-	Peng et al. (2020)
MIL-125(Ti)/PVDF	2 hr	-	100 µL	-	-	-	100	-	Zhou et al. (2020)
MSH@UiO-66- NH_2-TFN	3 hr	-	-	-	3×10^5	-	-[b]	-	Gohain et al. (2020)
MQ_{HCMC}	24 hr	9	300 µL	300 µL	3.5×10^6	4.2×10^6	99.84	100	Cihanoğlu and Alsoy Altınkaya (2020)
PSf-g-pMBHBA	24 hr	25	0.1 ml	0.1 ml	6×10^5	-	99.93	-	Wang et al. (2019b)
CA/LCNF 9	24 hr	-	1 ml	-	10^5	-	47	-	Yang et al. (2020)
ZGONH/PES (1.0 wt %)	6 hr	6	10 ml	10 ml	10^6	10^6	81.1	85.7	Ahmad et al. (2020)
EB	24 hr	9	300 µL	300 µL	3.5×10^6	4.2×10^6	-	-	This Study
Citric acid doped ES	24 hr	9	300 µL	300 µL	3.5×10^6	4.2×10^6	100	100	

[a]in the unit of gram, [b] antibacterial rates were not reported

5.3.3. Antibiofouling Performance of the Membranes

We evaluated the antibiofouling properties of the membranes with 5-cycle dynamic bacteria filtration tests. As seen in Figure 5.8, the unmodified EB membrane displayed 70% and 61% flux declines after filtering 935 L/m^2 of *E.coli* and *S.aureus* solutions, respectively. The same filtration scenario resulted in 12% and 21% flux declines for the citric acid doped ES membrane, suggesting that the acid doping provided anti-biofouling property. The flux of the EB membrane decreased continuously during filtration with both bacteria solutions in each cycle. In contrast, the doped ES membrane displayed stable fluxes after the initial drop.

The flux recoveries of the pristine membrane after *E.coli* and *S.aureus* filtration were 52.05±1.09 % and 52.19±1.03 % at the end of the fifth cycle (Figure 5.9). The irreversible biofouling on this membrane increased gradually up to about 48% for both *E.coli* and *S.aureus* filtration. Hence, the bacteria colonization on the surface and increased biofilm thickness over time caused the continuous flux decline for the unmodified membrane (Figure 5.8). As seen in Figure 5.9, the *FRR* for the ES membrane remained constant over 5 filtration cycles. Most fouling on this membrane was reversible and dead bacteria accumulated on the surface were quickly removed after 10 min washing with PBS, resulting in high *FRR* (94.02±1.18% and 92.59±1.10 % at the end of the fifth cycle *E.coli* and *S.aureus* filtrations, respectively).

The accumulation of bacterial population on the pristine EB membrane was clearly observed with SEM pictures, as shown in Figures 5.10.a and 5.10.c. In contrast, the doped membrane surface was free of bacteria (Figures 5.10.b and 5.10.d). The citric acid doping enhanced the surface hydrophilicity, hence, weakened the interaction of bacteria with the surface. Additionally, the nearly net-zero surface charge (Figure 5.4) prevented the electrostatic interaction of the bacteria with the surface. Hence, the anti-adhesion property, combined with the high antibacterial activity, improved the biofouling resistance of the doped membrane (Scheme 5.2). Previous studies also reported higher resistance to cell attachment for hydrophilic, uncharged surfaces (Chiang et al., 2012; Krishnan et al., 2008; Hibbs et al., 2016).

Although many studies tested the biofouling tendency of the membranes with the *E.coli* and *S.aureus* filtration, a fair comparison of the anti-biofouling performances is only possible if the initial fluxes of the membranes are similar. Kim et al., 2012 reported

reduced flux declines with the decreased initial flux of the silver-containing membrane during the filtration of *E.coli* solution. Given this limitation, we only found one study that used the cross-flow filtration and reported the same initial flux as ours (Zhang et al., 2018a). Although the *E.coli* concentration used in our study was 100 times higher (1.3×10^7 CFU/cm^2) than theirs (4.8×10^5 CFU/cm^2) and we used dead-end filtration, the flux declines observed were found similar (12% in this study and 11.5% in the study of Zhang et al., 2018a). In cross-flow, the permeate flux does not drop as fast when compared to dead-end filtration (Koltuniewicz et al., 1995). Thus, our membrane will most probably exhibit even lower flux decline under cross-flow filtration conditions.

Biocidal nanomaterials including silver (Zodrow et al., 2009; Koseoglu-Imer et al., 2013; Sawada et al., 2012), copper (Ben-Sasson et al., 2014), TiO_2 (Mishra and Mukhopadhyay, 2017; Samree et al., 2020), and GO (Hu et al., 2019; Li et al., 2016) are commonly attached to the surface of UF membranes to eliminate biofouling. The synthesis of these nanomaterials requires long preparation steps and the use of harsh chemicals (Zhang et al., 2018a; Patwardhan et al., 2018). Also, most membranes are first functionalized to attach these antibacterial agents (Mukherjee and De, 2018; Makvandi et al., 2021). In contrast, the citric acid used in this study can be easily doped through a simple, one-step filtration without any need for the post treatment of the membrane. Furthermore, the citric acid is from natural sources and there is no hazardous waste generated during the doping process. In conclusion, we propose a green + green solution to the current membrane production due to the source of the antibacterial agent and the simplicity of the doping method (Scheme 5.3).

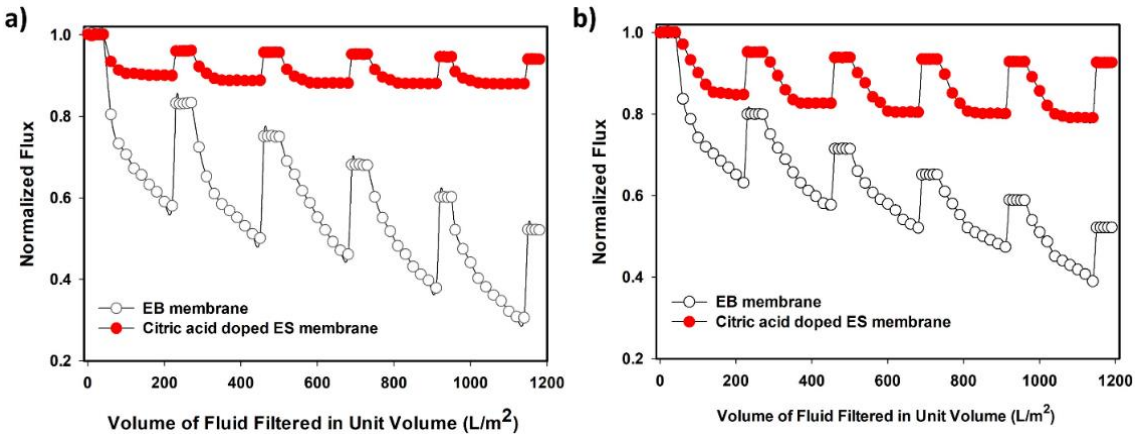

Figure 5.8. Normalized flux of the EB membrane and citric acid doped ES membranes as a function of volume filtered per unit area during a) *E.coli* and b) *S.aureus* filtrations. Initial water fluxes of the membranes: ~50 L/m^{2}hr

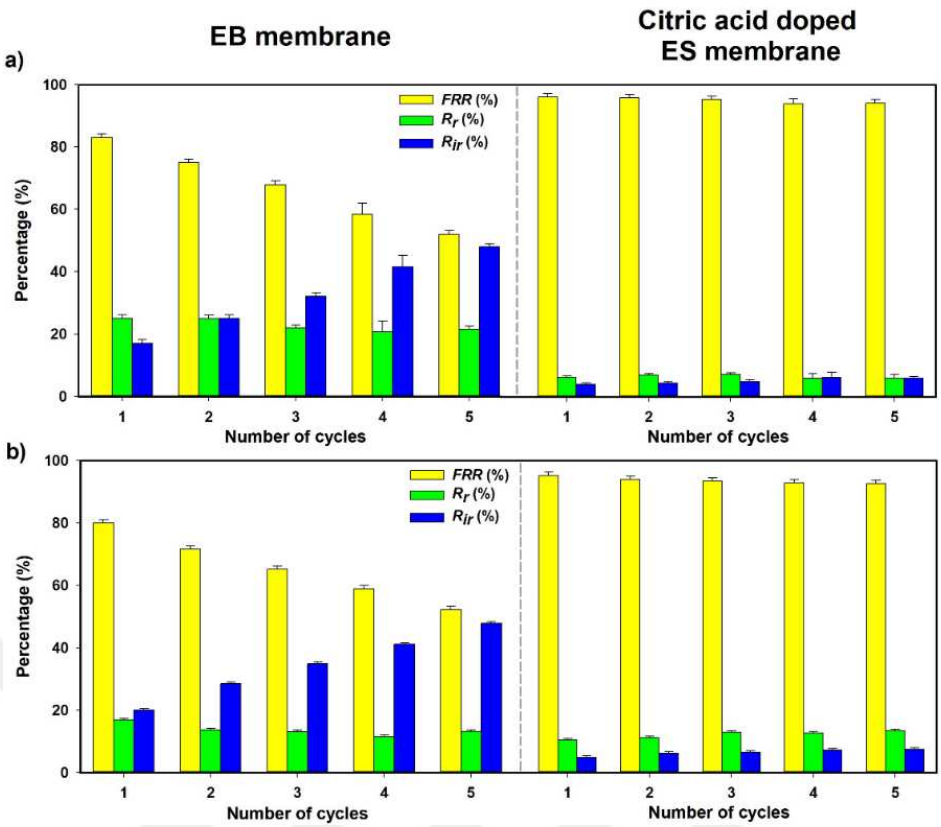

Figure 5.9. Flux recovery ratio and biofouling resistances of the membranes during a) *E.coli* and b) *S.aureus* filtrations

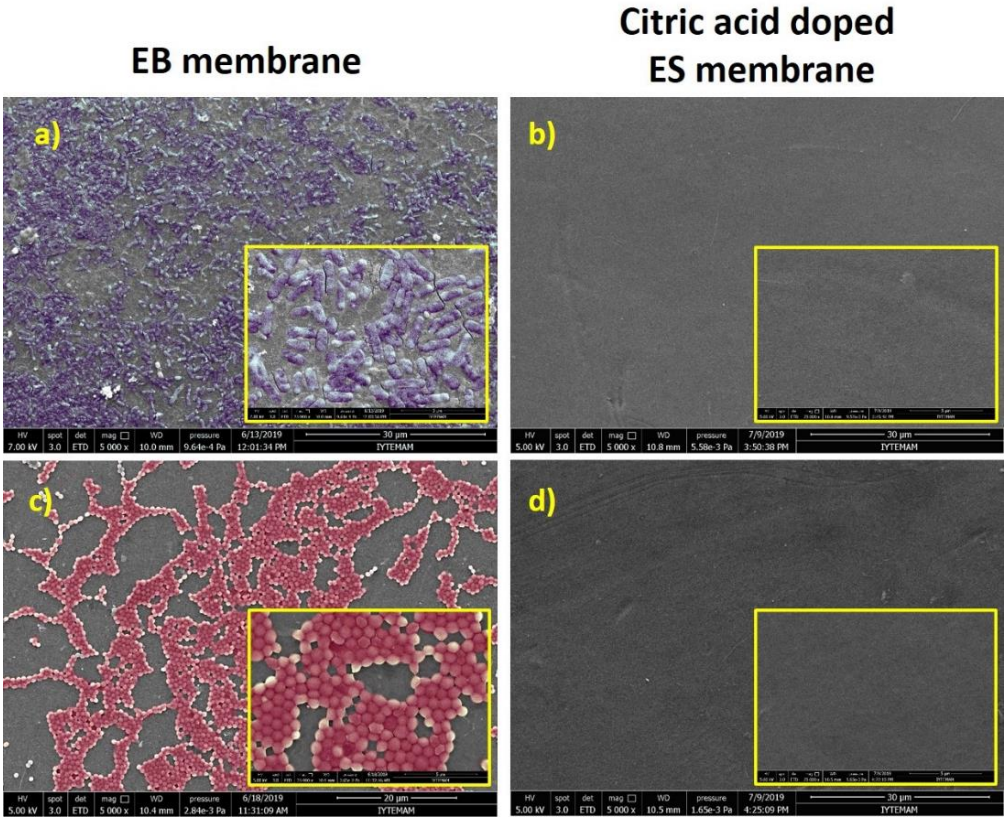

Figure 5.10. Surface SEM images of the membranes at the end of 1st cycle (a,b) *E.coli* and (c,d) *S.aureus* filtrations

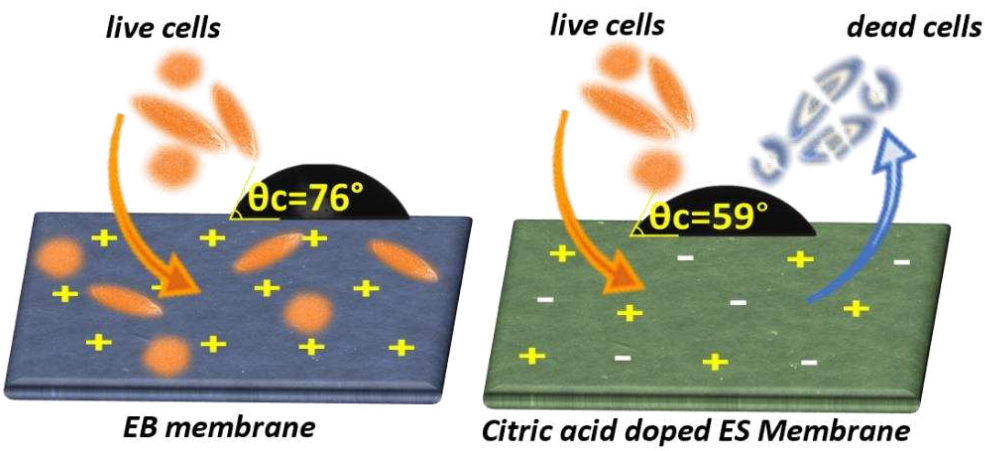

Scheme 5.2. Anti-adhesive properties of the pristine EB and citric acid doped ES membranes

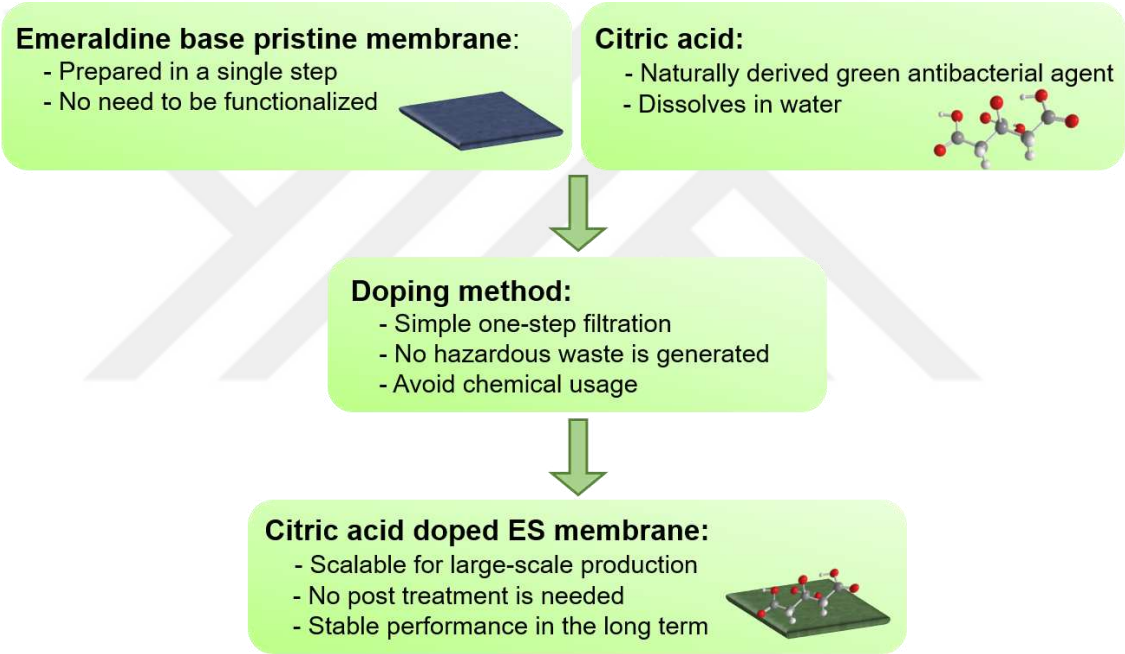

Scheme 5.3. Applied strategies in this study to produce greener membrane

5.3.4. Antibacterial Stability of Citric Acid Doped ES Membrane

Antibacterial membranes kill bacteria through release (release-killing) or direct contact of antibacterial agents with bacteria (contact-killing). We determined the killing mechanism of the citric acid doped membrane in two steps by first determining the amount of citric acid leached from the membrane and then by measuring the antibacterial activity of the leached membrane against *E.coli* and *S.aureus*. The EB membrane contains benzenoid amine and quinonoid imine groups. During doping, the imine groups are

preferentially protonated by citric acid (Kang et al., 1990) resulting in positively charged nitrogen. The ionization product of citric acid, $C_6H_7O_7^-$, then ionically bonds to the positively charged nitrogen as illustrated in Scheme 5.1. We evaluated the leaching of citric acid by storing the membrane in 1 M NaCl solution which represents a harsh environment since high salt concentration can rupture ionic bond (Spruijt et al., 2012). Figure 5.11.a shows that after 5-month storage, a tiny amount, only 1.97% of citric acid loaded to the membrane released into NaCl solution. The leached citric acid consisted of the free acid molecules physically adsorbed to the chains. The released amount did not change between 30 and 150 days, demonstrating the strong bonding of the citric acid to the ES membrane. As shown in Figure 5.11.b, the same *PWP* and the rejection values measured within 5 months of storage also confirmed the stability of the doped membrane. After one-month storage in 1 M NaCl solution, the antibacterial activity of the citric acid doped ES membrane against *E.coli* and *S.aureus* did not change (Figure 5.12), when compared with the fresh counterpart (Figure 5.7.b and 5.7.d). Both the antibacterial activity and leaching test results demonstrated that the citric acid doped membrane kills bacteria through contact killing mode (Scheme 5.4). This conclusion was further supported with the dynamic bacteria filtration studies. The change in antibiofouling property of the citric acid doped membrane during 5-cycle bacteria filtration (filtering 935 L/m^2 of *E.coli* and *S.aureus* solutions) was found negligible (Figure 5.8).

In general, the inactivation of bacteria through contact-killing is described in 4 steps: Binding of antibacterial agents to cell membranes by ionic and/or hydrophobic interactions (Zhang et al., 2016a; Nagandran et al., 2020; Samantaray et al., 2019; Wen et al., 2019b), damage of cell membrane, degradation of DNA and damage of intracellular compartment (Zeiger et al., 2014). Although our data showed that the citric acid doped ES membrane inactivates bacteria through contact-killing mechanism, the exact bactericidal mechanism remains unclear and can be investigated as a comprehensive study in the future.

The antibacterial nanoparticles are commonly used to mitigate the biofilm formation on membrane surfaces through release-killing mechanism. However, their continuous release results in a shorter lasting period of the membrane and may cause toxic effects on the environment and human health. Citric acid has a favorable ecological profile with very low aquatic toxicity and fast biodegradability (Tolls et al., 2009). Considering a minimal amount of citric acid released into high salinity water, we can conclude that the membrane developed in this study does not pose any risk to the

environment. Based on leaching and bacteria filtration tests, it can also be suggested that the anti-biofouling properties of the citric acid doped membrane can be stable in long-term filtration.

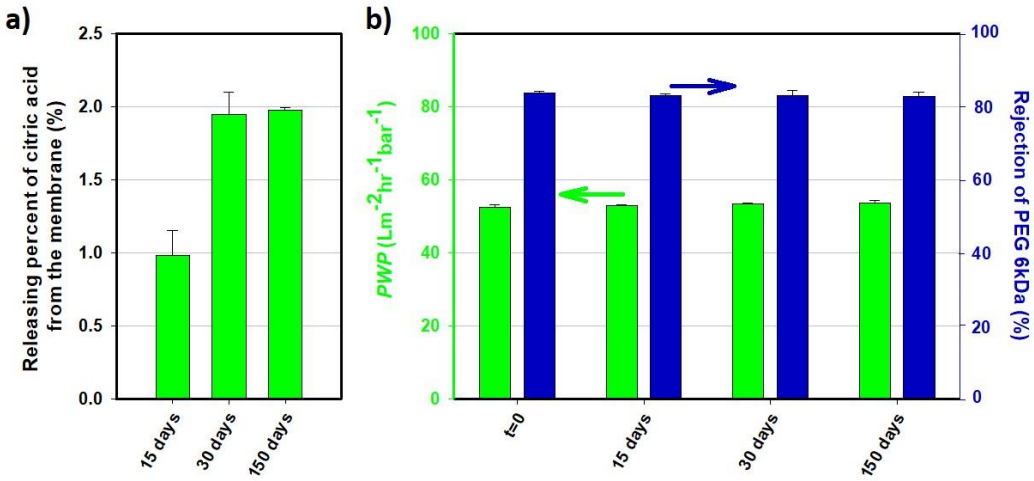

Figure 5.11. Stability test results of citric acid doped ES membrane

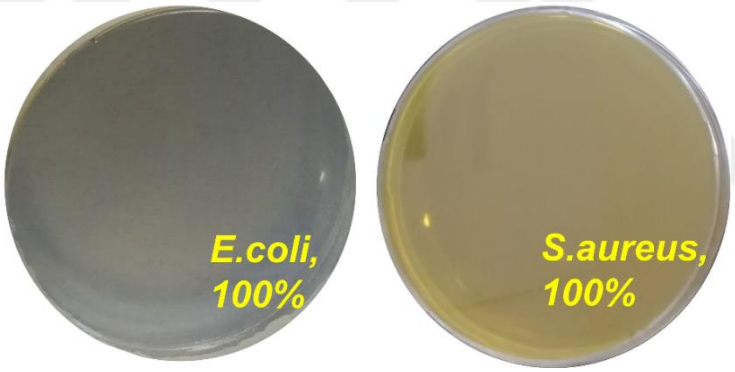

Figure 5.12. Bactericidal rates within 24 hr incubation time for the citric acid doped ES membranes after 1-month storage in 1 M NaCl solution (Bacteria suspensions were diluted 100-fold, before spreading on these plates)

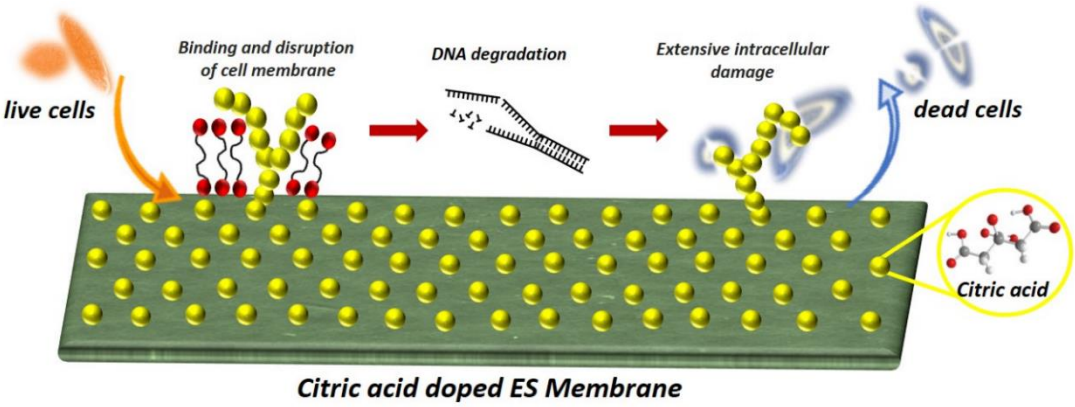

Scheme 5.4. Bacteria killing mechanism of the citric acid doped ES membrane

5.4. Conclusion

The present study aimed to enhance the anti-biofouling performance of the PANI-based UF membrane through citric acid doping. The doping was carried out with a one-step, simple filtration of acid. The doped membrane exhibited excellent antibacterial activity against Gram-negative and Gram-positive bacteria in comparison to the pristine membrane. Improved biofouling resistance resulted from the combination of anti-adhesion and antibacterial properties. Slight flux decline observed for the doped membrane during filtration of bacteria solution was almost fully recovered after washing with PBS. However, the pristine PANI membrane could not inhibit the biofilm formation, and an intense bacterial population remained on its surface at the end of each filtration cycle followed by washing. Leaching experiments demonstrated that the doped citric acid was stable in the structure. Also, the antibacterial activity of the citric acid doped ES membrane against *E.coli* and *S.aureus* did not change after one-month storage in 1 M NaCl solution. The results suggest that the doped ES membrane has a great potential for desalination applications where the biofouling resistance and stability under high salinity are two important criteria for the membrane selection.

Due to the growing concern of global environmental pollution, green synthesis of membranes is needed to reach sustainable development goals. In this respect, we aimed to reduce the number of preparation steps by choosing the right antibacterial agent for the membrane polymer. We used a naturally derived antibacterial agent, and its minor release into the environment does not cause any toxic effect on the aquatic environment. Also, neither the antibacterial agent nor the support membrane requires functionalization before loading. These choices and the protocol adopted in this study contributed to sustainable membrane development. In addition, the scale-up of the protocol is easy for large-scale sustainable production.

CHAPTER 6

CONCLUSION

This thesis study aimed to manufacture high-performance (antifouling /antibiofouling properties), long-term stable, cost-effective membranes needed for water and energy sustainability. The primary motivation was to develop strategies for green membrane production with fast, simple, facile, and easily scalable fabrication procedures that can be adapted for large-scale production.

Chapter 2 reported a new class of acid-resistant UF membrane fabricated from PANI based on its self-acid doping ability. The doped membrane's chemical structure and separation performance were not adversely affected by acid exposure, even after 30 days of exposure to the H_2SO_4 solution under static conditions. The membrane was also tested in realistic conditions through filtration of alumina sol synthesized in a highly acidic H_2SO_4 solution. The results have shown that 99% recovery of the aluminum sulfate particles is possible with the doped PANI membrane due to the hydrophilic, relatively smooth, and antifouling surface created by acid doping. The positive impacts of membrane filtration on the chemical and physical properties of the aluminum sulfate powder and the energy cost were determined by comparing it with the existing drying methods. The features such as long-term acid stability, high particle recovery, low fouling tendency, and low materials and processing costs make acid-doped PANI membrane a potential candidate for producing aluminum sulfate powder from alumina sol. On the other hand, the membrane can also be used in numerous other applications to treat acid-containing feeds.

In Chapter 3, the feasibility of using a membrane to improve the sustainability of silica nanopowder production was demonstrated. Poly (ether imide sulfone) has been used for membrane production due to its superior chemical resistance, high thermal-oxidative stability, and good processability. The membranes were modified with amine-functionalized TiO_2 nanoparticles. The modified membrane demonstrated good long-term leaching stability in 40% ethanol and silica synthesis solution and maintained its permeability and rejection characteristics under static and dynamic conditions. Additionally, recovering 99.5% of the nanoparticles was provided thanks to the high

antifouling property of the membrane. A high flux recovery ratio (> 93%) was obtained by only backwashing with water. Gravity-settling without energy can easily separate silica nanoparticles and water in the backwashing solution. Compared to classical freeze-drying and oven-drying methods, integrating membranes into silica nanopowder production can reduce energy consumption and utility cost. In addition, the solvent and catalyst recovered in the permeate stream can be reused in the synthesis, reducing disposal and purchasing costs. It was shown that membrane-assisted nanopowder production could minimize the adverse effects caused by commonly used conventional drying methods and make the process more sustainable and environmentally friendly.

Chapter 4 reported a novel catalytically active polydopamine-modified poly (ether sulfone) membrane immobilized with an alumina-calcium oxide catalyst. The stability test showed that 95% of the initially loaded particles were still on the surface after storing the membrane in a reactant mixture for up to 1 month. Unchanged biodiesel yields and butanol fluxes of the membrane during one month of storage were other evidence for the catalyst stability. We demonstrated the advantages of the flow-through mode of operation by measuring the biodiesel yields under batch and continuous conditions. During filtration, the biodiesel yield decreased in the first three cycles and stayed constant, while a continuous decrease was observed under static conditions. In each cycle, the equilibrium limitation for the yield was overcome only when the membrane was operated under pressure. We found a strong relationship between the flux and yield declines. Our results demonstrated that the main reason for the decrease in catalytic activities was the fouling on the catalyst surface which was quickly removed by backwashing with butanol. It is concluded that integrating membrane technology can make biodiesel production more cost-effective and environmentally friendly.

Studies in Chapter 5 aimed to enhance the anti-biofouling property of the PANI based UF membrane by utilizing its self-acid doping ability. A naturally derived biodegradable agent, citric acid, was used as a dopant. Acid doping increased the hydrophilicity, made the surface nearly electroneutral, and imparted biocidal characteristics to the membrane. Biofouling was simulated by filtering bacteria suspensions, and reversible fouling on the doped membrane was quickly removed by simple washing, leading to a high flux recovery ratio. The flux, rejection, and antibacterial activity values did not change after being stored in 1 M NaCl solution for up to five months, demonstrating the antibacterial agent's stability. The protocol proposed in this study is fast, simple, facile, and easily scalable for large-scale production. Using a green

antibacterial agent and its loading with a one-step process without consuming chemicals or functionalizing the support makes the proposed method environmentally friendly.

In conclusion, the efforts in developing membranes for nanopowder and biofuel production can help minimize the negative economic and environmental consequences, thus resulting in increasingly green and more sustainable chemical processes. In addition, membrane manufacturing strategies developed in this thesis study can form a basis for large-scale production. This thesis's applications and membrane fabrications have been proven and optimized at the laboratory scale. For future work, we suggest translating the laboratory scale into the pilot scale to validate all the processes and measure data that simulate the industrial scale process.

REFERENCES

Aburabie, J., Villalobos, L.F., Peinemann, K.-V., 2017. Composite membrane formation by combination of reaction-induced and nonsolvent-induced phase separation. Macromol. Mater. Eng. 302, 1700131.

Aburabie, J.H., Puspasari, T., Peinemann, K.-V., 2020. Alginate-based membranes: Paving the way for green organic solvent nanofiltration. J. Membr. Sci. 596, 117615.

Aca-Aca, G., Loría-Bastarrachea, M.I., Ruiz-Treviño, F.A., Aguilar-Vega, M., 2018. Transesterification of soybean oil by PAAc catalytic membrane: Sorption properties and reactive performance for biodiesel production. Renew. Energy 116, 250-257.

Ahmad, N., Samavati, A., Nordin, N., Jaafar, J., Ismail, A.F., Malek, N., 2020. Enhanced performance and antibacterial properties of amine-functionalized ZIF-8-decorated GO for ultrafiltration membrane. Sep. Purif. Technol. 239, 13.

Akin, O., 2021. Butyl esters production from canola oil over heterogeneous base catalysts, Izmir Institute of Technology.

Albrecht, W., Seifert, B., Weigel, T., Schossig, M., Holländer, A., Groth, T., Hilke, R., 2003. Amination of poly(ether imide) membranes using di- and multivalent amines. Macromol. Chem. Phys. 204, 510-521.

Alele, N., Streubel, R., Gamrad, L., Barcikowski, S., Ulbricht, M., 2016. Ultrafiltration membrane-based purification of bioconjugated gold nanoparticle dispersions. Sep. Purif. Technol. 157, 120-130.

Alenazi, N.A., Hussein, M.A., Alamry, K.A., Asiri, A.M., 2017. Modified polyether-sulfone membrane: a mini review. Des. Monomers Polym. 20, 532-546.

Alenazi, N.A., Hussein, M.A., Alamry, K.A., Asiri, A.M., 2018. Nanocomposite-based aminated polyethersulfone and carboxylate activated carbon for environmental application. A real sample analysis. J. Carb. Res. 4, 30.

Ali, A., Drioli, E., Macedonio, F., 2017. Membrane engineering for sustainable development: A perspective. Appl. Sci. 7, 1026.

Ali, F.A.A., Alam, J., Shukla, A.K., Alhoshan, M., Ansari, M.A., Al-Masry, W.A., Rehman, S., Alam, M., 2019. Evaluation of antibacterial and antifouling properties of silver-loaded GO polysulfone nanocomposite membrane against Escherichia coli, Staphylococcus aureus, and BSA protein. React. Funct. Polym. 140, 136-147.

Al-Juboori, R.A., Yusaf, T., 2012. Biofouling in RO system: Mechanisms, monitoring and controlling. Desalination 302, 1-23.

Anand, A., Unnikrishnan, B., Wei, S.-C., Chou, C.P., Zhang, L.-Z., Huang, C.-C., 2019. Graphene oxide and carbon dots as broad-spectrum antimicrobial agents – a mini review. Nanoscale Horiz. 4, 117-137.

Argyle, M.D., Bartholomew, C.H., 2015. Heterogeneous catalyst deactivation and regeneration: a review. Catalyst 5, 145-269.

Asadi Tashvigh, A., Luo, L., Chung, T.-S., Weber, M., Maletzko, C., 2018. A novel ionically cross-linked sulfonated polyphenylsulfone (sPPSU) membrane for organic solvent nanofiltration (OSN). J. Membr. Sci. 545, 221-228.

Asadi Tashvigh, A., Elshof, M.G., Benes, N.E., 2021. Development of thin-film composite membranes for nanofiltration at extreme pH. ACS Appl. Polym. Mater. 3, 5912–5919.

Atchariyawut, S., Feng, C., Wang, R., Jiraratananon, R., Liang, D.T., 2006. Effect of membrane structure on mass-transfer in the membrane gas–liquid contacting process using microporous PVDF hollow fibers. J. Membr. Sci. 285, 272-281.

Atrak, K., Ramazani, A., Taghavi Fardood, S., 2018. Green synthesis of amorphous and gamma aluminum oxide nanoparticles by tragacanth gel and comparison of their photocatalytic activity for the degradation of organic dyes. J. Mater. Sci.: Mater. Electron. 29, 8347-8353.

Ba, C., Langer, J., Economy, J., 2009. Chemical modification of P84 copolyimide membranes by polyethylenimine for nanofiltration. J. Membr. Sci. 327, 49-58.

Bai, L., Wu, H., Ding, J., Ding, A., Zhang, X., Ren, N., Li, G., Liang, H., 2020. Cellulose nanocrystal-blended polyethersulfone membranes for enhanced removal of natural organic matter and alleviation of membrane fouling. Chem. Eng. J. 382, 122919.

Baker, R.W., 2012. Membrane Technology and Applications, 3rd ed., John Wiley and Sons, Ltd., New York, NY.

Barakat, M., 2011, New trends in removing heavy metals from industrial wastewater. Arab. J. Chem. 4, 361-377.

Baskar, G., Aiswarya, R., 2016. Trends in catalytic production of biodiesel from various feedstocks. Renewable Sustainable Energy Rev. 57, 496-504.

Batista, A., Vieira, A., Rodrigues, H.S., Almeida Silva, T., Assunção, R., Beluomini, M., Rezende, H., Hernandez-Terrones, M.G., 2015. Production and physicochemical characterization of methylic and ethylic biodiesel from canola oil. Revista Brasileira de Engenharia de Biossistemas 8, 289.

Beck, A.J., Whittle, J.D., Bullett, N.A., Eves, P., Mac Neil, S., McArthur, S.L., Shard, A.G., 2005. Plasma co-polymerisation of two strongly interacting monomers: acrylic acid and allylamine. Plasma Process. Polym. 2, 641-649.

Beltrán, J.M., Koo-Oshima, S., 2006. Water desalination for agricultural applications. FAO Land and water discussion paper, 5, 48.

Ben-Sasson, M., Zodrow, K.R., Genggeng, Q., Kang, Y., Giannelis, E.P., Elimelech, M., 2014. Surface functionalization of thin-film composite membranes with copper nanoparticles for antimicrobial surface properties. Environ. Sci. Technol. 48, 384-393.

Bernstein, R., Belfer, S., Freger, V., 2011. Bacterial attachment to RO membranes surface-modified by concentration-polarization-enhanced graft polymerization. Environ. Sci. Technol. 45, 5973-5980.

Beveridge, T.J., 1999. Structures of gram-negative cell walls and their derived membrane vesicles. J. Bacteriol. 181, 4725-4733.

Bharathiraja, D.B., Sutha, M., Krishnamoorthy, S., Masi, C., Dinakarkumar, Y., Ramanujam, P.K., 2018. Calcium oxide nanoparticles as an effective filtration aid for purification of vehicle gas exhaust. In Energy, Environment, and Sustainability, pp: 181-192.

Blinova, N.V., Stejskal, J., Trchová, M., Prokeš, J., Omastová, M., 2007. Polyaniline and polypyrrole: A comparative study of the preparation. Eur. Polym. J. 43, 2331-2341.

Blinova, N.V., Stejskal, J., Trchová, M., Prokeš, J., 2008. Control of polyaniline conductivity and contact angles by partial protonation. Polym. Int. 57, 66-69.

Boeva, Z.A., Sergeyev, V.G., 2014. Polyaniline: Synthesis, properties, and application. Polym Sci Ser C 56 (2014) 144-153.

Bonhomme, L., Doyle, J., Greenizen, K., Gagne, G., Devin, S., Lombard, G., Smith, V., Kavonian, M., 2012. Centrifugal Filter, US8357296B2.

Boricha, A.G., Murthy, Z.V.P., 2009. Preparation, characterization, and performance of nanofiltration membranes for the treatment of electroplating industry effluent. Sep. Purif. Technol. 65, 282-289.

Bowen, R.W., Doneva, T.A., 2000. Atomic force microscopy characterization of ultrafiltration membranes: Correspondence between surface pore dimensions and molecular weight cut-off. Surf. Interface Anal. 29, 544-547.

Brundtland, G., 1987. Report of the World Commission on environment and development: Our common future. United Nations General Assembly Document A/42/427.

Burn, S., Hoang, M., Zarzo, D., Olewniak, F., Campos, E., Bolto, B., Barron, O., 2015. Desalination techniques-a review of the opportunities for desalination in agriculture. Desalination 364, 2-16.

Casimiro, M.H., Silva, A.G., Alvarez, R., Ferreira, L.M., Ramos, A.M., Vital, J., 2014. PVA supported catalytic membranes obtained by γ-irradiation for biodiesel production. Radiat. Phys. Chem. 94, 171-175.

Causserand, C., Rouaix, S., Akbari, A., Aimar, P., 2004. Improvement of a method for the characterization of ultrafiltration membranes by measurements of tracers retention. J. Membr. Sci 238, 177-190.

Chaudhary, M., Maiti, A., 2020. Fe-Al-Mn@chitosan based metal oxides blended cellulose acetate mixed matrix membrane for fluoride decontamination from water: Removal mechanisms and antibacterial behavior. J. Membr. Sci. 611, 118372.

Chen, Y., Zhang, Y., Zhang, H., Liu, J., Song, C., 2013. Biofouling control of halloysite nanotubes-decorated polyethersulfone ultrafiltration membrane modified with chitosan-silver nanoparticles. Chem. Eng. J. 228, 12-20.

Cheng, C., Li, S., Zhao, W., Wei, Q., Nie, S., Sun, S., Zhao, C., 2012. The hydrodynamic permeability and surface property of polyethersulfone ultrafiltration membranes with mussel-inspired polydopamine coatings. J. Membr. Sci. 417-418, 228-236.

Chiang, Y.-C., Chang, Y., Higuchi, A., Chen, W.-Y., Ruaan, R.-C., 2009. Sulfobetaine-grafted poly(vinylidene fluoride) ultrafiltration membranes exhibit excellent antifouling property. J. Membr. Sci. 339, 151-159.

Chiang, Y.-C., Chang, Y., Chuang, C.-J., Ruaan, R.-C., 2012. A facile zwitterionization in the interfacial modification of low bio-fouling nanofiltration membranes. J. Membr. Sci. 389, 76-82.

Chougala, L.S., Yatnatti, M.S., Linganagoudar, R.K., Kamble, R., Kadadevarmath, J.S., 2017. A simple approach on synthesis of TiO_2 nanoparticles and its application in dye sensitized solar cells. J. Nano- Electron. Phys. 9, 6.

Cicek, N., Franco, J.P., Suidan, M.T., Urbain, V., 1998. Using a membrane bioreactor to reclaim wastewater. J. Am. Water Works Assoc. 90, 105-113.

Cihanoğlu, A., Alsoy Altınkaya, S., 2018. A facile approach for preparation of positively charged nanofiltration membranes by in-situ crosslinking between polyamide-imide and polyethylenimine. Sep. Purif. Technol 207, 353-362.

Cihanoğlu, A., Schiffman, J.D., Alsoy Altınkaya, S., 2022. Biofouling-resistant ultrafiltration membranes via codeposition of dopamine and cetyltrimethylammonium bromide with retained size selectivity and water flux. ACS Appl. Mater. Interfaces 14, 38116-38131.

Combe, C., Molis, E., Lucas, P., Riley, R., Clark, M.M., 1999. The effect of CA membrane properties on adsorptive fouling by humic acid. J. Membr. Sci. 154, 73-87.

Corzo-González, Z., Loria-Bastarrachea, M., Hernandez Nuñez, E., Aguilar-Vega, M., Gonzalez-Díaz, M., 2017. Preparation and characterization of crosslinked PVA/PAMPS blends catalytic membranes for biodiesel production. Polym. Bull. 74, 2741-2754.

Çakmakce, M., Kayaalp, N., Koyuncu, I., 2008. Desalination of produced water from oil production fields by membrane processes. Desalination 222, 176-186.

Das, R., Ali, S.B.A. Hamid, S. Ramakrishna, Z.Z. Chowdhury, Carbon nanotube membranes for water purification: A bright future in water desalination. Desalination 336 (2014) 97-109.

da Silva Burgal, J., Peeva, L.G., Kumbharkar, S., Livingston, A., 2015. Organic solvent resistant poly(ether-ether-ketone) nanofiltration membranes. J. Membr. Sci. 479, 105-116.

de Souza Araki, M., Coutinho, C.M., Gonçalves, L.A.G., Viotto, L.A., 2010. Solvent permeability in commercial ultrafiltration polymeric membranes and evaluation of the structural and chemical stability towards hexane. Sep. Purif. Technol. 71, 13-21.

Dehghani Kiadehi, A., Jahanshahi, M., Rahimpour, A., Ghoreyshi, A.A., 2014. Fabrication and evaluation of functionalized nano-titanium dioxide (F-NanoTiO_2)/ polysulfone (PSf) nanocomposite membranes for gas separation. IJChE 11, 40-49.

Delcour, J., Ferain, T., Deghorain, M., Palumbo, E., Hols, P., 1999. The biosynthesis and functionality of the cell-wall of lactic acid bacteria. Antonie van Leeuwenhoek 76, 159-184.

Diallo, M.S., Fromer, N.A., Jhon, M.S., 2013. Nanotechnology for sustainable development: retrospective and outlook. J. Nanopart. Res. 15, 2044.

Dittmeyer, R., Svajda, K., Reif, M., 2004. A review of catalytic membrane layers for gas/liquid reactions. Topics in Catalysis 29, 3-27.

Dizge, N., Aydiner, C., Imer, D.Y., Bayramoglu, M., Tanriseven, A., Keskinler, B., 2009. Biodiesel production from sunflower, soybean, and waste cooking oils by transesterification using lipase immobilized onto a novel microporous polymer. Bioresour. Technol. 100, 1983-1991.

Dobosz, K.M., Kuo-LeBlanc, C.A., Emrick, T., Schiffman, J.D., 2019. Antifouling ultrafiltration membranes with retained pore size by controlled deposition of zwitterionic polymers and poly(ethylene glycol). Langmuir 35, 1872-1881.

Dognani, G., Hadi, P., Ma, H., Cabrera, F.C., Job, A.E., 2019. D.L.S. Agostini, B.S. Hsiao, Effective chromium removal from water by polyaniline-coated electrospun adsorbent membrane. Chem. Eng. J. 372, 341-351.

Ebnesajjad, S., 2003. 13 - Properties of Fluoropolymers, in: S. Ebnesajjad (Ed.) Melt Processible Fluoroplastics, William Andrew Publishing, Norwich, NY, 375-447.

Eevera, T., Rajendran, K., Saradha, S., 2009. Biodiesel production process optimization and characterization to assess the suitability of the product for varied environmental conditions. Renew. Energy 34, 762-765.

Endo, N., Takeda, Y., Matsusaki, K., Higa, M., 2001. Separation and concentration of trace ion with polyaniline. Anal. Sci. 17 (2001) i1109-1112.

Enten, A.C., Leipner, M.P.I, Bellavia, M.C., King, L.E., Sulchek, T.A., 2020. Optimizing flux capacity of dead-end filtration membranes by controlling flow with pulse width modulated periodic backflush. Sci. Rep. 10, 896.

Falca, G., Musteata, V.-E., Behzad, A.R., Chisca, S., Nunes, S.P., 2019. Cellulose hollow fibers for organic resistant nanofiltration. J. Membr. Sci. 586, 151-161.

Feng, Y., Lin, X., Li, H., He, L., Sridhar, T., Suresh, A.K., Bellare, J., Wang, H., 2014. Synthesis and characterization of chitosan-grafted BPPO ultrafiltration composite membranes with enhanced antifouling and antibacterial properties. Ind. Eng. Chem. Res. 53, 14974-14981.

Feng, Y., Weber, M., Maletzko, C., Chung, T.-S, 2019, 2019. Fabrication of organic solvent nanofiltration membranes via facile bioinspired one-step modification. Chem. Eng. Sci. 198, 74-84.

Frey, R.G., Halloran, J.W., 1984. Compaction behavior of spray-dried alumina. J. Am. Ceram. Soc. 67, 199-203.

Fu, Z.-J., Wang, Z.-Y., Liu, M.-L., Cai, J., Yuan, P.-A., Wang, Q., Xing, W., Sun, S.-P., 2021. Dual-layer membrane with hierarchical hydrophobicity and transport channels for nonpolar organic solvent nanofiltration. AIChE J. 67, 17138.

Gaborski, T.R., Snyder, J.L., Striemer, C.C., Fang, D.Z., Hoffman, M., Fauchet, P.M., McGrath, J.L., 2010. High-performance separation of nanoparticles with ultrathin porous nanocrystalline silicon membranes. ACS Nano 4, 6973-6981.

Georgopoulou, M., Kontakiotis, E., Nakou, M., 1994. Evaluation of the antimicrobial effectiveness of citric acid and sodium hypochlorite on the anaerobic flora of the infected root canal. Int. Endod. J. 27, 139-143.

Gerstandt, K., Peinemann, K.-V., Skilhagen, S.E., Thorsen, T., Holt, T., 2008. Membrane processes in energy supply for an osmotic power plant. Desalination 224, 64-70.

Gohain, M.B., Pawar, R.R., Karki, S., Hazarika, A., Hazarika, S., Ingole, P.G., 2020. Development of thin film nanocomposite membrane incorporated with mesoporous synthetic hectorite and MSH@UiO-66-NH_2 nanoparticles for efficient targeted feeds separation, and antibacterial performance. J. Membr. Sci. 609, 17.

Gomes, E.C., Oliveira, M.A.S., 2012. Chemical polymerization of aniline in hydrochloric acid (HCl) and formic acid (HCOOH) media. Differences between the two synthesized polyanilines. Am. J. Polym. Sci. 2, 5-13.

Gonzalez-Munoz, M.J., Rodriguez, M.A., Luque, S., Alvarez, J.R., 2006. Recovery of heavy metals from metal industry waste waters by chemical precipitation and nanofiltration. Desalination 200, 742–744.

GRV, Grand View Research, Market analysis report, GVR-1-68038-808-4. https://www. grandviewresearch.com/industry-analysis/nanosilica-market, 2017 (accessed 11 January 2022).

Gungormus, E., Altinkaya, S., 2020. A high-performance acid-resistant polyaniline based ultrafiltration membrane: Application in the production of aluminium sulfate powder from alumina sol. Chem. Eng. J. 389, 124393.

Guo, H., Wang, Z., Liu, Y., Huo, P., Gu, J., Zhao, F., 2020. Synthesis and characterization of novel zwitterionic poly(aryl ether oxadiazole) ultrafiltration membrane with good antifouling and antibacterial properties. J. Membr. Sci. 611, 118337.

Gupta, V., Vinod, C.P., Kulkarni, G.U., Lahiri, G.K., Maity, N., Bhaduri, S., 2005. Polyethersulfone supported titanium complexes as ethylene polymerization catalysts. Curr. Sci. 88, 1162.

Hangzhou Cobetter Filtration Equipment Co Ltd, 2022. Ultrafiltration centrifuge tube assembly, CN216964168U.

Hapońska, M., Nurra, C., Abelló, S., Makkee, M., Salvadó, J., Torras, C., 2019. Membrane reactors for biodiesel production with strontium oxide as a heterogeneous catalyst. Fuel Process. Technol. 185, 1-7.

Harries, R., 1985. A field trial of seeded reverse osmosis for the desalination of a scaling type mine water. Desalination 56, 227-236.

Hatchett, D.W., Josowicz, M., Janata, J., 1999. Acid doping of polyaniline: Spectroscopic and electrochemical studies. J. Phys. Chem. B 103, 10992-10998.

Hayrynen, K., Pongracz, E., Vaisanen, V., Pap, N., Manttari, M., Langwaldt, J., Keiski, R.L., 2009. Concentration of ammonium and nitrate from mine water by reverse osmosis and nanofiltration. Desalination 240, 280–289.

He, M., Gao, K., Zhou, L., Jiao, Z., Wu, M., Cao, J., You, X., Cai, Z., Su, Y., Jiang, Z., 2016. Zwitterionic materials for antifouling membrane surface construction. Acta Biomater. 40, 142-152.

He, M., Yuan, T., Dong, W., Li, P., Jason Niu, Q., Meng, J., 2019. High-performance acid-stable polysulfonamide thin-film composite membrane prepared via spinning-assist multilayer interfacial polymerization. J. Mater. Sci. 54, 886-900.

Hegab, H.M., Zou, L., 2015. Graphene oxide-assisted membranes: Fabrication and potential applications in desalination and water purification. J. Membr. Sci. 484, 95-106.

Hendrix, K., Vanherck, K., Vankelecom, I.F., 2012. Optimization of solvent resistant nanofiltration membranes prepared by the in-situ diamine crosslinking method. J. Membr. Sci. 421, 15-24.

Hendrix, K., Van Eynde, M., Koeckelberghs, G., Vankelecom, I.F.J., 2013. Crosslinking of modified poly(ether ether ketone) membranes for use in solvent resistant nanofiltration. J. Membr. Sci. 447, 212-221.

Hessien, M.M., Rashad, M.M., Zaky, R.R., Abdel-Aal, E.A., ElBarawy, K.A., 2009. Controlling the synthesis conditions for silica nano sphere from semi burned rice straw. Mater. Sci. Eng. B 162, 14-21.

Hibbs, M.R., McGrath, L.K., Kang, S., Adout, A., Altman, S.J., Elimelech, M., Cornelius, C.J., 2016. Designing a biocidal reverse osmosis membrane coating: Synthesis and biofouling properties. Desalination 380, 52-59.

Hoseinpour, H., Peyravi, M., Nozad, A., Jahanshahi, M., 2016. Static and dynamic assessments of polysulfonamide and poly(amide-sulfonamide) acid-stable membranes. J. Taiwan. Inst. Chem. Eng. 67, 453-466.

Hou, R., Zhang, D., Duan, X.X., Wang, X.H., Wang, S.T., Sun, Z., 2016. Fabrication of $H_3PW_{12}O_{40}$/agarose membrane for catalytic production of biodiesel through esterification and transesterification. Rsc Advances 6, 81794-81801.

Hou, S., Dong, X., Zhu, J., Zheng, J., Bi, W., Li, S., Zhang, S., 2017. Preparation and characterization of an antibacterial ultrafiltration membrane with N-chloramine functional groups. J. Colloid Interface Sci. 496, 391-400.

Hu, M.Y., Cui, Z.Y., Li, J., Zhang, L., Mo, Y.H., Dlamini, D.S., Wang, H., He, B.Q., Li, J.X., Matsuyama, H., 2019. Ultra-low graphene oxide loading for water permeability, antifouling and antibacterial improvement of polyethersulfone/sulfonated polysulfone ultrafiltration membranes. J. Colloid Interface Sci. 552, 319-331.

Huang, X., 2011. Separator technologies for lithium–ion batteries. J. Solid State Electrochem. 15, 649-662.

Huang, X., McVerry, B.T., Marambio-Jones, C., Wong, M.C.Y., Hoek, E.M.V., Kaner, R.B., 2015. Novel chlorine resistant low-fouling ultrafiltration membrane based on a hydrophilic polyaniline derivative. J. Mater. Chem. A 3, 8725-8733.

Jalal, T.A., Prada, I.D.C., Tayouo, R., Giannelis, E.P., Nunes, S.P., 2014. Reactive phase inversion for manufacture of asymmetric poly (ether imide sulfone) membranes. React. Funct. Polym. 85, 1-10.

Jung, M.R., Horgen, F.D., Orski, S.V., Rodriguez V., Beers, K.L, Balazs, G.H., Jones, T.T., Work, T.M., Brignac, K.C., Royer, S.-J., Hyrenbach, K.D., Jensen, B.A., Lynch, J.M., 2018. Validation of ATR FT-IR to identify polymers of plastic marine debris, including those ingested by marine organisms. Mar. Pollut. Bullet. 127, 704-716.

Ibrahim, K.A., 2017. Synthesis and characterization of polyaniline and poly(aniline-co-o-nitroaniline) using vibrational spectroscopy. Arab. J. Chem. 10, S2668-S2674.

JCPDS-ICDD, 200. PDF-2 Database, International Centre for Diffraction Data, Pennsylvania.

Jeon, J.-Y., 2012. Permeation properties of thermo-chemically stable ultrafiltration membranes of copoly (bis[4-(3-aminophenoxy)phenyl]sulfone/3,3′,4,4′-benzo phenonetetracarboxyl/pyromellite) imides. Desalination 296, 46-52.

Jeppesen, T., Shu, L., Keir, G., Jegatheesan, V., 2009. Metal recovery from reverse osmosis concentrate. J. Clean. Prod. 17, 703-707.

Juby, G., 1992. Membrane desalination of service water from gold mines. J. South Afr. Inst. Min. Metall. 92, 69.

Junior, M., Silva, L., Claro, P., Sanfelice, R., Oliveira, J., Ugucioni, J.C., Correa, D., Tonoli, G.H.D., 2019. Cellulose nanofibrils modification with polyaniline aiming at enhancing electrical properties for application in flexible electronics. Cellul. Chem. Technol. 53, 775-786.

Kakihana, Y., Cheng, L., Fang, L.-F., Wang, S.-Y., Jeon, S., Saeki, D., Rajabzadeh, S., Matsuyama, H., 2017. Preparation of positively charged PVDF membranes with improved antibacterial activity by blending modification: Effect of change in membrane surface material properties. Colloids Surf, A Physicochem Eng Asp. 533, 133-139.

Kang, B., Li, Y.-D., Liang, J., Yan, X., Chen, J., Lang, W.-Z., 2016. Novel PVDF hollow fiber ultrafiltration membranes with antibacterial and antifouling properties by embedding N-halamine functionalized multi-walled carbon nanotubes (MWNTs). RSC Adv. 6, 1710-1721.

Kang, E.T., Neoh, K.G., Khor, S.H., Tan, K.L., Tan, B.T.G., 1990. X.p.s. studies of charge transfer interactions in some polyaniline complexes. Polym. 31, 202-207.

Kang, E.T., Neoh, K.G., Tan, K.L., 1998. Polyaniline: A polymer with many interesting intrinsic redox states. Prog. Polym. Sci. 23, 277-324.

Kang, G., Cao, Y., Zhao, H., Yuan, Q., 2008. Preparation and characterization of crosslinked poly (ethylene glycol) diacrylate membranes with excellent antifouling and solvent-resistant properties. J. Membr. Sci. 318, 227-232.

Karimi, A., Khataee, A., Safarpour, M., Vatanpour, V.K., 2020. Development of mixed matrix ZIF-8/polyvinylidene fluoride membrane with improved performance in solvent resistant nanofiltration. Sep. Purif. Technol. 237, 116358.

Karkhanechi, H. , Takagi, R., Matsuyama, H., 2014. Enhanced antibiofouling of RO membranes via polydopamine coating and polyzwitterion immobilization. Desalination 337, 23-30.

Khajouei, M., Jahanshahi, M., Peyravi, M., 2018. Biofouling mitigation of TFC membrane by in-situ grafting of PANI/Cu couple nanoparticle. J. Taiwan Inst. Chem. Eng. 85, 237-247.

Kim, D., Salazar, O.R., Nunes, S.P., 2016. Membrane manufacture for peptide separation. Green Chem., 18, 5151-5159.

Kim, D., Nunes, S.P., 2017. Poly(ether imide sulfone) membranes from solutions in ionic liquids. Ind. Eng. Chem. Res. 56, 14914-14922.

Kim, J.H., Cook, M., Park, S.H., Moon, S.J., Kim, J.F., Livingston, A.G., Lee, Y.M., 2018. A compact and scalable fabrication method for robust thin film composite membranes. Green Chem., 20, 1887-1898.

Kim, J., 2020. Recent progress on improving the sustainability of membrane fabrication. J. Membr. Sci. Res. 6, 241-250.

Kim, Y., Rana, D., Matsuura, T., Chung, J.-W., 2012. Towards antibiofouling ultrafiltration membranes by blending silver containing surface modifying macromolecules. Chem. Commun. 48, 693-695.

Koberg, M., Gedanken, A., 2013. Chapter 9 - Using microwave radiation and SrO as a catalyst for the complete conversion of oils, cooked oils, and microalgae to biodiesel. New and Future Developments in Catalysis. S. L. Suib. Amsterdam, Elsevier: 209-227.

Koltuniewicz, A.B., Field, R.W., Arnot, T.C., 1995. Cross-flow and dead-end microfiltration of oily-water emulsion. Part I: Experimental study and analysis of flux decline. J. Membr. Sci. 102, 193-207.

Komlenic, R., 2010. Rethinking the causes of membrane biofouling. Filtr. Sep. 47, 26-28.

Koschuh, W., Thang, V.H., Krasteva, S., Novalin, S., Kulbe, K.D., 2005. Flux and retention behaviour of nanofiltration and fine ultrafiltration membranes in filtrating juice from a green biorefinery: a membrane screening. J. Membr. Sci. 261, 121-128.

Koseoglu-Imer, D.Y., Kose, B., Altinbas, M., Koyuncu, I., 2013. The production of polysulfone (PS) membrane with silver nanoparticles (AgNP): Physical properties, filtration performances, and biofouling resistances of membranes. J. Membr. Sci. 428, 620-628.

Krishnan, S., Weinman, C.J., Ober, C.K., 2008. Advances in polymers for anti-biofouling surfaces. J. Mater. Chem. 18, 3405-3413.

Kumar, R., Ismail, A.F., 2015. Fouling control on microfiltration/ultrafiltration membranes: Effects of morphology, hydrophilicity, and charge. J. Appl. Polym. Sci. 132, 21.

Kwon, S., Messing, G.L., 1997. The effect of particle solubility on the strength of nanocrystalline agglomerates: Boehmite. Nanostruct. Mater. 8, 399-418.

Lackner, M.B., 2015. Kirk-Othmer Encyclopedia of Chemical Technology. Wiley and Sons: New York, NY, USA.

Le Phuong, H.A., Ayob, N.A.I., Blanford, C.F., Rawi, N.F.M., Szekely, G., 2019. Nonwoven membrane supports from renewable resources: Bamboo fiber reinforced poly(lactic acid) composites. ACS Sustain. Chem. Eng7, 11885-11893.

Lee, J.M., Frankiewicz, T.C., 2005. Treatment of produced water with an ultrafiltration (UF) membrane—a field trial. SPE Annual Technical Conference and Exhibition, Society of Petroleum Engineers.

Lee, K.P., Arnot, T.C., Mattia, D., 2011. A review of reverse osmosis membrane materials for desalination—development to date and future potential. J. Membr. Sci. 370, 1-22.

Lee, H., Yanilmaz, M., Toprakci, O., Fu, K., Zhang, X., 2014. A review of recent developments in membrane separators for rechargeable lithium–ion batteries. Energy Environ. Sci. 7, 3857-3886.

Lee, J.S., Saka, S., 2010. Biodiesel production by heterogeneous catalysts and supercritical technologies. Bioresour. Technol. 101, 7191-7200.

Lee, J.S., Heo, S.A., Jo, H.J, Min, B.R., 2016. Preparation and characteristics of cross-linked cellulose acetate ultrafiltration membranes with high chemical resistance and mechanical strength. React. Funct. Polym. 99, 114-121.

Li, H.J., Cao, T.M., Qin, J.J., Jie, X.M., Wang, T.H., Liu, J. H., Yuan, Q., 2006. Development and characterization of anti-fouling cellulose hollow fiber UF membranes for oil–water separation J. Membr. Sci. 279, 328-335.

Li, J., Liu, X., Lu, J., Wang, Y., Li, G., Zhao, F., 2016. Anti-bacterial properties of ultrafiltration membrane modified by graphene oxide with nano-silver particles. J. Colloid Interface Sci. 484, 107-115.

Li, X., Pang, R., Li, J., Sun, X., Shen, J., Han, W., Wang, L., 2013. In situ formation of Ag nanoparticles in PVDF ultrafiltration membrane to mitigate organic and bacterial fouling. Desalination 324, 48-56.

Li, X.L., Zhu, L.P., Zhu, B.K., Xu, Y.Y., 2011. High-flux and anti-fouling cellulose nanofiltration membranes prepared via phase inversion with ionic liquid as solvent. Sep. Purif. Technol. 83, 66-73.

Liang, Y., Li, C., Li, S., Su, B., Hu, M.Z., Gao, X., Gao, C., 2020. Graphene quantum dots (GQDs)-polyethyleneimine as interlayer for the fabrication of high performance organic solvent nanofiltration (OSN) membranes. Chem. Eng. J. 380, 122462.

Lin, J., Ye, W., Baltaru, M.C., Tang, Y.P., Bernstein, N.J., Gao, P., Balta, S., Vlad, M., Volodin, A., Sotto, A., Luis, P., Zydney, A.L., Bruggen, B.V., 2016. Tight ultrafiltration membranes for enhanced separation of dyes and Na_2SO_4 during textile wastewater treatment. J. Membr. Sci. 514, 217-228.

Lipnizki, F., Hausmanns, S., Ten, P.-K., Field, R.W., Laufenberg, G., 1999. Organophilic pervaporation: prospects and performance. Chem. Eng. J. 73, 113-129.

Liu, C., Faria, A.F., Ma, J., Elimelech, M., 2017. Mitigation of biofilm development on thin-film composite membranes functionalized with zwitterionic polymers and silver nanoparticles. Environ. Sci. Technol. 51, 182-191.

Liu, C., Liu, Y., Guo, Y., Wang, C., Hu, Z., Zhang, C., 2019a. High-hydrophilic and salt rejecting PA-g/co-PVP RO membrane via bionic sand-fixing grass for pharmaceutical wastewater treatment. Chem. Eng. J. 357, 269-279.

Liu, F.C., Dong, P., Lu, W., Sun, K., 2019b. On formation of AlOC bonds at aluminum/polyamide joint interface. Appl. Sur. Sci. 466, 202-209.

Liu, M., Yao, G., Cheng, Q., Ma, M., Yu, S., Gao, C., 2012. Acid stable thin-film composite membrane for nanofiltration prepared from naphthalene-1,3,6-trisulfonylchloride (NTSC) and piperazine (PIP). J. Membr. Sci. 415-416, 122-131.

Liu, M.J., Tzou, K., Gregory, R.V., 1994. Influence of the doping conditions on the surface energies of conducting polymers. Synth. Met. 63, 67-71.

Liu, Q., Xu, G.-R.J.D.V., 2016. Graphene oxide (GO) as functional material in tailoring polyamide thin film composite (PA-TFC) reverse osmosis (RO) membranes. Desalination 394, 162-175.

Liu, T.-Y., Bian, L.-X., Yuan, H.-G., Pang, B., Lin, Y.-K., Tong, Y., Van der Bruggen, B., Wang, X.-L., 2015. Fabrication of a high-flux thin film composite hollow fiber nanofiltration membrane for wastewater treatment. J. Membr. Sci. 478, 25-36.

Liu, X.-L., Li, Y.-S., Zhu, G.-Q., Ban, Y.-J., Xu, L.-Y., Yang, W.-S., 2011. An organophilic pervaporation membrane derived from metal–organic framework nanoparticles for efficient recovery of bio-alcohols. Angew. Chem. Int. Ed. 50, 10636- 10639.

Liu, Y., Chen, X., 2013. High permeability and salt rejection reverse osmosis by a zeolite nano-membrane. Phys. Chem. Chem. Phys. 15, 6817-6824.

Liu, Y., Ai, K., Lu, L., 2014. Polydopamine and its derivative materials: Synthesis and promising applications in energy, environmental, and biomedical fields. Chem. Rev. 114, 5057-5115.

Liyanage, D.D., Thamali, R.J.K.A., Kumbalatara, A.A.K., Weliwita, J.A., Witharana, S., 2016. An analysis of nanoparticle settling times in liquids. J. Nanomater. 2016, 7061838.

Loeb, S., Sourirajan, S., 1960. Sea-water demineralization by means of a semipermeable membrane: UCLA Water Resources Center Report WRCC-34, Los Angelos, California.

Lohokare, H.R., Chaudhari, H.D., Kharul, U.K., 2018. Solvent and pH-stable poly(2,5-benzimidazole) (ABPBI) based UF membranes: Preparation and characterizations. J. Membr. Sci. 563, 743-751.

Louie, J.S., Pinnau, I., Ciobanu, I., Ishida, K.P, Ng, A., Reinhard, M., 2006. Effects of polyether–polyamide block copolymer coating on performance and fouling of reverse osmosis membranes. J. Membr. Sci 280, 762-770.

Lotero, E., Liu, Y., Lopez, D.E., Suwannakarn, K., Bruce, D.A., Goodwin, J.G., 2005. Synthesis of biodiesel via acid catalysis. Ind. Eng. Chem. Res. 44, 5353-5363.

Luo, J., Ding, L., Su, Y., Wei, S., Wan, Y., 2010. Concentration polarization in concentrated saline solution during desalination of iron dextran by nanofiltration. J. Memb. Sci. 363, 170-179.

Luo, Q., He, B., Liang, M., Kong, A., Li, J., 2017. Continuous transesterification to produce biodiesel under HTCC/Na_2SiO_3/NWF composite catalytic membrane in flow-through membrane reactor. Fuel 197, 51-57.

Makvandi, P., Iftekhar, S., Pizzetti, F., Zarepour, A., Zare, E.N., Ashrafizadeh, M., Agarwal, T., Padil, V.V.T., Mohammadinejad, R., Sillanpaa, M., Maiti, T.K., Perale, G., Zarrabi, A., Rossi, F., 2021. Functionalization of polymers and nanomaterials for water treatment, food packaging, textile and biomedical applications: a review. Environ. Chem. Lett. 19, 583-611.

Mallevialle, J., Odendaal, P., Wiesner, M.R., 1996. Water treatment membrane processes, New York, McGraw-Hill.

Manoharan, R.K., Ayyaru, S., Ahn, Y.-H., 2020. Auto-cleaning functionalization of the polyvinylidene fluoride membrane by the biocidal oxine/TiO_2 nanocomposite for anti-biofouling properties. New J. Chem. 44, 807-816.

Manttari, M., Nystrom, M., 2004. Ultrafiltration and nanofiltration in the pulp and paper industry using cross-rotational (CR) filters. Water Sci. Technol. 50, 229-238.

Manttari, M., Viitikko, K., Nystrom, M., 2006. Nanofiltration of biologically treated effluents from the pulp and paper industry. J. Membr. Sci. 272, 152-160.

Mao, Z., Cao, Y., Jie, X., Kang, G., Zhou, M., Yuan, Q., 2010. Dehydration of isopropanol–water mixtures using a novel cellulose membrane prepared from cellulose/N-methylmorpholine-N-oxide/H_2O solution. Sep. Purif. Technol., 72, 28-33.

Marino, T., Galiano, F., Molino, A., Figoli, A., 2019. New frontiers in sustainable membrane preparation: Cyrene™ as green bioderived solvent. J. Membr. Sci. 580, 224-234.

Matsuura, T., 2001. Progress in membrane science and technology for seawater desalination—a review. Desalination 134, 47-54.

Max, J.-J., Chapados, C., 2013. Aqueous ammonia and ammonium chloride hydrates: Principal infrared spectra. J. Mol. Struct. 1046, 124-135.

Mazinani, S., Darvishmanesh, S., Ehsanzadeh, A., Van der Bruggena, B., 2017. Phase separation analysis of Extem/solvent/non-solvent systems and relation with membrane morphology. J. Membr. Sci. 526, 301-314.

McKeen, L.W., 2016. 1 - Fluoropolymers, in: L.W. McKeen (Ed.) Fluorinated Coatings and Finishes Handbook (Sec. Ed.), William Andrew Publishing, Oxford, 1-12.

Meisterjahn, B., Wagner, S., von der Kammer, F., Hennecke, D., Hofmann, T., 2016. Silver and gold nanoparticle separation using asymmetrical flow-field flow fractionation: Influence of run conditions and of particle and membrane charges. J. Chromatogr., A 1440, 150-159.

Menardo, C., Nechtschein, M., Rousseau, A., Travers, J.P., Hany, P., 1988. Investigation on the structure of polyaniline: 13C n.m.r. and titration studies. Synth. Met. 25, 311-322.

Meng, J., Cao, Z., Ni, L., Zhang, Y., Wang, X., Zhang, X., Liu, E., 2014. A novel salt-responsive TFC RO membrane having superior antifouling and easy-cleaning properties. J. Membr. Sci. 461, 123-129.

Meng, Z.-H., 2012. Chapter 13 - Molecularly imprinted sol-gel sensors, in: S. Li, Y. Ge, S.A. Piletsky, J. Lunec (Eds.), Molecularly imprinted sensors, Elsevier, Amsterdam, 2012, pp. 303-337.

Meseguer-Lloret, S., Molins-Legua, C., Campíns-Falcó, P., 2005. Selective determination of ammonium in water based on HPLC and chemiluminescence detection. Analytica Chimica Acta 536, 121-127.

Miceli, M., Frontera, P., Macario, A., Malara, A., 2021. Recovery/reuse of heterogeneous supported spent catalysts. Catalyst 11, 591.

Millipore Corporation, 2022. Amicon Ultra-0.5 Centrifugal Filter Unit. https://www.sigmaaldrich.com/TR/en/product/mm/ufc5003 (accessed 10 October 2022).

Minami, K., 1994. A trial of high performance anaerobic treatment on wastewater from a kraft pulp mill. Desalination 98, 273-283.

Mishra, G., Mukhopadhyay, M., 2017. Flux improvement, rejection, surface energy and antibacterial properties of synthesized TiO_2-Mo.HNTs/PVC nanocomposite ultrafiltration membranes. New J. Chem. 41, 15049-15057.

Mojet, B.L., Ebbesen, S.D., Lefferts, L., 2010. Light at the interface: The potential of attenuated total reflection infrared spectroscopy for understanding heterogeneous catalysis in water. Chem. Soc. Rev. 39, 4643-55.

Mudalige, T.K., Qu, H., Sánchez-Pomales, G., Sisco, P.N., Linder, S.W., 2015. Simple functionalization strategies for enhancing nanoparticle separation and recovery with asymmetric flow field flow fractionation. Anal. Chem. 87, 1764-1772.

Mudalip, S.K.A., Bakar, M.R.A., Adam, F., Mudalip, P.J.A., 2013. Structures and hydrogen bonding recognition of mefenamic acid form I crystals in mefenamic acid/ethanol solution. Int. J. Chem. Eng. Appl. 4, 124-128.

Mukherjee, M., De, S., 2018. Antibacterial polymeric membranes: a short review. Environ. Sci. Water Res. Technol. 4, 1078-1104.

Mulder, M., 1996. Basic principles of membrane technology. Kluwer Academic Publisher.

Musa, I.A., 2016. The effects of alcohol to oil molar ratios and the type of alcohol on biodiesel production using transesterification process. Egypt. J. Pet. 25, 21-31.

Nagandran, S., Goh, P.S., Ismail, A.F, Wong, ., T.W., Binti Wan Dagang, W.R.Z., 2020. The recent progress in modification of polymeric membranes using organic macromolecules for water treatment. Symmetry 12, 239.

Nimcevic, D., Puntigam, R., Wörgetter, M., Gapes, J.R., 2000. Preparation of rapeseed oil esters of lower aliphatic alcohols. JAOCS 77, 275-280.

Ogoshi, T., Hasegawa, Y., Aoki, T., Ishimori, Y., Inagi, S., Yamagishi, T., 2011. Reduction of emeraldine base form of polyaniline by Pillar [5] arene based on formation of poly(pseudorotaxane) structure. Macromolecules 44, 7639-7644.

Pappu, V.K.S., Yanez, A.J., Peereboom, L., Muller, E., Lira, C.T., Miller, D.J., 2011. A kinetic model of the Amberlyst-15 catalyzed transesterification of methyl stearate with n-butanol. Bioresour. Technol.102, 4270-4272.

Paramonova, S., 2016. Re-viewing industrial energy-efficiency improvement using a widened system boundary. Doctoral dissertation, Linköping University, Sweden.

Pardal, A.C., Encinar, J.M., González, J.F., Martínez, G., 2010. Transesterification of rapeseed oil with methanol in the presence of various co-solvents. Third International Symposium on Energy from Biomass and Waste, Venice, Italy.

Parida, S.K., Dash, S., Patel, S., Mishra, B.K., 2006. Adsorption of organic molecules on silica surface. Adv. Colloid Interface Sci. 121, 77-110.

Park, S.-H., Kwon, S.J., Shin, M.G., Park, M.S., Lee, J.S., Park, C.H., Park, H., Lee, J.-H., 2018. Polyethylene-supported high performance reverse osmosis membranes with enhanced mechanical and chemical durability. Desalination 436, 28-38.

Patwardhan, S.V., Manning, J.R.H., Chiacchia, M., 2018. Bioinspired synthesis as a potential green method for the preparation of nanomaterials: Opportunities and challenges. Curr. Opin. Green Sustain. Chem. 12, 110-116.

Peng, C., Xing, S., Yuan, Z., Xiao, J., Wang, C., Zeng, J., 2012. Preparation and anti-icing of superhydrophobic PVDF coating on a wind turbine blade. Appl. Surf. Sci. 259, 764-768.

Peng, N., Chung, T.-S., Chng, M.L., Aw, W., 2010. Evolution of ultra-thin dense-selective layer from single-layer to dual-layer hollow fibers using novel Extem® polyetherimide for gas separation. J. Membr. Sci. 360, 48-57.

Peng, S., Chen, Y., Jin, X., Lu, W., Gou, M., Wei, X., Xie, J., 2020. Polyimide with half encapsulated silver nanoparticles grafted ceramic composite membrane: Enhanced silver stability and lasting anti–biofouling performance. J. Membr. Sci. 611, 118340.

Penha, F.M., Rezzadori, K., Proner, M.C., Zanatta, V., Zin, G., Tondo, D.W., de Oliveira, J.V., Petrus, J.C.C., Luccio, M.D., 2015. Influence of different solvent

and time of pre-treatment on commercial polymeric ultrafiltration membranes applied to non-aqueous solvent permeation. Eur. Polym. J. 66, 492-501.

Ping, M., Zhang, X., Liu, M., Wu, Z., Wang, Z., Surface modification of polyvinylidene fluoride membrane by atom-transfer radical-polymerization of quaternary ammonium compound for mitigating biofouling. J. Membr. Sci. 570-571, 286-293.

Platt, S., Nyström, M., Bottino, A., Capannelli, G., 2004. Stability of NF membranes under extreme acidic conditions. J. Membr. Sci. 239, 91-103.

Ponthieu, E., Payen, E., Pajonk, G.M., Grimblot, J., 1997. Comparison of drying procedures for the preparation of alumina powders with the system Al-alkoxide/tertiary butanol/water. J. Sol-Gel Sci. Technol. 8, 201-206.

Prince, J.A., Bhuvana, S., Anbharasi, V., Ayyanar, N., Boodhoo, K.V.K, Singh, G., 2014. Self-cleaning Metal Organic Framework (MOF) based ultrafiltration membranes - A solution to bio-fouling in membrane separation processes. Sci. Rep. 4, 6555.

Purvis, B., Mao, Y., Robinson, D., 2019. Three pillars of sustainability: in search of conceptual origins. Sustain. Sci. 14, 681-695.

Qin, J.J., Wai, M.N., Do, M.H., 2005. Integrated ultrafiltration/nanofiltration process for reclamation of wastewater from metal plating industry. Abstr. Pap. Am. Chem. Soc. 229, U924-U924.

Qin, L., Yang, L., Yang, J., Weber, R., Ranguelova, K., Liu, X., Lin, B., Li, C., Zheng, M., Liu, G., 2021. Photoinduced formation of persistent free radicals, hydrogen radicals, and hydroxyl radicals from catechol on atmospheric particulate matter. iScience 24, 102193.

Qu, P., Tang, H., Gao, Y., Zhang, L., Wang, S., 2010. Polyethersulfone composite membrane blended with cellulose fibrils. BioResources 5, 14.

Rahman, I.A., Vejayakumaran, P., Sipaut, C.S., Ismail, J., Bakar, M.A., Adnan, R., Chee, C.K., 2007. An optimized sol–gel synthesis of stable primary equivalent silica particles. Colloids Surf. A Physicochem. Eng. Asp. 294, 102-110.

Rahman, I.A., Vejayakumaran, P., Sipaut, C.S., Ismail, J., Chee, J.K., 2008. Effect of the drying techniques on the morphology of silica nanoparticles synthesized via sol–gel process. Ceram. Int. 34, 2059-2066.

Rajasekharan, V., Viswanathan, S., Manisankar, P., 2013. Electrochemical evaluation of anticorrosive performance of organic acid doped polyaniline based coatings. Int. J. Electrochem. Sci. 8, 11327-11336.

Rasool, M.A., Vankelecom, I.F.J., 2019. Use of γ-valerolactone and glycerol derivatives as bio-based renewable solvents for membrane preparation. Green Chem. 21, 1054–1064.

Razali, M., Kim, J.F., Attfield, M., Budd, P.M., Drioli, E., Lee, Y.M., Szekely, G., 2015. Sustainable wastewater treatment and recycling in membrane manufacturing. Green Chem. 17, 5196-5205.

Razi, F., Sawada, I., Ohmukai, Y., Maruyama, T., Matsuyama, H., 2012a. The improvement of antibiofouling efficiency of polyethersulfone membrane by functionalization with zwitterionic monomers. J. Membr. Sci. 401-402, 292-299.

Razi, F., Sawada, I., Ohmukai, Y., Maruyama, T., Matsuyama, H., 2012b. Surface functionalization by grafting (2-Dimethylamino)ethyl methacrylate methyl chloride quaternary salt (DMAEMAq) onto hollow fiber polyethersulfone (PES) membranes for improvement of antibiofouling properties. Solvent Extr. Res. Dev. Jpn. 19,101-115.

Ren, W., Ai, Z., Jia, F., Zhang, L., Fan, X., Zou, Z., 2007. Low temperature preparation and visible light photocatalytic activity of mesoporous carbon-doped crystalline TiO_2. Appl. Catal. B 69, 138-144.

Ricci, B.C., Ferreira, C.D., Aguiar, A.O., Amaral, M.C.S., 2015. Integration of nanofiltration and reverse osmosis for metal separation and sulfuric acid recovery from gold mining effluent. Sep. Purif. Technol. 154, 11-21.

Ricci, B.C., Ferreira, C.D., Marques, L.S., Martins, S.S., Reis, B.G., Amaral, M.C.S., 2017. Assessment of the chemical stability of nanofiltration and reverse osmosis membranes employed in treatment of acid gold mining effluent. Sep. Purif. Technol. 174, 301-311.

Rimbu, G., Stamatin, I., Jackson, C.L., Scott, K., 2006. The morphology control of polyaniline as conducting polymer in fuel cell technology. J. Optoelectron. Adv. Mater. 8, 670-674.

Rodríguez, B., Oztürk, D., Rosales, M., Flores, M., García, A.J.J.o.M.S., 2018. Antibiofouling thin-film composite membranes (TFC) by in situ formation of Cu-(m-phenylenediamine) oligomer complex. Biomaterials 53, 6325-6338.

Rubio, F., Rubio, J., Oteo, J.L., 1998. A FT-IR study of the hydrolysis of tetraethylorthosilicate (TEOS). Spectrosc. Lett. 31, 199-219.

Rundquist, E.M., Pink, C.J., Livingston, A.G., 2012. Organic solventnanofiltration: a potential alternative to distillation for solvent recovery from crystallisation mother liquors. Green Chem. 14, 2197-2205.

Saeki, D., Tanimoto, T., Matsuyama, H., 2014. Anti-biofouling of polyamide reverse osmosis membranes using phosphorylcholine polymer grafted by surface-initiated atom transfer radical polymerization. Desalination 350, 21-27.

Samantaray, P.K., Madras, G., Bose, S., 2019. The key role of modifications in biointerfaces toward rendering antibacterial and antifouling properties in polymeric membranes for water remediation: A critical assessment. Adv. Sustain. Syst 3, 1900017.

Samree, K., Srithai, P.-u., Kotchaplai, P., Thuptimdang, P., Painmanakul, P., Hunsom, M., Sairiam, S., 2020. Enhancing the antibacterial properties of PVDF membrane by hydrophilic surface modification using titanium dioxide and silver nanoparticles. Membranes 10, 289.

Sawada, I., Fachrul, R., Ito, T., Ohmukai, Y., Maruyama, T., Matsuyama, H., 2012. Development of a hydrophilic polymer membrane containing silver nanoparticles with both organic antifouling and antibacterial properties. J. Membr. Sci. 387-388, 1-6.

Saxena, M., Ray, P., Singh, P.S., Bhattacharya, A., 2015. Studies towards understanding the effect of hexane on polysulfone membranes. Polym. Bull. 72, 2157-2169.

Seyedpour, S.F., Rahimpour, A., Najafpour, G., 2019. Facile in-situ assembly of silver-based MOFs to surface functionalization of TFC membrane: A novel approach toward long-lasting biofouling mitigation. J. Membr. Sci. 573, 257-269.

Shen, J., Shahid, S., Sarihan, A., Patterson, D.A., Emanuelsson, E.A.C, 2018. Effect of polyacid dopants on the performance of polyaniline membranes in organic solvent nanofiltration, Sep. Purif. Technol. 204, 336-344.

Sherwood J., De bruyn, M., Constantinou, A., Moity, L., McElroy, C.R., Farmer, T.J., Duncan, T., Raverty, W., Hunta A.J., Clark, J.H., 2014. Dihydrolevoglucosenone (Cyrene) as a bio-based alternative for dipolar aprotic solvents. Chem. Commun. 50, 9650-9652.

Shi, W., He, B., Ding, J., Li, J., Yan, F., Liang, X., 2010. Preparation and characterization of the organic–inorganic hybrid membrane for biodiesel production. Bioresour. Technol. 101, 1501-1505.

Shi, W., He, B., Li, J., 2011. Esterification of acidified oil with methanol by SPES/PES catalytic membrane. Bioresour. Technol. 102, 5389-5393.

Shi, W., He, B., Cao, Y., Li, J., Yan, F., Cui, Z., Zou, Z., Guo, S., Qian, X., 2013. Continuous esterification to produce biodiesel by SPES/PES/NWF composite catalytic membrane in flow-through membrane reactor: Experimental and kinetic studies. Bioresour. Technol. 129, 100-107.

Shi, W., Yang, M., Li, H., Zhou, R., Zhang, H., 2015. Preparation and characterization of sulfonated poly (ether sulfone) (SPES)/Phosphotungstic acid (PWA) hybrid membranes for biodiesel production. Catal. Lett. 145, 1581–1590.

Shi, W., Li, H., Zhou, R., Qin, X., Zhang, H., Su, Y., Du, Q., 2016a. Preparation and characterization of phosphotungstic acid/PVA nanofiber composite catalytic membranes via electrospinning for biodiesel production. Fuel 180, 759-766.

Shi, W., Li, H., Zhou, R., Zhang, H., Du, Q., 2016b. Biodiesel production from soybean oil by quaternized polysulfone alkali-catalyzed membrane. Bioresour. Technol. 210, 43-48.

Shi, W., Li, H., Yu, B., Zhang, H., Su, Y., 2021. Biodiesel production catalyzed by polyvinyl guanidineacetic membrane. Catal. Lett. 151, 153-163.

Shi, W., Li, T., Li,H., Du, Q., Zhang, H., Qin, X., 2022. Continuous biodiesel production from acidic oil using a combination of the acid-, alkali-catalyzed membrane and GO/PVDF separation membrane. J. Ind. Eng. Chem. 107, 268-279.

Shinde, D.B, Cao, L., Wonanke, A.D.D., Li, X., Kumar, S., Liu, X., Hedhili, M.N., Emwas, A.-H., Addicoat, M., Huang, K.-W., Lai, Z., 2020. Pore engineering of ultrathin covalent organic framework membranes for organic solvent nanofiltration and molecular sieving. Chem. Sci. 11, 5434-5440.

Shuit, S.H., Ong, Y.T., Lee, K.T., Subhash, B., Tan, S.H., 2012. Membrane technology as a promising alternative in biodiesel production: A review. Biotechnol. Adv. 30, 1364-1380.

Singh, S., Khulbe, K.C., Matsuura, T. , Ramamurthy, P. , 1998. Membrane characterization by solute transport and atomic force microscopy. J. Membr. Sci. 142, 111-127.

Skilhagen, S.E., Dugstad, J.E., Aaberg, R.J., 2008. Osmotic power–power production based on the osmotic pressure difference between waters with varying salt gradients. Desalination 220, 476-482.

Smith, J.J., Wayman, B.E., 1986. An evaluation of the antimicrobial effectiveness of citric acid as a root canal irrigant. J. Endod. 12, 54-58.

Soleimani Dorcheh, A., Abbasi, M.H., 2008. Silica aerogel; Synthesis, properties and characterization. J. Mater. Process. Technol. 199, 10-26.

Soroko, I., Bhole, Y., Livingston, A.G., 2011. Environmentally friendly route for the preparation of solvent resistant polyimide nanofiltration membranes. Green Chem. 13, 162-168.

Spruijt, E., van den Berg, S.A., Stuart, M.A.C., van der Gucht, J., 2012. Direct measurement of the strength of single ionic bonds between hydrated charges. ACS Nano 6, 5297–5303.

Su, L.-C., Xie, Z., Zhang, Y., Nguyen, K.T., Yang, J., 2014. Study on the Antimicrobial properties of citrate-based biodegradable polymers. Front Bioeng. Biotechnol. 2, 23-23.

Sun, S.P., Hatton, T.A., Chung, T.-S., 2011. Hyperbranched polyethyleneimine induced cross-linking of polyamide−imide nanofiltration hollow fiber membranes for effective removal of ciprofloxacin. Environ. Sci. Technol. 45, 4003-4009.

Sun, X.-F., Qin, J., Xia, P.-F., Guo, B.-B., Yang, C.-M., Song, C., Wang, S.-G., 2015. Graphene oxide–silver nanoparticle membrane for biofouling control and water purification. Chem. Eng. J. 281, 53-59.

Szekely, G., Jimenez-Solomon, M.F., Marchetti, P., Kima, J.F., Livingston, A.G., 2014. Sustainability assessment of organic solvent nanofiltration: from fabrication to application. Green Chem. 16, 4440-4473.

Steiner, T., 2002. The hydrogen bond in the solid state. Angew. Chem. Int. Ed. 41, 48-76.

Tasselli, F., 2016. Non-solvent induced phase separation process (NIPS) for membrane preparation, in: E. Drioli, L. Giorno (Eds.) Encyclopedia of Membranes. Springer, Boston, MA.

Thangaraj, B., Solomon, P., Muniyandi, B., Srinivasan, R., Lin, L., 2018. Catalysis in biodiesel production-a review. Clean Energy 3.

Thuy, N.T., Minh, D.L., 2012. Size effect on the structural and magnetic properties of nanosized Perovskite $LaFeO_3$ prepared by different methods. Adv. Mater. Sci. Eng. 380306.

Tian, F., Xu, B., Li, Y., Deng, J., Zhang, H., Peng, R., 2020. A highly active, readily synthesized and easily separated graphene oxide (GO)/Polyethersulfone (PES) catalytic membrane for biodiesel production. Chemistry Select 5, 1676-1682.

Tolls, J., Berger, H., Klenk, A., Meyberg, M., Müller, R., Rettinger, K., Steber, J., 2009. Environmental safety aspects of personal care products--a European perspective. Environ. Toxicol. Chem. 28, 2485-2489.

Trchová, **M.,** Šeděnková, **I.,** Tobolková, **E.,** Stejskal, **J., 2004.** FTIR spectroscopic and conductivity study of the thermal degradation of polyaniline films**.** Polym. Degrad. Stab. 86**,** 179-185.

Tripathi, B.P., Dubey, N.C., Choudhury, S., Simon, F., Stamm, M., 2013. Antifouling and antibiofouling pH responsive block copolymer based membranes by selective surface modification. J. Mater. Chem. B 1, 3397-3409.

Trimm, D., 2001. The regeneration or disposal of deactivated heterogeneous catalysts. Appl Catal A-Gen 212, 153-160.

Trimpert, C., Boese, G., Albrecht, W., Richau, K., Weigel, T., Lendlein, A., Growth, T., 2006. Poly(ether imide) membranes modified with poly(ethylene imine) as potential carriers for epidermal substitutes. Macromol. Biosci. 6, 274-284.

Tsai, W.-B., Chien, C.-Y., Thissen, H., Lai, J.-Y., 2011. Dopamine-assisted immobilization of poly(ethylene imine) based polymers for control of cell–surface interactions. Acta Biomaterialia 7, 2518-2525.

Turkkul, B., Deliismail, O., Seker, E., 2020. Ethyl esters biodiesel production from Spirulina sp. and Nannochloropsis oculata microalgal lipids over alumina-calcium oxide catalyst. Renew. Energy 145, 1014-1019.

Umdu, E.S., 2008. Methyl ester production from vegetable oils on heterogeneous basic catalysts, Izmir Institute of Technology.

Ursino, C., Simone, S., Donato, L., Santoro, S., De Santo, M.P., Drioli, E., Di Nicolòb, E., Figoli, A., 2016. ECTFE membranes produced by non-toxic diluents for organic solvent filtration separation. RSC Advances 6, 81001-81012.

USEPA, 2008. Environmental Laws Applicable to Construction and Operation of Biodiesel Production Facilities, EPA-907-B-08-001. US Environmental Protection Agency, Washington, DC.

Van Goethem, C., Mertens, M., Cirujano, F.G., Seo, J.W., De Vos, D., Vankelecom, I.F.J., 2018. Improved MOF nanoparticle recovery and purification using crosslinked PVDF membranes. Chem. Commun. 54, 7370-7373.

Vankelecom, I.F.J., 2002. Polymeric Membranes in Catalytic Reactors. Chem. Rev. 102, 3779-3810.

Vanherck, K., Koeckelberghs, G., Vankelecom, I.F.J., 2013. Crosslinking polyimides for membrane applications: A review. Prog. Polym. Sci. 38, 874-896.

Varma, H.K., Mani, T.V., Damodaran, A.D., Warrier, K.G., Balachandran, U., 1994. Characteristics of alumina powders prepared by spray-drying of boehmite sol. J. Am. Ceram. Soc. 77, 1597-1600.

Vicente, G., Martínez, M., Aracil, J., 2004. Integrated biodiesel production: a comparison of different homogeneous catalysts systems. Bioresour. Technol. 92, 297-305.

Wang, C., Li, Z., Cao, L., Cheng, B.J.M.R., 2018. A superhydrophilic and anti-biofouling polyphenylene sulfide microporous membrane with quaternary ammonium salts. Macromol. Res. 26, 800-807.

Wang, H., Wei, Z., Wang, H., Jiang, H., Li, Y., Wu, C., 2019a. An acid-stable positively charged polysulfonamide nanofiltration membrane prepared by interfacial polymerization of polyallylamine and 1,3-benzenedisulfonyl chloride for water treatment. RSC Adv. 9, 2042-2054.

Wang, H.-T., Ao, D., Lu, M.-C., Chang, N., 2020. Alteration of the morphology of polyvinylidene fluoride membrane by incorporating MOF-199 nanomaterials for improving water permeation with antifouling and antibacterial property. J. Chin. Chem. Soc. 67, 1807-1817.

Wang, J., Sun, H., Gao, X., Gao, C., 2014. Enhancing antibiofouling performance of polysulfone (PSf) membrane by photo-grafting of capsaicin derivative and acrylic acid. Appl. Surf. Sci. 317, 210-219.

Wang, J., Wang, Z., Wang, J., Wang, S., 2015. Improving the water flux and bio-fouling resistance of reverse osmosis (RO) membrane through surface modification by zwitterionic polymer. J. Membr. Sci. 493, 188-199.

Wang, Q., Wang, J., Gao, X., Yu, H., Ma, Z., Zhang, Y., Gao, C., 2019b. Antibiofouling polysulfone ultrafiltration membranes via surface grafting of capsaicin derivatives. Water Sci. Technol. 79, 1821-1832.

Wang, S., Liu, F., Gao, C., Wan, T., Wang, L., Wang, L., Wang, L., 2019c. Enhancement of the thermoelectric property of nanostructured polyaniline/carbon nanotube composites by introducing pyrrole unit onto polyaniline backbone via a sustainable method. Chem. Eng. J. 370, 322-329.

Wang, S.-Y., Fang, L.-F., Zhu, B.-K., Matsuyama, H., 2021. Enhancing the antifouling property of polymeric membrane via surface charge regulation. J. Colloid Interface Sci. 593, 315-322.

Wang, X., Jing, S., Liu, Y., Liu, S., Tan, Y., 2017. Diblock copolymer containing bioinspired borneol and dopamine moieties: Synthesis and antibacterial coating applications. Polymer 116, 314-323.

Weatherly, C.A., Woods, R.M., Armstrong, D.W., 2014. Rapid analysis of ethanol and water in commercial products using ionic liquid capillary gas chromatography with thermal conductivity detection and/or barrier discharge ionization detection. J. Agric. Food Chem, 62, 1832-1838.

Weinwurm, F., Drljo, A., Friedl, A., 2015, Lignin Concentration by Nanofiltration and pre-cipitation in a lignocellulose biorefinery, in: P.S. Varbanov, J.J. Klemes, S.R.W.Alwi, J.Y. Yong, X. Liu (Eds.) Pres15: Process Integration, Modelling and Optimisation for Energy Saving and Pollution Reduction, Aidic Servizi Srl, Milano, 901-906.

Wen, Y., Zhang, X.R., Chen, M., Wu, Z.C., Wang, Z.W., 2019a. Characterization of antibiofouling behaviors of PVDF membrane modified by quaternary ammonium compound - combined use of QCM-D, FCM, and CLSM. J. Water Reuse Desalination 9, 18-30.

Wen, Y., Chen, Y., Wu, Z., Liu, M., Wang, Z., 2019b. Thin-film nanocomposite membranes incorporated with water stable metal-organic framework CuBTTri for mitigating biofouling. J. Membr. Sci 582, 289-297.

Wu, X., Leung, D.Y.C., 2011. Optimization of biodiesel production from camelina oil using orthogonal experiment. Appl. Energy 88, 3615-3624.

Wu, C., Wang, Z., Liu, S., Xie, Z., Chen, H., Lu, X., 2018. Simultaneous permeability, selectivity and antibacterial property improvement of PVC ultrafiltration membranes via in-situ quaternization. J. Membr. Sci. 548, 50-58.

Xia, J., Liu, S., Pallathadka, P.K., Chng, M.L., Chung, T.-S., 2010. Structural determination of Extem XH 1015 and its gas permeability comparison with polysulfone and Ultem via molecular simulation. Ind. Eng. Chem. Res. 49, 12014-12021.

Xu, F., Song, Y., Wei, M., Wang, Y., 2018. Water flow through interlayer channels of two-dimensional materials with various hydrophilicities. J. Phys. Chem. C 122, 15772-15779.

Xu, J.-W., Wang, Y., Yang, Y.-F., Ye, X.-Y., Yao, K., Ji, J., Xu, Z.-K., 2015. Effects of quaternization on the morphological stability and antibacterial activity of

electrospun poly(DMAEMA-co-AMA) nanofibers. Colloids Surf. B Biointerfaces 133, 148-155.

Yang, C., Xu, W., Nan, Y., Wang, Y., Gao, C., Hu, Y., Chen, X., 2019, Preparation and characterization of acid and solvent resistant polyimide ultrafiltration membrane. Appl. Surf. Sci. 483, 278-284.

Yang, C.S., Kim, J.S., Choi, J.-W., Kwon, M.H., Kim, Y.J., Choi, J.G., Kim, G.T., 2000. XPS study of aluminum oxides deposited on PET thin film. J Ind Eng Chem 6, 149-156.

Yang, S.J., Wang, T.H., Tang, R., Yan, Q.L., Tian, W.Q., Zhang, L.P., 2020. Enhanced permeability, mechanical and antibacterial properties of cellulose acetate ultrafiltration membranes incorporated with lignocellulose nanofibrils. Int. J. Biol. Macromol. 151, 159-167.

Yang, Y.-F., Li, Y., Li, Q.-L., Wan, L.-S., Xu, Z.-K., 2010. Surface hydrophilization of microporous polypropylene membrane by grafting zwitterionic polymer for anti-biofouling. J. Membr. Sci. 362, 255-264.

Ye, Q., Zhou, F., Liu, W., 2011. Bioinspired catecholic chemistry for surface modification. Chem. Soc. Rev 40, 4244-4258.

Yeerken, T., Wang, G., Li, H., Liu, H.L., Yu, W.D., 2019. Chemical stable, superhydrophobic and self-cleaning fabrics prepared by two-step coating of a polytetrafluoroethylene membrane and silica nanoparticles. Text. Res. J. 89, 4827-4841.

Yin, J.-Z., Xiao, M., Song, J.-B., 2008. Biodiesel from soybean oil in supercritical methanol with co-solvent. Energy Convers. Manag. 49, 908-912.

Yoldas, B.E., 1975. Alumina gels that form porous transparent Al_2O_3. J. Mater. Sci. 10, 1856-1860.

Yu, L., Zhang, Y., Zhang, B., Liu, J., Zhang, H., Song, C., 2013. Preparation and characterization of HPEI-GO/PES ultrafiltration membrane with antifouling and antibacterial properties. J. Membr. Sci. 447, 452-462.

Yu, Q., Qin, Y., Han, M., Pan, F., Han, L., Yin, X., Chen, Z., Wang, L., Wang, H., 2020. Preparation and characterization of solvent-free fluids reinforced and plasticized polylactic acid fibrous membrane. Int. J. Biol. Macromol. 161, 122.

Zaidi, A., Simms, K., Kok, S., 1992. The use of micro/ultrafiltration for the removal of oil and suspended solids from oilfield brines. Water Sci. Technol. 25, 163-176.

Zaloum, R., Lessard, S., Mourato, D., Carriere, J., 1994. Membrane bioreactor treatment of oily wastes fromametal transformation mill. Water Sci. Technol. 30, 21-27.

Zeiger, M., Solioz, M., Edongué, H., Arzt, E., Schneider, A.S., 2014. Surface structure influences contact killing of bacteria by copper. MicrobiologyOpen 3, 327-332.

Zeng, Y. Wang, L., Zhang, L., Yu, J.Q., 2018. An acid resistant nanofiltration membrane prepared from a precursor of poly(s-triazine-amine) by interfacial polymerization. J. Membr. Sci. 546, 225-233.

Zeng, Z., Yu, D., He, Z., Liu, J., Xiao, F.X., Zhang, Y., Wang, R., Bhattacharyya, D., Tan, T.T., 2016. Graphene oxide quantum dots covalently functionalized PVDF membrane with significantly-enhanced bactericidal and antibiofouling performances. Sci. Rep. 6, 20142.

Zhang, L., Lin, Y., Cheng, L., Yang, Z., Matsuyama, H., 2019a. A comprehensively fouling- and solvent-resistant aliphatic polyketone membrane for high-flux filtration of difficult oil-in-water micro- and nanoemulsions. J. Membr. Sci. 582, 48-58.

Zhang, W., Shi, Z., Zhang, F., Liu, X., Jin, J., Jiang, L., 2013. Superhydrophobic and superoleophilic PVDF membranes for effective separation of water-in-oil emulsions with high flux. Adv. Mater. 25, 2071-2076.

Zhang, Y., Shao, H., Wu, C. and Hu, X., 2001. Formation and characterization of cellulose membranes from N-Methylmorpholine-N-oxide solution. Macromol. Biosci. 1, 141-148.

Zhang, H., Ding, J., Qiu, Y., Zhao, Z., 2012. Kinetics of esterification of acidified oil with different alcohols by a cation ion-exchange resin/polyethersulfone hybrid catalytic membrane. Bioresour. Technol. 112, 28-33.

Zhang, H., Tian, F., Xu, L., Peng, R., Li, Y., Deng, J., 2020a. Batch and continuous esterification for the direct synthesis of high qualified biodiesel from waste cooking oils (WCO) with Amberlyst-15/Poly (vinyl alcohol) membrane as a bifunctional catalyst. Chem. Eng. J. 388, 124214.

Zhang, J., Li, X., He, B., Song, Y., Ji, Y., Cui, Z., Li, J., Younas, M., 2020b. Biodiesel production through heterogeneous catalysis using a novel poly (phenylene sulfide) catalytic membrane. Energy & Fuels 34, 7422-7429.

Zhang, L.L., Tang, Y.Y., Jiang, X.H., Yu, L.M., Wang, C.Y., 2020c. Highly dual antifouling and antibacterial ultrafiltration membranes modified with silane coupling agent and capsaicin-mimic moieties. Polymers 12, 17.

Zhang, W., Cheng, W., Ziemann, E., Be'er, A., Lu, X., Elimelech, M., Bernstein, R., 2018b. Functionalization of ultrafiltration membrane with polyampholyte hydrogel and graphene oxide to achieve dual antifouling and antibacterial properties. J. Membr. Sci. 565, 293-302.

Zhang, W., Yang, Y., Ziemann, E., Be'er, A., Bashouti, M.Y., Elimelech, M., Bernstein, R., 2019b. One-step sonochemical synthesis of a reduced graphene oxide – ZnO nanocomposite with antibacterial and antibiofouling properties. Environ. Sci. Nano 6, 3080-3090.

Zhang, X., Ma, J., Tang, C.Y., Wang, Z., Ng, H.Y., Wu, Z., 2016a. Antibiofouling polyvinylidene fluoride membrane modified by quaternary ammonium compound: Direct contact-killing versus induced indirect contact-killing. Environ. Sci. Technol. 50, 5086-5093.

Zhang, X., Wang, Z., Chen, M., Liu, M., Wu, Z., 2016b. Polyvinylidene fluoride membrane blended with quaternary ammonium compound for enhancing anti-biofouling properties: Effects of dosage. J. Membr. Sci. 520, 66-75.

Zhang, X., Wang, Z., Chen, M., Ma, J., Chen, S., Wu, Z., 2017. Membrane biofouling control using polyvinylidene fluoride membrane blended with quaternary ammonium compound assembled on carbon material. J. Membr. Sci. 539, 229.

Zhang, X.R., Wang, Z.W., Tang, C.Y.Y., Ma, J.X., Liu, M.X., Ping, M., Chen, M., Wu, Z.C., 2018b. Modification of microfiltration membranes by alkoxysilane polycondensation induced quaternary ammonium compounds grafting for biofouling mitigation. J. Membr. Sci. 549, 165-172.

Zhang, Y., Wang, Z., Lin, W., Sun, H., Wu, L., Chen, S., 2013. A facile method for polyamide membrane modification by poly(sulfobetaine methacrylate) to improve fouling resistance. J. Membr. Sci. 446, 164-170.

Zhang, Y., Sun, H., Sadam, H., Liu, Y., Shao, L., 2019c. Supramolecular chemistry assisted construction of ultra-stable solvent-resistant membranes for angstrom-sized molecular separation. Chem. Eng. J. 371, 535-543.

Zhang, Z., Chen, S., Chang, Y., Jiang, S., 2006. Surface grafted sulfobetaine polymers via atom transfer radical polymerization as superlow fouling coatings. J. Phys. Chem. B 110, 10799-10804.

Zhao, D.L., Chung, T.-S., 2018. Applications of carbon quantum dots (CQDs) in membrane technologies: A review. Water Res. 147, 43-49.

Zhao, S., Huang, L., Tong, T., Zhang, W., Wang, Z., Wang, J., Wang, S., 2017. Antifouling and antibacterial behavior of polyethersulfone membrane incorporating polyaniline@silver nanocomposites. Environ. Sci. Water Res. Technol. 3, 710-719.

Zhong, N., Li, L., Xu, X., Cheong, L.-Z., Xu, Z., Li, B., 2013. High yield of monoacylglycerols production through low-temperature chemical and enzymatic glycerolysis. Eur. J. Lipid Sci. Technol. 115, 684-690.

Zhou, S.Y., Gao, J., Zhu, J.Y., Peng, D.L., Zhang, Y.M., Zhang, Y.T., 2020. Self-cleaning, antibacterial mixed matrix membranes enabled by photocatalyst Ti-MOFs for efficient dye removal. J. Membr. Sci. 610, 10.

Zhu, M., He, B., Shi, W., Feng, Y., Ding, J., Li, J., Zeng, F., 2010. Preparation and characterization of PSSA/PVA catalytic membrane for biodiesel production. Fuel 89, 2299-2304.

Zhu, Y., Dou, P., He, H., Lan, H., Xu, S., Zhang, Y., He, T., Niu, J., 2020. Improvement of permeability and rejection of an acid resistant polysulfonamide thin-film composite nanofiltration membrane by a sulfonated poly (ether ether ketone) interlayer. Sep. Purif. Technol. 239, 116528.

Zhu, Z., Jiang, J., Wang, X., Huo, X., Xu, Y., Li, Q., Wang, L., 2017. Improving the hydrophilic and antifouling properties of polyvinylidene fluoride membrane by incorporation of novel nanohybrid GO@SiO_2 particles. Chem. Eng. J. 314, 266

Zodrow, K., Brunet, L., Mahendra, S., Li, D., Zhang, A., Li, Q., Alvarez, P.J.J., 2009. Polysulfone ultrafiltration membranes impregnated with silver nanoparticles show improved biofouling resistance and virus removal. Water Res. 43, 715

APPENDIX A

PERMISSIONS FOR REPRODUCING PUBLISHED ARTICLES

All permissions have been taken to reproduce the full text presented in Chapters 2, 3, and 5 through the Copyright Clearance Center. All documentation of the approvals is listed on the following pages.

Chapter 2

CCC RightsLink

Home | Help | Email Support | Elif Güngörmüş Deliismail

A high-performance acid-resistant polyaniline based ultrafiltration membrane: Application in the production of aluminium sulfate powder from alumina sol

Author: Elif Gungormus,Sacide Alsoy Altinkaya
Publication: Chemical Engineering Journal
Publisher: Elsevier
Date: 1 June 2020

© 2020 Elsevier B.V. All rights reserved.

Journal Author Rights

Please note that, as the author of this Elsevier article, you retain the right to include it in a thesis or dissertation, provided it is not published commercially. Permission is not required, but please ensure that you reference the journal as the original source. For more information on this and on your other retained rights, please visit: https://www.elsevier.com/about/our-business/policies/copyright#Author-rights

BACK CLOSE WINDOW

© 2022 Copyright - All Rights Reserved | Copyright Clearance Center, Inc. | Privacy statement | Data Security and Privacy | For California Residents | Terms and ConditionsComments? We would like to hear from you. E-mail us at customercare@copyright.com

Chapter 3

RightsLink

Home | Help | Email Support | Elif Güngörmüş Deliismail

A new-generation poly (ether imide sulfone) based solvent resistant ultrafiltration membrane for a sustainable production of silica nanopowder

Author: Elif Gungormus,Sacide Alsoy Altinkaya
Publication: Separation and Purification Technology
Publisher: Elsevier
Date: 1 January 2023

© 2022 Elsevier B.V. All rights reserved.

Journal Author Rights

Please note that, as the author of this Elsevier article, you retain the right to include it in a thesis or dissertation, provided it is not published commercially. Permission is not required, but please ensure that you reference the journal as the original source. For more information on this and on your other retained rights, please visit: https://www.elsevier.com/about/our-business/policies/copyright#Author-rights

BACK CLOSE WINDOW

© 2022 Copyright - All Rights Reserved | Copyright Clearance Center, Inc. | Privacy statement | Data Security and Privacy | For California Residents | Terms and ConditionsComments? We would like to hear from you. E-mail us at customercare@copyright.com

Chapter 5

RightsLink

Home | Help | Email Support | Elif Güngörmüş Deliismail

Facile fabrication of Anti-biofouling polyaniline ultrafiltration membrane by green citric acid doping process

Author: Elif Gungormus,Sacide Alsoy Altinkaya
Publication: Separation and Purification Technology
Publisher: Elsevier
Date: 15 December 2021

© 2021 Elsevier B.V. All rights reserved.

Journal Author Rights

Please note that, as the author of this Elsevier article, you retain the right to include it in a thesis or dissertation, provided it is not published commercially. Permission is not required, but please ensure that you reference the journal as the original source. For more information on this and on your other retained rights, please visit: https://www.elsevier.com/about/our-business/policies/copyright#Author-rights

BACK CLOSE WINDOW

© 2022 Copyright - All Rights Reserved | Copyright Clearance Center, Inc. | Privacy statement | Data Security and Privacy | For California Residents | Terms and ConditionsComments? We would like to hear from you. E-mail us at customercare@copyright.com

APPENDIX B

SUPPLEMENTARY INFORMATION FOR CHAPTER 3

Synthesis of colloidal silica suspension:

Silica nanoparticles were synthesized by varying ethanol concentration in the ethanol-water mixture as 13%, 38%, and 50%. Increasing this ratio from 13 to 38% did not significantly change the mean particle size (Figure B.1) but doubled the zeta potential value (-12.75±0.50 mV for 13% ethanol concentration in the ethanol-water mixture, -24.63±0.69 mV for 38% ethanol concentration in the ethanol-water mixture, Figure B.2). Nanoparticle formation was not successful above the ethanol concentration of 38% due to gel formation. Since the particles carrying zeta potential of -24.63±0.69 mV will have a higher colloidal stability and lower interaction with a negatively charged membrane surface, 38% ethanol concentration in the ethanol-water mixture was chosen for the synthesis of silica nanoparticles.

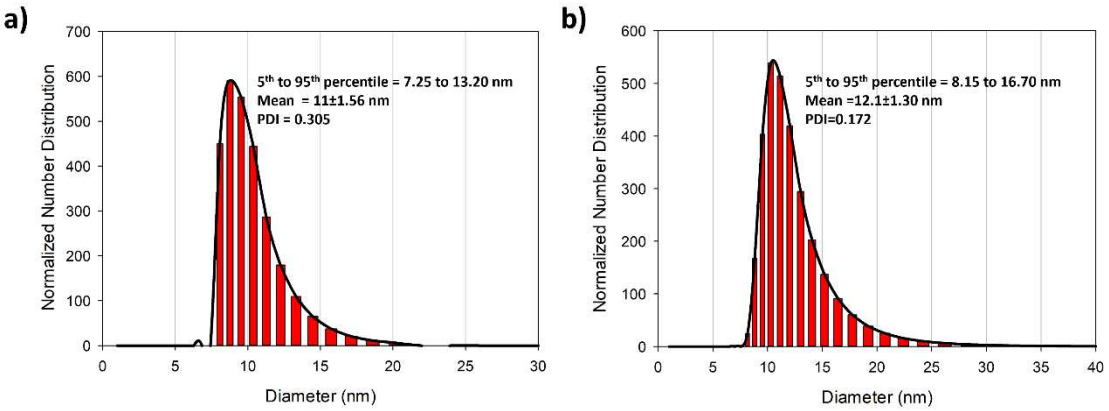

Figure B.1. Particle size distributions of the colloidal silica suspension prepared in a) 13% and b) 38% ethanol concentration in ethanol-water mixture

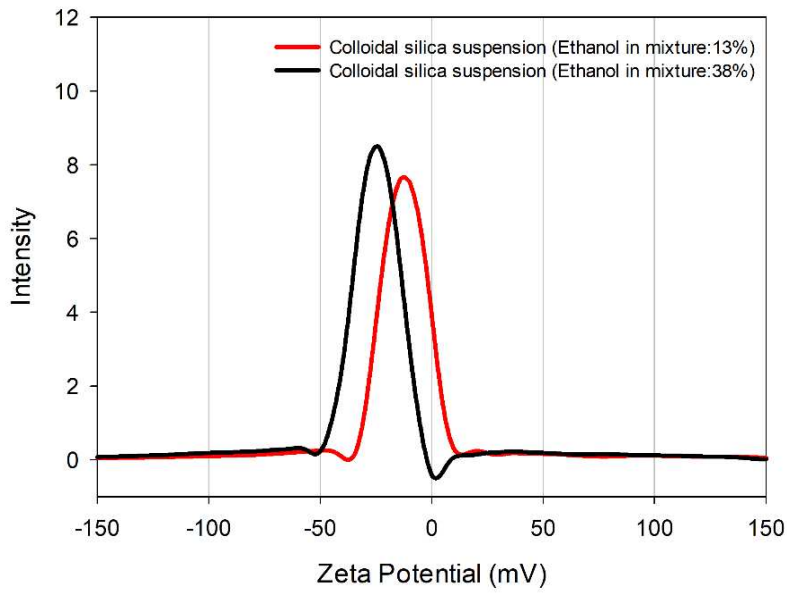

Figure B.2. Zeta potential of the colloidal silica suspension prepared in 13% and 38% ethanol concentration in ethanol-water mixture

Characterization of the pristine and amine-functionalized TiO_2 coated poly (ether imide sulfone) membranes:

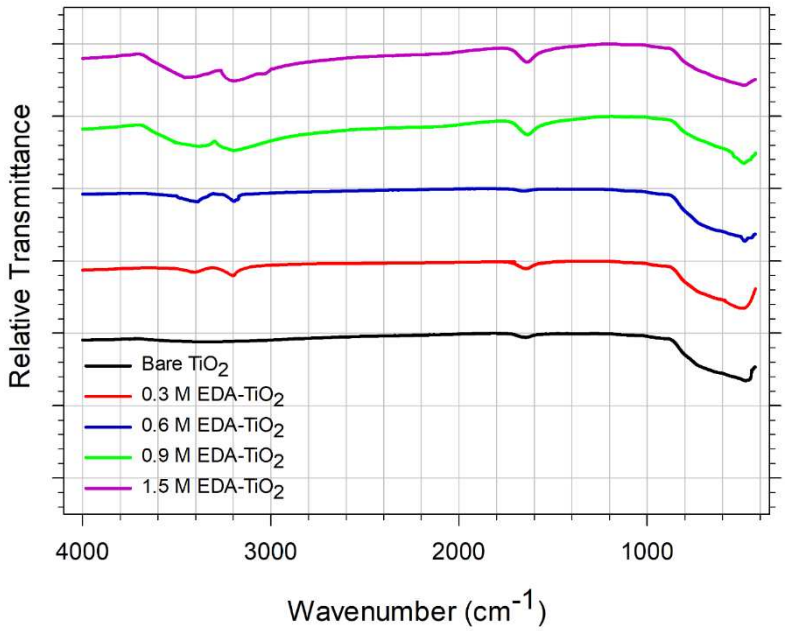

Figure B.3. ATR-FTIR spectra of the amine-functionalized TiO_2 prepared using different EDA concentrations

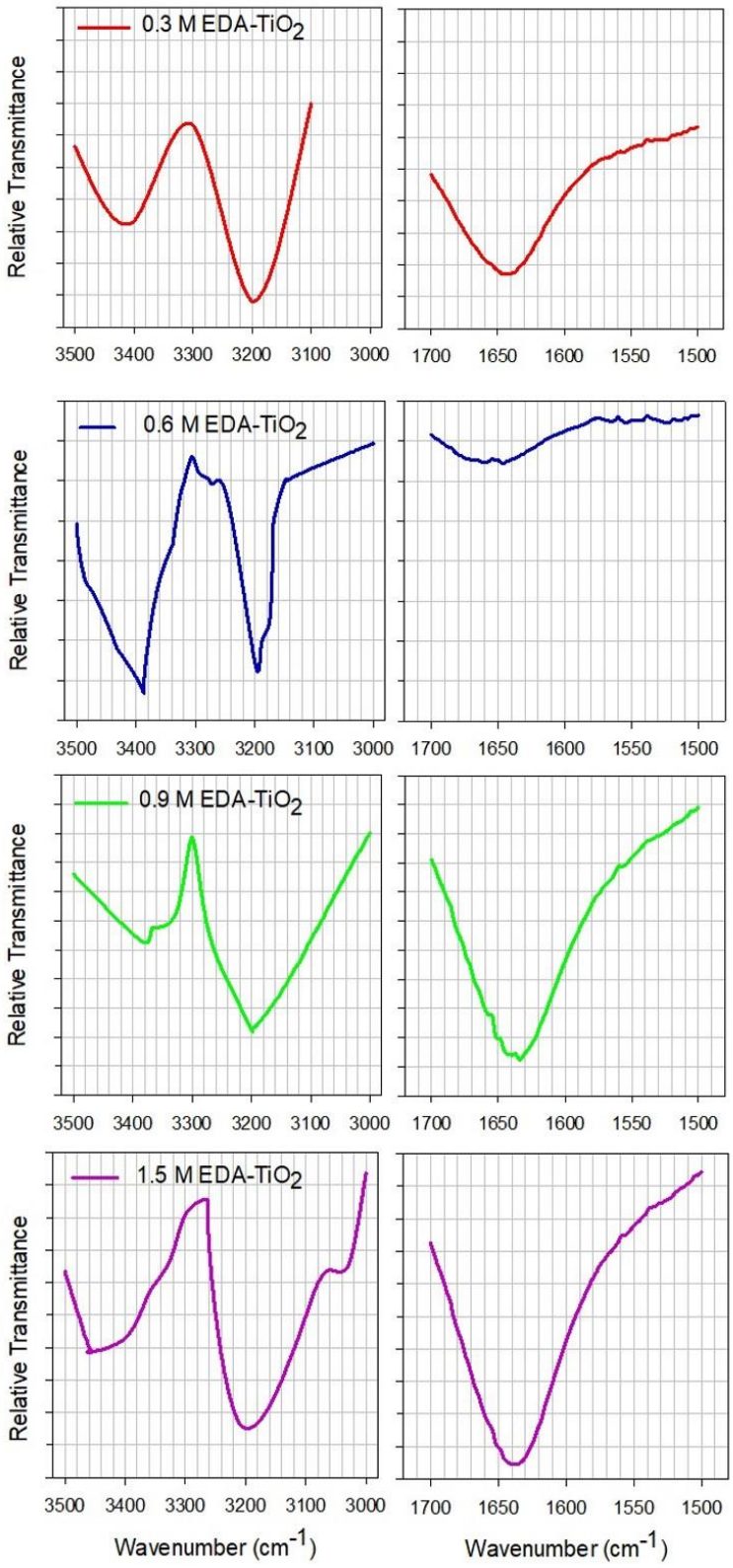

Figure B.4. Detailed ATR-FTIR spectra of the amine-functionalized TiO_2 prepared using different EDA concentrations

Table B.1. Normalized peak area of the amine-functionalized TiO_2 nanoparticles prepared using different EDA concentrations

EDA (M)	Peak Area for Ti-OH (A_1)	Peak Area for –NH (A_2)	A_2/A_1
0.3	0.26	0.41	1.58
0.6	0.19	0.50	2.63
0.9	0.34	0.79	2.32
1.5	0.42	1	2.38

Table B.2. The change of average size and zeta potentials of the bare TiO_2 and amine-functionalized TiO_2 prepared using different EDA concentrations

EDA (M)	Mean Particle Size (nm)	PDI	Zeta Potential (mV)
0	50.9±2.9	0.37	-34.82±0.95
0.3	55.6±3.1	0.29	-36.06±1.21
0.6	60.23±2.80	0.32	-39.90±0.31
0.9	183±2	0.30	-28.83±0.05
1.5	206±11	0.46	-26.64±0.66

Table B.3. The effects of coating time and temperature of the amine-functionalized TiO_2 nanoparticles on the PWP of the modified membranes

Coating Temperature (°C)	Coating Time (min)	PWP ($Lm^{-2}h^{-1}bar^{-1}$)
20	0	70.23±0.65
	30	70.10±0.62
	60	70.37±0.35
	90	70.36±0.17
50	0	70.23±0.65
	30	72.96±0.71
	60	73.04±0.24
	90	73.74±0.38
70	0	70.23±0.65
	30	75.32±0.31
	60	81.65±0.72
	90	81.81±1.03
90	0	70.23±0.65
	30	75.95±0.49
	60	81.59±0.67
	90	81.55±0.32

Silica nanopowder production by membrane filtration:

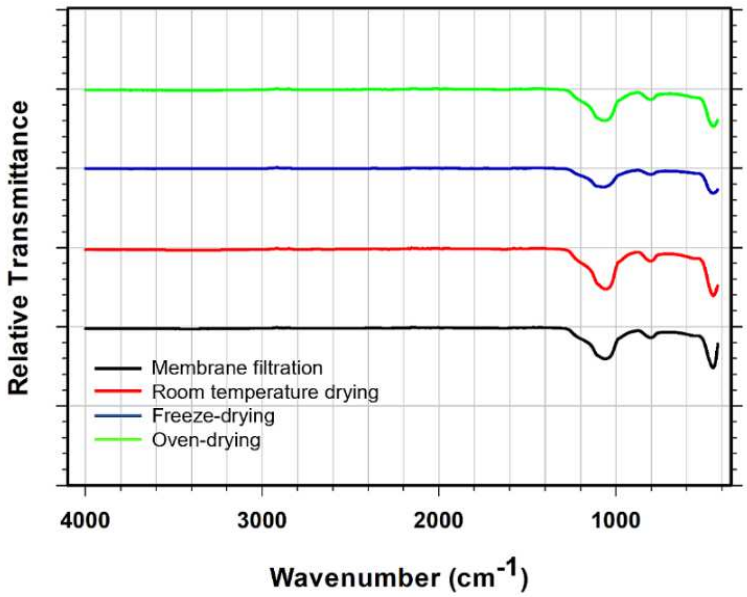

Figure B.5. ATR-FTIR spectra of the silica nanopowder produced by membrane filtration and traditional drying methods

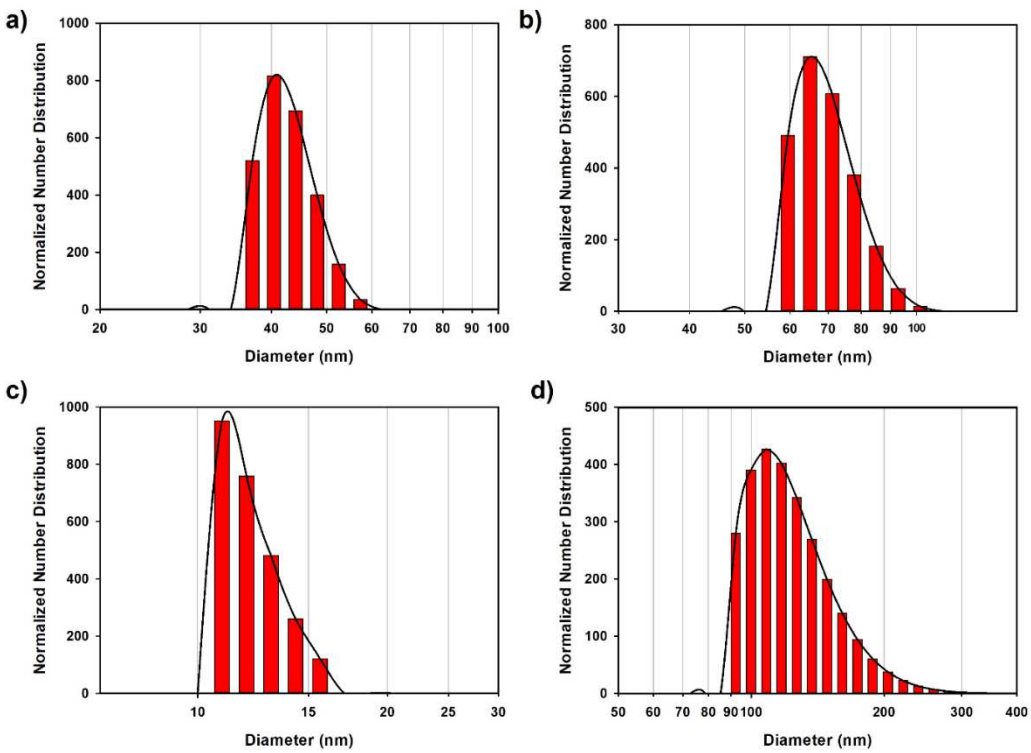

Figure B.6. Particle size distributions of silica nanopowder produced by a) membrane filtration, b) room-temperature drying, c) freeze-drying, and d) oven-drying

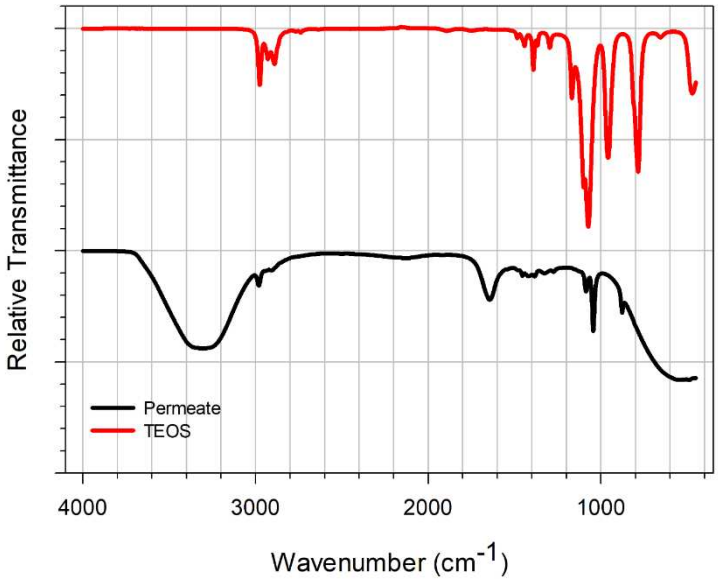

Figure B.7. ATR-FTIR spectra of TEOS and the permeate obtained from filtering colloidal silica suspension by the amine-functionalized TiO_2 coated poly (ether imide sulfone) membranes

VITA

Education

Ph.D.	Chemical Engineering, Izmir Institute of Technology, İzmir, Turkey Thesis: "Development of innovative polymeric membranes using green approaches for water and energy sustainability" Advisor: Prof. Dr. Sacide ALSOY ALTINKAYA	2022
M.Sc.	Environmental Engineering, Izmir Institute of Technology, İzmir, Turkey Thesis: "Ambient air persistent organic pollutant monitoring, backtrajectory modeling, and health risk assessment" Advisor: Prof. Dr. Aysun SOFUOĞLU	2015
B.S.	Chemical Engineering, Izmir Institute of Technology, İzmir, Turkey Senior thesis: "Preparation and characterization of polysulfone based hemodialysis membranes through superoxide dismutase/catalase enzymes immobilization" Advisor: Prof. Dr. Sacide ALSOY ALTINKAYA	2012

Academic Experience

Research Assistant	Chemical Engineering, Izmir Institute of Technology, Izmir, Turkey	2013-
Project Assistant	TUBITAK 112Y325 Project: Monitoring of persistent organic pollutants in ambient air and soil samples at selected urban and background sites in Turkey	2013-2015 (18 Months)
Project Assistant	TUBITAK 113Y500 Project: Determination of the levels and sources of organic and inorganic pollutants causing air pollution in and around Dilovası Industrial Zone	2016 (6 Months)

Honors and Awards

Global Winner of Future Infrastructure Star Challenge 2021 (1st place award)
Bentley Systems Incorporated
Project: Mini-Modular-Plant for Digitized Sustainable Campus

Honor- High Honors Certificates
Izmir Institute of Technology
2008-2012

Publications

Gungormus, E., Tuncel S., Tecer, L.H., Sofuoglu, S.C., 2014. Inhalation and dermal exposure to atmospheric polycyclic aromatic hydrocarbons and associated carcinogenic risks in a relatively small city. Ecotoxicology and Environmental Safety 108, 106-113.

Ugranli, T., Gungormus, E., Kavcar, P., Demircioglu, E., Odabasi, M., Sofuoglu, S.C., Lammel G., Sofuoglu, A., 2016. POPs in a major conurbation in Turkey: Ambient air concentrations, seasonal variation, inhalation and dermal exposure, and associated carcinogenic risks. Environmental Science and Pollution Research 23 (22), 22500-22512.

Ugranli, T., Gungormus E., Sofuoglu, A., Sofuoglu, S.C., 2016. Chapter: Indoor Air Quality in Chemical Laboratories, in Comprehensive Analytical Chemistry; Elsevier, 73, 859-878.

Birgül, A., Kurt-Karakus, P.B, Alegria, H., Gungormus, E., Celik, H., Cicek, T., Can-Güven, E., 2017. Polyurethane foam (PUF) disk passive samplers derived polychlorinated biphenyls (PCBs) concentrations in the ambient air of Bursa-Turkey: Spatial and temporal variations and health risk assessment. Chemosphere, 168, 1345-1355.

Dumanoglu, Y., Gaga, E., Gungormus, E., Sofuoglu, S.C., Odabasi, M., 2017. Spatial and seasonal variations, sources, air-soil exchange, and carcinogenic risk assessment for PAHs and PCBs in air and soil of Kutahya, Turkey, the province of thermal power plants. Science of the Total Environment, 580, 920-935.

Kurt-Karakus, P.B, Cicek, T., Sofuoglu, S.C, Celik, H., Gungormus, E., Gedik, K., Sofuoglu, A., Okten, H.E., Birgul, A., Alegria, H., Jones, K.C, 2018. The first countrywide monitoring of selected POPs: Polychlorinated biphenyls (PCBs), polybrominated diphenyl ethers (PBDEs) and selected organochlorine pesticides (OCPs) in the atmosphere of Turkey. Atmospheric Environmet, 177, 154-165.

Kurt-Karakus, P.B., Alegria, H., Birgul, A., Gungormus, E., Jantunen, L., 2018. Organophosphate ester (OPEs) flame retardants and plasticizers in air and soil from a highly industrialized city in Turkey. Science of The Total Environment, 625,555-565.

Cetin, B., Yurdakul, S., Gungormus, E., Ozturk, F., Sofuoglu, S.C., 2018. Source apportionment and carcinogenic risk assessment of passive air sampler-derived PAHs and PCBs in a heavily industrialized region. Science of the Total Environment, 633, 30-41.

Gungormus, E., Alsoy Altınkaya S., 2020. A high-performance acid-resistant polyaniline based ultrafiltration membrane: Application in the production of aluminium sulfate powder from alumina sol. Chemical Engineering Journal, 389, 124393.

Gungormus, E., Sofuoglu, A., Celik, H., Gedik, K., Mulder, M., Lammel, G., Sofuoglu, S.C., Okten, E., Ugranli, T., Birgul, A., Jones, K.C., Kurt-Karakus, P.K., 2021. Selected Persistent Organic Pollutants in Ambient Air in Turkey: Regional Sources and Controlling Factors. Environmental Science and Technology, 55, 14, 9434–9443.

Gungormus, E., Alsoy Altınkaya S., 2021. Facile fabrication of Anti-biofouling polyaniline ultrafiltration membrane by green citric acid doping process. Separation and Purification Technology, 279, 119756.

Gungormus, E., Alsoy Altınkaya S., 2023. A new-generation poly (ether imide sulfone) based solvent resistant ultrafiltration membrane for a sustainable production of silica nanopowder. Separation and Purification Technology, 304, 122351